To the Graduate Council:

I am submitting herewith a thesis written by Sher Mohammed entitled "The Effect of Welding Conditions on the Low Temperature Transformation and Properties of the Weld HAZ of Low Alloy Steels for Use in Light Water Reactors." I have examined the final copy of this thesis for form and content and recommend that it be accepted in partial fulfillment of the requirements for the degree of Master of Science, with a major in Metallurgical Engineering.

Carl D. Lundin, Major Professor

We have read this thesis
and recommend its acceptance:

Charlie R. Brooks

E. E. Stansbury

Accepted for the Council:

L. Evans Haak

Vice Chancellor
Graduate Studies and Research

THE EFFECT OF WELDING CONDITIONS ON THE LOW TEMPERATURE TRANSFORMATION AND PROPERTIES OF THE WELD HAZ OF LOW ALLOY STEELS FOR USE IN LIGHT WATER REACTORS

A Thesis

Presented for the

Master of Science

Degree

The University of Tennessee, Knoxville

Sher Mohammed

November 1981

3055542

ACKNOWLEDGMENTS

The support of Oak Ridge National Laboratory is acknowledged. The author wishes to express his appreciation to Mr. H. B. Thompson and his talented group of expert machinists, R. Bellamy, J. French, B. Love, W. Morrell, who skillfully machined test specimens necessary for the successful completion of this effort. Appreciation is also extended to Mr. T. A. Long and his group of electronics technicians for maintaining critical instrumentation during the testing phase of the program. A special note of appreciation is extended to Mr. M. Neal who was called upon many times to repair instruments that were crucial to the successful completion of this study and often worked beyond the call of duty to insure the instruments operated properly.

Appreciation is also extended to Dr. C. D. Lundin, from whom came wise counsel and guidance during this study. Recognition is given also to Dr. E. E. Stansbury and Dr. C. R. Brooks, for their continued encouragement, advice and assistance during the course of this investigation.

ABSTRACT

This research is directed toward the effect of welding procedures on the fabrication of low alloy steels (SA 508 and SA 533) for pressure vessel use. During fabrication of Low Alloy Steels used in Light Water Reactor construction, preheat for welding, and in some instances, the maintenance of preheat after welding, is employed to avoid fabrication problems. The employment of preheat is aimed primarily at the elimination of HAZ cracking, which is normally attributed to cold cracking due to hydrogen and the low temperature transformation of austenite to martensite. It is beneficial to achieve a higher fracture toughness in the weld HAZ relative to that of the adjacent base material and it has been observed that untempered HAZ regions normally show lower toughness; but a properly PWHT HAZ shows superior toughness, especially if the structure is martensitic. In addition to modifying the metallurgical structure, PWHT is applied to reduce or eliminate the residual welding stresses. Materials containing carbide forming alloy elements often exhibit precipitation of the alloy carbides within the grains of the weld HAZ during PHWT and serve to strengthen the matrix in comparison to the grain boundary. The creep strain necessary to relieve the residual stresses is forced into the weakened grain boundary region and consequently extensive grain boundary deformation may induce cracks in the HAZ. This problem of reheat cracking can be eliminated by controlling the compositions of the materials.

In order to approach the preheat problem, the continuous cooling transformation and isothermal transformation behavior has been determined dilatometrically and by resistivity measurements. This

documentation of CCT and I-T behavior is unique in that it includes the full spectrum of cooling and hold behavior and is extended to weld HAZ situations. The two HAZ regions correspond to coarse-grained region (2400°F peak) which lies adjacent to the fusion zone and the refined region (1650°F peak) in the outer extremeties of the HAZ. The transformation products resulting from exposure to peak temperature of 2400 and 1650°F were determined metallographically. The result of CCT behavior showed that the higher peak temperature (2400°F) causes the bainite nose to shift to significantly longer times. It was also observed for the coarse-grained region, that the CCT behavior for both steels is identical. Comparative energy input/thickness values were also calculated for equivalent cooling rates.

The reheat cracking tendency for both steels was evaluated by metallographic studies of simulated HAZ structures subjected to PWHT cycles and simultaneous restraint. Both SA 533 and SA 508 cracked intergranularly. The stress rupture parameter (this is the product of the stress for a rupture life of ten (10) minutes and the corresponding reduction of area) calculated for both steels showed that SA 508 was more susceptible to reheat cracking than SA 533.

Cold cracking tests comprised of the Battelle Test and University of Tennessee's Hydrogen Susceptibility Test were conducted. These tests indicated that for SA 508, a higher preheat temperature is required to avoid cracking than for SA 533. Further, the Hydrogen Susceptibility Test results show that SA 508 composition is more susceptible to hydrogen embrittlement than is the composition of SA 533.

The charpy impact toughness was determined for the various HAZ transformation products by simulating the HAZ structures. It was

found that tempered martensite is far superior to tempered bainite in regards to the HAZ toughness. For an untempered martensitic structure, a post-weld hold at 600°F was injurious to the as-welded HAZ toughness, but superior toughness could be achieved by PWHT. Grain refining thermal cycles do not improve toughness per se if the transformation product is untempered bainite. The heat flow associated with and peak temperatures reached by additional passes are considered necessary for optimum HAZ toughness.

It is recommended that during welding of SA 533 and SA 508, weld energy input should be controlled to obtain a cooling rate faster than the critical cooling rate for bainite, and thus form a primarily martensitic structure. PWHT of this structure is recommended after welding in order to temper the martensite and optimize the HAZ behavior.

TABLE OF CONTENTS

CHAPTER		PAGE
I.	INTRODUCTION	1
II.	LITERATURE REVIEW	5
	Effect of Heat Treatment on Weld HAZ	5
	Weld HAZ and Its Toughness	10
	Transformation Products in Weld HAZ	17
	Stress Relief Cracking of Weld HAZ	26
	Hydrogen Embrittlement	30
III.	EXPERIMENTAL PROCEDURES	32
	Materials	32
	Isothermal Transformation Behavior	33
	Continuous Cooling Transformation Behavior	35
	CCT Obtained by Resistivity Measurements	35
	Manual Measurements at Room Temperature	35
	Measurements of Resistivity at Elevated Temperature Under Digital Computer Control	39
	CCT Behavior Obtained Dilatometrically	44
	The Gleeble	44
	Programming	45
	The Dilatometer	48
	Evaluation of Cold Cracking	51
	Underbead Crack Test	53
	Hydrogen Susceptibility Test	53
	Stress Relief Cracking	58
	Charpy Impact Toughness of HAZ	61

CHAPTER PAGE

IV. RESULTS AND DISCUSSION 64
Isothermal Transformation Behavior 64
Continuous Cooling Transformation Behavior 80
CCT Behavior Obtained by Resistivity Measurements . . 81
SA 533 Grade B Class 1 81
SA 508 Class 2 83
CCT Behavior for the HAZ Exposure Obtained by the Gleeble Dilatometric Method 96
SA 533 Grade B Class 1 96
SA 508 Class 2 105
Hardenability of SA 533 and SA 508 127
Cold Cracking 131
Battelle Underbead Cracking Test 134
Results of Hydrogen Susceptibility Testing 136
Stress Relief Cracking 139
Charpy V-Notch Toughness of Simulated HAZ Microstructures 150
SA 533 Grade B Class 1 152
SA 508 Class 2 161
V. CONCLUSIONS 173
BIBLIOGRAPHY 176
APPENDICES 183
APPENDIX A 184
APPENDIX B 192
VITA 195

LIST OF TABLES

TABLE		PAGE
1.	Chemical Compositions of the Materials	6
2.	Mechanical Properties of the Materials	7
3.	Percentage Composition for Material SA 533 Gr. B Cl. 1 and SA 508 Cl. 2	34
4.	Cooling Rates of Material A-533 from Curves a to l of Figure 35	84
5.	Cooling Rates of Material A-508 from Curves a to p of Figure 39	90
6.	Results of Battelle Underbead Cracking Tests	135
7.	Results of University of Tennessee Hydrogen Susceptibility Tests	135
8.	The Values Obtained in SRC Test for Rupture Life of 10 minutes	143
A-1.	Schedule of Salt Bath Heat Treatment of SA 533 (3T) and SA 508 (8M) Specimens	185
A-2.	Thermal Treatments and Stresses Employed in Stress Relief Cracking Test	186
A-3.	Thermal Treatments Employed in Charpy V-notch Test	187
A-4.	Energy Inputs as a Function of Plate Thickness for SMAW Process	188
A-5.	Data Obtained by Stress-Relief Cracking Test	189
A-6.	Data of Charpy Test Obtained for SA 533 steel, Tested @ -25°F.	190
A-7.	Data of Charpy Test Obtained for SA 508 steel, Tested @ 72°F.	191

LIST OF FIGURES

FIGURE		PAGE
1.	Schematic view of a typical large pressure vessel . . .	2
2.	Submerged-arc weldment hardness traverse at quarter-thickness location. The region of the heat-affected zone that is most sensitive to reheat cracks exhibits the highest hardness. (Canonico[1])	12
3.	Charpy V-notch impact properties of 125 ksi tensile-strength alloy steel with different structures	14
4.	Charpy V-notch impact test results for specimens from three levels in a SA-533 Grade B Class 1 plate 305 mm (12 in.) thick. Code: closed dot, surface in longitudinal direction. Open triangle, 1/4 thick in longitudinal direction. Closed diamond, 1/2 thick in longitudinal direction.	15
5.	Isothermal Transformation Diagram for A 302, Grade C, Steel. (The actual cooling data are superimposed on the diagram.)	19
6.	CCT Diagram of Steel 'B'. Composition: C 0.17%, Si 0.26%, Mn 0.84%, P 0.05%, S 0.06%, Cr 0.4%, Ni 0.84%, Mo 0.62%.	21
7.	Comparison of grain sizes in simulated (for a peak temperature of 1350°C) and real heat affected zones for the indicated cooling times between 800 and 500°C.	23
8.	Partial Continuous Cooling Transformation Diagram of SA 533 steel	25
9.	Isothermal transformation diagram for ASTM A 302 Grade C steel. (The analysis for A 302 Grade C is identical to that of A 533 Grade B.) The rapid cooling rate near the fusion line in combination with the coarse austenite grains will result in a microstructure that is predominantly martensitic.	36
10.	Schematic representation of resistivity measurement at room temperature	38
11.	Block configuration of operational devices for electrical resistivity measurement	41

FIGURE PAGE

12. Flow chart of master program ERM 42

13. Schematic representation of resistivity vs. temperature curves 43

14. Block diagram of Electronic Control Mechanism 47

15. A high-speed dilatometer 50

16. Schematic representation of dilation vs. temperature curves. 52

17. Underbead Cracking Test specimen 54

18. Hydrogen Susceptibility Test specimen 56

19. Schematic representation of apparatus used to strain specimen 57

20. Stress relief cracking specimen used in Gleeble 59

21. Schematic representation of reheat cracking studies 60

22. Details of charpy specimen preparation 62

23. Isothermal transformation diagram of SA 533 Gr. B Cl. 1 steel. 65

24. Isothermal transformation diagram of SA 508 Cl. 2 steel. 66

25. Specimen 3T0A (held for 1 sec. @ 550°F) shows fully martensitic structure. HRC 50. Super picral etch 68

26. Specimen 3T1B (held for 10 sec. @ 800°F) Shows Bainitic-Martensitic structure. HRC 44. Super picral etch 69

27. Specimen 3T3E (held for 10^3 secs. @ 1250°F). Shows Ferritic-Martensitic structure. HRC 44. Super picral etch 70

28. Specimen 8M0A (held for 1 sec. @ 550°F). Shows fully martensitic structure. HRC 52. Super picral etch 72

FIGURE PAGE

29. Specimen 8M2B (held for 10^2 secs. @ 800°F). Shows Bainitic-martensitic structure. HRC 33. Super picral etch 73

30. Specimen 8M3E (held for 10^3 secs. @ 1250°F) Shows Ferritic-Martensitic structure. HRC 49. Super picral etch 74

31. Specimen 8M4E (held for 10^4 secs. @ 1250°F). Shows Ferritic-Pearlitic-Martensitic structure. HRC 34. Super picral etch 76

32. Pearlitic-Ferritic Structure of specimen 8M4E. (held for 10^4 secs. @ 1250°F). Super picral etch. SEM 77

33. Comparison of I-T behavior for SA 533 with SA 508 steel 78

34. Comparison of I-T diagrams of SA 533 (above) with SA 302 (provided by Luken's Steel Co.) 79

35. Continuous Cooling Transformation diagram of SA 533 Gr. B Cl. 1 steel 82

36. Fully martensitic structure representing curve 'a'. Cooling rate 167°F/sec. @ 1300°F. Super picral etch 85

37. Bainitic structure representing curve 'g'. Cooling rate 4.5°F/sec. @ 1300°F. Super picral etch 86

38. Microstructures representing curve 'k'. Cooling rate 0.1°F/sec. @ 1300°F. Super picral etch. 87

39. Continuous Cooling Transformation diagram of SA 508 Cl. 2 steel 89

40. Fully Martensitic structure representing curve 'a'. Cooling rate 198°F/sec. @ 1300°F. Super picral etch. 91

41. Bainitic structure representing curve 'i'. Cooling rate 6°F/sec. @ 1300°F. Super picral etch 92

42. Microstructures representing curve 'p'. Cooling rate 0.018°F/sec. @ 1300°F. Super picral etch. 93

FIGURE PAGE

43. Comparison of CCT behavior for SA 533 with SA 508 steel 94

44. Continuous Cooling Transformation diagram of SA 533 Gr.B Cl. 1 for a peak temperature of 1650°F. 97

45. Microstructure corresponding to energy input 20KJ/in., 1650°F peak temperature. HRC 48. Super picral etch 99

46. Microstructure corresponding to energy input of 136KJ/in., 500°F preheat, 1650°F peak temperature. HRC 21. Super picral etch 100

47. Continuous Cooling Transformation diagram of SA 533 Gr.B Cl. 1 for a peak temperature of 2400°F. 101

48. Microstructure corresponding to energy input of 50KJ/in., 2400°F peak temperature. HRC 44. Super picral etch 102

49. Microstructure corresponding to energy input of 136KJ/in., 500°F preheat, 2400°F peak temperature. HRC 25. Super picral etch 103

50. Effect of peak temperature on continuous cooling transformation behavior of SA 533 Gr.B Cl. 1 steel 104

51. Continuous Cooling Transformation diagram of SA 508 Cl. 2 for a peak temperature of 1650°F 106

52. Microstructure corresponding to energy input of 32 KJ/in., 1650°F peak temperature HRC 44. Super picral etch 107

53. Microstructure corresponding to energy input of 136KJ/in., 500°F preheat, 1650°F peak temperature. HRC 25. Super picral etch 108

54. Continuous Cooling Transformation diagrams of SA 508 Cl. 2 of peak temperature of 2400°F 109

55. Microstructure corresponding to energy input of 50KJ.in., 2400°F peak temperature. HRC 47. Super picral etch 111

FIGURE PAGE

56. Microstructure corresponding to energy input of 136KJ/in., 500°F preheat, 2400°F peak temperature. HRC 27. Super picral etch 112

57. Effect of peak temperature on continuous cooling transformation behavior of SA 508 Cl. 2 steel 113

58. Comparison of Continuous Cooling Transformation behavior of SA 533 and SA 508 for a peak temperature of 2400°F 114

59. Comparison of CCT behavior of steel 'B' with SA 508 steel 116

60. Energy input vs. cooling rates for steel plates utilizing SMAW process 118

61. Continuous Cooling Transformation behavior of SA 533 for a peak temperature of 1650°F (energy inputs correspond to 2 in. steel plate). 119

62. Continuous Cooling Transformation behavior of SA 533 for a peak temperature of 1650°F (energy inputs correspond to 3 in. steel plate). 120

63. Continuous Cooling Transformation behavior of SA 533 for a peak temperature of 2400°F (energy inputs correspond to 2 in. steel plate). 121

64. Continuous Cooling Transformation behavior of SA 533 for a peak temperature of 2400°F (energy inputs correspond to 3 in. steel plate). 122

65. Continuous Cooling Transformation behavior of SA 508 for a peak temperature of 1650°F (energy inputs correspond to 2 in. steel plate). 123

66. Continuous Cooling Transformation behavior of SA 508 for a peak temperature of 1650°F (energy inputs correspond to 3 in. steel plate). 124

FIGURE PAGE

67. Continuous Cooling Transformation behavior of SA 508 for a peak temperature of 2400°F (energy inputs correspond to 2 in. steel plate). 125

68. Continuous Cooling Transformation behavior of SA 508 for a peak temperature of 2400°F (energy inputs correspond to 3 in. steel plate). 126

69. Hardenability curves for SA 508 and SA 533 steels 128

70. Correlation of CCT and hardenability curves of SA 533 . . 129

71. Correlation of CCT and hardenability curves of SA 508 . . 130

72. Hardenability curves for SA 508 and SA 533 steels, austenitized at 2200°F 132

73. Microstructures show underbead cracks for specimens welded @ 32°F. The top section of micrographs is weld metal. Super picral etch 137

74. Macrographs of cracks observed in University of Tennessee Hydrogen Susceptibility Test specimens 138

75. Stress rupture properties at 1150°F of simulated grain coarsened weld HAZ of SA 508 and SA 533 141

76. Fracture behavior observed in SRC test of SA 533 steel. (Martensitic structure.) 145

77. Fracture behavior observed in SRC test of SA 533 steel. (Bainitic structure.) 146

78. Fracture behavior observed in SRC test of SA 508. (Martensitic structure.). 147

79. Fracture behavior observed in SRC test of SA 508. (Bainitic structure.) 149

80. Charpy V-notch toughness as related to different HAZ thermal cycles for SA 533 Gr. 151

81. Microstructural behavior observed in SA 533 steel for Cycle II. 153

FIGURE PAGE

82. Microstructural behavior observed in SA 533 steel for Cycle VI 154

83. Microstructural behavior observed in SA 533 steel for multiple cycles (Cycle II) 156

84. Microstructural behavior observed in SA 533 steel for multiple cycles (Cycle VI) 157

85. Microstructural behavior observed in SA 533 steel for Cycle II and held @ 600°F 158

86. Microstructural behavior observed in SA 533 steel for Cycle VI and held @ 600°F 159

87. Microstructural behavior observed in SA 533 steel for Cycle VI and held @ 300°F 160

88. Charpy V-notch toughness as related to different HAZ thermal cycles for SA 508 Cl. 2 162

89. Microstructural behavior observed in SA 508 steel for Cycle II 163

90. Microstructural behavior observed in SA 508 steel for Cycle VI 164

91. Microstructural behavior observed in SA 508 steel for multiple cycles (Cycle II) 165

92. Microstructural behavior observed in SA 508 steel for multiple cycles (Cycle VI) 166

93. Microstructural behavior observed in SA 508 steel for Cycle II and held @ 600°F 168

94. Microstructural behavior observed in SA 508 steel for Cycle VI and held @ 600°F 169

95. Microstructural behavior observed in SA 508 steel for Cycle II and held @ 300°F 170

96. Microstructural behavior observed in SA 508 steel for Cycle VI and held @ 300°F 171

A-1. Lateral expansion values for charpy specimens of SA 533 Gr. B Cl. 1 exposed to different HAZ thermal cycles. . . 193

A-2. Lateral expansion values for charpy specimens of SA 508 Cl. 2 exposed to different HAZ thermal cycles . . . 194

CHAPTER I

INTRODUCTION

The pressure vessels used as the primary containment for Light-Water nuclear power plants are fabricated from thick-walled plate or forgings by welding.[1] Figure 1 provides a schematic view indicating the various components that are joined together to produce a large pressure vessel. The main course sections in Figure 1 are constructed from plate or forgings.

The pressure vessel material used for the primary containment of the light-water nuclear power plants in the United States represent only two base metal compositions. These steels are identified as SA 533 Grade B Class 1 and SA 508 Class 2. The SA before the specification number indicates that the material has been accepted for use by the ASME code. A steel that is employed in the fabrication of a nuclear pressure vessel must satisfy the requirements of the SA specification, which indicate the limits on chemical composition, permissible melting and processing practices, and minimum mechanical properties, as well as other criteria that are established by the ASME code, the Federal Register, and NRC Regulatory Guides.

The purpose of this research was to conduct a weldability investigation on the two materials which constitute a significant fraction of the low alloy steels employed for heavy section light water reactor utilization, namely SA 533 Grade B Class 1 and its closely allied sister forging material, SA 508 Class 2.

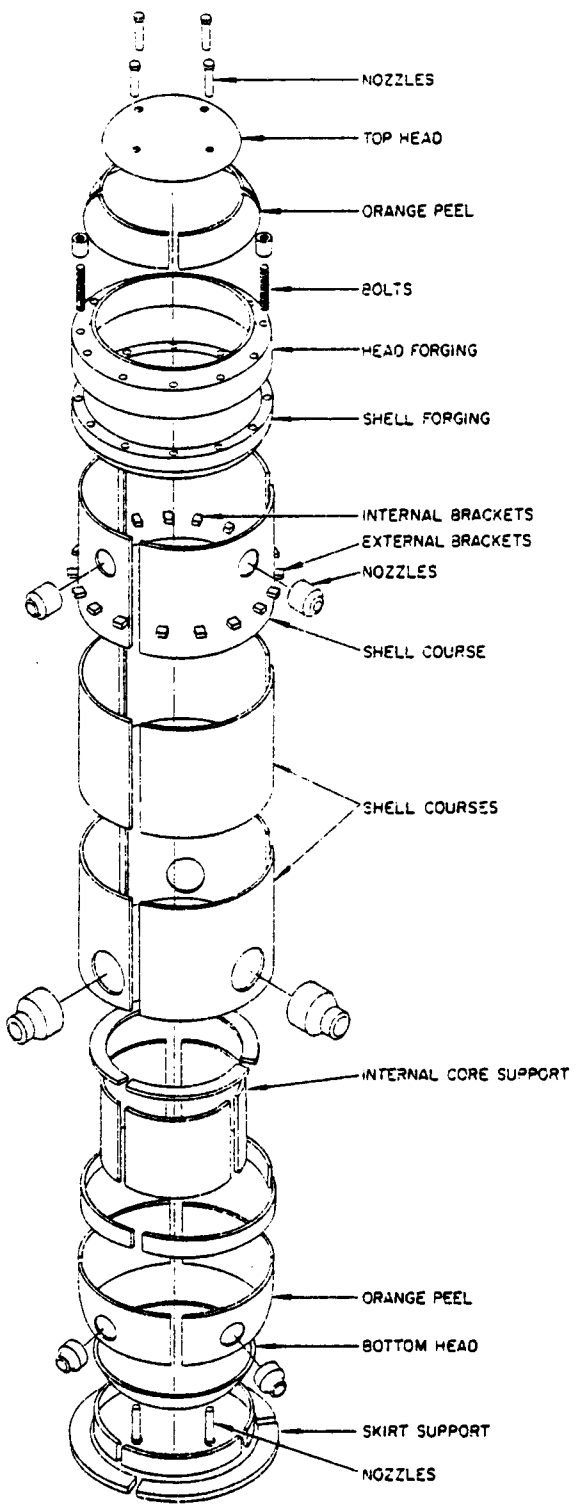

Figure 1. Schematic view of a typical large pressure vessel.

In the fabrication of the low alloy steels used in light water reactor construction, control of welding energy input, preheat for welding, and in some instances the maintenance of preheat after welding are employed to avoid fabrication problems. The employment of preheat is aimed primarily at the elimination of HAZ cracking, especially in the coarse-grained region adjacent to the weld fusion line. The weld metal is not immune to cracking problems but since the carbon content is low, the problem is rarely encountered. The occurrence of the cracking is normally attributed to two causes:

1. Cold cracking due to hydrogen in the HAZ (picked up from the weld metal in most instances), the low temperature transformation of austenite to martensite and the restraint and residual stresses.
2. Reheat cracking which is due to compositional effects, including residual elements and the stress state, caused by the original transformation during welding or the thermal cycles of PWHT.

There is only a limited extent to which the development of residual stresses in heavy section welding can be minimized, so most preventative measures for cold cracking revolve around the elimination of hydrogen and the control of the transformation of austenite to martensite. To these ends, low hydrogen welding procedures are employed and preheating and maintenance thereof throughout welding, is used to retard cooling, thus modifying the martensite transformation and permitting hydrogen to escape before transformation takes place. These procedures are very effective, although the application of preheat and its maintenance throughout welding is costly. In light of our current energy situation, it would

be desirable from a conservation point of view, to minimize preheating and holding at preheat temperatures, but without adversely affecting product fabricability or performance. However, we do not have sufficient knowledge of the metallurgical response in the HAZ to scientifically determine the required procedures. It is to this end that this research is directed.

CHAPTER II

LITERATURE REVIEW

The light-water nuclear reactor (LWR) pressure vessels are fabricated from one of two low alloy, high strength steels. The quenched-and-tempered alloys are identified as SA 533 Grade B Class 1, or SA 508 Class 2 in the ASME Boiler and Pressure Vessel Code. The range of chemical compositions of both alloys is given in Table 1.[2] Note that SA 508 has higher C, Ni and Mo content, plus it also contains some Cr and V, whereas SA 533 is higher in Mn content and contains no Cr or V. The minimum mechanical property requirements for the SA specification of both materials are given in Table 2. Both materials tend to have similar mechanical properties, except that SA 508 has higher tensile strength and lower percentage reduction in area as compared to SA 533.

Effects of Heat Treatment on Weld HAZ

The majority of pressure vessels are made by forming flat plate into cylindrical shapes, pressing spherical shaped heads, joining these by fusion welding and incorporating forged components, such as nozzles, to produce the vessel. There are several main disadvantages associated with the majority of these welding operations.[3] Firstly, high residual stresses are undesirable in thick vessels, both from the fabrication and service behavior standpoints. Secondly, local high hardness values and associated embrittlement in the heat affected zones are of concern, particularly in chemical vessels, both from the corrosion viewpoint and risk of hydrogen cracking. The most common method of reducing these

TABLE 1

CHEMICAL COMPOSITIONS OF THE MATERIALS

MATERIALS	% COMPOSITION						
	C	Mn	Ni	Mo	Cr	Si	V
SA 533 GR B CL 1	0.25 max	1.15 - 1.50	0.4 - 0.7	0.45 - 0.60	—	0.15 - 0.30	—
SA 508 CL 2	0.27 max	0.5 - 1.0	0.5 - 1.0	0.55 - 0.70	0.25-0.45	0.15 0.40	0.05

TABLE 2

MECHANICAL PROPERTIES OF THE MATERIALS

ELEMENTS	TENSILE STRENGTH MPa	YIELD STRENGTH M Pa	ELONGATION (%)	REDUCTION IN AREA (%)
SA-533 GRADE B CLASS 1	550-690 (80,000-100,000psi)	345 (50,000psi)	18	62
SA-508 CLASS 2	500-725 (80,000-105,000psi)	345 (50,000psi)	18	38

residual stresses and high hardness levels is to carry out a heat treatment below the lower critical temperature of the material, to induce sufficient plastic flow to reduce the stresses to an acceptable level and distribution. In addition, this treatment has the metallurgical effect of tempering the material resulting in recovery of ductility and decreasing hardness.

In general, it has been recognized for a long time that material strengths are degraded by exposure to elevated temperatures; however, little consideration has been paid to quantifying these effects in pressure vessels materials which undergo post weld heat treatment (PWHT). This is an area which many design codes tend to neglect. One factor in this historical neglect is the smaller size and the simplicity of the majority of pressure vessels as compared to reactor vessels and thus, they did not require long periods of PWHT during fabrication. However, with the advent of large nuclear reactor and petro-chemical pressure vessels, the increased thickness and the complexity requires that the fabricator adopt multiple PWHT which can often total 20 to 40 hours or more duration. The requirements dictating long time PWHT are:

1. Thickness of the vessels.
2. Highly restrained welds at nozzles.
3. Long manufacturing cycles making it unwise to leave component parts of the vessel in the as-welded condition for extended periods.
4. Increased use of more complex low alloy steels.

Since a nuclear vessel is fabricated by welding, the entire vessel is given a final post weld heat treatment (PWHT) for 1 hour per inch of thickness. Usually, the PWHT temperature is between 595 and 620°C

(1100 and 1150°F). During fabrication vessel components are given short-time intermediate PWHT, and total PWHT time for some weldments may exceed 40 hours.

For low alloy steels, even long periods of PWHT are normally beneficial to HAZ cleavage resistance in situations where precipitation hardening effects are small, e.g., Ni-Mo, Ni-Cr-Mo, Mn-Cr-Mo-V steels.[3,4] Steels with high V and Cu contents, however, can give secondary hardening in the HAZ, particularly at high carbon levels, and some embrittlement may result unless the PWHT temperature is carefully chosen.[5] The maximum levels of V and Cu that can be tolerated from the HAZ toughness viewpoint will depend on other alloying elements present, and each steel type must be considered separately. Where secondary hardening is likely, PWHT conditions that cause overaging in the HAZ are normally chosen to develop maximum toughness although underaging of high V steels at approximately 520°C (968°F) is occasionally practiced in Germany. Dolby[6] concluded that PWHT will generally improve HAZ toughness of all grades unless high levels of elements present are capable of secondary hardening. Even if the toughness is reduced on PWHT, critical defect sizes may be increased due to the reduction of the residual stress level.

In addition to PWHT, the effect of preheat and post weld holds must be considered. SA 533 Grade B and SA 508 Class 2 materials fall under ASME P3 and are treated similarly when preheat is employed for welding. While preheat is not mandatory under ASME III, Appendix D suggests 250°F for P3 materials over 5/8" thick. Most fabricators find that for material 4 to 6 inches thick and greater, 250°F preheat and interpass temperature is not sufficient to prevent fabrication problems and utilize higher

temperatures, and on occasion, maintain these temperatures throughout welding and then hold at temperature for various times after welding. In the case of nozzles, (severe restraint) it has been customary for some fabricators to hold preheat until post weld heat treatment is performed (often an inordinately long time). If the carbon equivalent calculation is used to predict preheat requirements, SA 508 and SA 533 yield a C.E. of approximately 0.70 (for the rich analysis), suggesting a preheat in the range of 400 - 700°F.

Weld HAZ and Its Toughness

The weld heat affected zones of welded components have long been considered to be the region of most concern for potential crack initiation and failure. The reason for this concern is historical, due to the fact many of the early failures were associated with HAZ cracks. The rationalization behind the HAZ cracks can be summarized as follows:

HAZ's exhibit high hardness in the low alloy steels and as hardness is increased, the toughness generally decreases. What is important from a structural viewpoint is not the hardness per se but the fracture toughness of the HAZ relative to that of the adjacent base material. It can be shown[7] that if the toughness of the HAZ is greater at any given temperature than the toughness of the parent material, then this concern over HAZ brittleness is not warranted.

Maximum embrittlement (low toughness) in the transformed HAZ is normally found in the grain-coarsened region where peak temperatures exceed about 1200°C (2192°F), whereas the fine-grained transformed HAZ usually shows the highest toughness of any HAZ region. The toughness of multipass welds is dependent on the proportion of HAZ which is refined

by successive weld passes and is a function of weld procedure. Dolby[6] notes that single pass unreheated HAZ regions normally show lower toughness than multipass HAZ's because of the increased proportion of grain refined structure sampled by the test specimen in the multipass case.

The fracture toughness at the toe of the heat-affected zone is an important factor in the integrity of weldments because such zones have the lowest resistance to fracture initiation. In addition, the occurrence of some cracks, such as reheat cracks and underbead or underclad cracks in the coarse-grained HAZ of welded low alloy steel, seem to reflect the low fracture toughness of such zones. Many efforts[8,9] have been made to assess the toe HAZ fracture toughness in connection with the selection and development of the parent metal, and the welding processes. Nevertheless, the assessment of the toe fracture toughness is one of the most troublesome problems to resolve because the fracture toughness depends to a large extent upon microstructural gradients such as variations of the microstructure and the grain size in the HAZ and because such microstructural characteristics are directly influenced by the thermal cycle during welding.

It is recognized[10] that the transformation in the HAZ of low alloy steels are determined by the maximum temperature and cooling rate reached. The resultant structures have properties depending on these transformations. The maximum value of the hardness occurs in the martensitic-bainitic microstructure of the most coarse-grained region in the vicinity of the fusion boundary and farther from the fusion boundary, the hardness generally decreases to that of the parent metal. A hardness traverse across a SA weldment made between two 30.5 cm (12 inch) thick plates of SA 533 Grade B Class 1 Steel[11] shows that the highest hardness is found in the HAZ. This is shown in Figure 2.

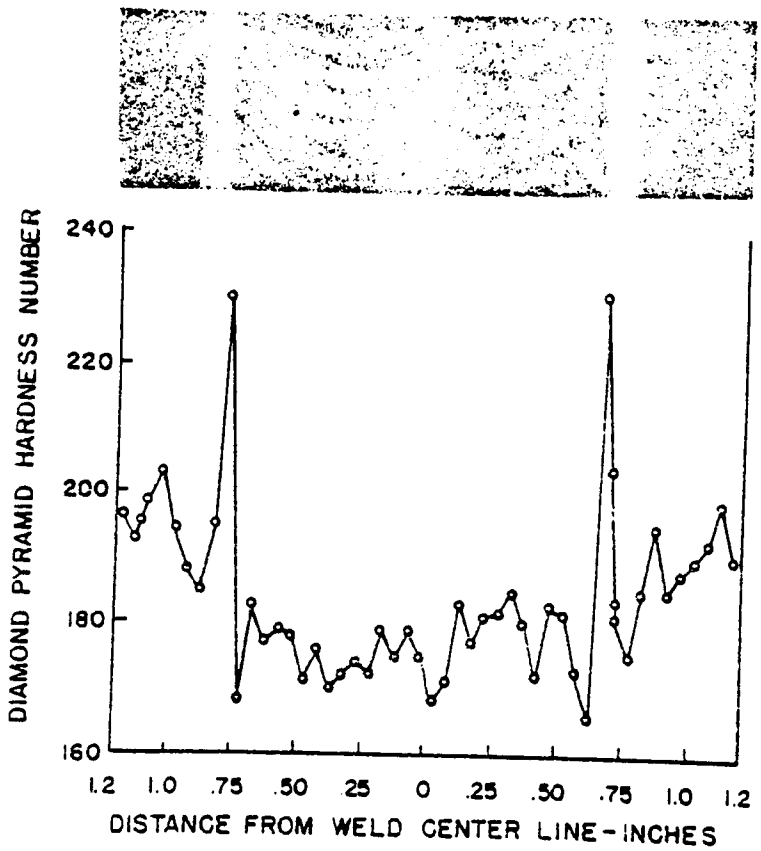

Figure 2. Submerged-arc weldment hardness traverse at quarter-thickness location. The region of the heat-affected zone that is most sensitive to reheat cracks exhibits the highest hardness. (Canonico [1]).

The HAZ of welds can possess superior tensile and toughness properties when compared to their chemically equivalent base metal.[1] This is particularly true for low alloy high strength steels that are correctly post weld heat treated. (Untempered martensite has poor toughness, but martensite that is correctly PWHT has superior properties.) Figure 3 shows an example of the influence of the microstructure on the Cv toughness of low alloy high strength steel.[12] (This figure does not represent the microstructures in SA 533 Grade B or SA 508 Class 2 steel; it is used only to illustrate the influence of microstructure on toughness.) It is evident that the structure with the best toughness is tempered martensite. The martensite plus bainite structure is less tough but still quite acceptable. The most rapid cooling rate occurs in conjunction with the coarse-grained region of the HAZ and thus, this region will exhibit the lowest temperature transformation product possible for the SA 508 Class 2 and SA 533 Grade B Class 1 steels. Therefore, if correctly tempered, the coarse-grained region of the HAZ can indeed be superior to the remainder of the structure. If incorrectly tempered, it will have the poorer toughness. The correct tempering temperature for these steels ranges from about 621 to 677°C (about 1150 to 1250°F).

In a similar manner, enhancement of the surface properties for thick plates has been observed in charpy v-notch tests.[13,14] Figure 4 shows the charpy-v energy curves obtained for material representing the surface, t/4, and midthickness locations. (The ASME code considers only t/4 properties when assessing the toughness of a nuclear pressure vessel.) The superior strength and toughness properties of the surface layers is attributed to the lower temperature microstructural constituents.[15] SA 533 Grade B steel transforms throughout its 12 inch thickness to bainite;

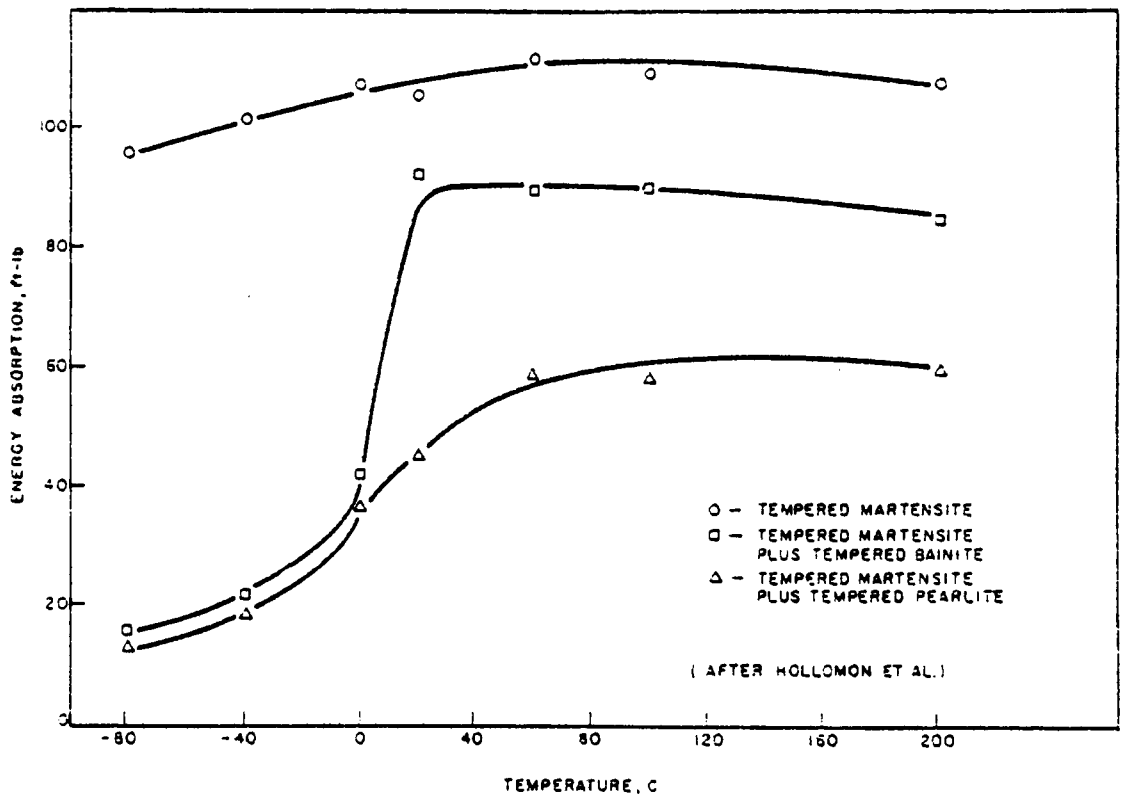

Figure 3. Charpy V-notch impact properties of 125 ksi tensile-strength alloy steel with different structures.

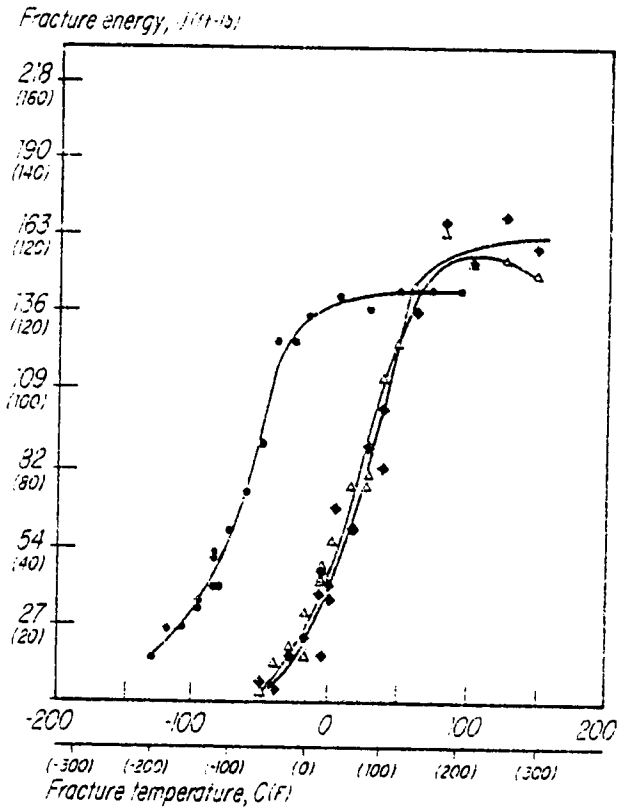

Figure 4. Charpy V-notch impact test results for specimens from three levels in a SA-533 Grade B Class 1 plate 305 mm (12 in.) thick. Code: closed dot, surface in longitudinal direction. Open triangle, 1/4 thick in longitudinal direction. Closed diamond, 1/2 thick in longitudinal direction.

however, the surface cools faster and transforms to lower bainite. It was experimentally determined[14] that the surface cools ten times faster than the midthickness location and about eight times faster than the t/4 location. Measured values were about 2.8, 0.33 and 0.25°C/s (5, 0.6 and 0.45°F/s), respectively, for these locations.

Recently, Grotke et al.[16] have simulated the HAZ microstructure of SA 508 Class 2 steel weldments using thermal cycles representative of commercial practice (about 3780 KJ/m (96 KJ/in)). They found that specimens heated to 1343°C (2450°F) and not tempered (post weld heat treated) had room temperature Cv energy values less than those of the quenched and tempered base metal. However, in all tests in which the specimens were given a multicycle thermal excursion representative of a multipass welding procedure, the Cv toughness of the HAZ microstructure was superior to that of the base metal.

The specimen blanks obtained from the weld thermal cycle simulations were also used for precracked charpy tests to obtain dynamic fracture toughness data for the simulated HAZ microstructure. The room temperature dynamic-fracture toughness of specimens heated to the peak temperature 2475°F (1343°C) was about 30% lower than that of the base metal. When the specimens were subjected to a thermal excursion simulating that of a multipass welding procedure, the HAZ toughness was superior to that of the base metal. Glover[17] mentioned in his literature survey that low toughness is found when the microconstituent existed as large blocky particles of lath martensite associated with bainitic carbides in segregated pools. Toughness was enhanced if the particles were fine, uniformly distributed

and in the form of higher carbon twinned martensite. Thus, the fine microstructure effects are important also in addition to the grain size.

Transformation Products in Weld HAZ

In order to understand the transformation products in the weld HAZ, it would be beneficial to correlate the transformation phenomena occurring during continuous cooling with isothermal data. The fundamental character of the isothermal diagram and its importance in understanding the heat treatment of steel are fully recognized. This diagram can, however, be quantitatively applied only when austenite is made to transform at substantially constant temperature. Davenport[18] has pointed out the need for correlating the transformation phenomena during continuous cooling with isothermal data and has outlined the principles of a "Cooling Transformation Diagram."

The isothermal diagram shows the fundamental transformation behavior of austenite at constant temperature; however, most actual heat treatments involve transformation as it occurs during cooling through a range of temperatures. The isothermal diagram is not, therefore, directly applicable to cooling transformation but can be used provided the relationship between the two types of transformation can be evaluated.

A cooling transformation diagram analogous to the isothermal diagram can be derived from isothermal data or determined experimentally.[19] It lies below and to the right of the corresponding isothermal diagram. The amount of the displacement, in general, increases with more rapid cooling up to the rate which just produces on cooling to room temperature a fully martensitic structure.

The derived relationship[19] between transformation on cooling and isothermal transformation may be employed to advantage in actual heat

treatments provided the cooling history is known; it may also be used for determining the rate of cooling necessary to achieve a desired final transformation product and combination of mechanical properties. The transformation which occurs during hardening, welding or heat treating by any method of controlled cooling can be predicted from the isothermal and the continuous cooling diagrams which aid in understanding and designing such heat treatments.

The properties of welds in low-alloy high-strength steels depend upon their microstructure as well as their composition. Therefore, the rate at which welds cool and transform from austenite after freezing exerts a strong influence on their properties. Since the cooling rates are dependent upon the conditions of welding, an understanding of the interaction of welding parameters on the cooling characteristics of weld metal is essential if reliable weldments are to be produced.[20]

An isothermal transformation diagram[14] representative of SA 533 Grade B steel is shown in Figure 5. Lukens Steel Company provided this isothermal diagram of an A 302, Grade C steel, which is quite similar to SA 533 Grade B steel. It should be noted that the I-T diagram for the ASTM A 302 Grade C steel contains a bainitic shelf and that the proeutectoid ferrite transformation is retarded.

The cooling rates superimposed (for approximation purposes only) on the I-T diagram imply that at the surface and 1/12 T locations, the structure does not contain any proeutectoid ferrite. The 1/4 T and 1/2 T locations may contain approximately 15 and 25% primary ferrite, respectively. However, it must be noted that ASTM A 533 Grade B is enriched in C, Mn, Mo and Ni, as compared to A 302 Grade C. If these factors (i.e, an I-T diagram instead of CCT diagram and an enriched chemical

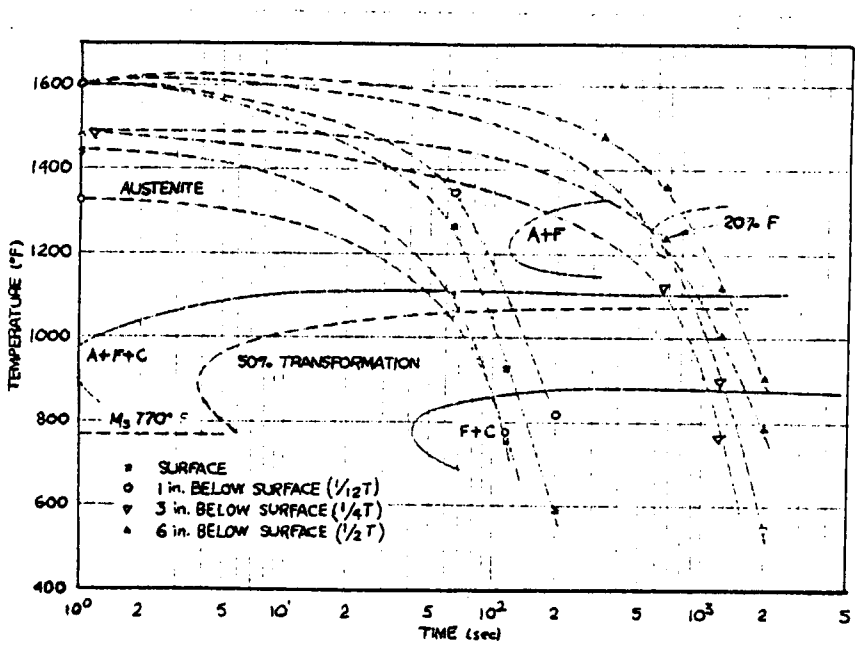

Figure 5. Isothermal Transformation Diagram for A 302, Grade C, Steel. (The actual cooling data are superimposed on the diagram.)

analysis) were taken into consideration, it would be expected that the I-T diagram in Figure 5 would be transposed to the right and downward. Hence, the absence of proeutectoid ferrite can be explained.

A CCT diagram by Fuji Maki H.[21] for a steel "B" is shown in Figure 6. This steel is similar in compositions to SA 508 steel, except that steel "B" is lower in carbon. The critical cooling rate for martensite formation is approximately 74°C/s and critical cooling rate for bainite formation without ferrite decomposition (bainite + martensite) is 11°C/s. All the steels tested by Fuji Maki[21] showed bainitic structures which were accompanied by proeutectoid ferrite for the range of practical cooling rates and therefore, it was reasoned that it would be very difficult to generate martensite in any commercial treatment.

Klumpes[22] discussed the Peak-Temperature-Cooling Time (PTCT) diagrams of SA 508 Class 2 and SA 533 Grade B Class 1 and made a comparison between real and simulated HAZ's. In order to construct the PTCT diagram for the steels, he performed several thermal cycles with peak temperatures of 1350, 1250, 1150, 1050 and 900°C and cooling times between 800 and 500°C of 5, 12, 24, 48, 96 and 480 seconds (giving cooling rates of 60, 25, 12.5, 6.25, 3 and 0.62°C/s).

The PTCT diagram for SA 508 Class 2 showed that Shielded Metal Arc Welding (SMAW) with a cooling rate about 50°C/s yields a martensitic structure in the HAZ with hardness between 450 and 500 HV30. Submerged Arc Welding (SAW) with preheat, with a cooling rate of about 11°C/s gives a martensitic-bainitic structure with hardnesses varying between 290 and 350 HV30. Electroslag Welding (cooling rate about

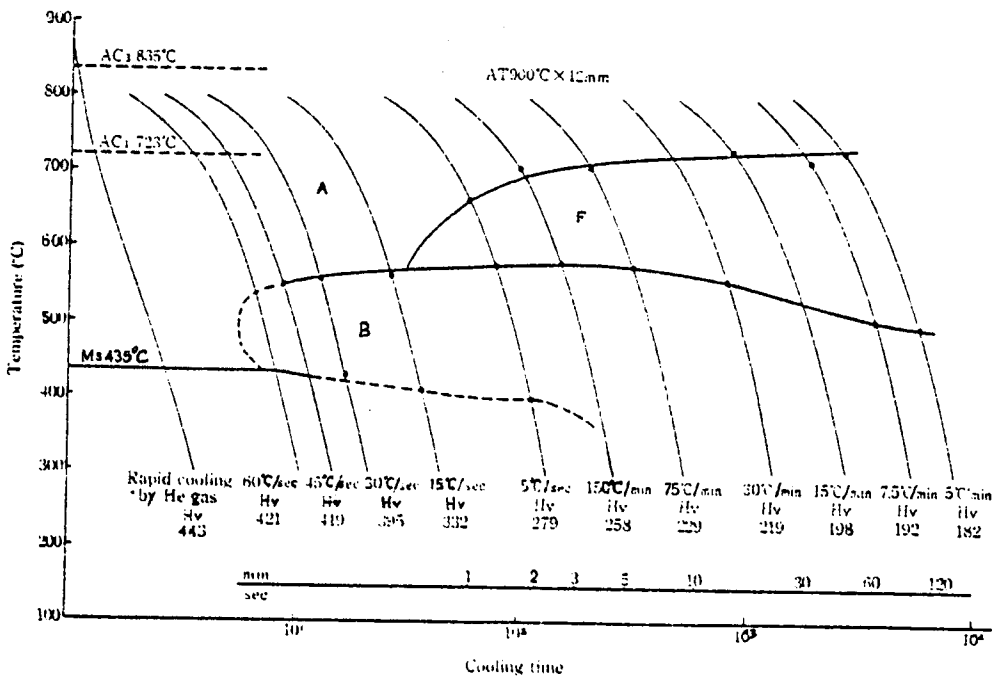

Figure 6. CCT Diagram of Steel 'B'. Composition: C 0.17%, Si 0.26%, Mn 0.84%, P 0.05%, S 0.06%, Cr 0.4%, Ni 0.84%, Mo 0.62%.

0.6°C/s) gives a bainite-ferrite structure with a hardness of 225 HV30.

It was noted that cooling time between 800 and 500°C of 12 seconds (i.e, cooling rate 25°C/s) gave the best toughness. Faster cooling rates deteriorated the toughness because of the increased amount of martensite in the structure. Slower cooling rates deteriorated the toughness because of grain growth. After a PWHT, the toughness of test specimens subjected to thermal cycles with faster cooling rates (cooling time less than 12 seconds) and peak temperature of 1350°C is deteriorated farther. For the slower cooling rate, the same heat treatment gives a recovery of the toughness properties.

In the PTCT diagram of SA 533 Grade B Class 1, for different cooling rates between 800 and 500°C, the hardnesses obtained were somewhat higher than those of SA 508 Class 2. The depth of hardening in case of SA 533 Grade B Class 1 exceeds that of SA 508 Class 2.

In the as-welded condition, the charpy-v transition temperature for material subjected to thermal cycles with peak temperatures of 1350°C is the lowest for cooling rates faster than 60°C/s (a fully martensitic structure). For these cooling rates, a heat treatment of 6 hours at 610°C deteriorates the toughness. For slower cooling rate, the same heat treatment has a very beneficial effect on the transition temperature expecially when compared to SA 508 Class 2.

For comparison of real and simulated HAZ microstructure Klumpes[22] took grain dimensions and hardnesses into consideration. The comparison of grain sizes between real and simulated HAZ (peak temperature of 1350°C) is given in Figure 7A for SA 508 Class 2, and in Figure 7B for SA 533 Grade B Class 1. The major cause of the difference in grain sizes is due to the steep temperature gradient occurring in real HAZ, which

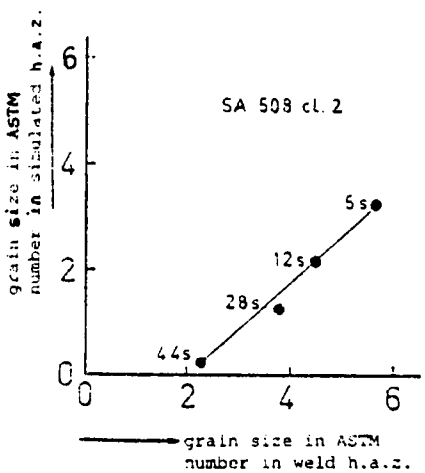

A

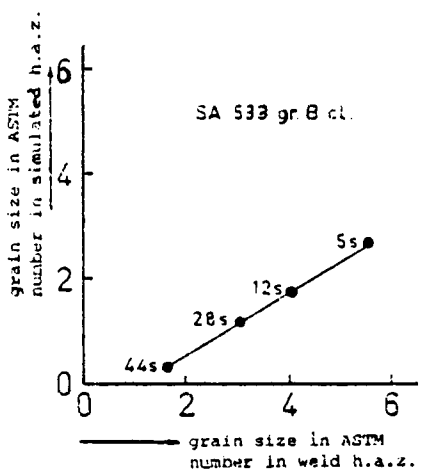

B

Figure 7. Comparison of grain sizes in simulated (for a peak temperature of 1350°C) and real heat affected zones for the indicated cooling times between 800 and 500°C.

hampers grain growth, whereas in simulated test specimens the grain growth is greater because of the relatively large volume of metal with the same temperature (i.e., less temperature gradient). Comparing hardnesses, it appears that the hardnesses in real HAZ are 30-40 HV30 higher than in the simulated HAZ for steel SA 508 Class 2. Steel SA 533 Grade B Class 1 gives a better agreement but some hardnesses in the real HAZ are higher than in the simulated ones. The differences in hardness correlate with grain sizes.

Klumpes[22] finally concluded that a PTCT diagram provides a good evaluation of HAZ, especially on predicting changes which occur by changing welding parameters.

The effect of preheat on transformations other than the effect on cooling rate is not obvious from CCT diagrams, especially since only incomplete diagrams are available. The partial CCT diagram shown in Figure 8 for SA 533 material does indicate that the transformations to bainite and martensite are the most important considerations but the diagram does not extend to the faster cooling rate characteristic of weld HAZ's in heavy plate. In this diagram, the bainite finish temperature is in close agreement with a calculated Ms temperature of 680°F and the extension of this bainite finish line would be expected to be the approximate Ms. A calculated value for the M_f (90%) would lie approximately 100°F below the Ms and the M_f (99%) would be approximately 200°F below the Ms. Utilizing these values, it would be predicted that the transformation from austenite to bainite and/or martensite would be complete at the preheat temperatures and the sole effect of preheat would be to drive off hydrogen. However,

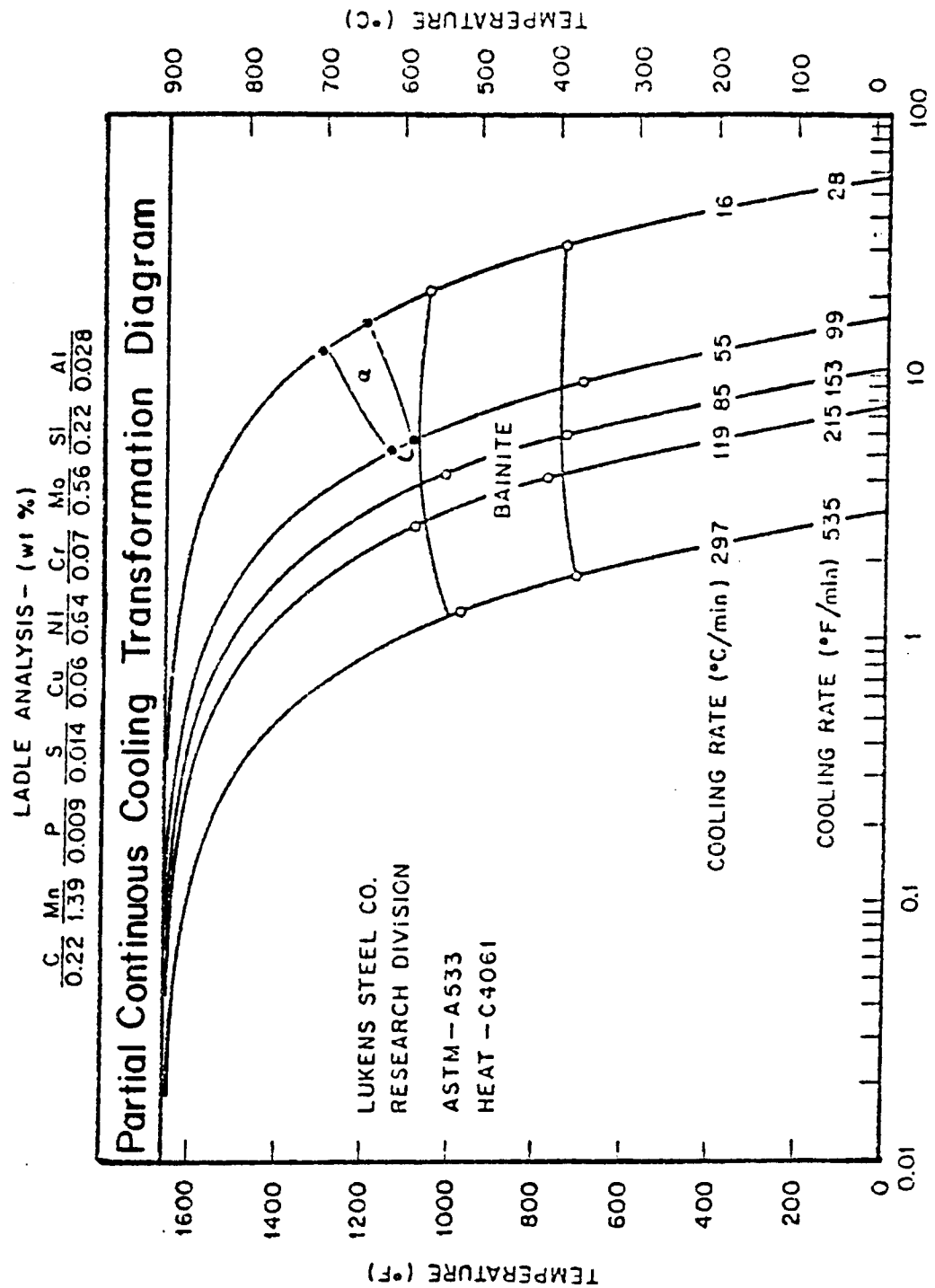

Figure 8. Partial Continuous Cooling Transformation Diagram of SA 533 steel.

the coarse-grained HAZ may transform differently than the continous cooling curve suggests for lower austenitize temperatures. Further, consider that subsequent thermal cycles may reaustenitize the HAZ or cause any remaining austenite to transform at higher temperatures to bainite or, alternately, may stabilize the austenite and retard its transformation even at preheat temperature.

Stress Relief Cracking of Weld HAZ

The term stress relief cracking is associated with the stress relief heat treatment of welded components. Stress relief heat treatment (PWHT) is usually applied to the welded structure to reduce or eliminate the residual welding stresses that have formed in the weldment when it has cooled to room temperature. The stress relieving of the residual stresses occurs by plastic flow and creep processes.[23] Materials containing carbide forming alloy elements often exhibit precipitation of the alloy carbides within the grains of the weld heat-affected zone during stress relief heat-treatment (PWHT) and serve to strengthen the matrix in comparison to the grain boundary. The creep strain necessary to relieve the residual stresses is forced into the weakened grain boundary region and consequently extensive grain boundary deformation may induce cracks in the heat-affected zone. Thus, this type of cracking has often been called "stress relief cracking" (SRC).

Investigations[24,25,26] have shown that the cracking is primarily intergranular in nature. The typical microstructural features which accompany and promote cracking are fine carbides precipitated within the grains of the heat affected zone in combination with a denuded or

a weakened grain boundary region. The creep strain normally accompanying thermal stress relief is forced into the weakened grain boundary region and the resulting extensive grain boundary deformation, usually accommodated by grain boundary sliding, produces intergranular cracks. The presence of grain boundary carbides often observed in the susceptible steels serves to further restrict the amount of grain boundary deformation that can be accommodated without cracking. The weld heat-affected zone is particularly susceptible to cracking, because it has undergone a high temperature thermal cycle which serves to resolution many carbides and subsequent reprecipitation may occur during thermal stress relief.

Detert[27] amd Lorenz[28] concluded that by heating to temperatures above 2300°F (1250°C) the alloy carbides are brought into solution, so that enhanced grain growth occur. After rapid cooling, the interior of the coarse austenitic grains transform into a hardened martensitic structure. During subsequent reheating such as in a creep test or during a post weld treatment for stress relief, the carbide forming elements such as Cr, Mo and V precipitate in the form of submicroscopic alloy carbides, which stabilize the hardened martensitic structure. Simultaneously at the site of former austenitic grain boundaries, coarse precipitates are formed.

Bertram and Banga[27] indicated that the extent of the low creep ductility of the coarse-grained structure of a heat-affected zone varies from steel to steel. It depends on the amount of alloying and on the kind of alloying element. Creep ductility measured in the coarse-grained structure of SA 533 type steel was of the order of at least 1 to 2 percent. Creep ductility of the same microstructure of SA 508

Class 2 steel was measured as low as a few tenths of a percent in certain heats. This may indeed be the reason for which the underclad cracking occurs more often in SA 508 Class 2 steel.

The tendency toward SRC increases with the degree of mechanical constraint imposed on the weld region, and it has recently been shown[29] that the SRC tendency is related to the purity of the steel. In a study of the Mn Mo Ni pressure vessel steels of the SA 533 B type, Brear and King[30] showed that a high purity heat (prepared by vacuum induction melting) was not susceptible to SRC. They reported that the cracking tendency increased with the value of the following impurity parameter (compositions in weight percentage).

$$0.20\,[Cu] + 0.44\,[S] + 1.0\,[P] + 1.8\,[As] + 1.0\,[Sn] + 2.7\,[Sb]$$

This parameter was obtained from experiments on laboratory heats of fixed base composition in which the impurity contents were systematically varied.

H. Nakamura[1] established an equation, based on extensive tests with low alloy high strength structural steels, that predict crack sensitivity based on the main alloying elements:

$$\Delta G = \%\,Cr + 3.3\,[\%Mo] + 8.1\,[\%V] - 2$$

A positive ΔG value indicates that a steel is sensitive to reheat cracking. Another formula exists,[29] which appears to be insufficiently rigorous, for low vanadium contents (0.05%).

$$P_{SR} = [\%Cr] + 2\,[\%Mo] + 10\,[\%V] + 7\,[\%Nb] + [\%Ti] - 2$$

Both forumlas, which were derived from an extensive series of welding tests, have the same limit value of 2.0, i.e., they contain the severity

of the testing procedure as a parameter. Nevertheless, the Nakamura formula has proven useful as a tool for preselecting steels for welding.

Applying Nakamura's equation to nominal compositions for SA 533 Grade B Class 1 steel (0.21% C, 0.17% Cr, 0.47% Mo, 0.48% Ni) and SA 508 Class 2 steel (0.26% C, 0.75% Mn, 0.45% Cr, 0.61% Mo, 0.81% Ni and 0.05% V) provides ΔG values of -0.27 and + 0.86 respectively,[1] which agrees with the work of Lorenz[28] and McMahon[29] that SA 508 steel is considerably more sensitive to reheat cracking than SA 533 Grade B.

Brear and King[30] showed that the presence of certain residual elements promotes Stress Relief Embrittlement (SRE) in HAZ structures in SA 533B/SA 508 (Mn-Ni-Mo) steels. This embrittlement is a consequence of the formation and growth of voids on prior austenite grain boundaries during stress relaxation which reduce the subsequent ductility and resistance to intergranular fracture. They identified the individual effects of the residual elements and showed that the susceptibility to SRE can be reduced in practice by control of residual element levels and by grain refinement.

Lindhagen and his colleague[31] did extensive study on the formation of microcracks during stress-relief annealing of a weldment in SA 508 Class 2, and they concluded that the coarse-grained HAZ has very low ductility at elevated temperatures and cracks form in the primary grain boundaries at small strains. Also, there was nothing to indicate that the presence of impurities in the material is the primary cause of the low ductility. It was also found that it is the high temperature strength of the structure which enables relaxation to occur to

some extent by grain boundary sliding and hence, crack formation. If a less strong steel is chosen such as SA 533 B which has a lower concentration of chromium, cracking could be avoided.

Hydrogen Embrittlement

Hydrogen embrittlement is another phenomenon of possible concern in vessel steels.[32] The potential source of hydrogen is that which is released by a corrosion reaction in the water environment. A critical appraisal of the applicable information has concluded that this is not a significant problem for low alloy steel vessel materials. The maximum probable concentration of corrosion-produced hydrogen appears to be an order of magnitude less than that required to produce measurable embrittlement in these steels. It is known that cold working can increase sensitivity to hydrogen embrittlement and this would be of potential concern in the locally deformed region resulting from warm prestressing. However, this should not be a serious problem based on some indirect reasoning. As indicated above, the concentration of the corrosion-released hydrogen is about an order of magnitude less than that necessary to cause embrittlement in the unstrained condition. With this apparent margin, the probable effects of prior plastic deformation should be fairly minor.

The literature review revealed that while certain phenomena in regards to the weldability, heat affected zone and cracking problems of SA 508 and SA 533 have been studied, insufficient information exists for the prediction of transformations and properties of the HAZ's. Thus, the efforts undertaken in the current study are aimed at understanding the isothermal transformation and continuous transformation

for both normal heat treatments and HAZ's. The effect of preheat, welding energy input and PWHT on the HAZ toughness and stress relief cracking potential is not adequately documented and this important area is addressed in the current study.

CHAPTER III

EXPERIMENTAL PROCEDURES

In this section a discussion of the experimental procedures used in the course of this investigation is presented.

Materials

A 6 inch thick ASTM SA 533 Grade B Class 1 plate was purchased by ORNL from Lukens Steel Company for their HSST program;[33] a portion of that material was used for this program. Their order specified that the steel:

1. meet the requirements of Sec III of the ASME Code for Class A nuclear vessels,
2. be vacuum degassed,
3. be made by the basic electric furnace process, and
4. have concentration of phosphorus and sulfur as low as possible but restricted to 0.012 and 0.015% maximum.

Heat treatment of SA 533 plate consisted in:

1. austenitizing at 1675 ± 25°F for a 6 hour hold period, followed by water quenching;
2. reaustenitizing at 1575 ± 25°F for a 6 hour hold period, followed by water quenching;
3. tempering at 1225 ± 25°F for a 6 hour hold period, followed by water quenching; and
4. Stress relieving at 1125 ± 25°F for a 1 hour hold period, followed by air cooling.[33]

The heat treatment for both plate and for forgings of SA 508 Class

2 is similar; austenitizing at 870 to 900°C (1600 to 1650°F), followed by a quench in highly agitated water or brine. The quenched steel is tempered, usually at 650 to 675°C (1200 to 1250°F) for a minimum of 1 hour per inch of thickness.[11] The composition for both steels is shown in Table 3. Note that SA 508 is higher in C, Ni, Mo, Cr and Si content, plus it contains some V, whereas, SA 533 is higher in Mn and contains no V.

The experiments conducted were to characterize and provide a thorough understanding of the transformation characteristics of SA 508 and SA 533 materials under the continuous cooling that occurs in the HAZ of welds, and to study the isothermal transformation behavior of these materials at low temperature (within the preheat range and above). The transformation products were studied as to their morphology and properties.

Isothermal Transformation Behavior

The isothermal transformation (I-T) behavior of austenite can best be studied by determining the transformation behavior at a series of temperatures below A_1, (by quenching small samples to the desired temperature in a liquid bath, allowing them to transform isothermally) and following the progress of the transformation metallographically or by dilatometric means. This procedure not only provides the rates of transformation at the various temperatures but also furnishes information as to the metallographic structures characteristic of the various temperatures of transformation and thus, permits the estimation of the properties of these microstructures.

Thus, to study the I-T behavior, 25 specimens of each material

TABLE 3

PERCENTAGE COMPOSITION FOR MATERIAL
SA 533 GR. B CL. 1 AND SA 508 CL.2

WEIGHT % COMPOSITION

MATERIALS	C	Mn	Ni	Mo	Cr	Si	P	S	Cu	V
SA 533 GR. B CL 1	0.21	1.38	0.46	0.47	0.17	0.18	0.010	0.014	0.12	—
SA 508 CL 2	0.26	0.75	0.81	0.61	0.45	0.26	0.010	0.014	—	0.05

SA 533 Grade B Class 1 and SA 508 Class 2, were cut into 0.5 inch cubes and heated to 1700°F, held for 1 hour, and then quenched in a salt bath. The specimens were held in salt bath for different time periods at five different temperatures. Lukens Steel Company provided an isothermal transformation diagram for ASTM SA 302 Grade C steel, which is shown in Figure 9. The analysis of SA 533 is similar to SA 302 and therefore, the transformation behavior of both steels should be similar. Based on this prediction, the times were selected to range from 1 to 10,000 seconds and temperatures were 550, 800, 950, 1150 and 1250°F. A complete schedule for both steels is shown in Table A-1 of Appendix A. After reaching the temperature of the molten bath, the samples were held for the required period of time, withdrawn and quickly quenched in cold water to room temperature. The cubes were sectioned and examined microstructurally. As the temperature of the molten bath (and consequently the transformation temperature) is changed, a series of data points are obtained which are used to construct the isothermal diagram.

Continuous Cooling Transformation Behavior

CCT Obtained by Resistivity Measurements

In order to study the behavior under continuous cooling transformation, electrical resistivity measurement (ERM) equipment was extensively used. This equipment was developed over several years at UTK[38] and recently adapted for computer control. Following is the descriptive procedure involved in measuring resistivity.

Manual Measurements at Room Temperature

The resistivity (ρ), of a rod sample was calculated from

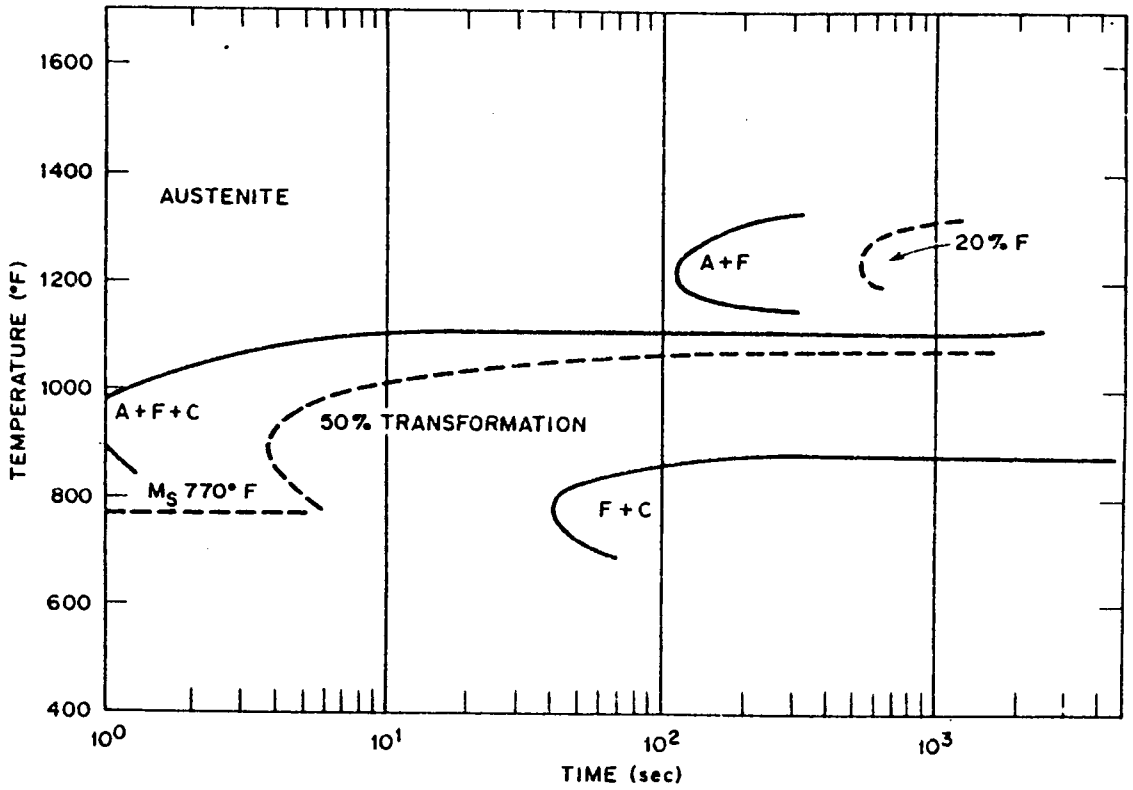

Figure 9. Isothermal transformation diagram for ASTM A 302 Grade C steel. (The analysis for A 302 Grade C is identical to that of A 533 Grade B.) The rapid cooling rate near the fusion line in combination with the coarse austenite grains will result in a microstructure that is predominantly martensitic.

$\rho = 0.7854VD^2/IL$; where D: diameter of a rod; L: sample length along axis; V: voltage-drop across length L; I: current passed through rod. The diameters of rods were measured with a micrometer having a vernier scale of 0.001 inch resolution. An average value for the diameter of each rod was evaluated through multiple reading both along the rod axis and around the rod circumference.

The sample length, L, was defined by the span between two knife edges which were glued to the cut ends of a quartz cylinder. The span was calibrated under a reflection optical microscope equipped with a precision traveling stage micrometer. A knife-edge standard of 2.5438 ± 0.0005 cm was prepared.

The resistivity was measured by mechanically fixing the rod across the top of the knife edges and connecting the ends to a precision controlled current source in series with a calibrated standard resistor as shown in Figure 10A. With a current passing, voltage-drops were measured between the knife edges, designated as V, and between the terminals of the standard resistor. The voltage drop across the standard resistor was divided by the calibrated value of its resistance to provide an accurate value of the electrical current, I.

Voltage drops were read with a digital voltmeter (5 1/2 digit), Data Precision Corp, model 3500 with an accuracy of ±4 microvolts in the full scale 0.12 volts. Readings were taken with the current in a forward and then in reverse direction and the values averaged to cancel thermal emf effects in the circuit. The reproducibility of the resistance measurements of a specimen with 0.02 ohm was ±6 micro-ohm, or ±0.06%. However, the absolute accuracy is limited by the ability to establish the diameter and uniformity of diameter of the rod which is

$$\frac{0.7856\,VD^2}{IL} = \rho$$

D = Diameter of a rod

L = Sample length along axis

V = Voltage drop across length L

I = Current passed through rod

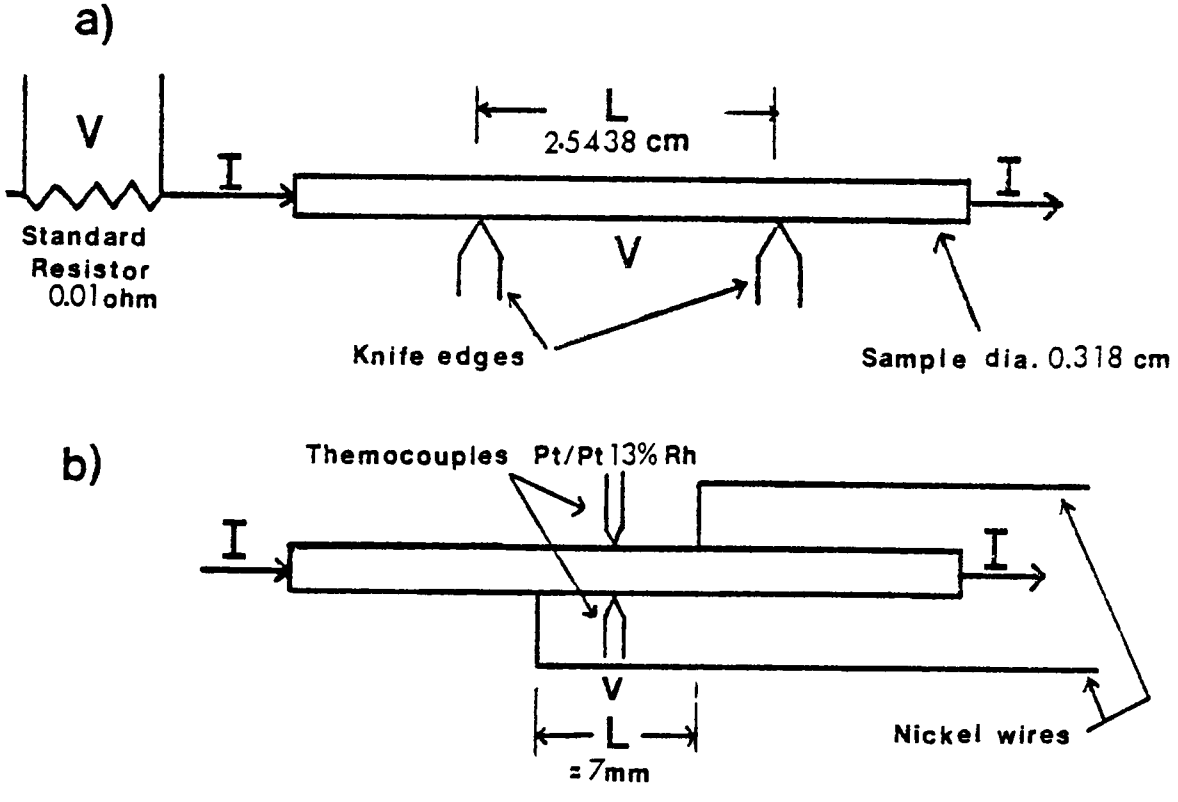

Figure 10. Schematic representation of resistivity measurement at room temperature.

about ±0.5%. As a consequence, the absolute accuracy of the resistivity measurements is set at 0.5%.

Measurements of Resistivity at Elevated Temperatures Under Digital Computer Control

A PDP 15/35 digital minicomputer was adopted to measure the resistivity of samples over wide ranges of heating and cooling rates. The computer, equipped with analog-to-digital converters, digital-to-analog converters and relay switching, allowed both resistivity measurements and temperature control to be programmed with great flexibility. FORTRAN IV language was used in programming.

The resistivity of the sample was first determined by manual measurement at room temperature. The two nickel wire probes, 0.020 inches in diameter, were spot welded about 7 mm apart near the center of the specimen. The actual distance was back calculated through the known resistivity and the voltage drop induced by a known current. Two Pt/Pt + 13% Rh thermocouples were spot welded on the specimen in the vicinities of the Ni-probes as shown in Figure 10B.

The specimen was suspended vertically in a 2.5 inch diameter ceramic tube lined with 0.010 inch thick nickel foil as a reflector to decrease the heat lost. Direct current to heat the specimen was supplied by vertical 1/4 inch diameter graded copper and then nickel rods. These rods along with ceramic tubes for thermocouple and voltage probe wires supported ten radiation shield disks which, with a series of radiation shields below the specimen, provided acceptable low heat loss. All of these leads passed through vacuum tight seals in the wall of the specimen chamber which was maintained at a vacuum of 5×10^{-5} Torr or lower.

A block configuration of the electrical resistivity measuring system is shown in Figure 11. The specimen is shown schematically in a horizontal position at the bottom of the figure. The three functions of the PDP 15/35 computer are represented at the top. Information to the computer included values of the parameters for the particular run, amplified thermocouple voltages, and the voltage drop along with the power supply. Information fed through computer operated switches in the several multipliers provided input to temperature input to temperature control algorithms with output response to the 90 ampere, six volt, specimen power supply. Operator communication to the computer was carried out with a keyboard terminal. Calculated values of the resistivity, specimen temperature, and other information on the operation of the system were output to the terminal and/or magnetic tape and the x-y plotter.

The computer operates through user written FORTRAN programs called TASKS which are requested by the user or by other tasks. A flow chart of the system of programs developed to operate the resistivity equipment, collect and process data, and output results in tabular or graphical form is shown in Figure 12. A master program called ERM receives user instructions such as specimen dimensions and the time-temperature history to be followed and then supervises the entire run following the flow chart shown in the figure.

Controlled cooling rates up to 0.5°C/min can be programmed. Faster cooling rates were obtained by blasting helium gas on the specimen. The cooling curves were recorded on a strip chart recorder. A schematic representation of resistivity vs. temperature curves is shown in Figure 13. The reaction-start and the reaction-stop temperatures were

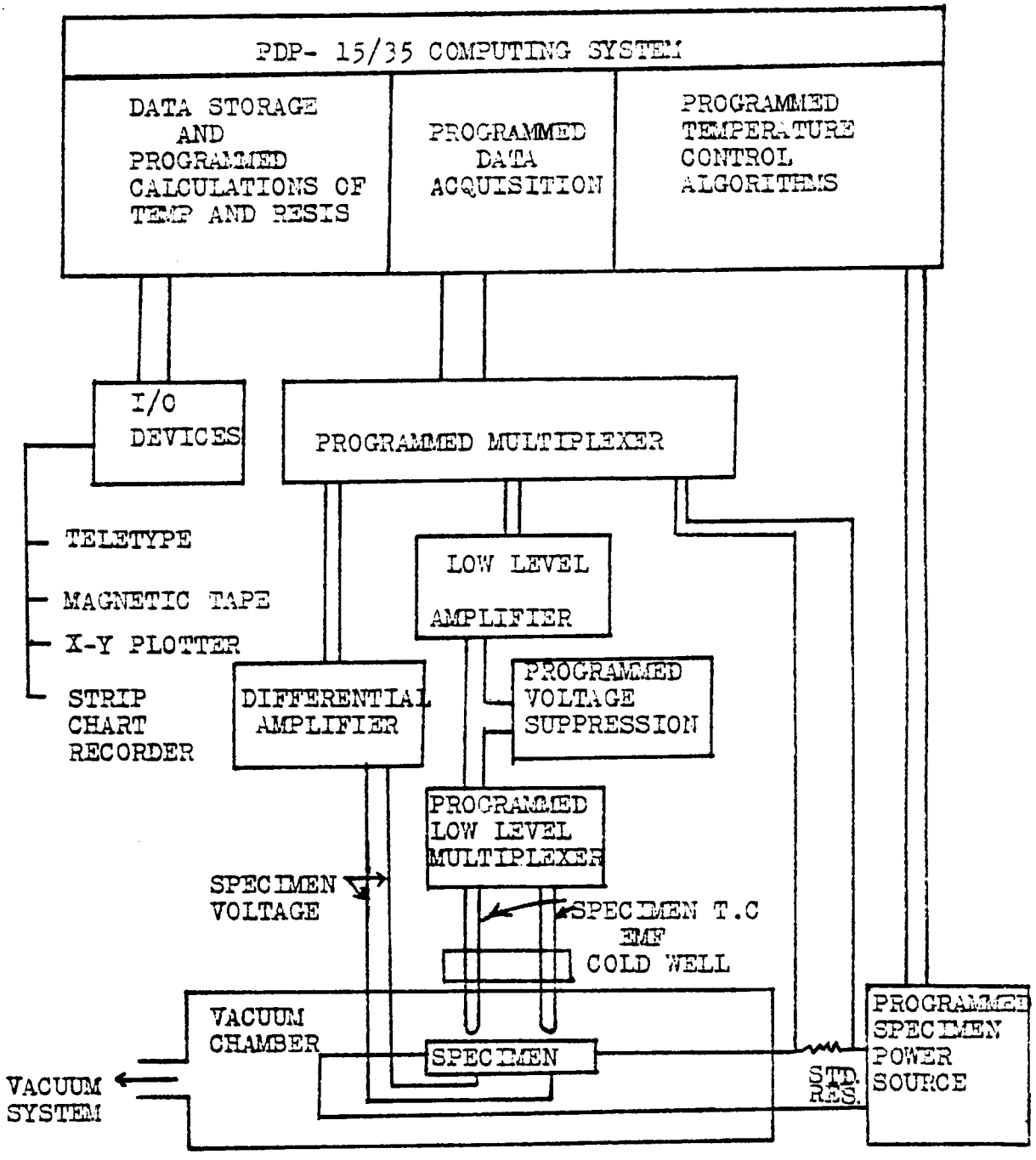

Figure 11. Block configuration of operational devices for electrical resistivity measurement.

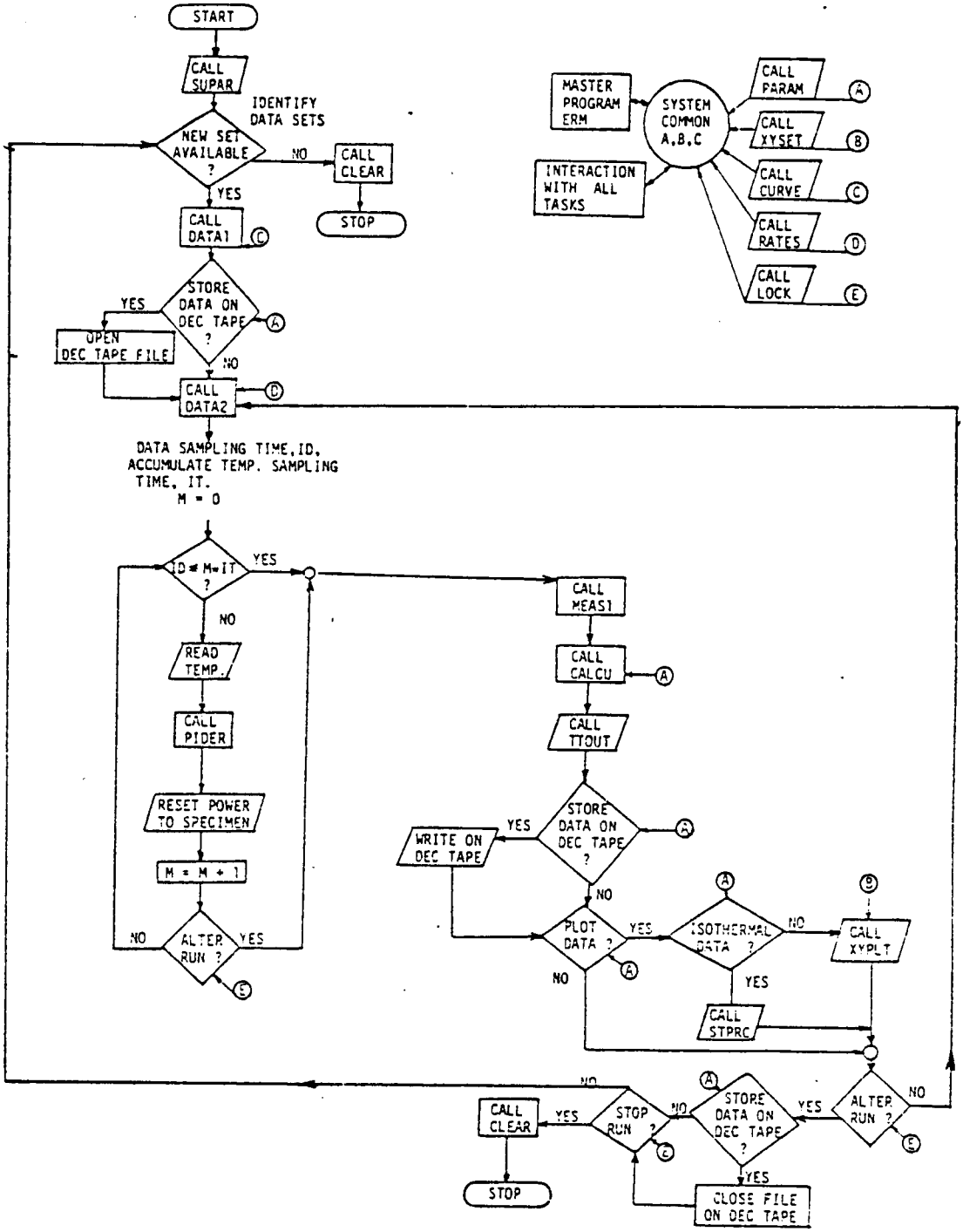

Figure 12. Flow chart of master program ERM.

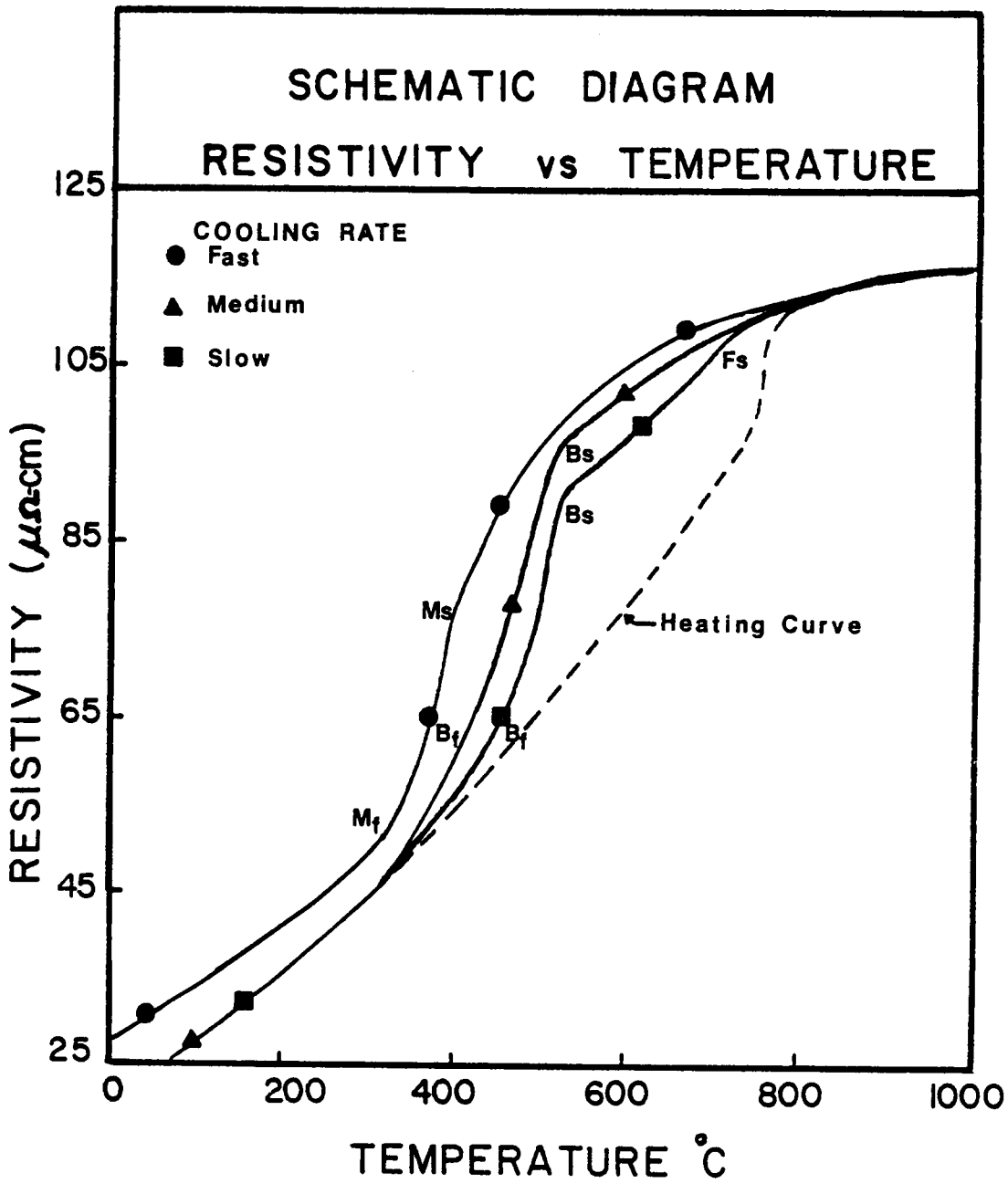

Figure 13. Schematic representation of resistivity vs. temperature curves.

evaluated by the change in slope. The strip chart recorder trace of temperature vs. time was used to develop the time base. The transformation temperatures as previously determined were located on the temperature-time trace. Zero time was taken at the peak temperature.

The pertinent times and temperatures for each of the transformations over a variety of cooling rates were then plotted on a temperature vs. log-time scale, thereby generating the continuous cooling transformation diagrams. The specimens with different cooling rates were saved for metallographic evaluations.

CCT Behavior Obtained Dilatometrically

The continuous cooling characteristics of SA 533 Grade B Class 1 and SA 508 Class 2, low alloy steels were investigated dilatometrically by utilizing the "Gleeble." This evaluation is directly related to weld HAZ transformations.

Specimens (0.25" dia., 3" in length) of SA 533 and SA 508 were subjected to different thermal cycles with peak temperatures of 2400°F ±40°F and 1650°F ±20°F, followed by cooling rates appropriate to the energy input and preheat. The dilational behavior of the specimens was monitored with a high speed dilatometer and, in this way, a continuous cooling transformation diagram was generated based upon thermal cycles which duplicate those found in the heat affected zone (HAZ) of arc welds.

The Gleeble

The device, called the Gleeble, developed at Rensselaer, reproduces the exact thermal cycle found at a particular point of interest near an actual weld in a specimen of suitable size for testing. Thus,

the microstructure found at the point of interest in the weld HAZ is created throughout the volume of the specimen experiencing the corresponding thermal cycle.

Briefly, the apparatus (Gleeble) consists of a proportional, variable rate, on-off, time-temperature controller that has the ability to duplicate, in a specimen of convenient size, the thermal conditions existing at any point in the HAZ of an arc weld. In operation, a specimen is clamped between two water-cooled copper jaws, one fixed and one movable, which are connected to the secondary of a transformer. The specimen is thus heated by its resistance to the passage of an electric current and is cooled by extraction of heat longitudinally to the water cooled jaws.

By use of a thermocouple welded to the specimen, the Gleeble compares a programmed reference signal to the specimen temperature 120 times per second and makes the necessary corrections. Any thermal cycle may be reproduced with heating rates up to 3000°F per second.

In addition, the device permits the investigator to evaluate high temperature mechanical properties by conducting a rapid tensile-test on the specimen at any point in the thermal cycle under investigation. Hot ductility tests, for example, can be performed by heating specimens to various temperatures in the hot-working range, and then pulling them in tension to fracture at strain rates approximating those experienced in hot working. Strain rate up to 20 inch per inch per sec. can be obtained, depending upon the effective gage length of the specimen.

Programming

The programming process involves establishing a reference potential

which varies with time in exact proportion to the desired variation of temperature with time. This is accomplished by the Gleeble reference generator, the electrical output of which is precisely the same as the output of a temperature measuring thermocouple subjected to the desired thermal cycle. Thus, a thermocouple of appropriate composition attached to a metallic specimen would provide an electrical output varying with time in a fashion identical to that of the reference generator if, and only if, the specimen experienced the desired thermal cycle. Any departure of the instantaneous temperature of the specimen from the desired thermal cycle would provide a thermocouple output voltage differing from that of the reference generator. Thus, by comparing the output of the thermocouple with that of the reference generator, an error-signal voltage can be obtained which indicates the directions and the magnitude of any instantaneous departure of the specimen temperature from the desired thermal cycle.

In order to obtain the rapid heating rates corresponding to actual weld thermal cycles, heating currents are passed directly through the specimen, causing the specimen to heat as a result of its own resistance to the flow of current. The specimen is held between massive, water-cooled copper jaws which are connected to the secondary of the main power transformer of the Gleeble. The jaws serve both to conduct the large heating currents to the specimen and to extract heat from the specimen during cooling.

The block diagram in Figure 14 shows the control circuit used in the Gleeble. The error signal (3) from the reference generator and control thermocouple is sampled by the chopper in the front end (B)

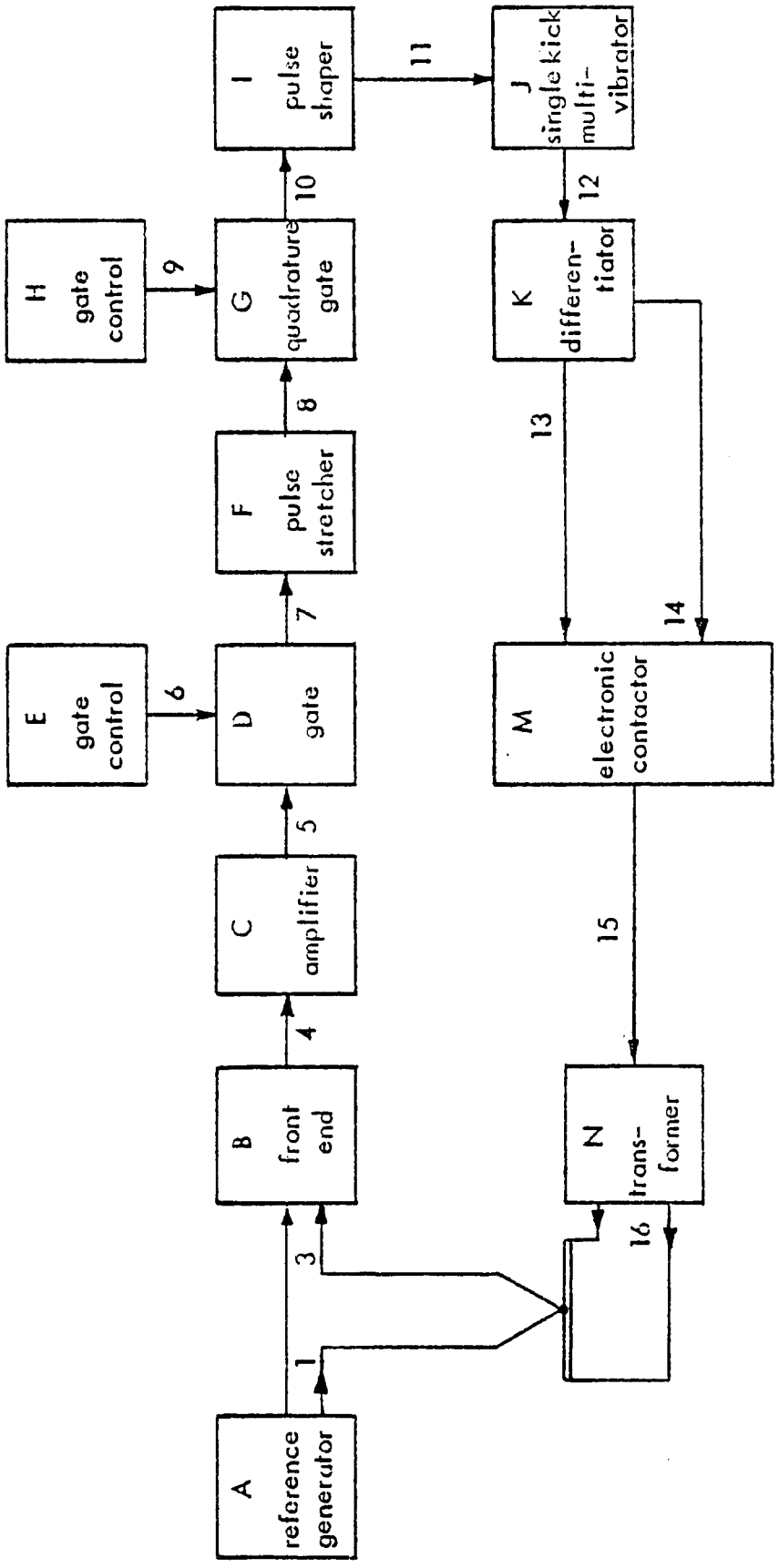

Figure 14. Block diagram of Electronic Control Mechanism.

every half cycle of the 60 cycle-per-second supply line voltage. This sampling of the error signal occurs for a brief interval during each half cycle when no heating current is flowing through the sample. This prevents voltages induced in the thermocouple leads by the heating current from interfering with the control operation.

The circuit in blocks (C) through (K) converts the error signal admitted at the front end (B) to a voltage signal suitable for controlling the electronic contactor (M). When the sample is below the correct temperature at a given time in the thermal cycle, the magnitude and polarity of the resulting error signal results in a firing of the electronic contactor (M). This in turn permits current of the proper magnitude to pass through the primary of the heating transformer (N) causing heating current to flow in the specimen. The circuit provides automatic rate-control action to bring the specimen temperature into correspondence rapidly without overshoot.

The rate-control action automatically adjusts the magnitude of the heating current to fit the instantaneous demand. Thus, the current magnitude is increased electronically when the specimen temperature is far below the desired temperature, and automatically decreased as the temperature nears the desired value. When the specimen is above temperature, the contactor will not fire and the specimen is cooled by the extraction of heat at the water-cooled jaws.

The overall dynamic response of the control maintains an accuracy of less than ±15°F of desired temperature at all times.

The Dilatometer

In order to generate a continuous cooling transformation diagram for SA 533 and SA 508 steels, a high-speed dilatometer was used, so

that volume changes accompanying the various allotropic transformations could be monitored and recorded. The dilatometer, shown in Figure 15, consists of a precision rectilinear transducer and a solid-hinge mechanical linkage. Quartz rods were used to contact the specimen.

Volume changes in the specimen were transmitted through the hinge to the rectilinear potentiometer which was in turn connected to a precision bridge circuit. The output of the bridge was connected to a channel in a recording oscillograph (Honeywell Visicorder M906 B) containing a galvanometer (M100-120) with a sensitivity of 11.0 microamperes per inch. In this manner, a continuous record of the dilational behavior of the specimen was produced.

The thermal cycles used in this investigation consisted of the weld thermal cycle corresponding to:

A	20 KJ/in.	Preheat	80°F.
I	32 KJ/in.	"	"
II	50 KJ/in.	"	"
III	100 KJ/in.	"	"
IV	136 KJ/in.	"	"
V	136 KJ/in.	"	300°F.
VI	136 KJ/in.	"	500°F.

Weld thermal cycles were calculated for 1 inch steel plate, for an initial plate temperature of 80°F, 300°F and 500°F. The CCT behavior studied was for the coarse-grained region using a peak temperature of 2400°F which lies next to the fusion zone and the refined region, using a peak temperature of 1650°F which is in the outer extremities of the HAZ. It should be noted that as the energy inputs and preheat

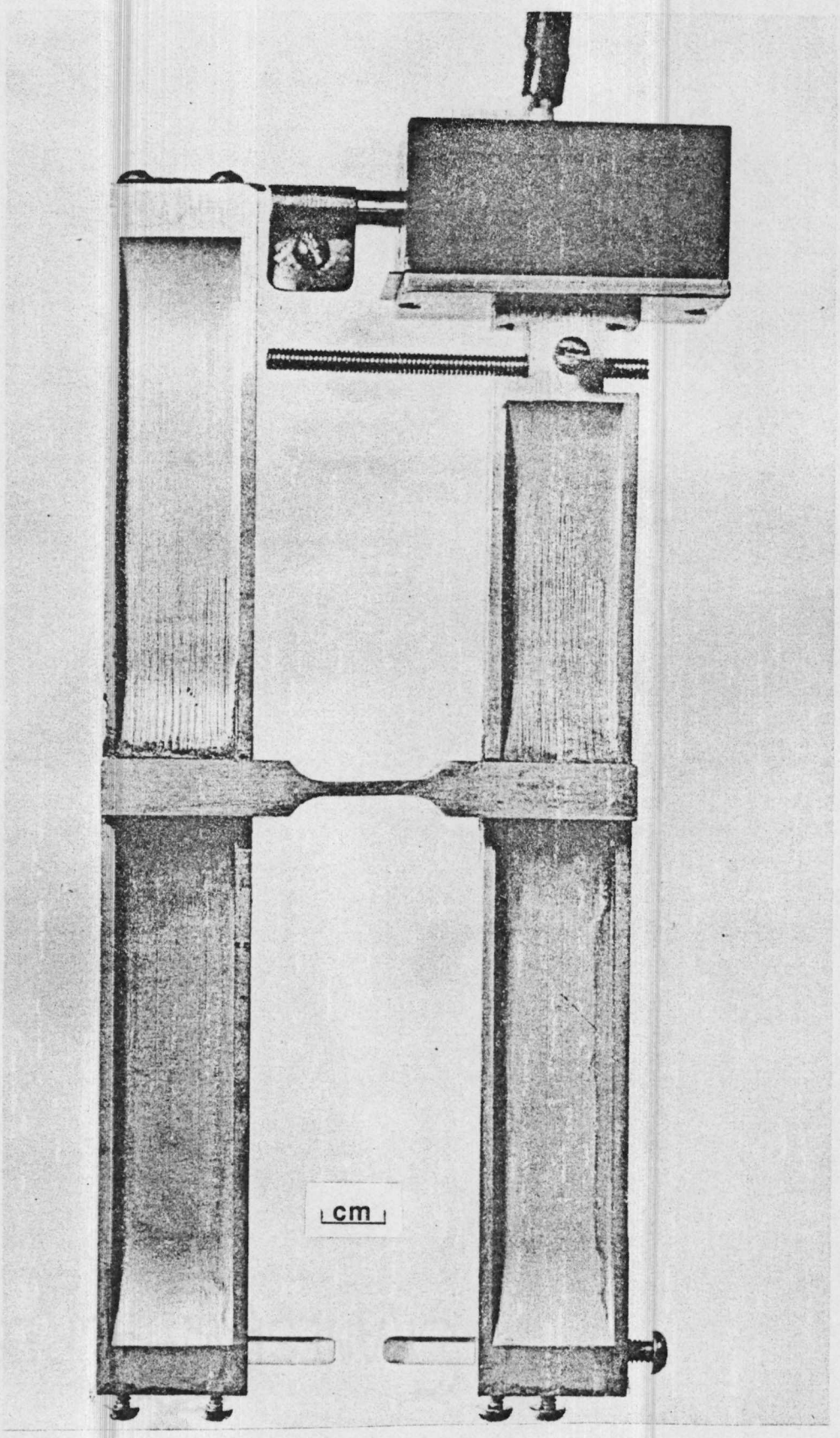

Figure 15. A high-speed dilatometer.

increases, the integrated time at peak temperature increases and the cooling rates decrease. Multiple runs were made for each of the weld thermal cycles studied, using a new specimen for each run in order to insure that the same initial microstructure was present.

Upon thermal cycling, two related traces were obtained,

1. a trace of dilation versus time and
2. a trace of temperature versus time.

From these data, plots of dilation versus temperature were constructed, as shown schematically in Figure 16. The reaction-start and the reaction-stop temperatures were chosen as the points where sensible departure from the smooth thermal contraction curve began. The transformation temperatures as previously determined were located on the temperature-time trace. Zero time for cooling was chosen at the peak temperature. The minimum peak temperature used was 1650°F. For the higher peak temperature, a time differential must be applied to evaluate the transformation equivalently (cooling time from 2400°F to 1650°F equals ≈ 10 sec.). The pertinent times and temperatures for each of the transformations over a variety of cooling rates were then plotted on a temperature versus log-time scale, thereby generating the continuous cooling transformation diagrams. The specimens with different thermal cycles were prepared for metallographic evaluation.

Evaluation of Cold Cracking

Cold cracks are usually formed in the base metal heat affected zones at low temperatures (usually below 200°F). Cracking in this range is almost invariably associated with the presence of dissolved and diffusable hydrogen. In order to study the cold cracking behavior of material SA 533 Grade B Class 1 and SA 508 Class 2 two experimental methods were employed:

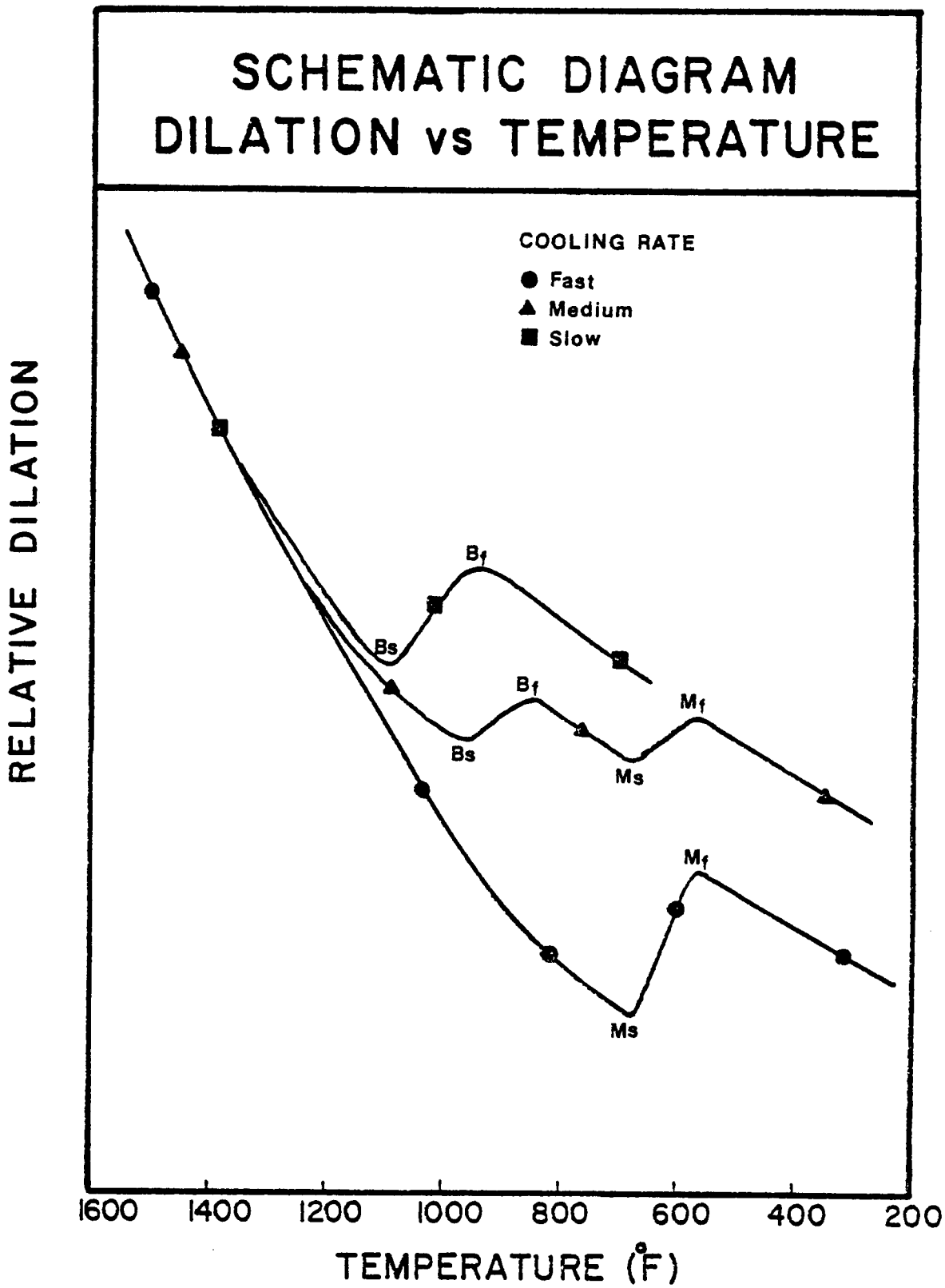

Figure 16. Schematic representation of dilation vs. temperature curves.

1. Underbead Crack Test and,
2. Hydrogen Susceptibility Test.

The experimental procedure for each of the tests is described as follows:

Underbead Crack Test

Battelle Memorial Institute[34] has developed a test for determining the underbead crack sensitivity of steels. Battelle samples, 2 inches wide by 3 inches long in the direction of rolling and 1 inch in thickness were cut from the material SA 533 Grade B Class 1 and SA 508 Class 2. A weld bead, 1 1/4 inches in length was deposited on the surface of each block, with a 1/8 inch diameter E6010 type electrode, a current of 100 amperes at 24 to 26 volts, and travel speed of 10 inches per minute. The small blocks were precooled or preheated to one of several temperatures such as 32°F, 85°F, 200°F, 300°F and 400°F. Upon completion of weld, the samples were held 24 hours at 60°F and then tempered to 1100°F for 1 hour. After PWHT the samples were sectioned longitudinally (along the centerline of the weld bead) to examine the underbead crack metallographically. The Battelle test specimen and the parameters used for this test are shown schematically in Figure 17.

Hydrogen Susceptibility Test (HST)

A testing procedure, developed at the University of Tennessee, reproduces hydrogen induced cracking in small laboratory scale specimens and allows direct observation of both initiation and

BATTELLE UNDERBEAD CRACKING TEST SPECIMEN

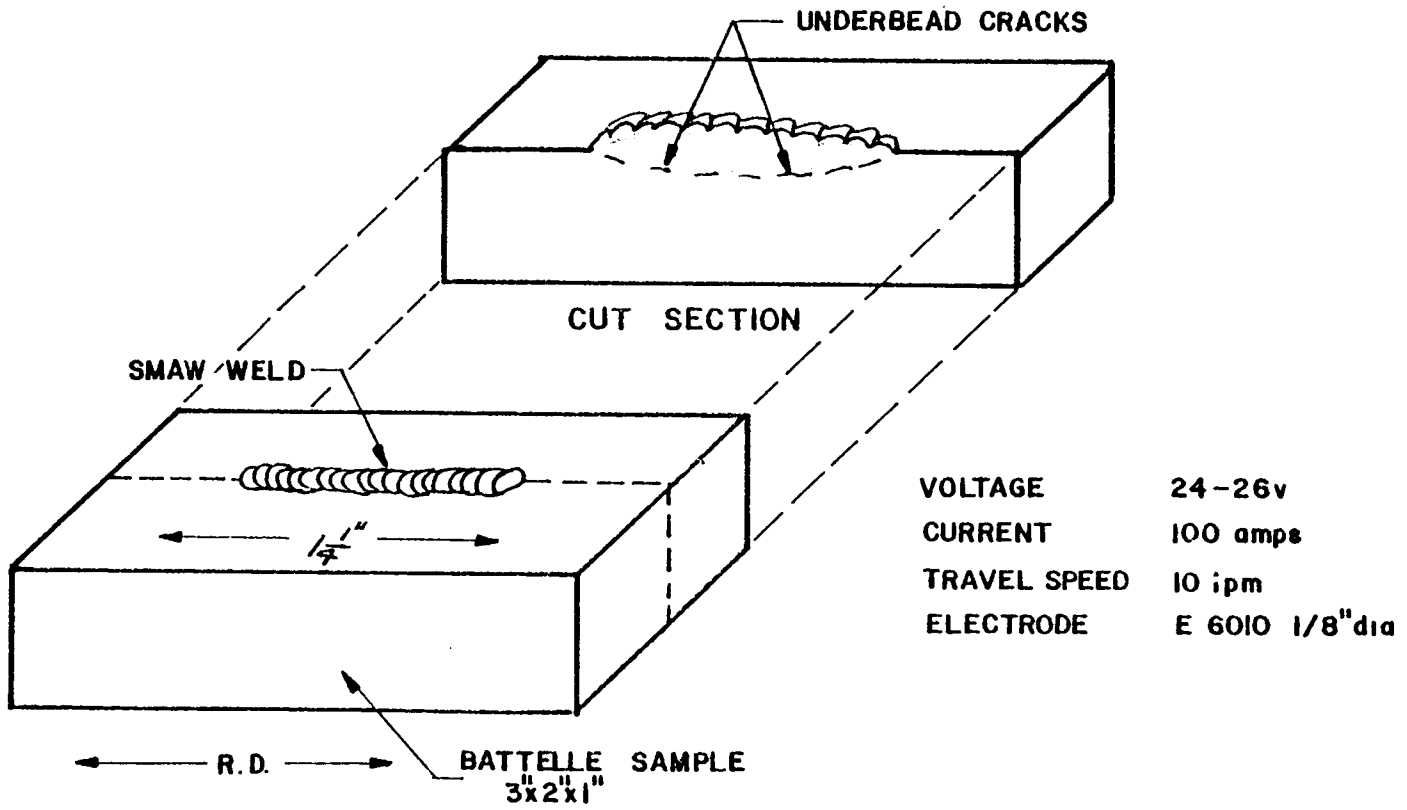

Figure 17. Underbead Cracking Test specimen.

propagation of the cracking. The specimens were prepared having a width of 5/8", 1 5/8" in length and 1/8" in thickness, in the rolling direction. Autogeneous GTA welds were made parallel to the rolling direction. During the deposition of the welds, hydrogen was added to the shielding gas to saturate the weld fusion zone with hydrogen. Figure 18 shows a schematic drawing of specimen, and parameters used during welding.

The testing device shown schematically in Figure 19 was designed and constructed to facilitate the study of hydrogen induced cracking. The testing device imposes an augmented strain on the welded surface of the bead on plate weld; about five minutes after welding, the samples are strained in the device. The approximate value of the augmented strain on the top surface of the weld in the longitudinal direction can be calculated by the relationship:

$$\varepsilon \tilde{=} \frac{t}{2R}$$

where ε = augmented strain in the outer fibers

t = thickness of specimen

R = radius of curvature of the die block (where $R \gg t$).

Therefore, either by substituting a die block with the appropriate radius of curvature, or by changing the thickness of the specimen, any desired augmented strain can be applied to the outer surface of the specimen. The augmented strain applied for SA 508 and SA 533 specimens was 4%; this strain is sufficient to cause cracking in the specimens and provide a conservative assessment of cracking sensitivity. The cracking was evaluated as a function of preheat temperatures of 32, 90, 300, 400, 500 and 600°F.

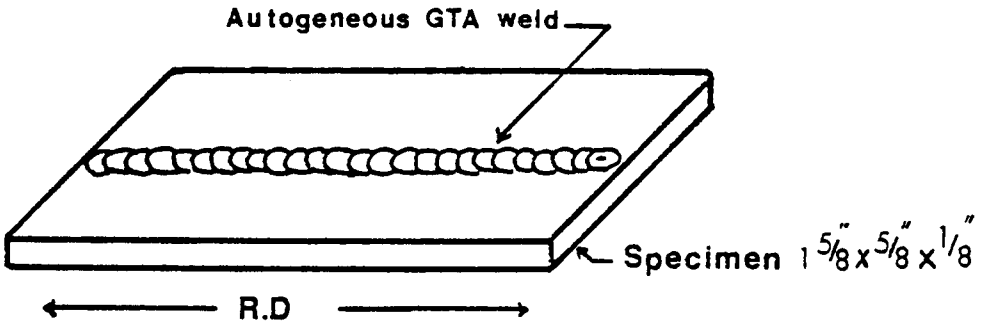

Current	80 – 100 amps
Voltage	10 v
Travel Speed	5 ipm
Shielding gas	5% H_2, 95% Ar, flow rate 30 CFH
Electrode	2% thoriated tungsten 1/16" dia. w/60° included point

Figure 18. Hydrogen Susceptibility Test specimen.

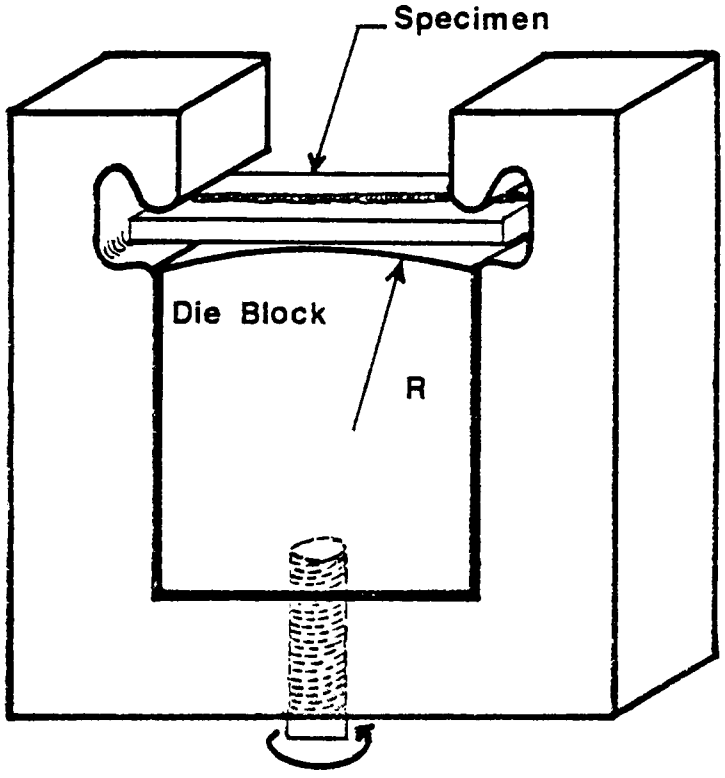

Figure 19. Schematic representation of apparatus used to strain specimen.

Stress Relief Cracking

Stress relief or reheat cracking may occur in the HAZ of welds in alloy steel during post weld heat treatment or during service at elevated temperature. Cracking is due to the combined effects of embrittlement and strain.

In order to reveal information about the phenomenon of stress relief cracking, HAZ structures were synthetically created by resistance heating and rapid cooling of base metal samples (0.25" dia. x 4.75" long) in the Gleeble. The specimen shown in Figure 20 was treated with different simulated welding cycles. A schematic representation of thermal treatment and stress applied is shown in Figure 21. After the desired HAZ thermalcycle the sample is reheated to 1150°F with stress being simultaneously applied. The basic thermal cycles employed for SRC tests were Cycle II (50KJ/in) and Cycle VI (136KJ/in, 500°F preheat) to create a martensitic and bainitic structure respectively in the simulated grain-coarsened region. The two transformation products were further tested with superimposed cycles (such as a hold at 600°F or multiple high temperature cycles) and also as function of stress. Table A-2 in Appendix A shows a complete schedule of the thermal treatments employed in SRC testing.

The specimens with simulated grain-coarsened weld HAZ microstructures PWHT at 1150°F, usually failed within a stress relieving time of 120 minutes. If the specimen did not fail within 120 minutes, the test was discontinued. The test data provided the reduction of area and time to failure for each specimen. The failed specimens were retained for metallographic and fractographic evaluations.

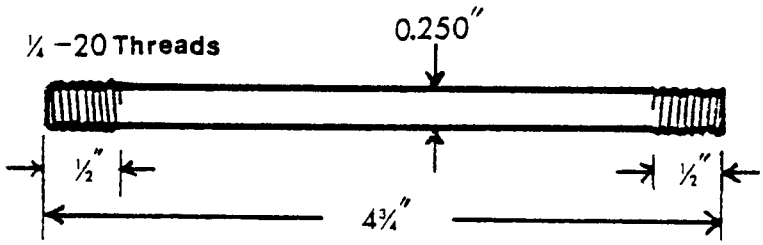

Figure 20. Stress relief cracking specimen used in Gleeble.

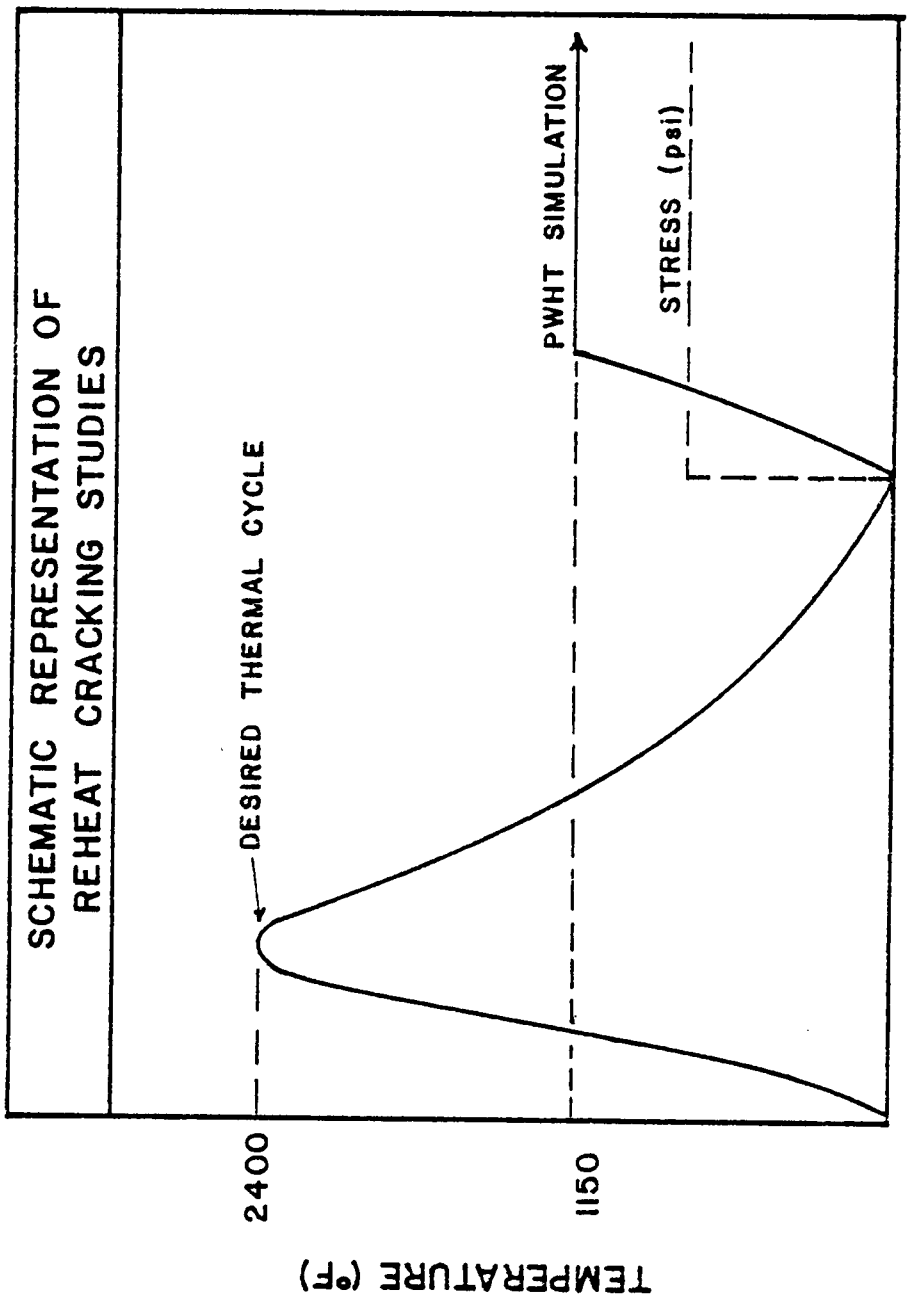

Figure 21. Schematic representation of reheat cracking studies.

Charpy Impact Toughness of HAZ

The Gleeble microstructure simulation technique for assessing the charpy notch toughness of HAZ structures was used in this investigation. The procedure involves subjecting a number of specimens to one or more peak temperature weld thermal cycles and then testing in the as-welded or PWHT condition.

The material used for charpy blanks was chosen from the 1/4t and 3/4t sections of the SA 533 and SA 508 6 in. plates. Charpy blanks were machined according to the dimensions shown in Figure 22 (rolling direction longitudinal). The charpy blanks were treated with different thermal cycles and post weld treatments in the Gleeble. A complete schedule of thermal heat treatments is shown in Table A-3 of Appendix A. The thermal cycles selected were Cycle II (50KJ/in) to obtain a fully martensitic structure and Cycle VI (136KJ/in, 500°F preheat) to obtain a fully bainitic structure.

Each specimen 0.42" x 0.42" x 2.5" in length was clamped in water cooled copper jaws of the Gleeble, and a fine wire thermocouple percussion welded to the specimen surface. The reference generator was adjusted to provide the proper time-temperature program and the specimen was subjected to the programmed thermal cycle. Each specimen was then removed from the apparatus, the thermocouple clipped to a length of approximately 1/2 inch, and the specimens were then stored at ambient temperature. The 1/2 inch length of thermocouple was left attached in order to serve as an index of the center of the volume of metal subjected to the desired thermal cycle so that the V-notches could be accurately located at a later date when the final machining was accomplished.

A total of 54 specimens were obtained for each material, out of which

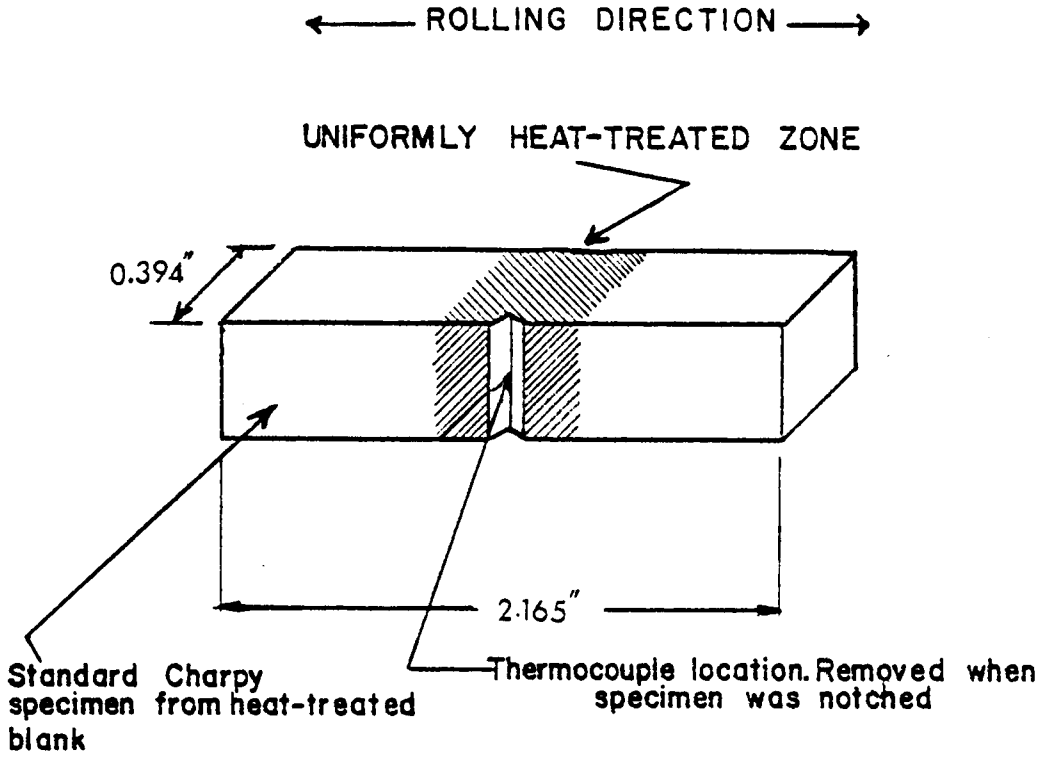

Figure 22. Details of charpy specimen preparation.

48 specimens were subjected to the selected thermal cycles and heat treatments (Table A-3 in Appendix A) and the remainder were tested to obtain base metal toughness. Out of 48 specimens, 24 were set aside for PWHT. For SA 533 the specimens were PWHT at 1150 ± 50°F for 40 hours, whereas, for SA 508 the specimens were PWHT at the same temperature for 24 hours. The time of PWHT is similar to what is commercially employed.

After the final machining of charpy blanks to the standard charpy bars of dimension 0.394" x 0.394" x 2.165" in length, the temperatures for the impact test were selected as -25°F for SA 533 material and 72°F for SA 508 material. These temperatures were based on the transition temperature obtained for the base metal of these materials. For each thermal treatment 3 charpy bars were tested and the average of three values were used to construct the bar graphs which represented energy absorbed (ft-lbs) and lateral expansion (mils) as a function of different thermal heat treatments. The broken bars were retained for metallographic and fractographic examinations.

CHAPTER IV

RESULTS AND DISCUSSION

In order to achieve a better understanding of the weldability of SA 533 and SA 508 steels one should have available suitable diagrams for predicting the microstructure after heat treatment and after welding the HAZ. Therefore, in order to provide fundamental information, both the isothermal and continuous cooling transformation behavior for steels SA 533 and SA 508 has been determined and the appropriate diagrams drawn.

Isothermal Transformation Behavior

The isothermal transformation diagrams for both SA 533 and SA 508 steels are shown in Figure 23 and 24 respectively. These diagrams have been drawn based on microstructural observations and the hardnesses obtained for the microconstituents.

At the austenitizing temperature, the steel is composed of a single constituent, austenite, which can exist as long as the temperature is maintained above a certain minimum temperature. When austenite is cooled below this critical temperature, it becomes unstable and transforms into a mixture of ferrite and carbide. For other than martensite this change of austenite requires a certain incubation period before the transformation begins and then a certain amount of time to complete the transformation.

The I-T diagram in Figure 23 represents the isothermal transformation behavior of SA 533 steel. It is observed that ferrite nose occurs at

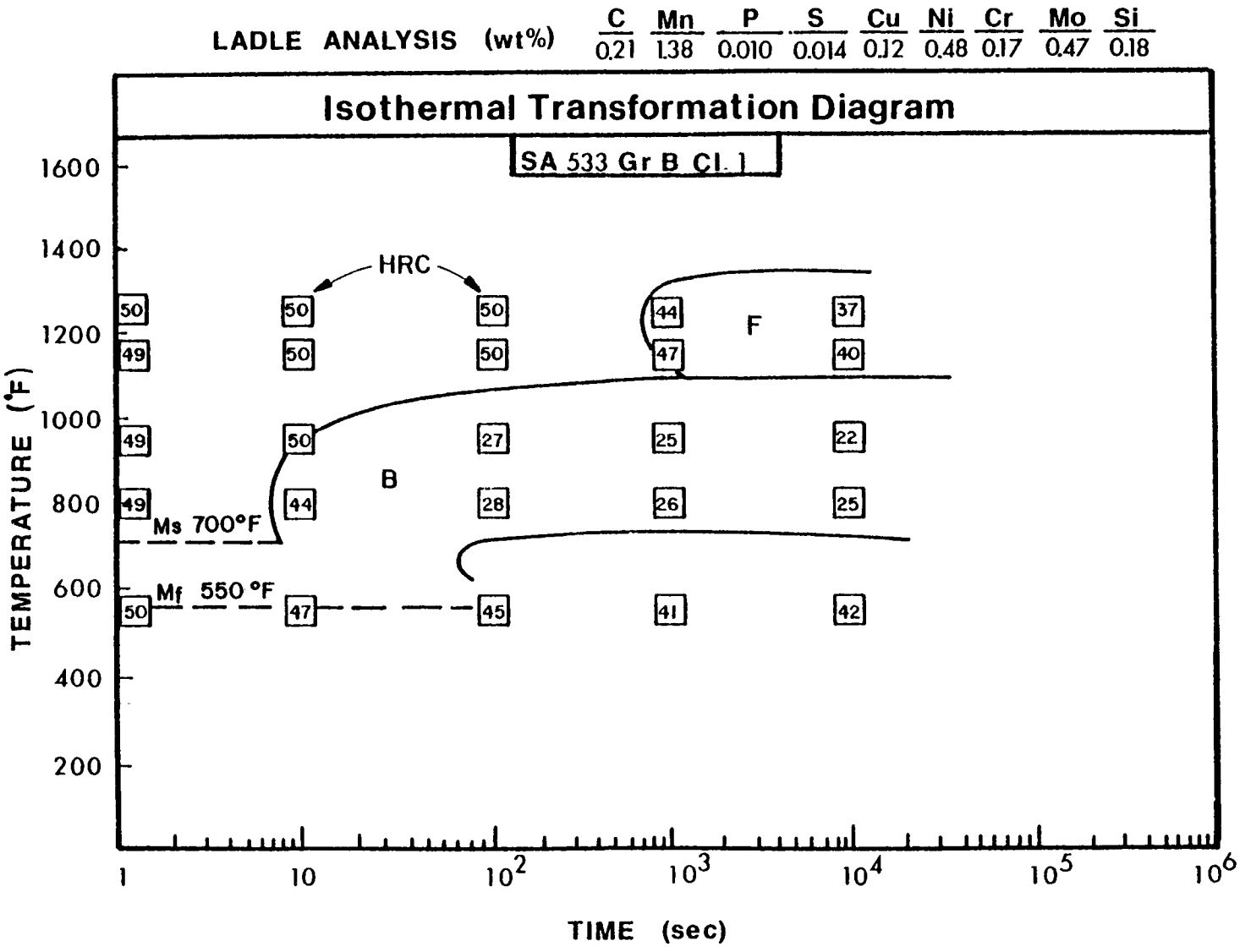

Figure 23. Isothermal transformation diagram of SA 533 Gr. B Cl. 1 steel.

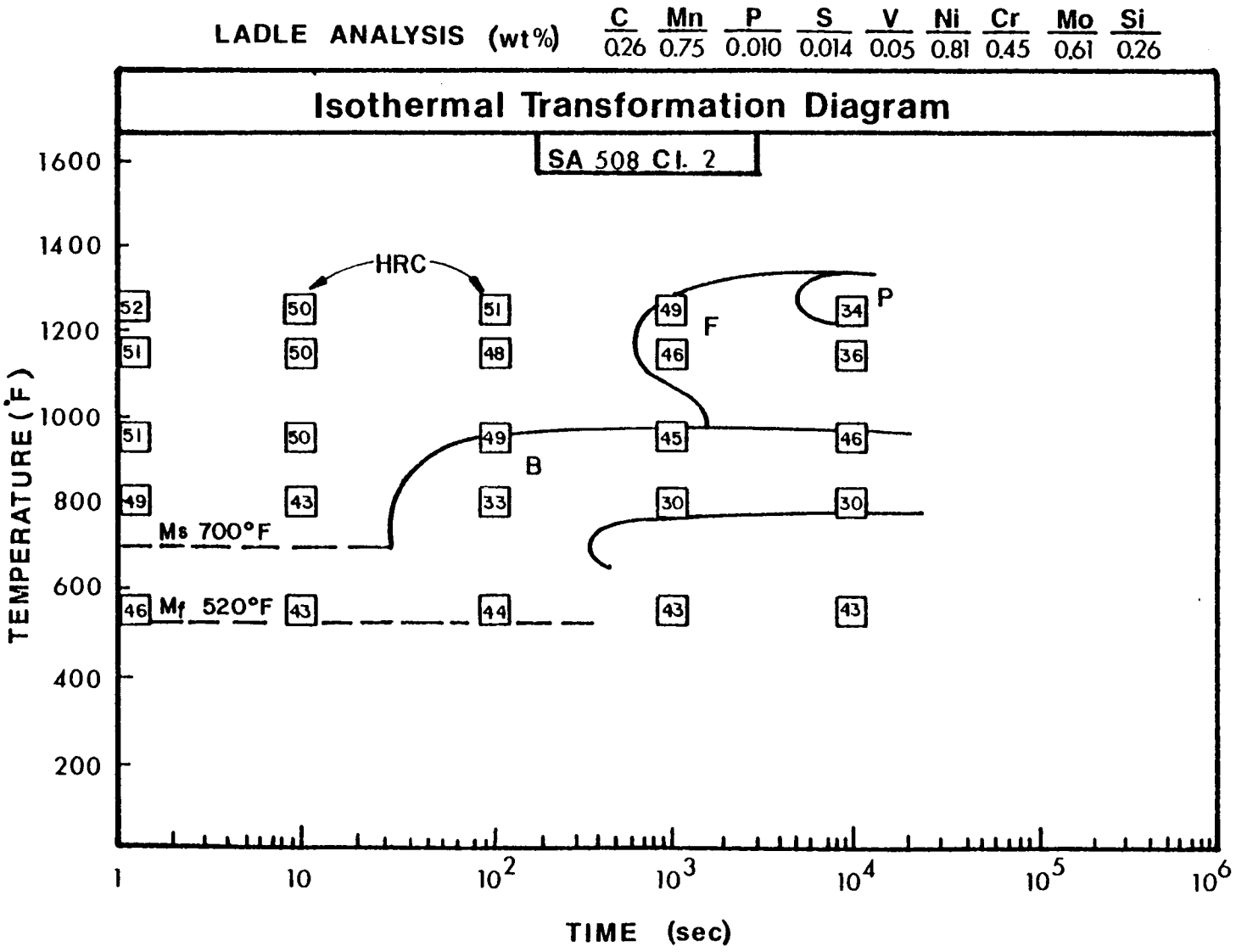

Figure 24. Isothermal transformation diagram of SA 508 Cl. 2 steel.

approximately 800 secs, and the bainite nose occurs at approximately 7 secs. Transformation to martensite (which in this steel occurs at temperatures of about 700°F), differs from transformation to ferrite, pearlite or bainite in that it is not diffusion controlled (time dependent), but occurs almost instantly upon cooling below the M_f and the percentage of transformation is dependent only on the temperature to which it is cooled (0-100% from Ms to M_f). Thus, in this steel, transformation to martensite will start on cooling at 700°F (designated as the Ms temperature), will be 90% complete on cooling at about 632°F (calculated value) and essentially 100% complete at about 550°F. In Figure 25 a fully martensitic structure is shown for a specimen quenched to 550°F from the austenitizing temperature.

Above 1100°F, ferrite is the primary constituent forming with the onset of pearlite at longer times in this temperature range. At temperatures below 1100°F, the constituent formed is bainite which consists of a non-lamellar aggregate of ferrite and carbides. The morphology of bainite changes gradually with transformation temperature, so that it is difficult to uniquely define outstanding characteristics. In Figure 26, the microstructure of specimen which was held at 800°F for 10 secs. shows martensite and bainite. On isothermal holding, the austenite begins to transform to bainite and the untransformed austenite remaining in the specimen at the instant it was quenched to room temperature appears in the final structure as martensite, which is a readily distinguishable transformation product. Similarly in Figure 27, a specimen held at 1250°F for 1000 secs. shows a ferritic and martensitic structure.

The I-T diagram in Figure 24 for SA 508 represents isothermal transformation behavior similar to what was observed for SA 533 steel. In

SA 533

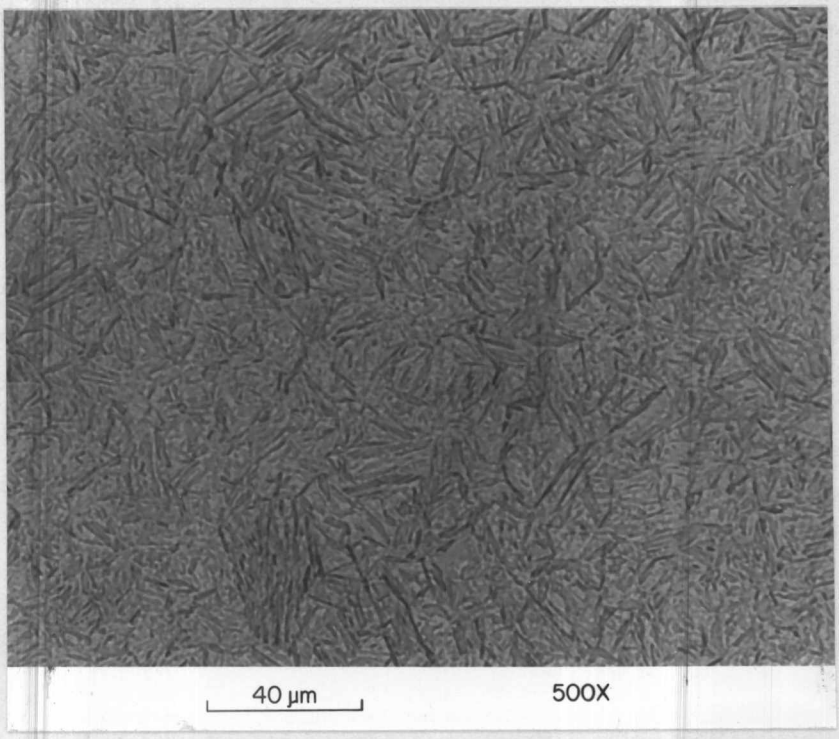

Figure 25. Specimen 3T0A (held for 1 sec. @ 550°F) shows fully martensitic structure. HRC 50. Super picral etch.

SA 533

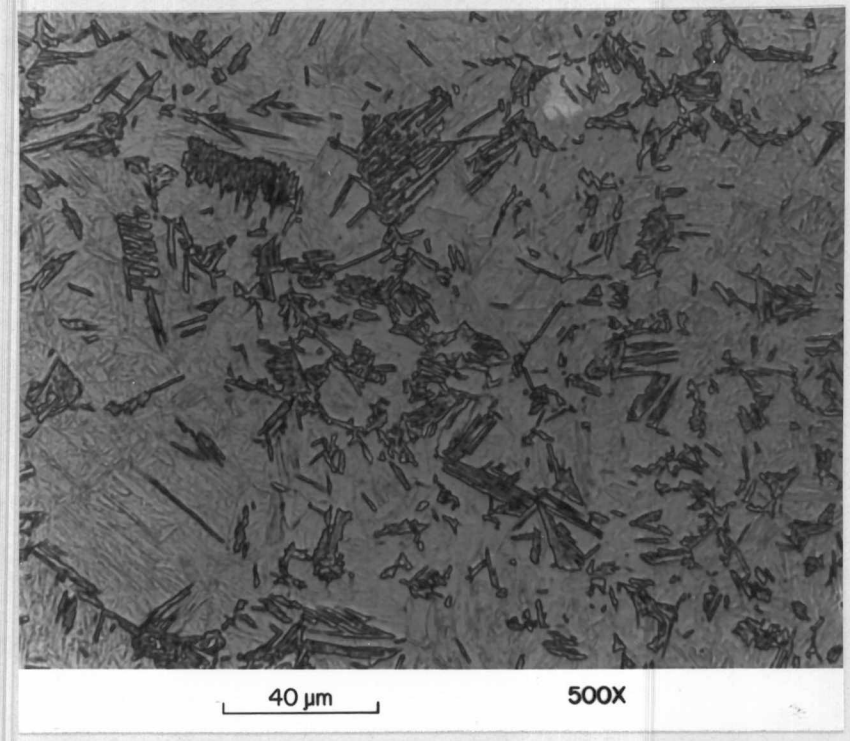

Figure 26. Specimen 3T1B (held for 10 sec. @ 800°F) Shows Bainitic-Martensitic structure. HRC 44. Super picral etch.

SA 533

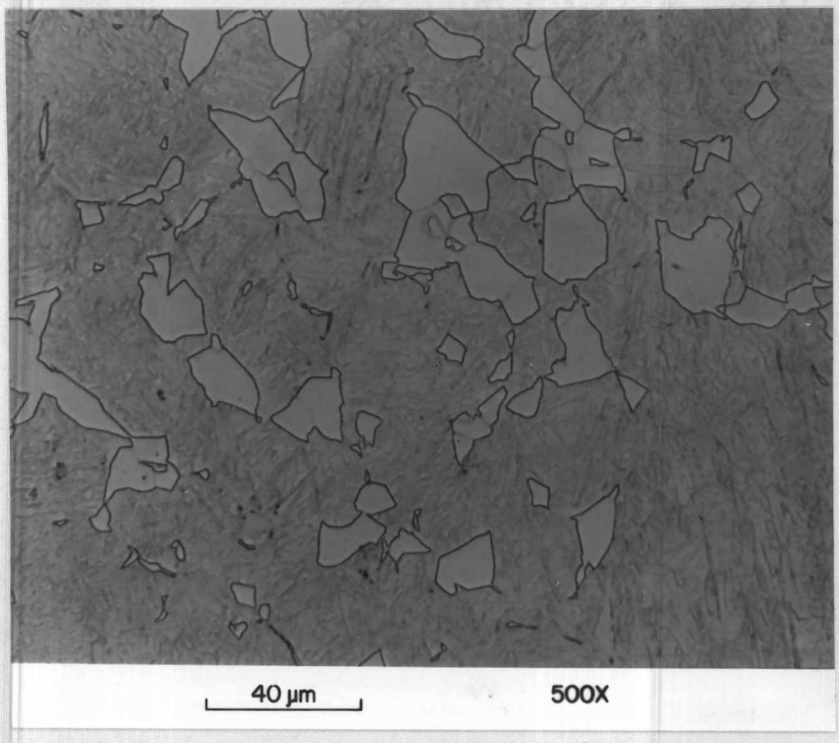

Figure 27. Specimen 3T3E (held for 10^3 secs. @ 1250°F). Shows Ferritic-Martensitic structure. HRC 44. Super picral etch.

this case, the ferrite nose has not changed position (start at 800 secs.) but at longer times (6000 secs.) another microconstituent, pearlite, is noted (the pearlite nose in SA 533 is apparently at times greater than 10^4 secs.).

In SA 508 steel the transformation to martensite occurs at approximately 700°F, it will be 90% complete (calculated value) on cooling at about 593°F and essentially 100% complete at about 550°F. In Figure 28, a fully martensitic structure is shown for a specimen quenched to 550°F from the austenitizing temperature of 1700°F.

Referring to Figure 29, representing the specimen held at 800°F for 100 secs., it is observed that most of the austenite transformed to bainite; the untransformed austenite remaining in the specimen at the instant it was quenched to room temperature appears in the final structure as martensite. It is concluded from this figure that austenite begins to transform to bainite at times less than 100 secs. Therefore, based on microstructure and hardnesses, it can be estimated that the bainite nose occurs at approximately 35 secs.

The specimens held at 950°F appear to have less bainite than the samples held at 800°F. The hardnesses correlated well with the microstructures, since the hardness is higher for the specimens held at 950°F than for the specimens held at 800°F. The observations suggest that the bainite start temperature for SA 508 steel is lower than observed in SA 533 steel.

Transformation of austenite to ferrite is observed in Figure 30 for the specimen held at 1250°F for 1000 secs.; the untransformed austenite appears in the final structure as martensite which was attained upon quenching. For the same holding temperature of 1250°F and longer time

SA 508

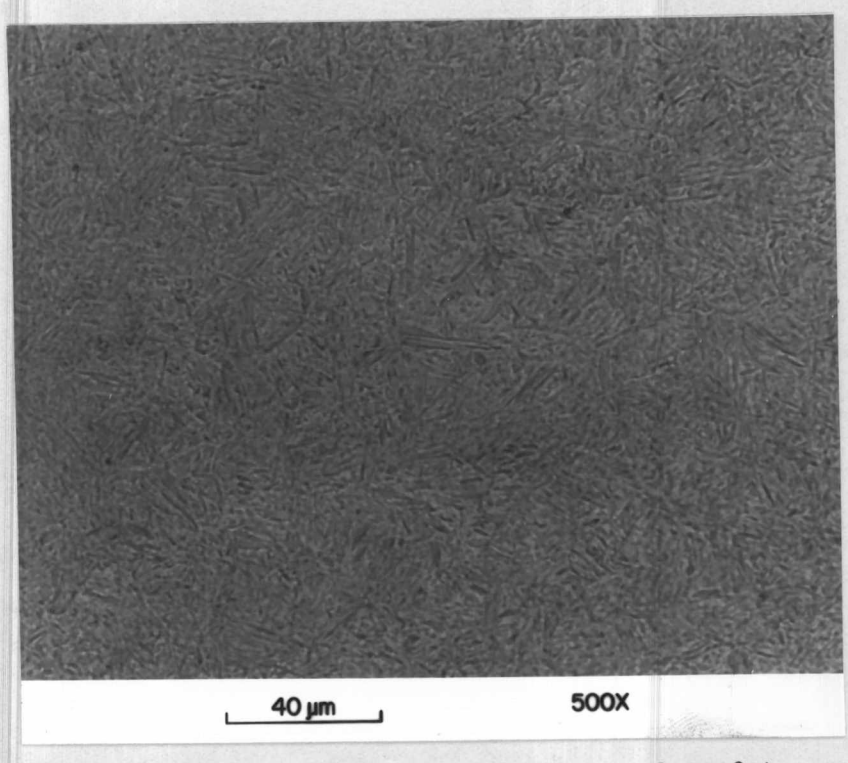

Figure 28. Specimen 8M0A (held for 1 sec. @ 550°F). Shows fully martensitic structure. HRC 52. Super picral etch.

SA 508

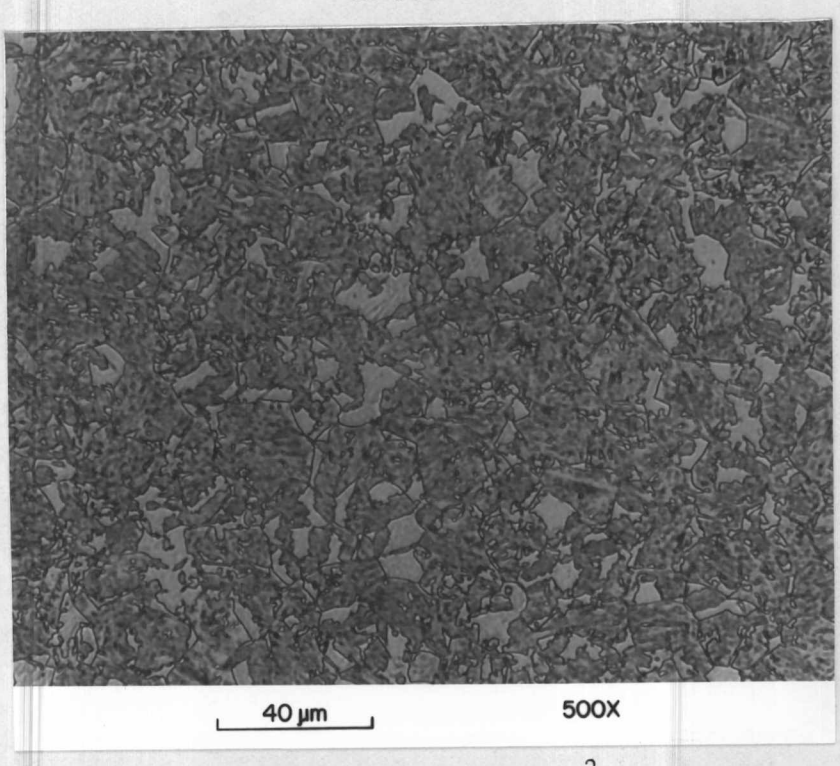

Figure 29. Specimen 8M2B (held for 10^2 secs. @ 800°F). Shows Bainitic-Martensitic structure. HRC 33. Super picral etch.

SA 508

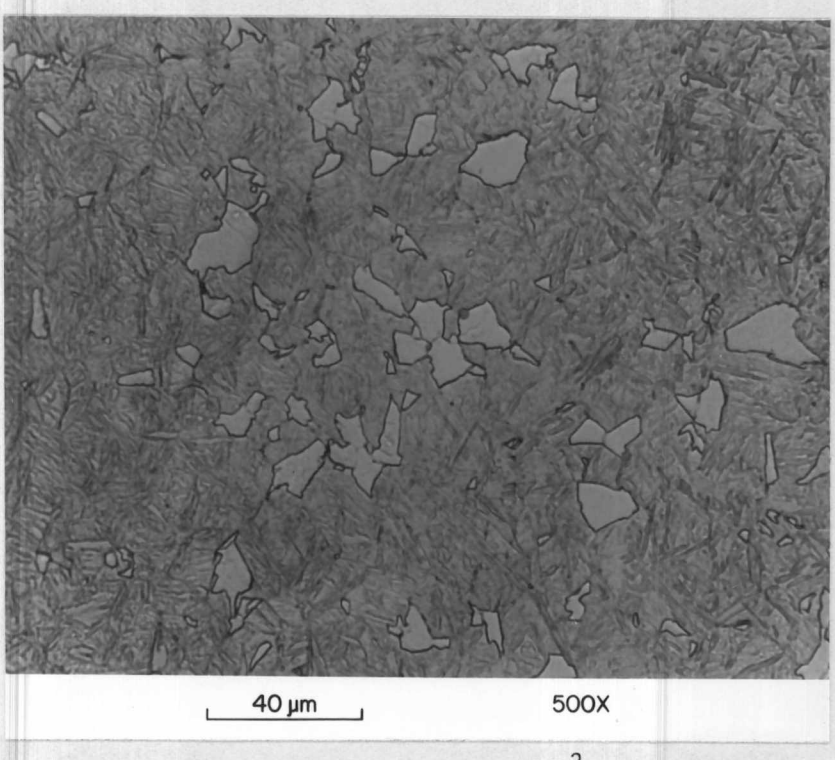

Figure 30. Specimen 8M3E (held for 10^3 secs. @ 1250°F) Shows Ferritic-Martensitic structure. HRC 49. Super picral etch.

of 10,000 secs., a new microconstituent, pearlite, is formed and is shown in Figure 31. This figure shows ferrite, martensite and pearlite. The lamellar appearance of pearlite is not clearly visible at this magnification due to its fine structure. To achieve better resolution of the pearlite, the scanning electron microscope (SEM) was utilized and pearlite laminations were clearly observed as shown in Figure 32.

Comparing the isothermal diagrams of SA 533 and SA 508 steels (Figure 33), it is clearly observed that the bainite nose for SA 508 steels is shifted to larger times, approximately 30 secs. The bainite start temperature for SA 508 is lower than the bainite start temperature for SA 533. The ferrite nose for both steels is identical, located at approximately 800 secs. A pearlite nose for SA 508 is seen at approximately 6000 secs., whereas no pearlite was formed in SA 533 for holds of up to 10,000 secs.

The Ms values for both steels are approximately 700°F and M_f value for SA 533 is estimated to be slightly higher than SA 508 steel. This estimation is based on the hardness values obtained at the hold temperature of 550°F for all times. It is estimated that M_f for SA 533 is 550°F, whereas M_f for SA 508 steel is approximately 520°F.

Luken Steel Company[14] indicates that since the analysis of SA 533 steel is similar to SA 302 steel, the transformation behavior of both steels should be nearly identical. To verify this, isothermal transformation diagrams for both SA 533 and SA 302 steels are compared in Figure 34. It is observed that transformation of the steels is not identical, the transformation for SA 533 starts at longer times than SA 302 steel.

SA 508

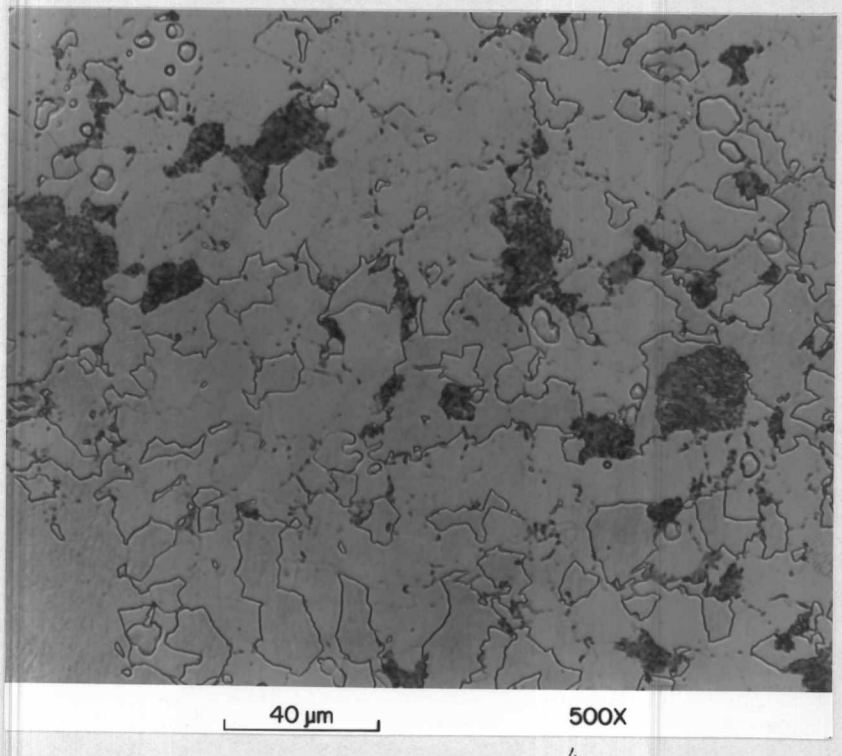

Figure 31. Specimen 8M4E (held for 10^4 secs. @ 1250°F). Shows Ferritic-Pearlitic-Martensitic structure. HRC 34. Super picral etch.

SA 508

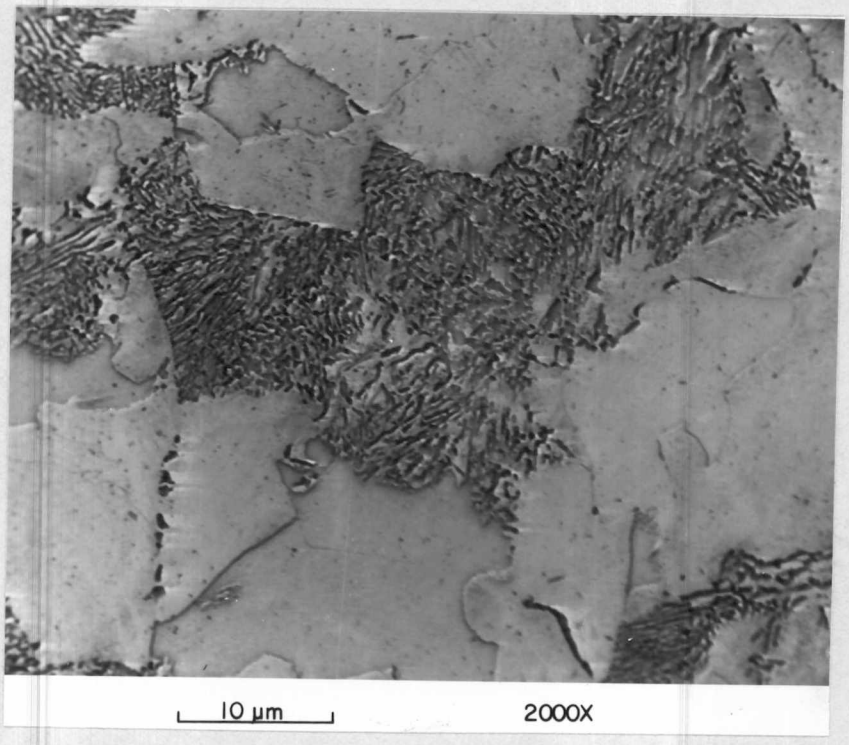

Figure 32. Pearlitic-Ferritic Structure of specimen 8M4E. (held for 10^4 secs. @ 1250°F). Super picral etch. SEM

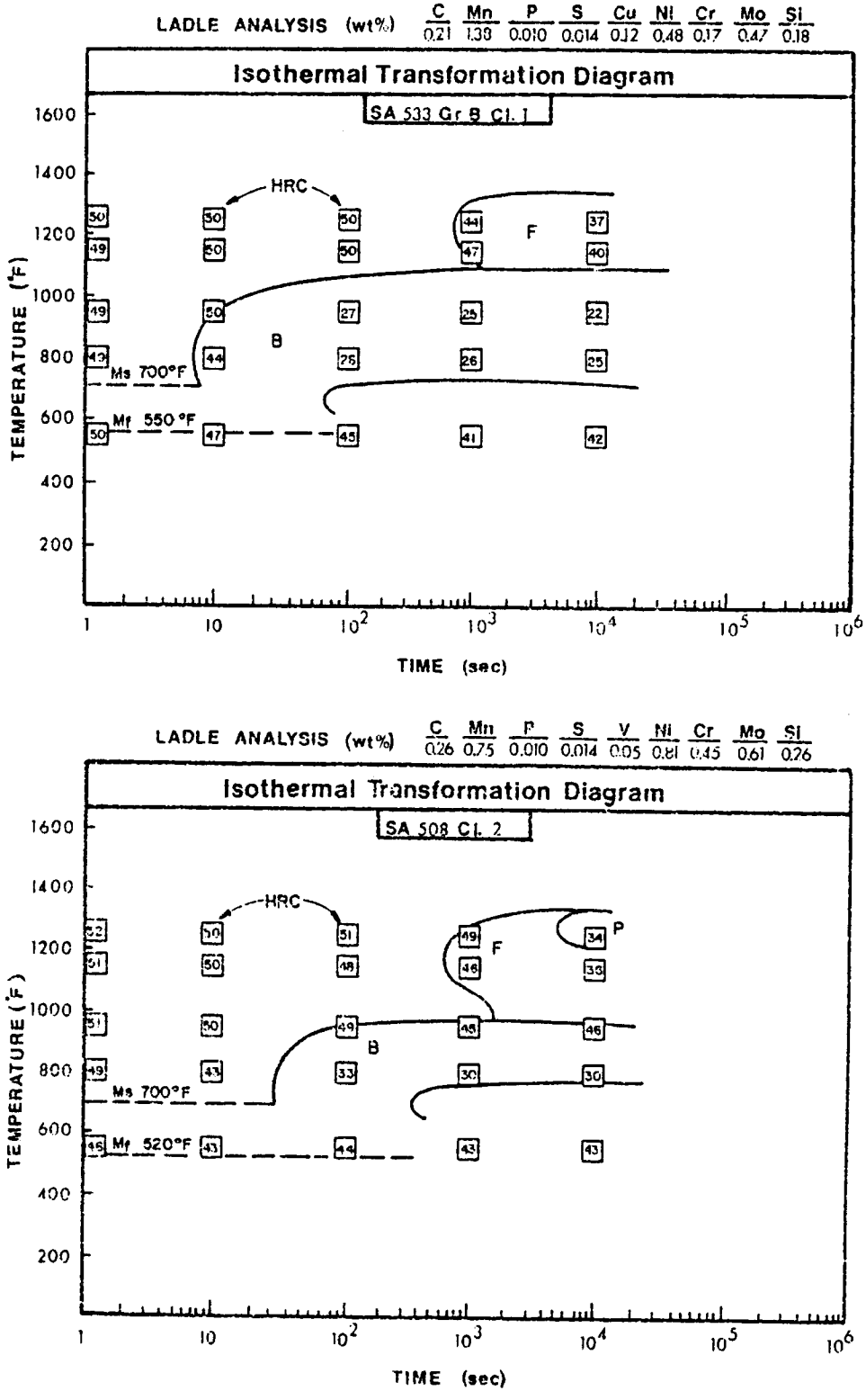

Figure 33. Comparison of I-T behavior for SA 533 with SA 508 steel.

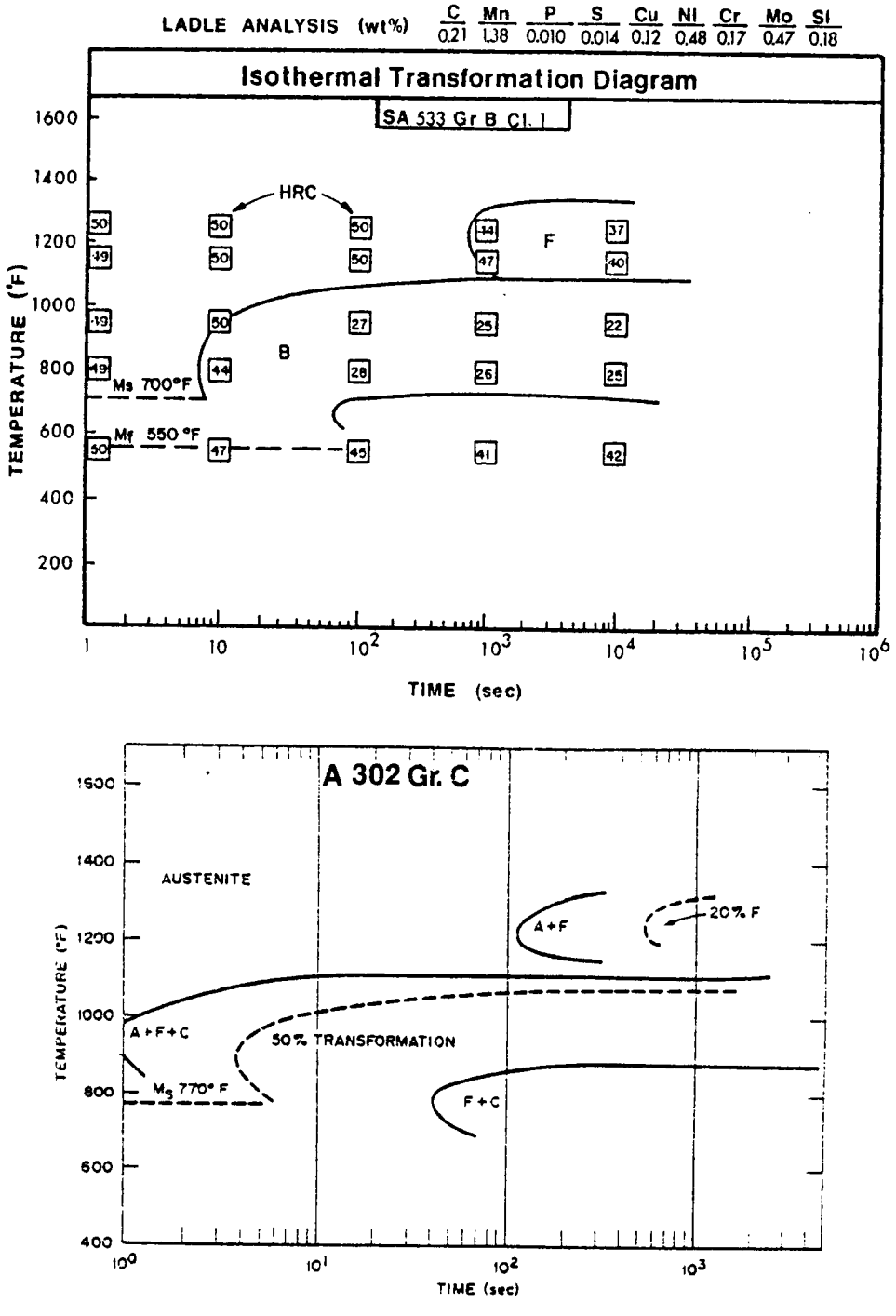

Figure 34. Comparison of I-T diagrams of SA 533 (above) with SA 302 (provided by Luken's Steel Co.).

The isothermal diagrams show the fundamental transformation behavior of austenite at constant temperature, however, most actual heat treatments involve transformation during cooling through a range of temperatures. The transformation which occurs during hardening, welding or heat treating by any method of controlled cooling can be approximated from the isothermal diagram but continuous cooling diagrams are more directly applicable. Therefore, continuous cooling transformation behavior for the weld HAZ of SA 533 and SA 508 has been documented.

Continuous Cooling Transformation Behavior

In recent years, the problem of materials selection has become increasingly complex. No longer is it sufficient to choose materials for service on the basis of perfunctory examination. Many investigators have shown that materials which are to be welded must be carefully examined as to the changes brought by the heat of welding.

By careful evaluation, it has been possible to predict the weldability of many steels and to avoid welding conditions which would lead to poor properties. One of the most powerful methods for evaluating weldability is through metallography. It has long been known that, in steel, the microstructure of the heat affected zone (HAZ) frequently determines the overall performance of a weld. Thus it is very useful indeed to be able to predict accurately the microstructure in the HAZ of a weld knowing only the welding parameters and the Continuous Cooling Transformtion (CCT) diagram.

There are many CCT diagrams available in the literature, however,

few of them are directly applicable to weld HAZ problems. For the most part, the thermal cycles used to generate the diagrams are not similar to weld thermal cycles. Austenitization is usually accomplished at temperatures which are usually only high enough to produce complete austenitization. The extreme grain coarsening seen near the fusion zone in an arc weld is seldom duplicated by the thermal cycles used. The slow heating rates and extended periods at elevated temperatures used in previous investigations afford a degree of homogeneity and solution of carbides which is unattainable in the HAZ of an arc weld.

It was decided therefore, to determine a continuous cooling transformation diagram for SA 533 Grade B Class 1 and SA 508 Class 2 steels in a manner which would render them applicable to predicting microstructures in the HAZ.

In order to study the behavior of continuous cooling transformation, two methods were employed, one by measuring the resistivity change of the material occurring on cooling and during transformation and secondly by measuring the dilation of the material as the volume changes occur during the various transformations.

CCT Behavior Obtained by Resistivity Measurements

SA 533 Grade B Class 1. The continuous cooling transformation behavior for SA 533 Grade B Class 1 is shown in Figure 35. The specimens were heated to the austenitizing temperature of 1650 ± 20°F, held for 10 minutes and then cooled in vacuum at a predetermined rate. Cooling curves from 'a' to 'g' were obtained by helium blast, whereas, curves 'h' to 'l' were obtained in vacuum at programmed rates. The

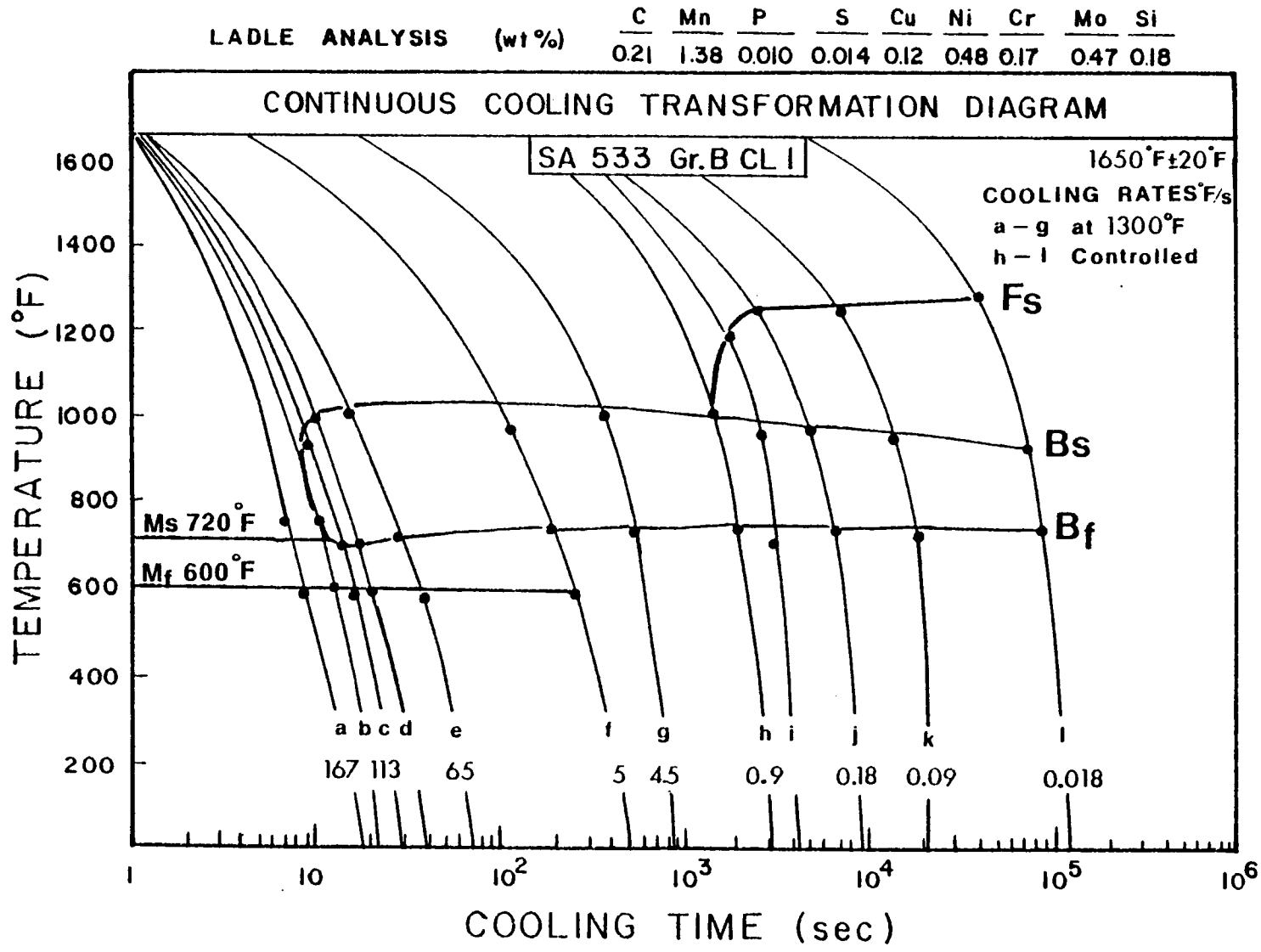

Figure 35. Continuous Cooling Transformation diagram of SA 533 Gr.B Cl 1 steel.

cooling rates obtained at 1300°F for curves 'a' to 'g' are shown at the end of each curve. Table 4 shows cooling rates obtained at 1300°F and 1000°F for curves 'a' to 'g' and the controlled linear cooling rates of curves from 'h' to 'l'.

When cooling under conditions applicable to curves 'a' and 'b' only martensite forms and two transformation temperatures were obtained - Ms and M_f, whereas, for curve 'c' three transformation temperatures were noticed, which indicates that the critical cooling rate for bainite is approximately 140°F/sec. at 1300°F. The calculated Ms (700°F) and M_{f90} (632°F) temperatures correlate well with the experimental transformation temperatures (Ms 720°F, M_f 600°F).

The bainite nose (Figure 35) occurs at approximately 9 seconds and ferrite nose at approximately 1500 seconds. Cooling curves from 'i' to 'l' show the ferrite start (Fs), and also that the Fs temperature decreases with increasing cooling rates. The critical cooling rate for ferrite is approximately 1°F/sec. at 1300°F. The F_f transformation temperature was difficult to detect by the ERM method.

Selected samples were examined metallographically. The specimen experiencing a cooling rate of 167°F/sec (curve 'a') formed a fully martensitic structure which is shown in Figure 36. The sample experiencing a cooling rate of 4.5°F/sec (curve 'g') resulted in a bainitic structure, and this is shown in Figure 37, and finally the specimen with slowest cooling rate of 0.09°F/sec (curve 'k') showed a ferritic, bainitic, pearlitic structure as shown in Figure 38A & B. The onset of the pearlite reaction was not documented in the CCT diagrams obtained by ERM.

TABLE 4

COOLING RATES OF MATERIAL A-533 FROM CURVES a TO l OF FIGURE 35

Cooling Curves	Helium Blast (psi)	Cooling rate @ 1300°F °C/sec.	°F/sec.	Cooling rate @ 1000°F °C/sec.	°F/sec.
a	30	93	167	62	111
b	15	76	137	51	92
c	5	63	113	49	88
d	2	43	77	41	74
e	0.5	37	65	19	34
f	<0.25	3	5	2	3.6
g	No He used	2.5	4.5	0.6	1.08

	Controlled Cooling Rate °C/sec.	°F/sec.
h	0.5	0.9
i	0.3	0.54
j	0.1	0.18
k	0.05	0.09
l	0.010	0.018

SA 533

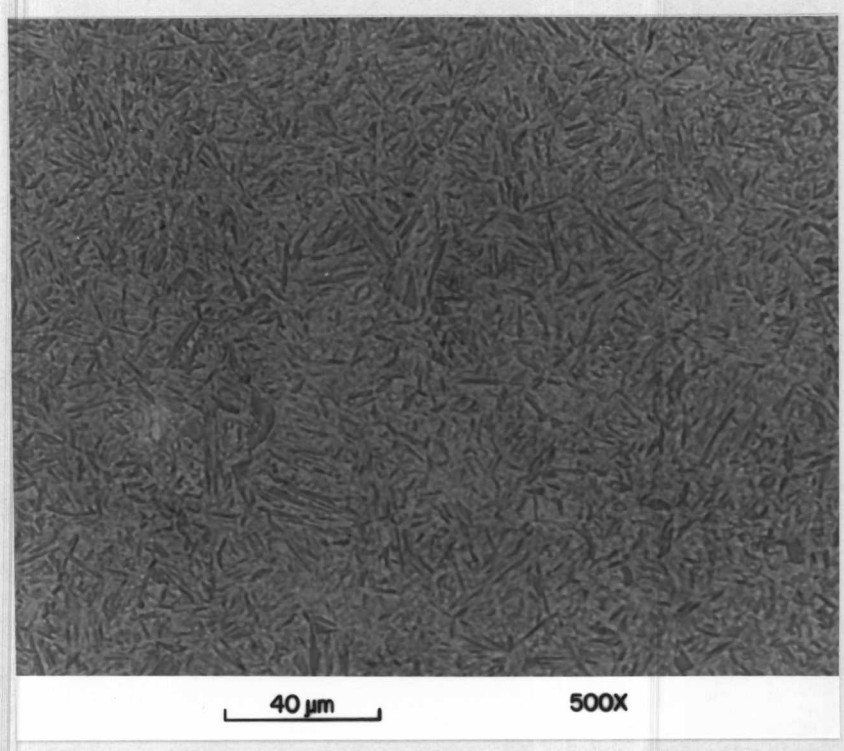

Figure 36. Fully martensitic structure representing curve 'a'. Cooling rate 167°F/sec. @ 1300°F. Super picral etch.

SA 533

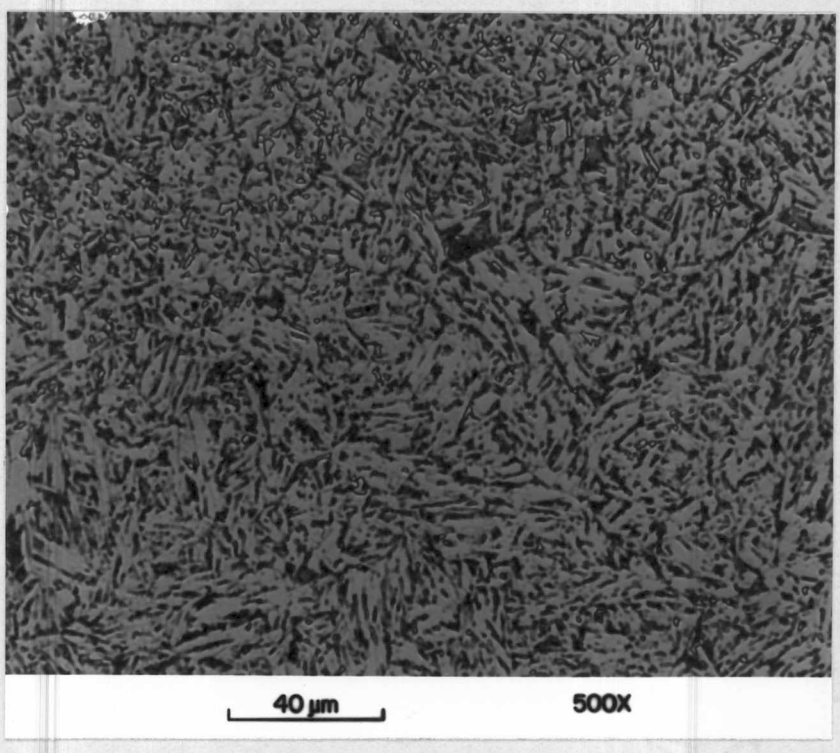

Figure 37. Bainitic structure representing curve 'g'. Cooling rate 4.5°F/sec. @ 1300°F. Super picral etch.

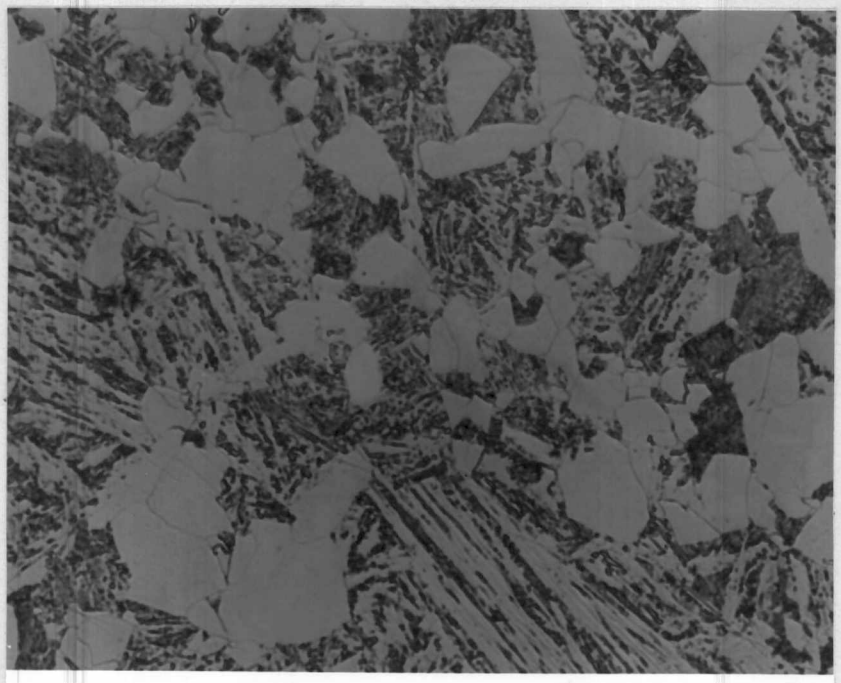

A) Ferritic-Bainitic-Pearlitic structure.

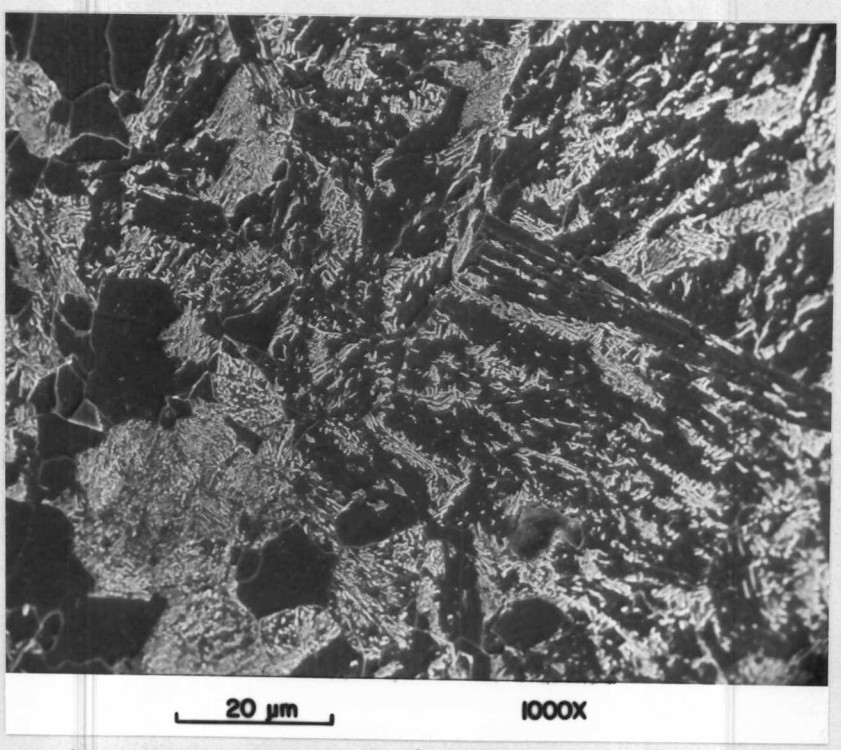

B) SEM Micrograph of A) above.

Figure 38. Microstructures representing curve 'k'. Cooling rate 0.1°F/sec. @ 1300°F. Super picral etch.

SA 508 Class 2. The continuous cooling transformation diagram for SA 508 Class 2 is shown in Figure 39. The heating and cooling of the sample was identical to that described for the SA 533 Grade B Class 1 specimens. Table 5 shows the cooling rates obtained at 1300°F and 1000°F for curves 'a' to 'i' and the controlled linear cooling rates for curves from 'j' to 'p'.

The cooling curves 'a' through 'f' show only the martensite transformation, whereas, curve 'g' exhibits three transformation reactions, indicating that critical cooling rate for the bainite start lies between curve 'f' and 'g' (approximately 50°F/sec. at 1300°F). The calculated Ms (685°F) and M_{f90} (593°F) temperatures, agree with the experimental values Ms (685°F), M_f (500°F).

It is observed from Figure 39 that bainite nose lies at approximately 40 seconds and ferrite nose lies at approximately 3000 seconds with the critical cooling rate for ferrite formation being approximately 0.25°F/sec. at 1300°F.

The samples exhibiting a cooling rate of 198°F/sec at 1300°F representing curve 'a' show a fully martensitic structure (Figure 40). Specimens with cooling rates of 6°F/sec. at 1300°F (curve 'i') reveal a fully bainitic structure which is shown in Figure 41. The specimen with the slowest cooling rate of 0.018°F/sec. representing curve 'p' formed ferrite and a bainite pearlite microstructure as shown in Figure 42A & B. Again the pearlite transformation was not uniquely revealed and may lie in the same range as bainite for very slow cooling.

The CCT diagrams for SA 533 and SA 508 are shown in Figure 43 for comparison. It is observed that the bainite nose of SA 508 is shifted further to the right (approximately 30 secs.), and has slower critical cooling rate, than for SA 533. The ferrite nose for SA 508 has also

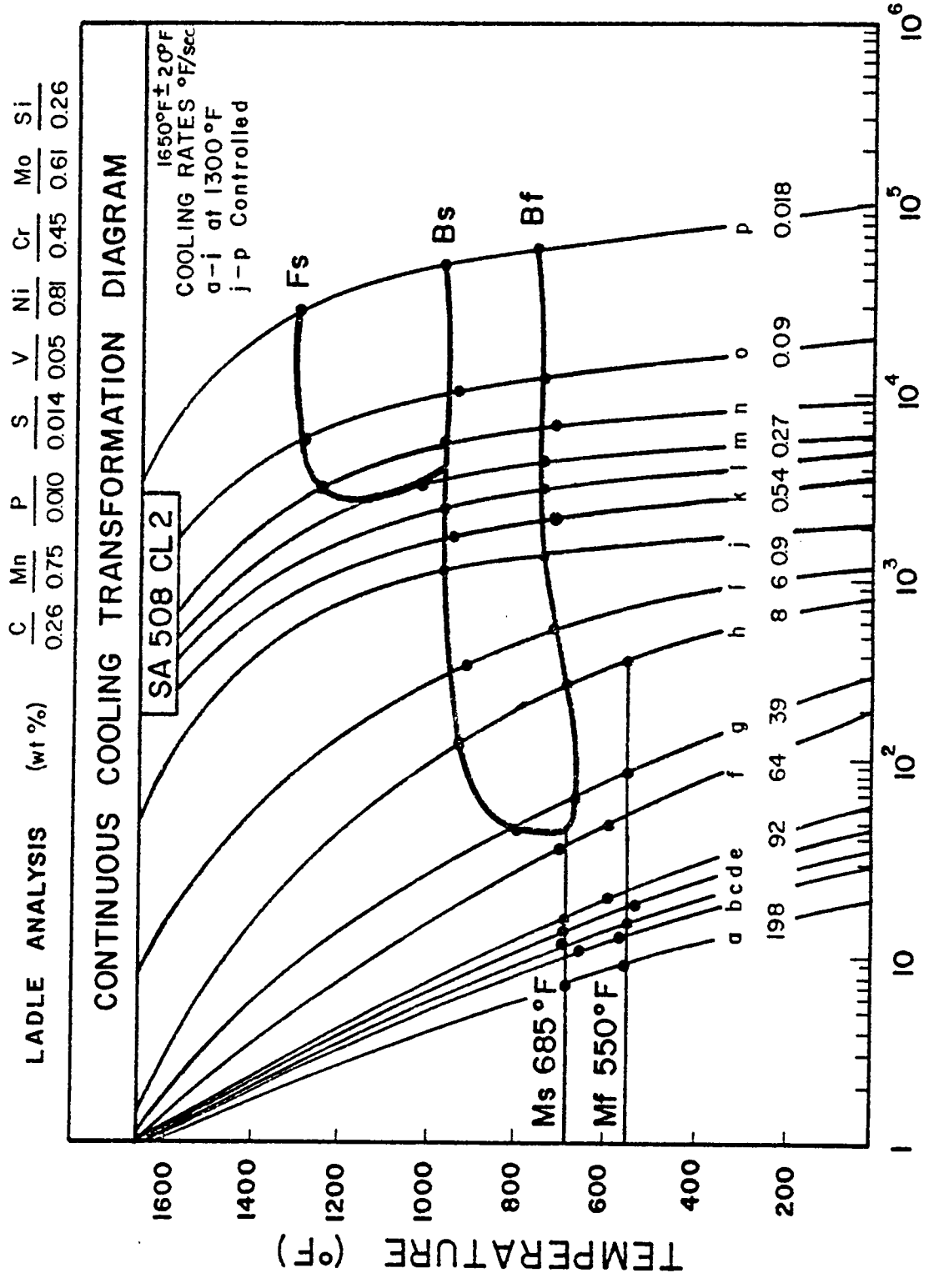

Figure 39. Continuous Cooling Transformation diagram of SA 508 Cl. 2 steel.

TABLE 5

COOLING RATES OF MATERIAL A-508 FROM CURVES a TO p OF FIGURE 39

Curves	Helium Blast (psi)	Cooling Rate @ 1300°F °C/sec.	°F/sec.	Cooling Rate @ 1000°F °C/sec.	°F/sec.
a	32	110	198	96	173
b	15	85.3	153	66	119
c	5	78	141	55.5	100
d	2	60	108	40	72
e	0.5	51	92	38.6	69
f	>0.25	35.4	64	15.5	28
g	0.25	21.6	39	9.3	17
h	<0.25	4.5	8	2.6	5
i	No He used	3.3	6	0.88	2

	Controlled Cooling Rate °C/sec.	°F/sec.
j	0.5	0.9
k	0.3	0.54
l	0.2	0.36
m	0.15	0.27
n	0.1	0.18
o	0.05	0.09
p	0.010	0.018

SA 508

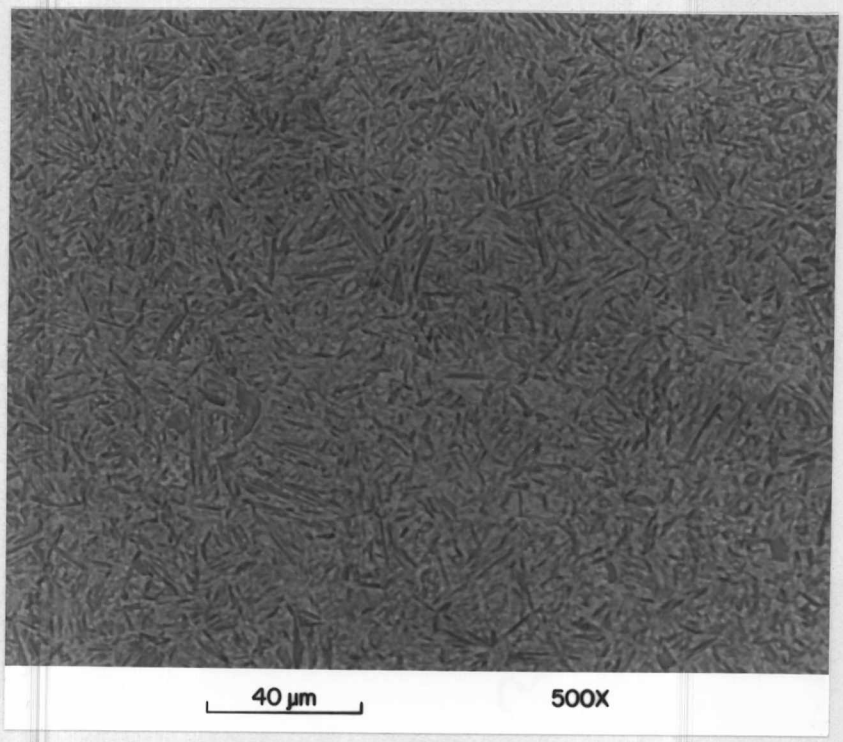

Figure 40. Fully Martensitic structure representing curve 'a'. Cooling rate 198°F/sec. @ 1300°F. Super picral etch.

SA 508

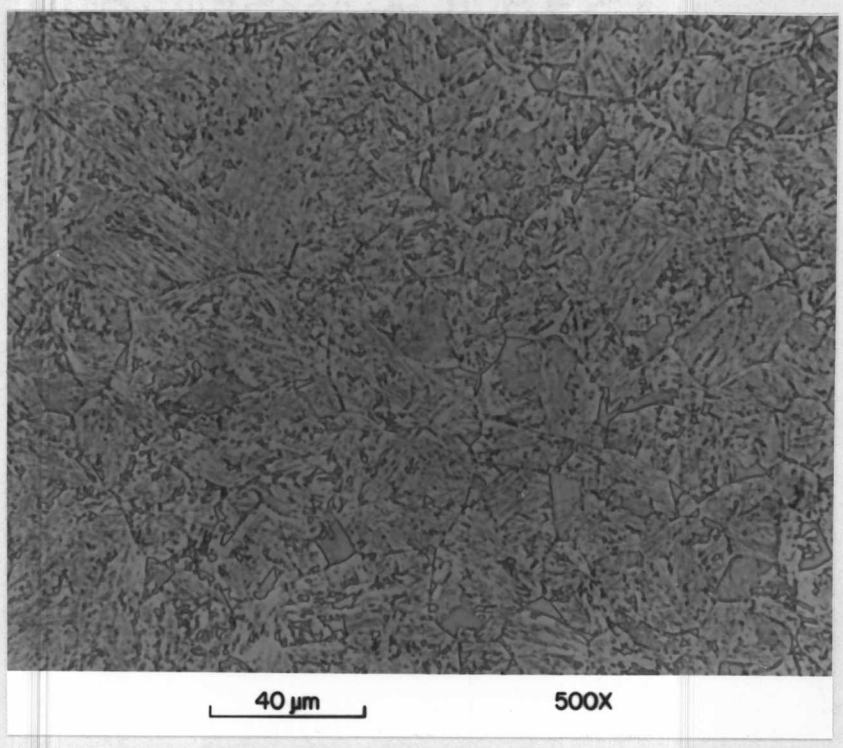

Figure 41. Bainitic structure representing curve 'i'. Cooling rate 6°F/sec. @ 1300°F. Super picral etch.

SA 508

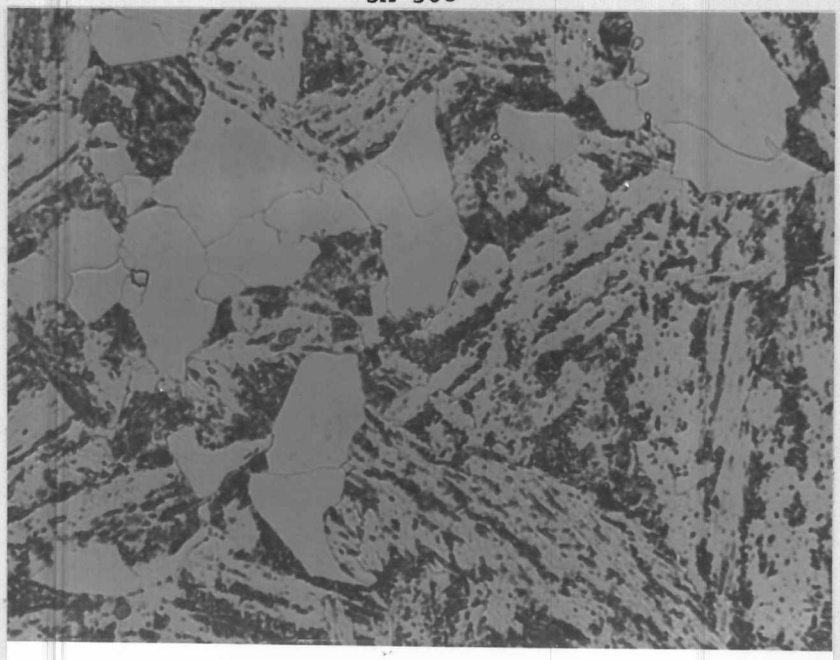

A) Ferritic-bainitic-pearlitic structure.

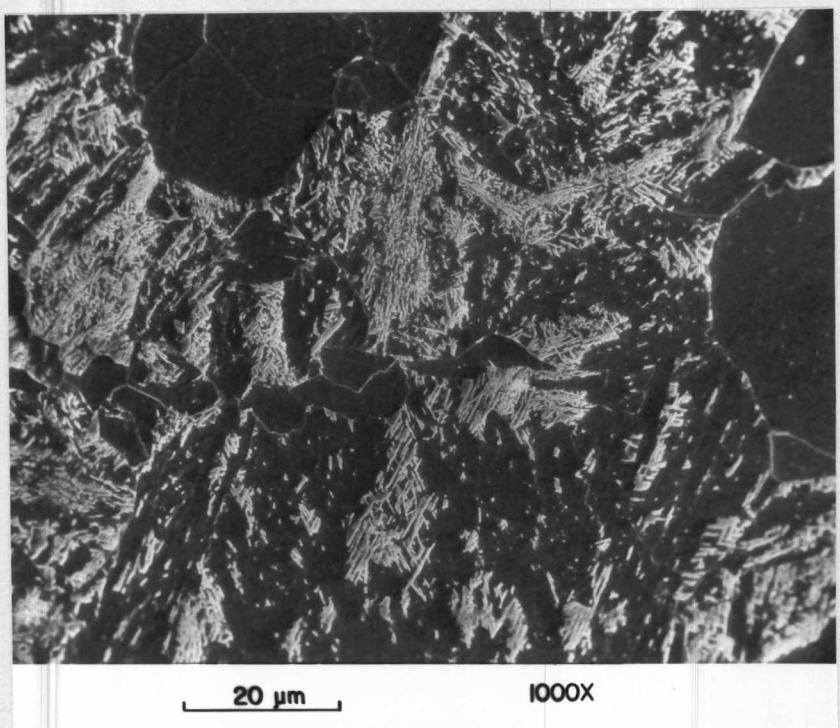

B) SEM micrograph of A) above.

Figure 42. Microstructures representing curve 'p'. Cooling rate 0.018°F/sec. @ 1300°F. Super picral etch.

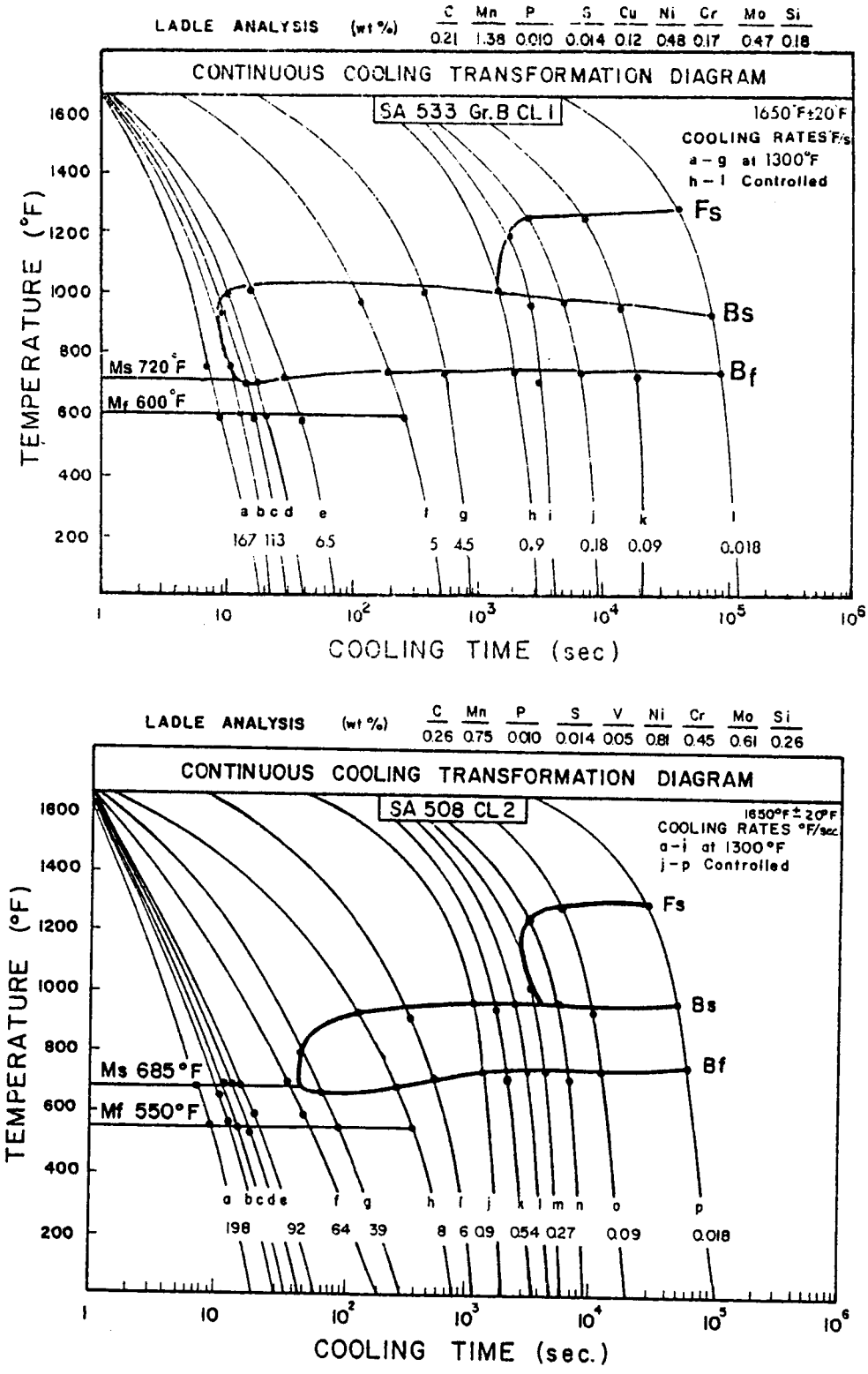

Figure 43. Comparison of CCT behavior for SA 533 with SA 508 steel.

shifted further to the right (approximately 1500 sec.). A careful observation of the bainite start temperature for both steels shows that bainite start temperature for SA 508 is a little lower than for SA 533. This observation also reflects the results of the isothermal transformation studies. It is observed that Ms and Mf temperatures of SA 508 steel are lower than those of SA 533 steel.

The transformation behavior observed with the slowest cooling rates in both steels showed bainitic, pearlitic and ferritic microconstituents. The transformation temperature for pearlite start (Ps) could not be uniquely detected. It is assumed that the transformation may be similar to the bainite transformation for very slow cooling occurring in the same temperature range.

Comparing the CCT behavior with I-T behavior, it is clearly observed that CCT transformation curves lie below and to the right of the corresponding isothermal transformation curves as would have been expected from previous work.[14]

It is readily predicted from the CCT diagrams that SA 508 steel has higher hardenability than SA 533 steel. Further, it should be noted that these CCT diagrams are not directly applicable to the weld HAZ, because the thermal cycles used to generate the diagrams are not similar to weld thermal cycles and the austenitizing temperature was only high enough to produce complete austenitization, but not high enough to produce grain coarsening which is usually noted near the fusion line in arc welds. Therefore, continuous cooling transformation diagrams were determined for both steels in a manner which render them applicable to predicting transformations and microstructures in the weld HAZ.

CCT Behavior for the HAZ Exposure Obtained by the Gleeble Dilatometric Method

CCT diagrams were obtained for two regions of the weld HAZ. The two peak temperatures chosen, represent the coarse-grained region (2400°F peak) which lies next to the fusion zone and the refined region (1650°F peak) in the outer extremities of the HAZ.

SA 533 Grade B Class 1. Using a peak temperature of 1650°F the behavior for SA 533 was obtained and is shown in Figure 44. Cooling curve 'A' represents the most rapid cooling attainable in the Gleeble corresponding to approximately 20 KJ/in (1" plate). With this rapid cooling all transformation was to martensite. Cooling conditions from I to VI all pass through the bainite region, revealing the Bs and B_f transformation temperatures and at the rapid rates reveal mixed bainite-martensite transformation. The ferrite region was not revealed since it would require slower cooling rates and thus welding energy inputs not characteristic of any reasonable welding process, except for possible electro-slag.

Note that the SA 533 CCT behavior obtained by the Gleeble dilatometric technique (Figure 44) correlates well with the CCT behavior obtained by ERM (Figure 35) albeit with different times at 1650°F. The gap between B_f and Ms lines shown in Figure 44 is due to the ability of Gleeble to clearly detect start and finish points, whereas ERM is not as sensitive in detecting the finish points. The Rockwell C hardness values are shown at the end of each cooling curve. The hardness values drop gradually as the microstructure changes from full martensitic to fully bainitic.

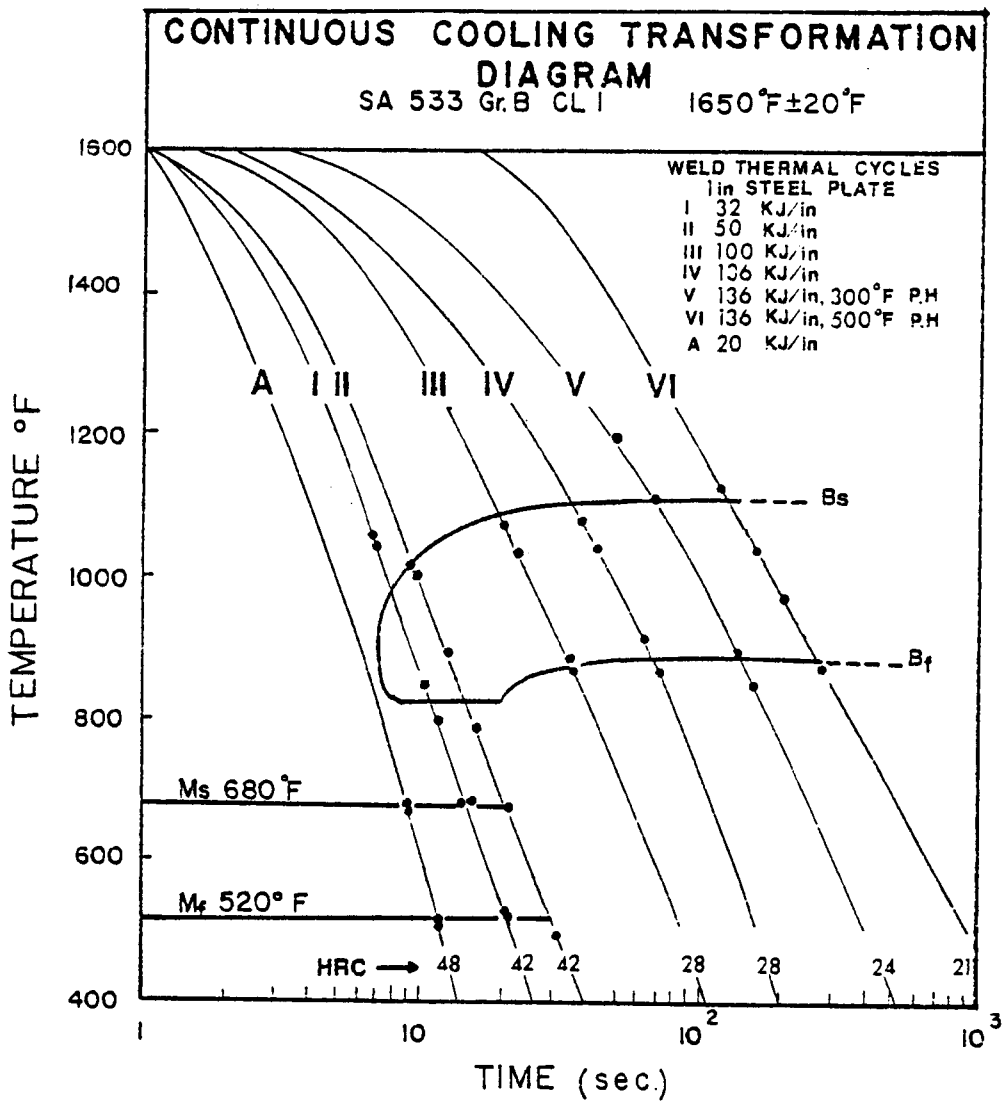

Figure 44. Continuous Cooling Transformation diagram of SA 533 Gr.B Cl 1 for a peak temperature of 1650°F.

The Ms and M_f were determined to be 680°F and 520°F, respectively. The martensitic microstructure produced by the fastest thermal cycle (curve A) corresponding to energy input of 20KJ/in. 80°F preheat (1" plate) is shown in Figure 45. For the slowest thermal cycle (curve VI) corresponding to energy input of 136KJ/in., 500°F preheat (1" plate), a bainitic structure results and is shown in Figure 46.

Similarly, thermal cycles with a 2400°F peak temperature were utilized in order to achieve a coarse-grained austenite with the maximum practical amount of the alloying elements present in solution and to effectively represent the HAZ near the fusion line. The CCT diagram using the 2400°F peak temperature cycle is shown in Figure 47. It should be noted that as the energy input increases, the integrated time at peak temperature increases and the cooling rate decreases. Cooling conditions II and III pass through the martensitic region whereas cooling conditions IV, V and VI pass through the bainitic region. The Ms and M_f in this case were 700°F and 520°F. The microstructures produced by thermal cycle II (50KJ/in., 80°F preheat) and thermal cycle VI (136KJ/in., 500°F preheat) are shown in Figures 48 and 49 respectively.

If one compares Figures 45 and 46 with Figures 48 and 49, it is clearly evident that the grain size for 2400°F peak temperature is much larger (approximately ASTM 2) than the grain size for the 1650°F peak temperature (approximately ASTM 13).

In order to clearly define the effect of peak temperature on CCT behavior, the CCT diagram obtained for peak temperature for 1650°F is superimposed on the CCT diagram for 2400°F peak temperature, as shown in Figure 50. It is observed that the higher peak temperature (2400°F)

SA 533

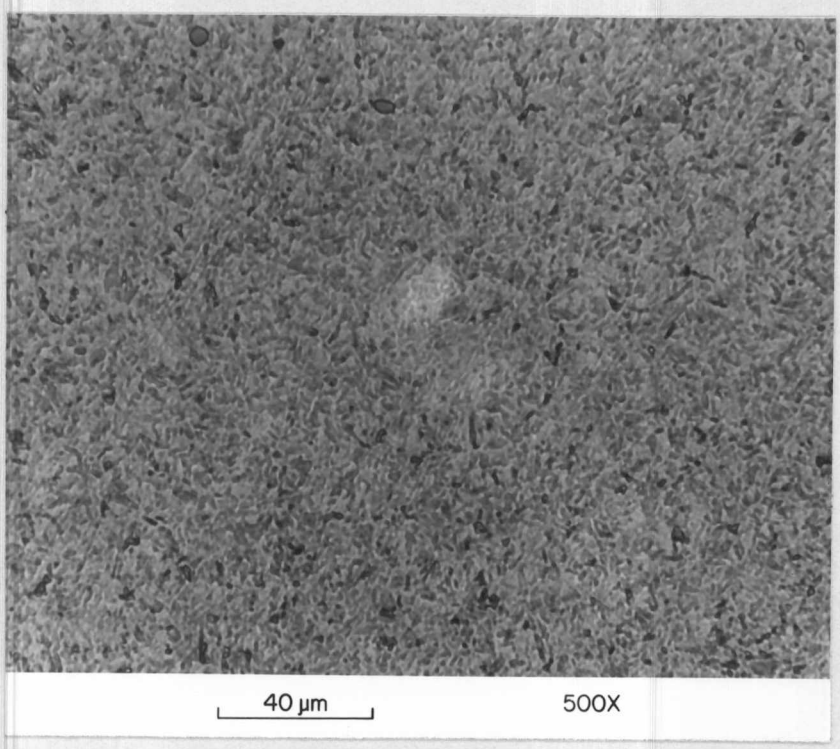

Figure 45. Microstructure corresponding to energy input 20KJ/in., 1650°F peak temperature. HRC 48. Super picral etch.

SA 533

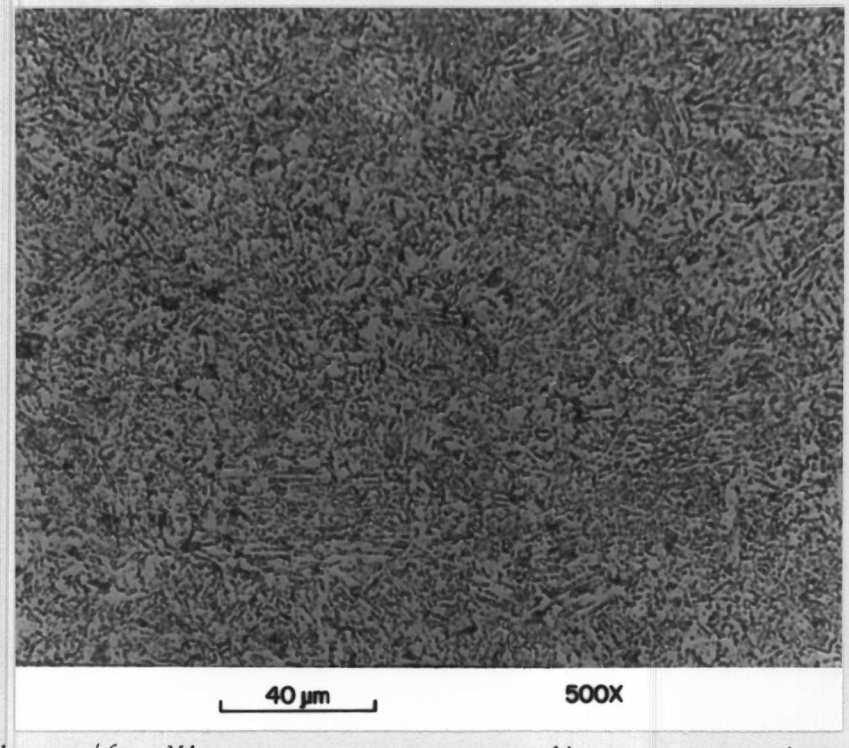

Figure 46. Microstructure corresponding to energy input of 136KJ/in., 500°F preheat, 1650°F peak temperature. HRC 21. Super picral etch.

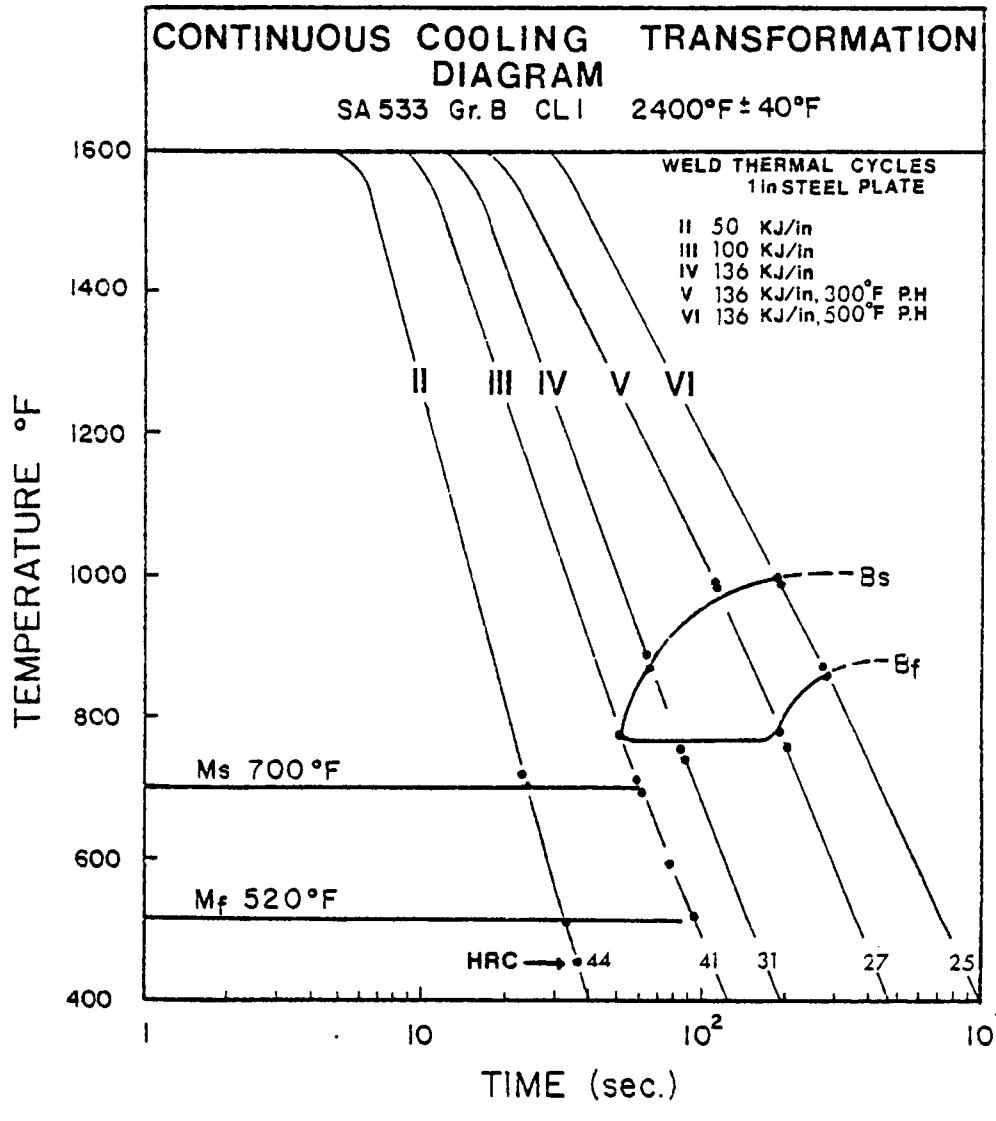

Figure 47. Continuous Cooling Transformation diagram of SA 533 Gr.B Cl 1 for a peak temperature of 2400°F.

SA 533

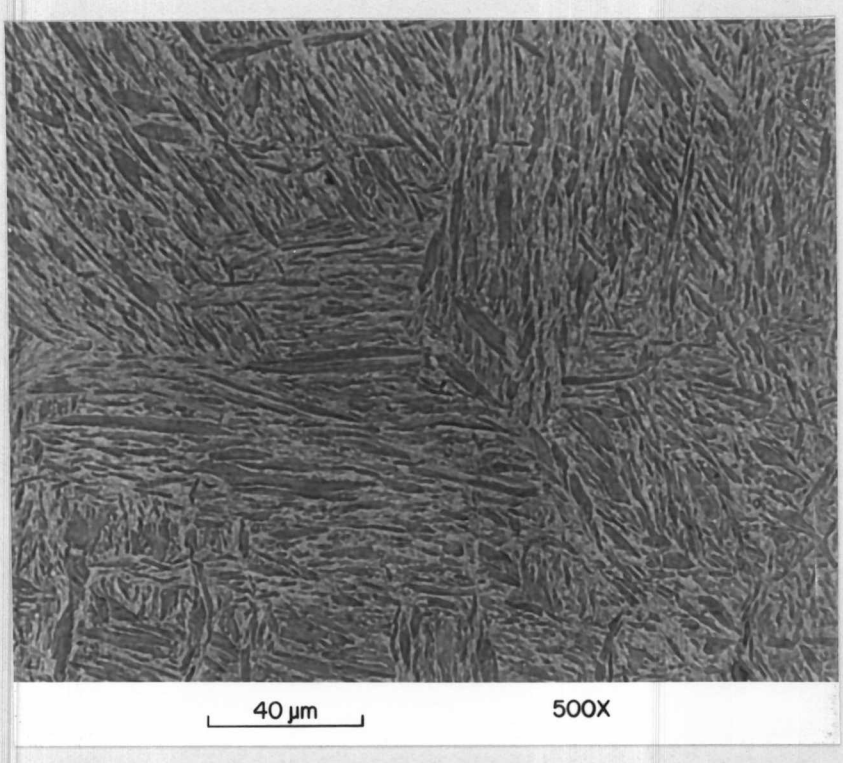

Figure 48. Microstructure corresponding to energy input of 50KJ/in., 2400°F peak temperature. HRC 44. Super picral etch.

SA 533

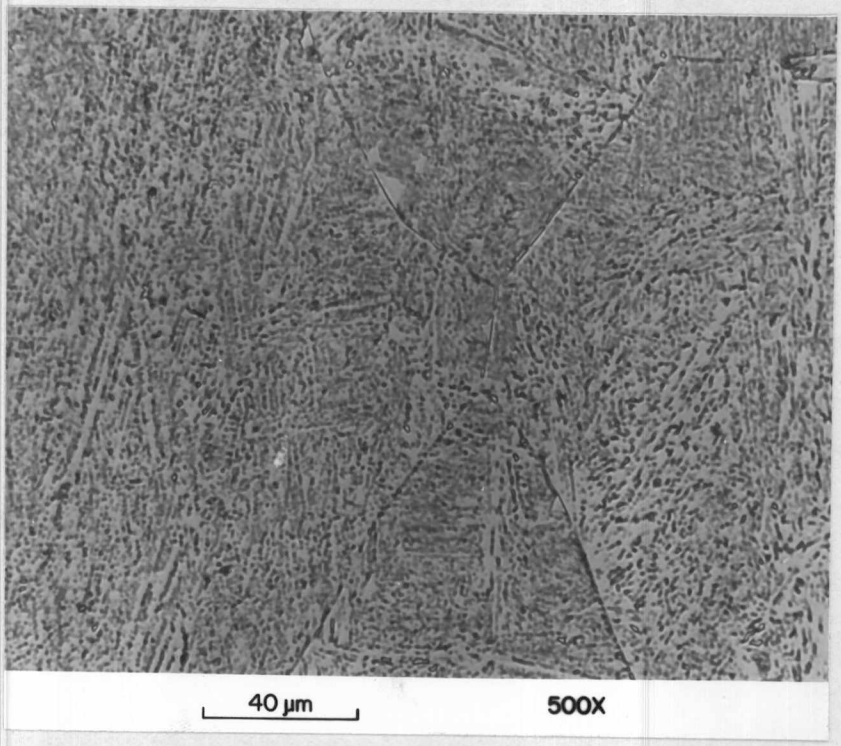

Figure 49. Microstructure corresponding to energy input of 136KJ/in., 500°F preheat, 2400°F peak temperature. HRC 25. Super picral etch.

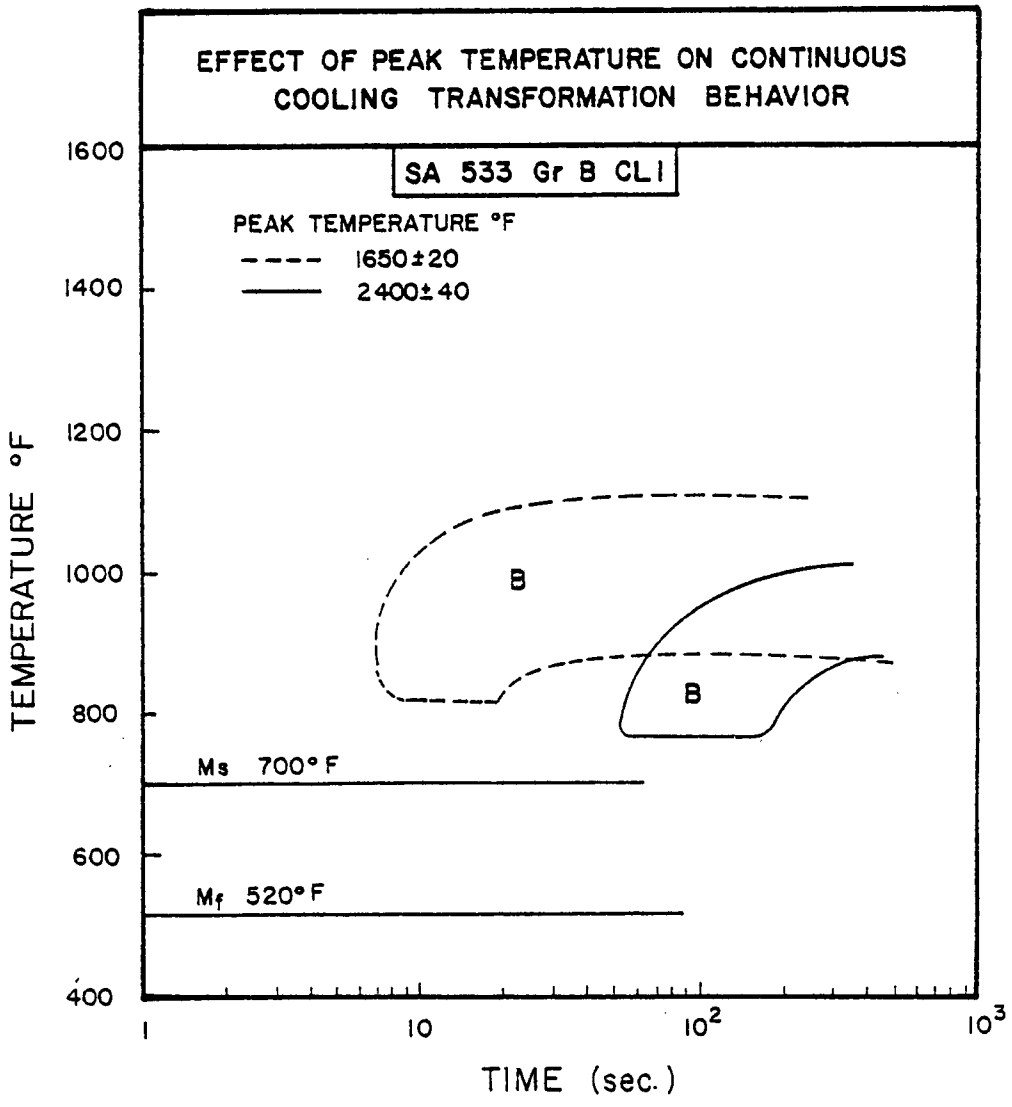

Figure 50. Effect of peak temperature on continuous cooling transformation behavior of SA 533 Gr.B Cl 1 steel.

caused the bainite nose to shift to the right and down, hence, lowering the Bs temperature taking into account the zero time difference the nose has shifted approximately 40 secs. and decreased approximately 100°F. The critical cooling rate shifts from 100°F/sec. to approximately 40°F/sec. at 1300°F. The Ms and M_f transformation temperatures are not significantly affected by the different peak temperatures.

SA 508 Class 2. The same thermal cycles utilized for determining CCT behavior for SA 533 steel were also used to determine CCT behavior for SA 508 steel. A CCT diagram for peak temperature of 1650°F is shown in Figure 51. It is observed that thermal cycle of 50KJ/in., 80°F preheat, yields a martensitic transformation, whereas in SA 533 steel, a more rapid thermal cycle of 32KJ/in., 80°F preheat did not give a martensitic transformation, this shows that the bainite nose for SA 508 steel is further to the right than that for SA 533 and the critical cooling rate shifts accordingly from 100°F/sec. to 60°F/sec. (at 1300°F.) The ERM results again correlate well with the CCT diagrams obtained in the Gleeble (1650°F for both). The Ms and M_f were determined to be 685°F and 540°F, respectively. The microstructures produced by thermal cycle I (32KJ/in., 80°F preheat) and thermal cycle VI (136KJ/in., 500°F preheat) are shown in Figures 52 and 53. These are the martensitic and bainitic transformation products, corresponding to SA 533 in Figures 45 and 46 respectively.

The CCT diagram for a higher peak temperature of 2400°F is shown in Figure 54. It is observed that the bainite start has shifted to longer times and lower temperatures. The Ms and M_f temperatures were determined to be

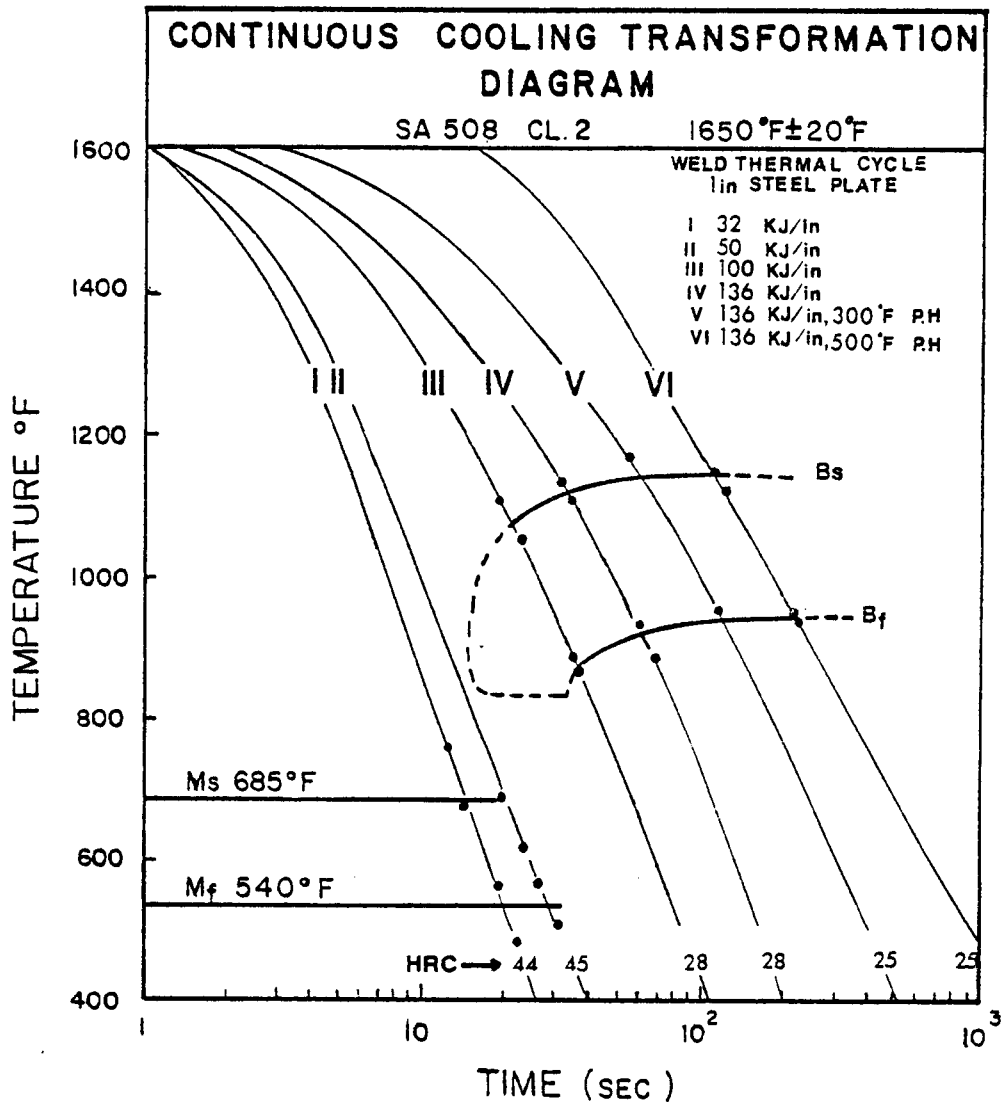

Figure 51. Continuous Cooling Transformation diagram of SA 508 Cl. 2 for a peak temperature of 1650°F.

SA 508

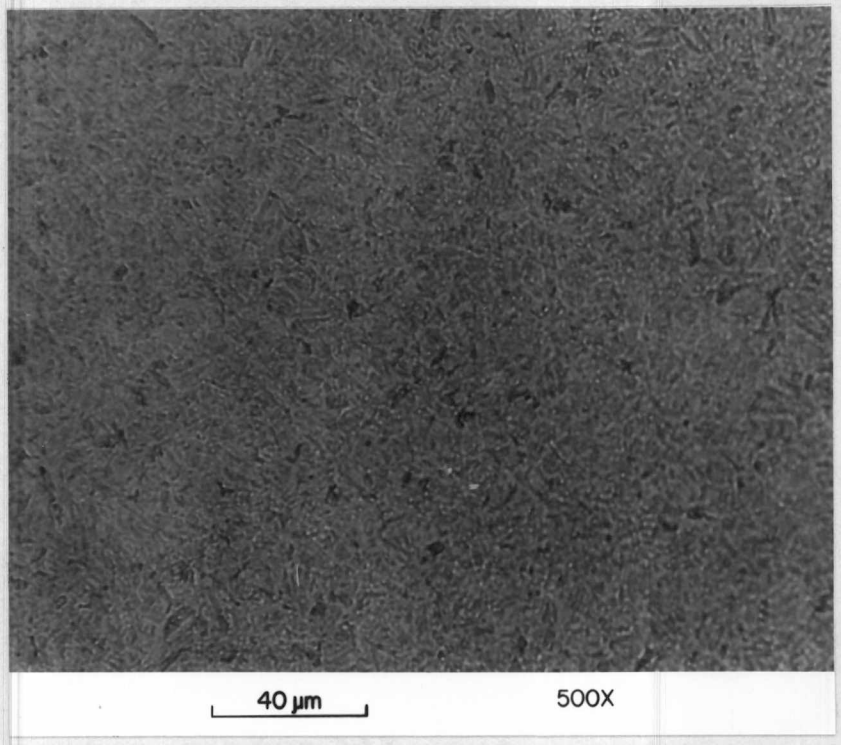

Figure 52. Microstructure corresponding to energy input of 32 KJ/in., 1650°F peak temperature HRC 44. Super picral etch.

SA 508

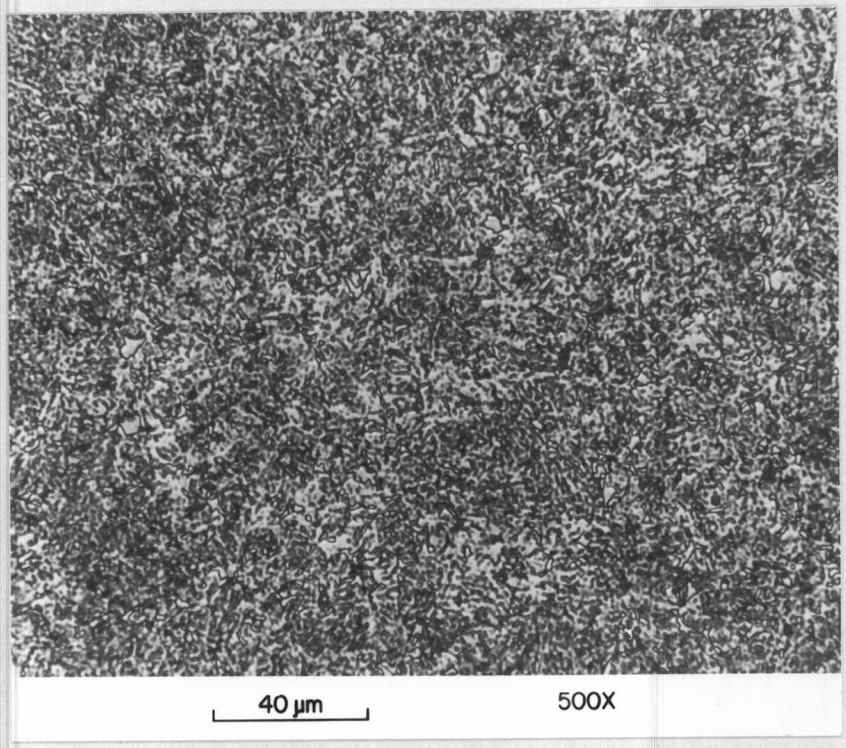

Figure 53. Microstructure corresponding to energy input of 136KJ/in., 500°F preheat, 1650°F peak temperature. HRC 25. Super picral etch.

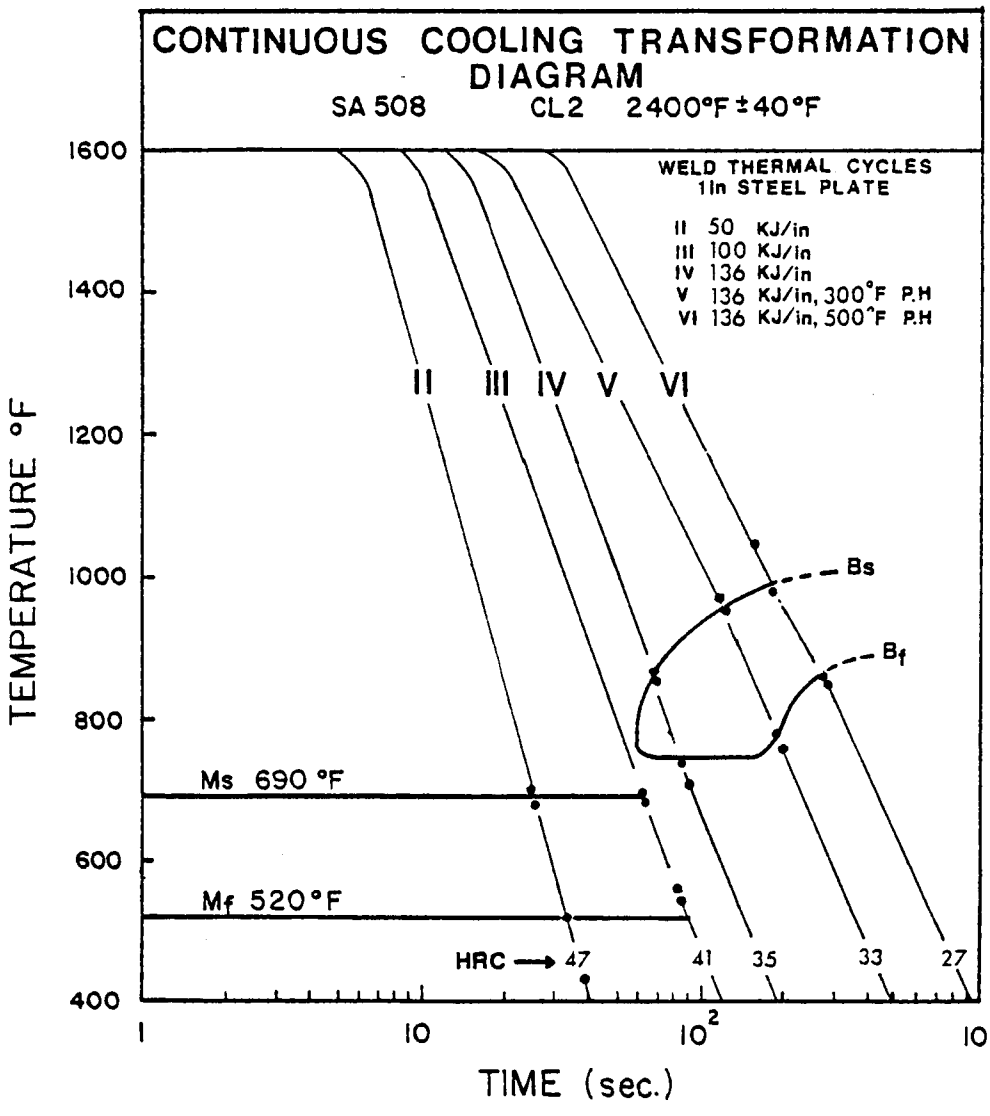

Figure 54. Continuous Cooling Transformation diagram of SA 508 Cl. 2 of peak temperature of 2400°F.

690°F and 520°F, respectively, very similar to the 1650°F Ms and M_f temperatures. The microstructures produced by thermal cycle II (50KJ/in., 80°F preheat) and thermal cycle VI (136KJ/in., 500°F preheat) are shown in Figures 55 and 56. In the case of SA 508 the ASTM grain size observed for 2400°F peak temperature is approximately 2 and for 1650°F peak temperature it is approximately 13. The data for SA 533 show identical grain sizes.

Superimposing the CCT diagram for the 1650°F peak temperature on the CCT diagram for the 2400°F peak temperature (Figure 57), it is observed that the shift of bainite nose is similar to what was observed in SA 533 steel, i.e., further to the right and to lower temperatures. (The cooling time start temperature alters this somewhat.) In this case, the nose has shifted approximately 30 secs. on the time scale and decreased in temperature approximately 100°F. Again the Ms and M_f transformation temperatures were unaffected by the different peak temperature exposures.

The CCT behavior of SA 533 and SA 508, utilizing a peak temperature of 2400°F, is virtually identical. Both CCT diagrams are shown in Figure 58. Thus, in the actual weld HAZ, both steels will have a similar transformation behavior for regions close to the fusion line. Further, it also indicates that both steels will have similar hardenability for higher peak temperatures. This conclusion is verified in the hardenability discussion to follow.

In order to note any difference in transformation characteristics upon holding at a peak temperature of 2400°F, specimens of SA 508 and SA 533 were held for 20 secs. and cooled under condition IV (136KJ/in, 80°F preheat, 1" plate.). It was observed that the transformation behavior did not change; the transformation obtained was similar to

SA 508

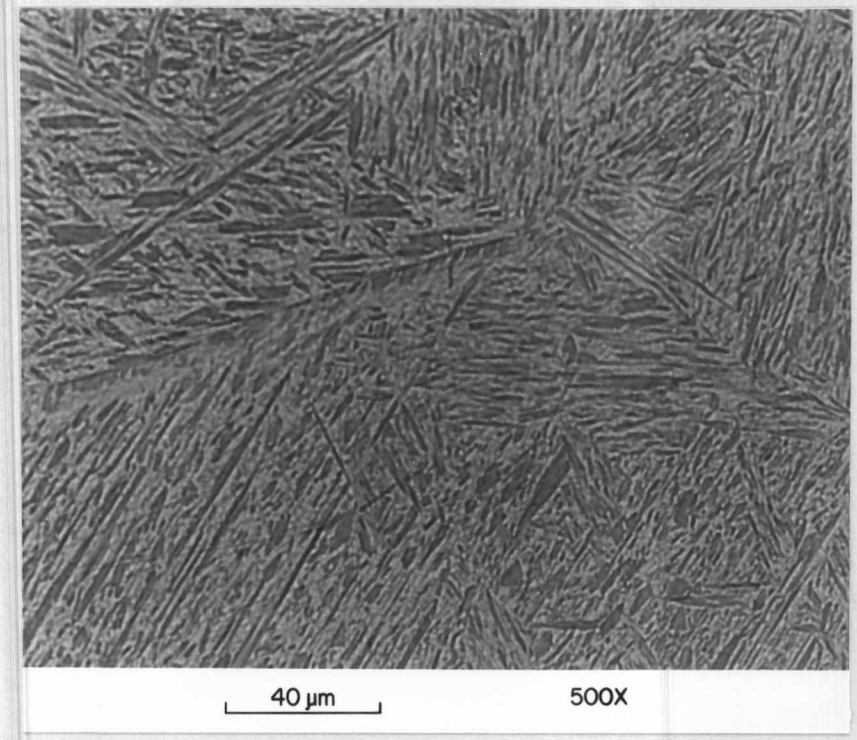

Figure 55. Microstructure corresponding to energy input of 50KJ/in., 2400°F peak temperature. HRC 47. Super picral etch.

SA 508

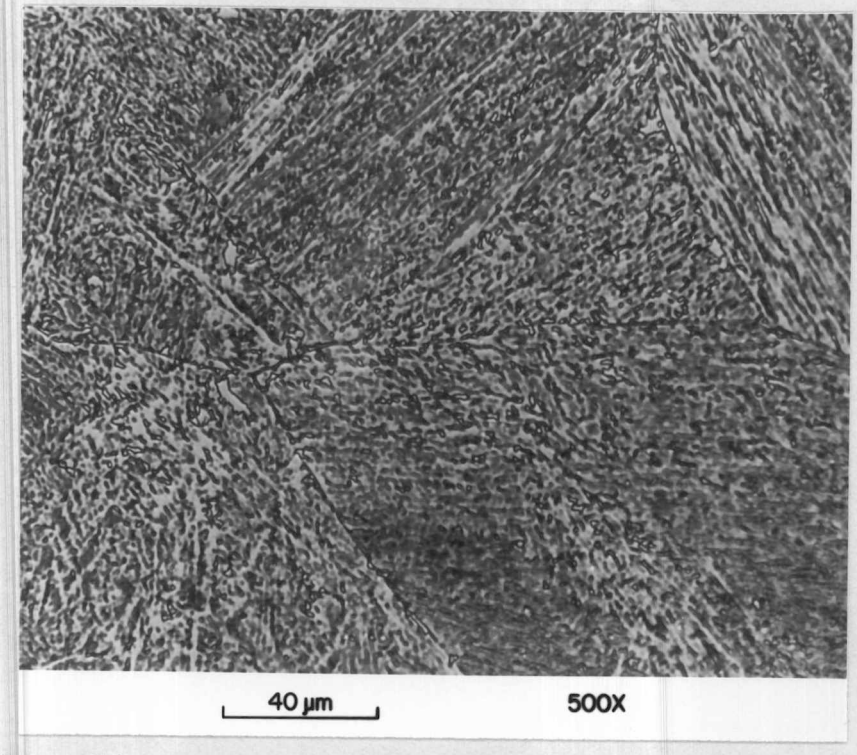

Figure 56. Microstructure corresponding to energy input of 136KJ/in., 500°F preheat, 2400°F peak temperature. HRC 27. Super picral etch.

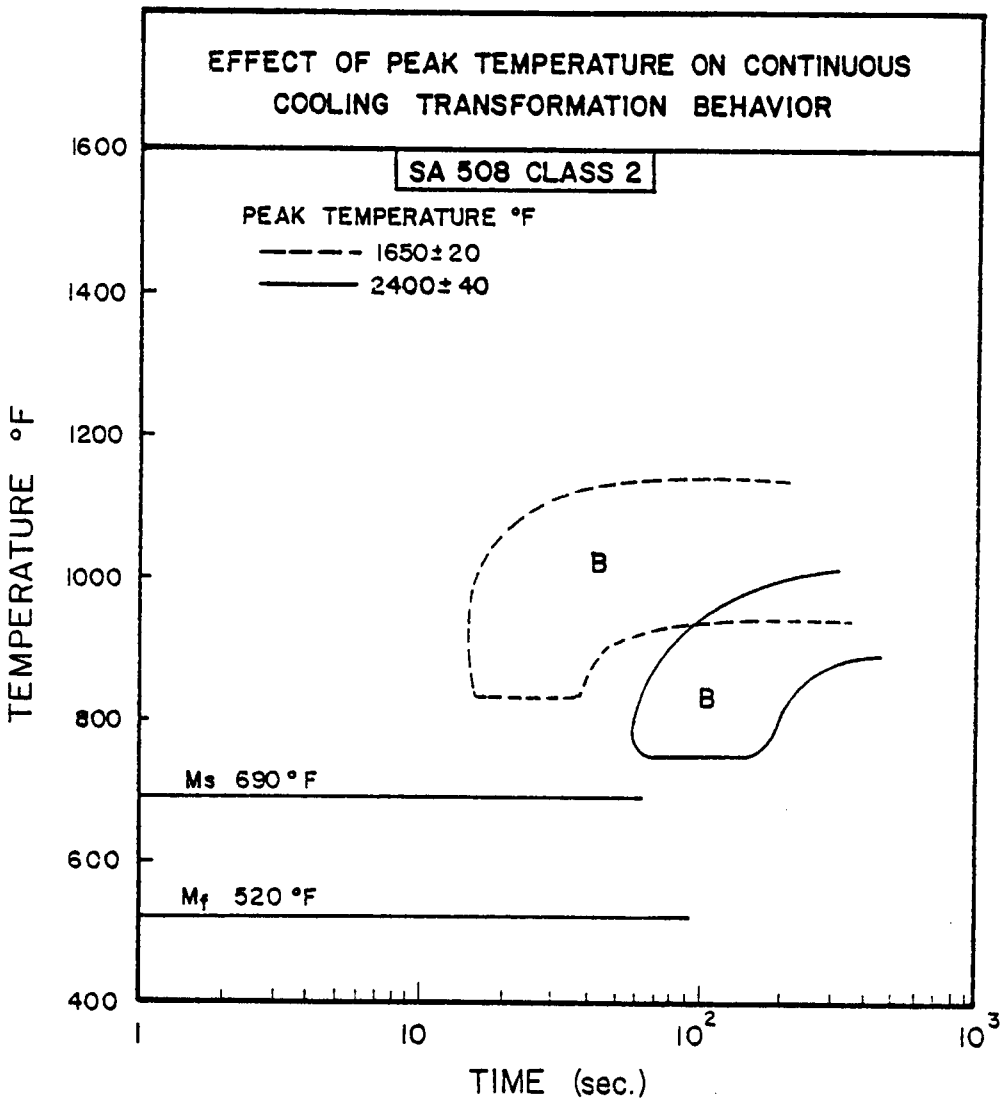

Figure 57. Effect of peak temperature on continuous cooling transformation behavior of SA 508 Cl. 2 steel.

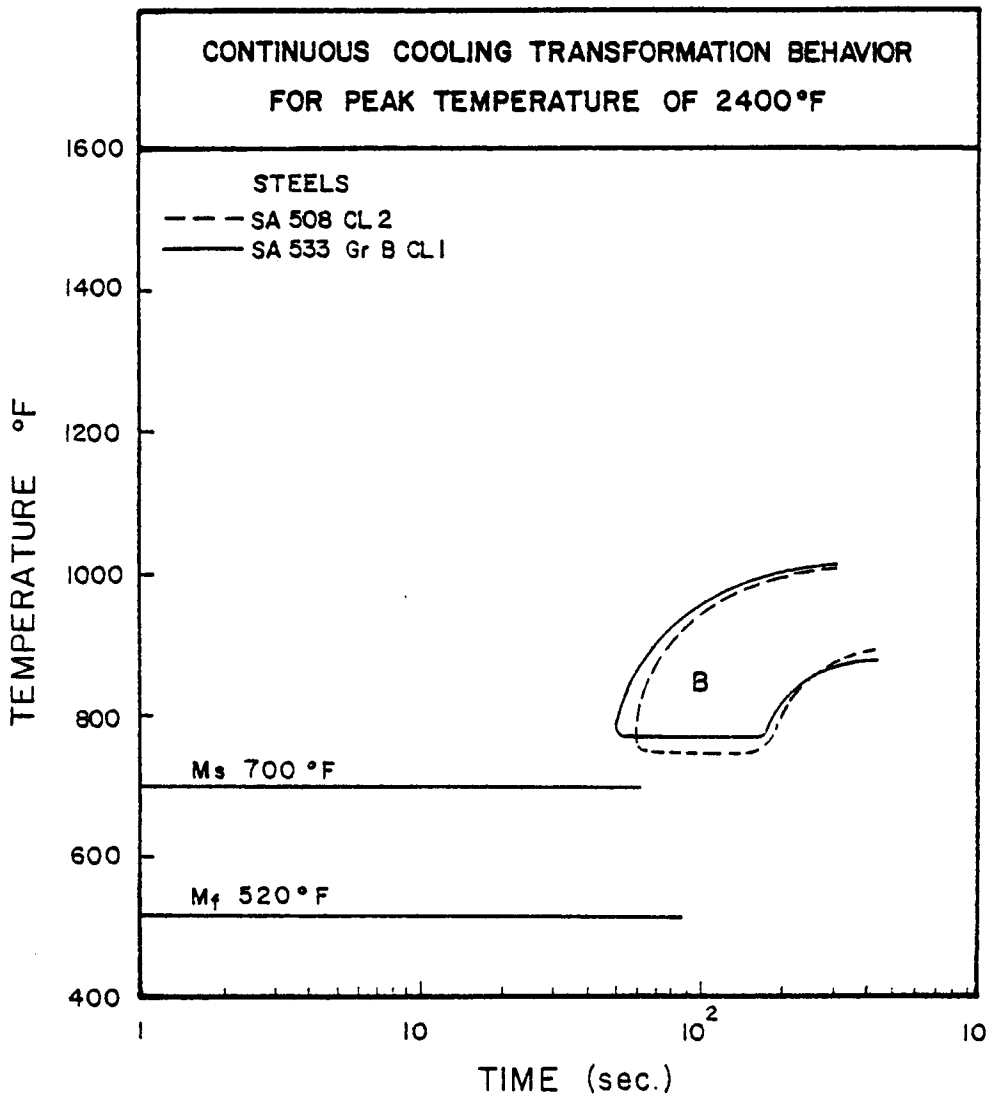

Figure 58. Comparison of Continuous Cooling Transformation behavior of SA 533 and SA 508 for a peak temperature of 2400°F.

what was observed for no holding with thermal cycle IV (136KJ/in, 80°F preheat) for both steels. This indicates that solution of alloy elements is rapid at the high peak temperatures. When a peak temperature of 1900°F was used with thermal cycle VI (136KJ/in, 500°F preheat), the transformation characteristics were similar to what were obtained by 2400°F peak temperature; this indicates that significant grain growth and solution also occurs at a 1900°F peak temperature.

Fuji Maki's[21] CCT diagram of steel "B" (see literature review), which is of a similar composition to SA 508 steel (except that steel "B" is lower in carbon content), is compared with the CCT diagram of SA 508 steel in Figure 59. Due to the lower carbon content, steel "B" has a faster critical cooling rate to avoid bainite transformation than does SA 508 steel. The critical cooling rate for steel "B" is approximately 133°F/sec, whereas for SA 508 steel it is approximately 50°F/sec. The ferrite nose in SA 508 steel is shifted further to the right than in steel "B".

Klumpes[22] discussed the PTCT diagrams of SA 508 and SA 533 exposed to several thermal cycles with peak temperatures ranging from 1650 to 2460°F. The PTCT diagrams of steels SA 508 and SA 533 showed that a cooling rate of 90°F/sec gives a fully martensitic structure. This cooling rate seems to be reasonable in comparison to the experimental results herein for SA 508 steel which had a critical cooling rate of 50°F/sec, but for SA 533 steel our experimental results show a critical cooling rate of 140°F/sec which indicates that Klumpes cooling rate of 90°F/sec would not be fast enough to form martensite. Klumpes mentioned that the depth of hardening in the case of SA 533 steel exceeds that of

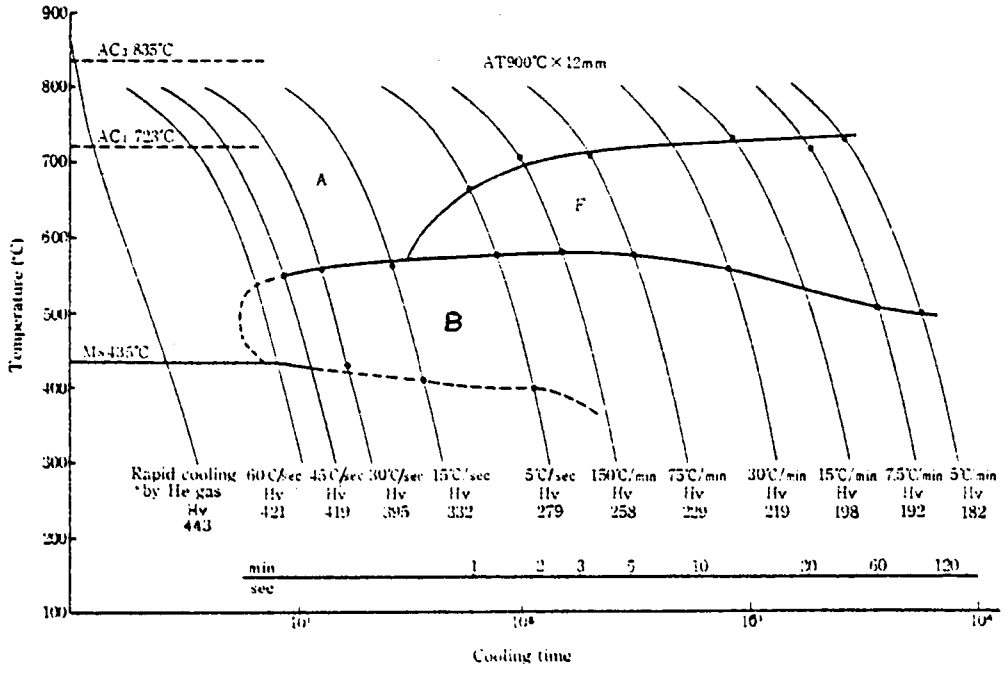

Composition : C 0.17%, Si 0.26%, Mn 0.84%, P 0.05%, S 0.06%, Cr 0.4%, Ni 0.84%, Mo 0.62%
CCT Diagram of Steel B

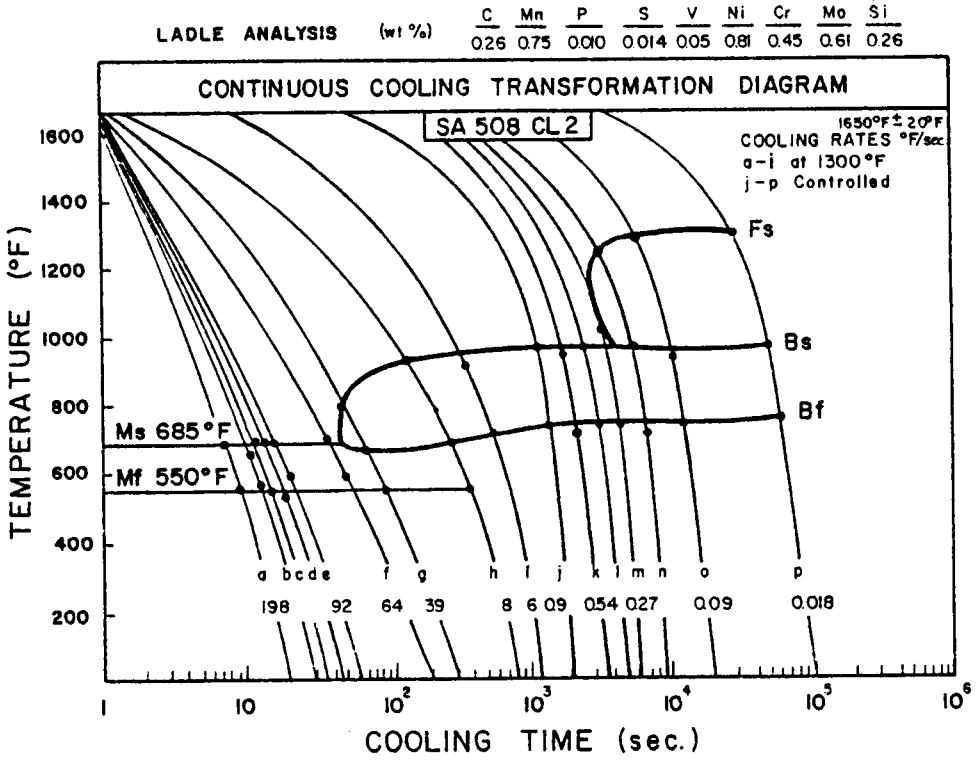

Figure 59. Comparison of CCT behavior of steel 'B' with SA 508 steel.

SA 508 steel, which means that for his steels the bainite nose in SA 533 is at a longer time than the bainite nose for SA 508. This result is totally the opposite of what we have obtained and is not predictable from chemical composition.

There is an interrelationship between energy input, preheat and plate thickness in regards to the similarity of cooling rates in welds. The thermal cycles calculated for use in this study were for 1" steel plate with different energy inputs and preheats and thus, for direct utility under other conditions the correlations predicted by other investigators are reviewed here for information. Signes[35] proposed a simple method which has been devised for predicting weld metal cooling rates for mild and low alloy steels. Using Signes method, different energy inputs were obtained for thicker plates with the same cooling rate as for 1 inch thick steel plate. These values have been summarized in Table A-4 of Appendix A and are graphically shown in Figure 60. Over 3 inches in plate thickness, the cooling rate does not change significantly with thickness (i.e., increasing the thickness further will have no influence on cooling rate). Note that Signes method gives the cooling rate of weld metals (i.e., centerline of the weld) not the HAZ. Jhaveri and his colleagues[35] mentioned that the cooling rate is a maximum on the weld centerline and the shape of the cooling rate distribution curve is such that the centerline cooling rate is only 5 to 10% higher than that in the weld HAZ, and is therefore representative of the cooling rate in the entire weld region. Figures 61 through 68 show thermal cycles for 2 inch and 3 inch plate thickness.

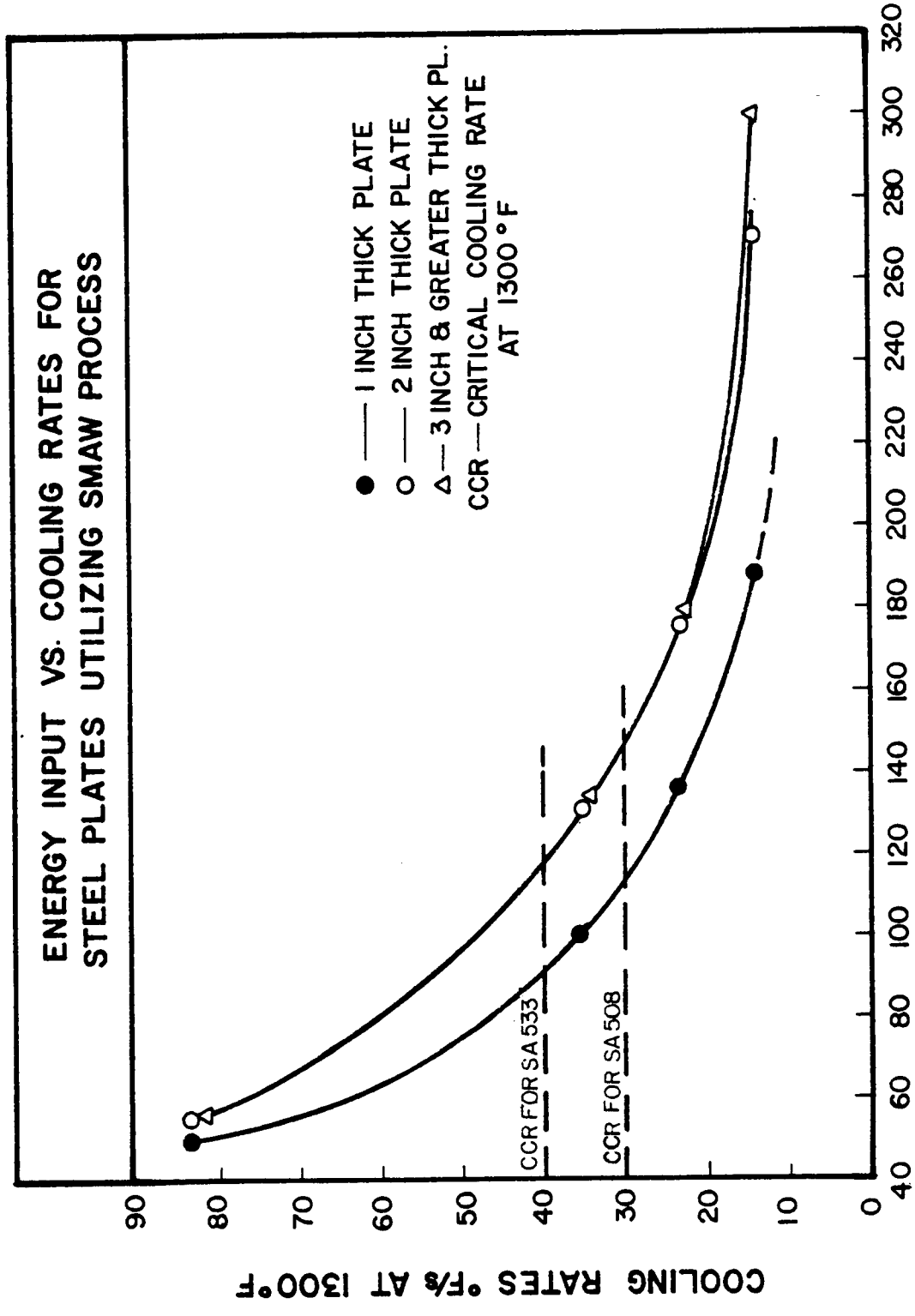

Figure 60. Energy input vs. cooling rates for steel plates utilizing SMAW process.

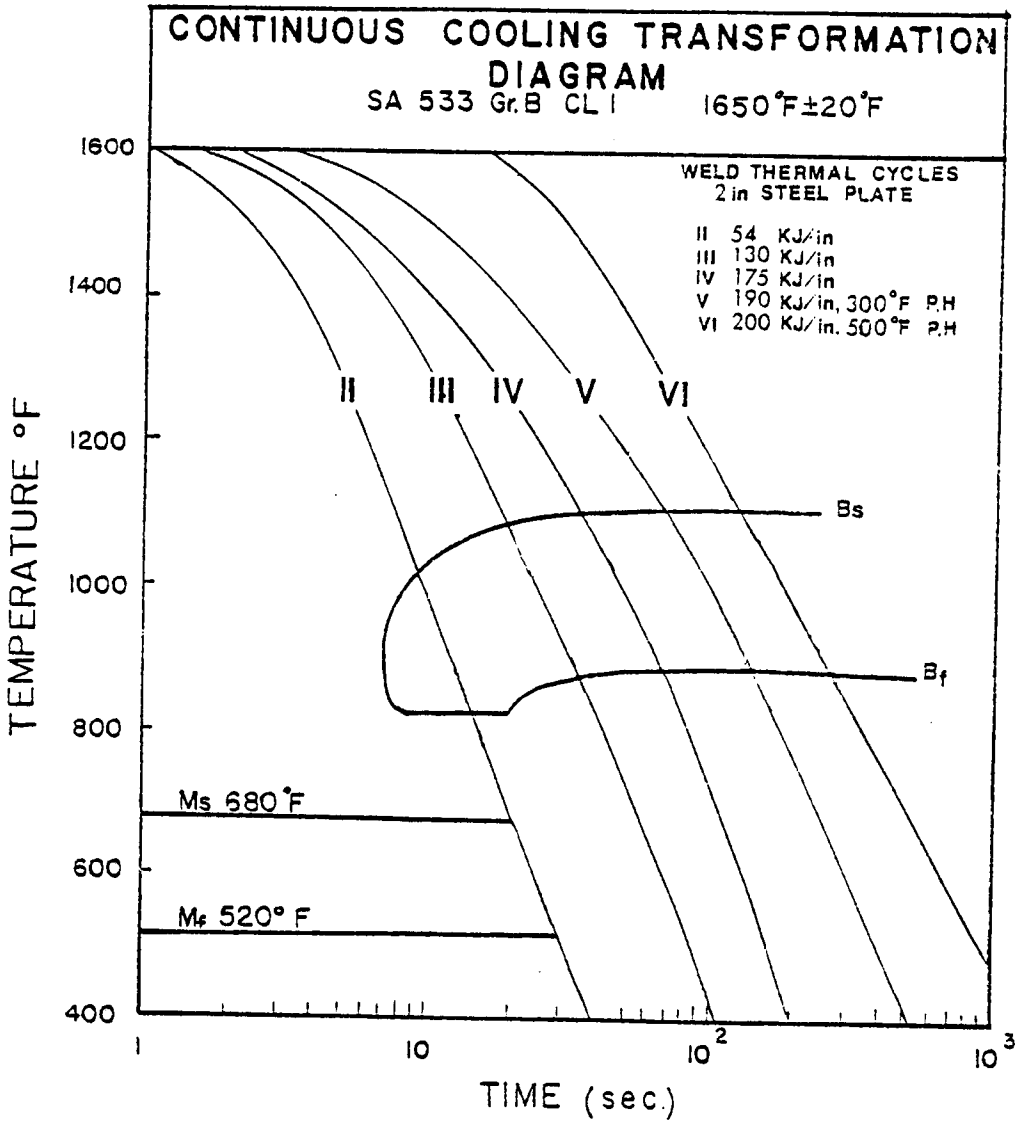

Figure 61. Continuous Cooling Transformation behavior of SA 533 for a peak temperature of 1650°F (energy inputs correspond to 2 in. steel plate).

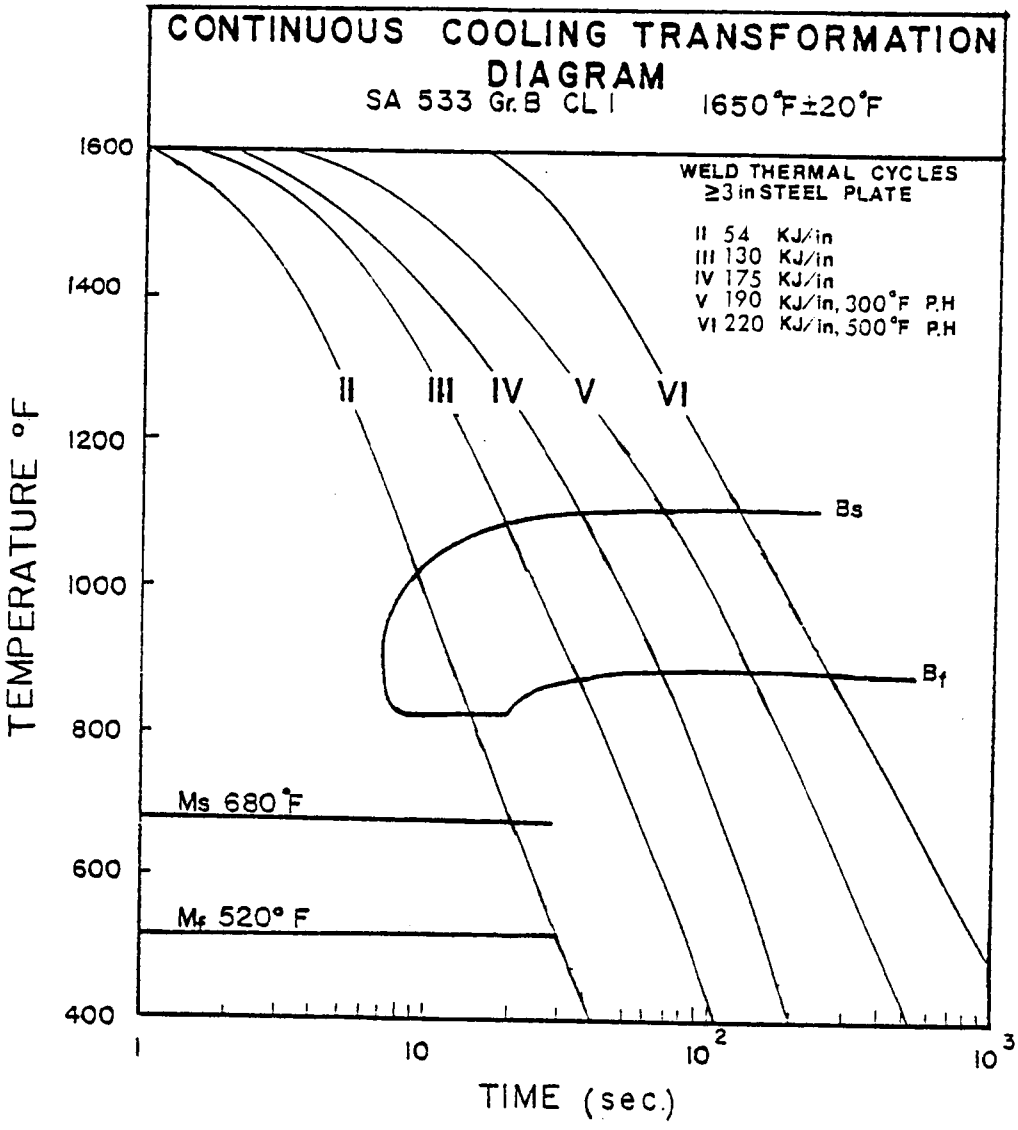

Figure 62. Continuous Cooling Transformation behavior of SA 533 for a peak temperature of 1650°F (energy inputs correspond to 3 in. steel plate.).

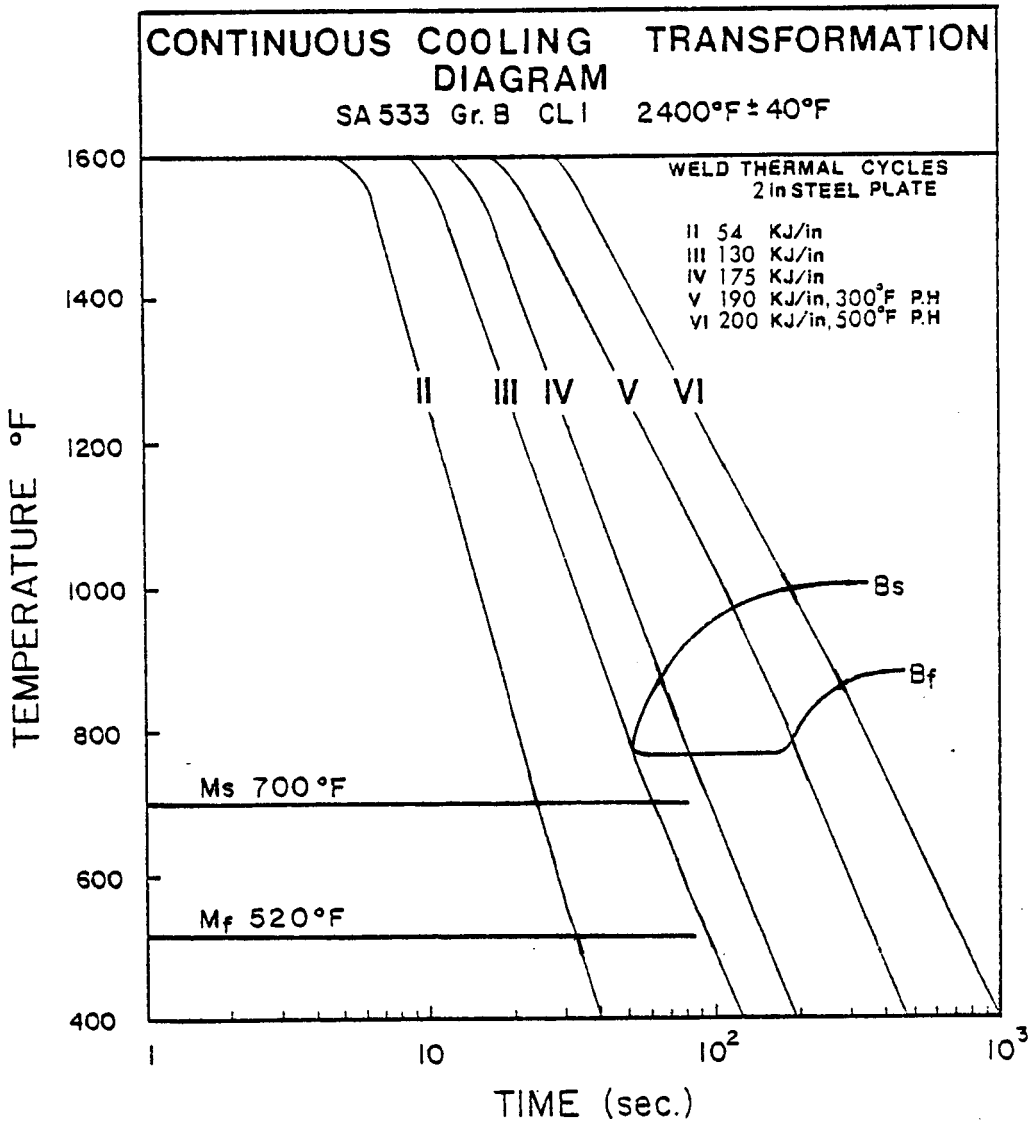

Figure 63. Continuous Cooling Transformation behavior of SA 533 for a peak temperature of 2400°F (energy inputs correspond to 2 in. steel plate).

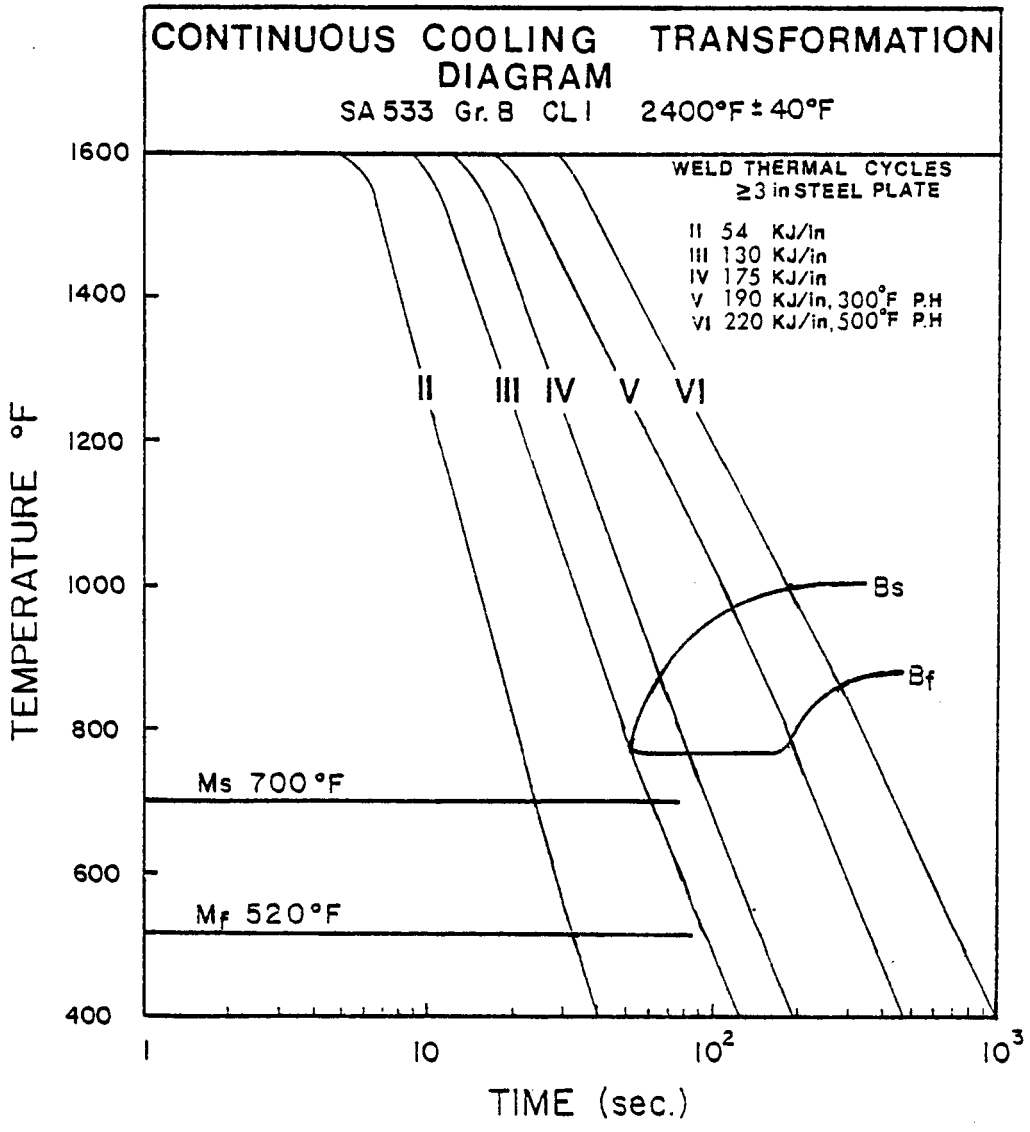

Figure 64. Continuous Cooling Transformation behavior of SA 533 for a peak temperature of 2400°F (energy inputs correspond to 3 in. steel plate).

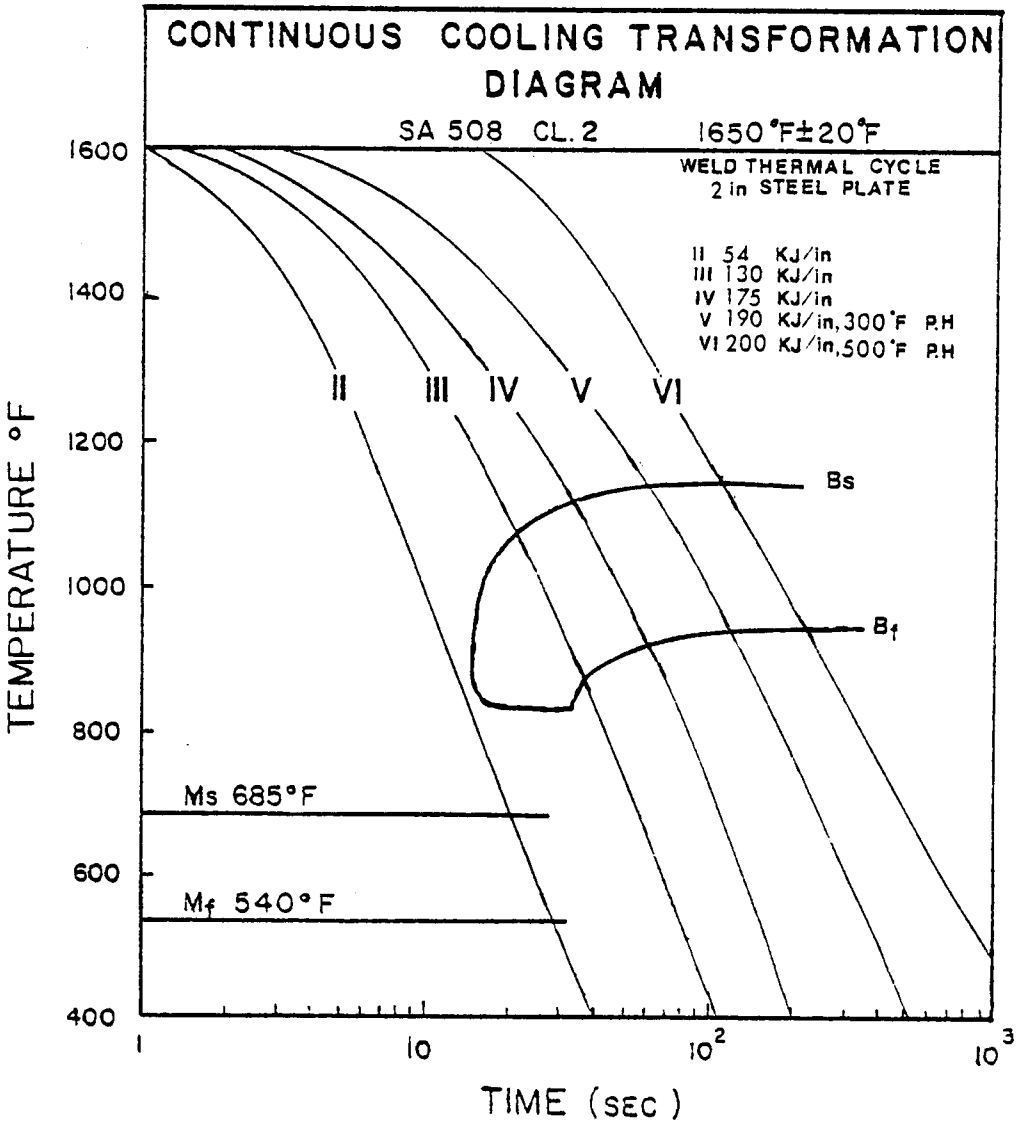

Figure 65. Continuous Cooling Transformation behavior of SA 508 for a peak temperature of 1650°F (energy inputs correspond to 2 in. steel plate).

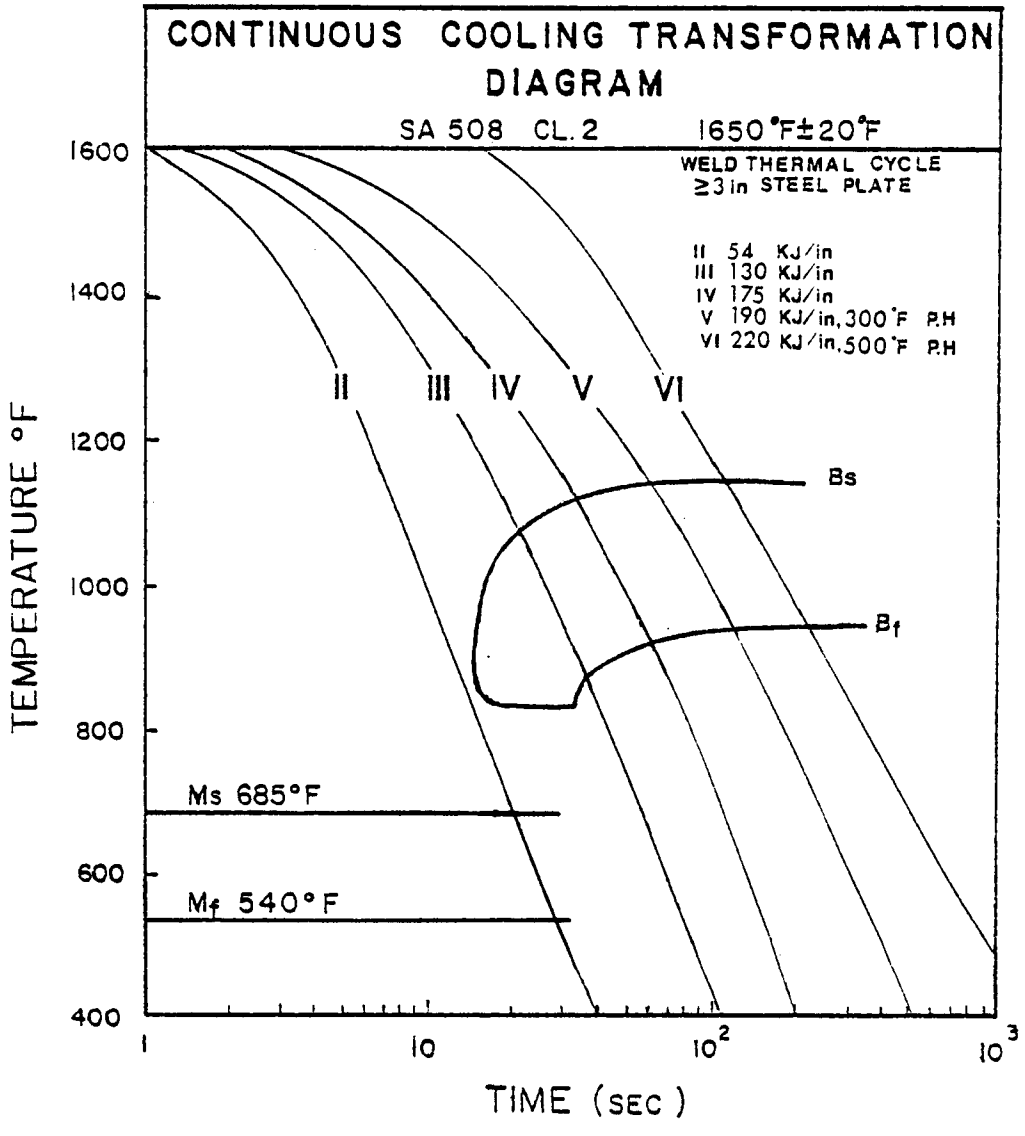

Figure 66. Continuous Cooling Transformation behavior of SA 508 for a peak temperature of 1650°F (energy inputs correspond to 3 in. steel plate).

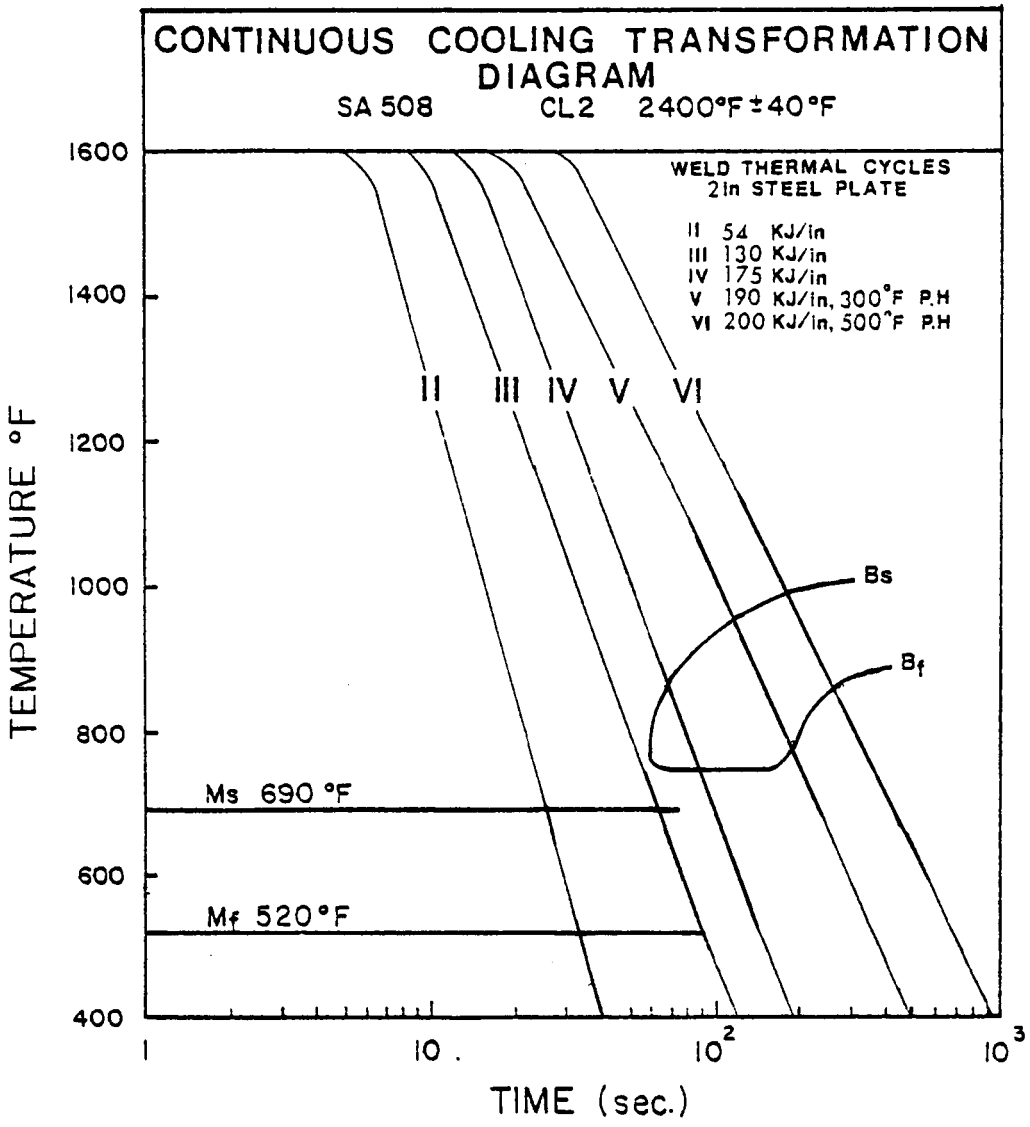

Figure 67. Continuous Cooling Transformation behavior of SA 508 for a peak temperature of 2400°F (energy inputs correspond to 2 in. steel plate).

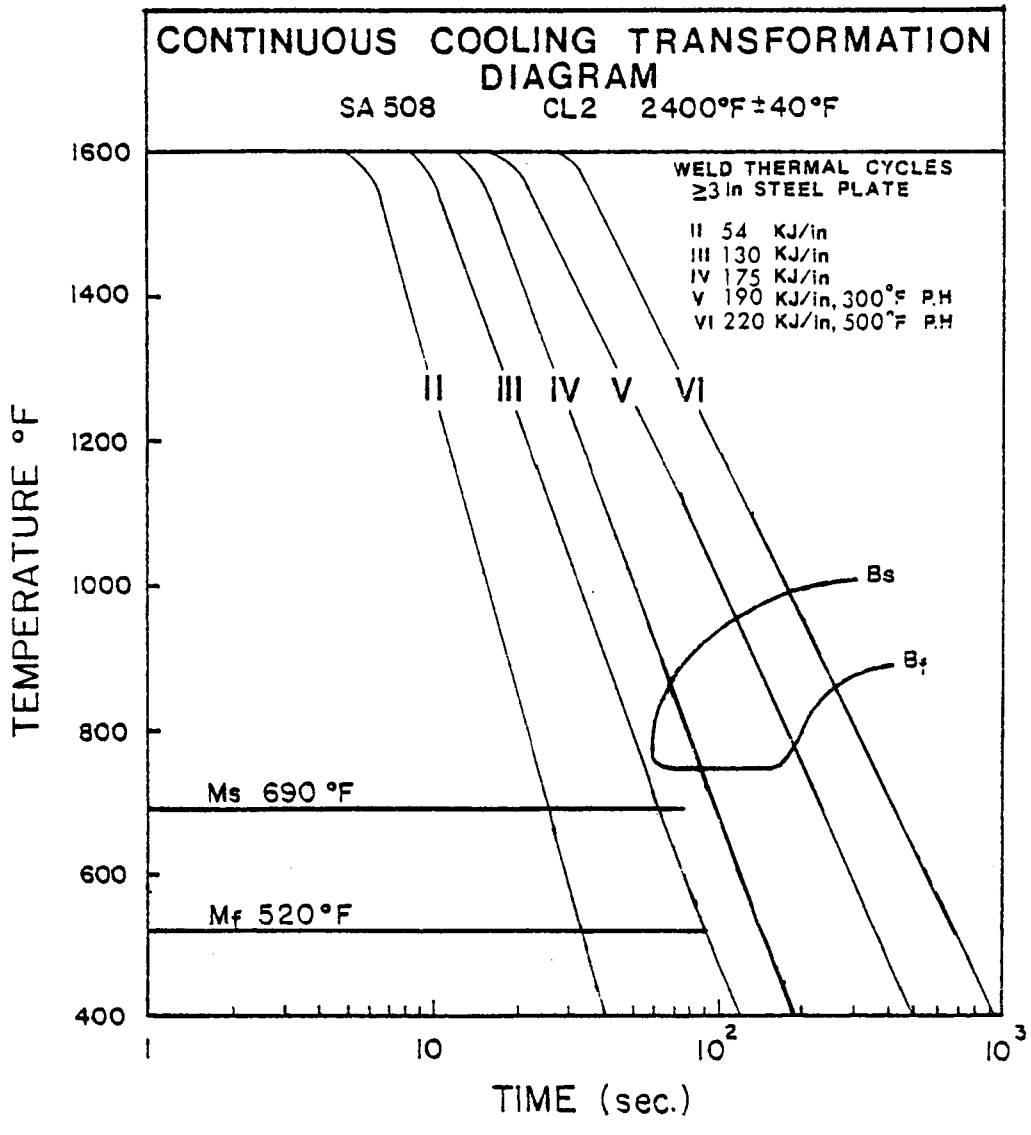

Figure 68. Continuous Cooling Transformation behavior of SA 508 for a peak temperature of 2400°F (energy inputs correspond to 3 in. steel plate).

Hardenability of SA 533 and SA 508

The study of hardenability in steel is the study of the transformation kinetics of austenite. Austenitizing temperatures for hardening heat treatments are usually chosen to be high enough so that all alloy additions are in solution, to maximize their hardenability effect, but not too high to coarsen the austenite grain size to the point that it detracts from toughness of the hardened steel. At higher austenitizing temperatures a more homogeneous austenite is achieved, which reduces nucleation sites for high-temperature transformation, thus increasing hardenability. Time at the austenitizing temperature also influences hardenability, primarily because time is needed to achieve austenite homogeneity.

Hardenability tests were conducted for SA 533 and SA 508 materials according to the ASTM standard A 255. The hardenability curves are shown in Figure 69. It is observed from Figure 69 that SA 508 has the higher hardenability than SA 533. Hardness at the quenched end for SA 533 is HRC 38 and for SA 508 is HRC 46. Hardenability curve for SA 508 shows a drop in hardness at approximate cooling rate of 42°F/sec at 1300°F. Similarly, the curve for SA 533 shows a drop in hardness at approximate cooling rate of 125°F/sec at 1300°F, and the hardness further decreases with slower cooling rates.

A correlation between the CCT behavior obtained by ERM with the hardenability curves is shown in Figures 70 and 71. It is noticed that critical cooling rate for SA 533 is approximately 140°F/sec at 1300°F, whereas, with the Jominy curve, a hardness drop is noticed at cooling rate of 125°F/sec at 1300°F. This hardness drop proves that bainite

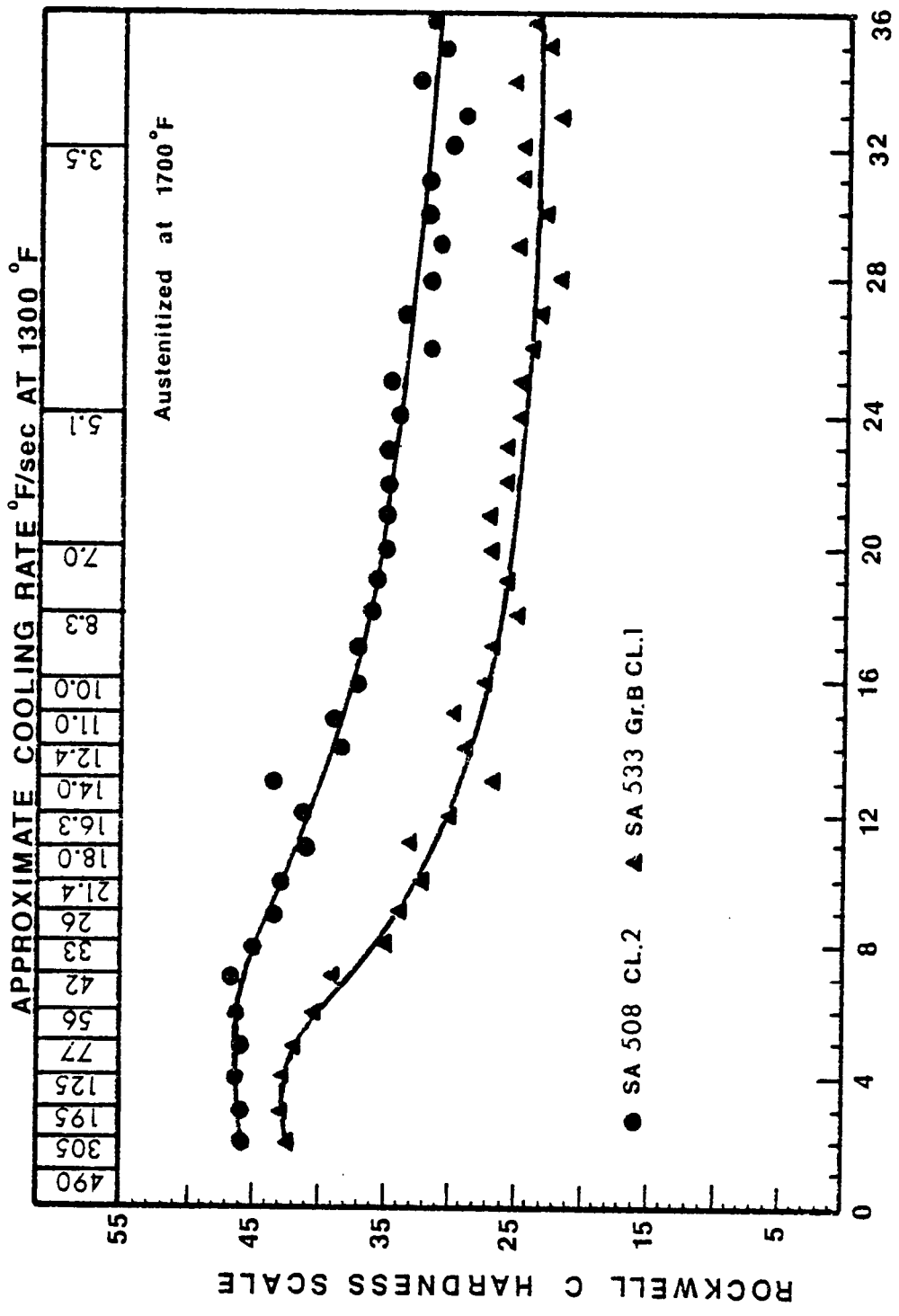

Figure 69. Hardenability curves for SA 508 and SA 533 steels.

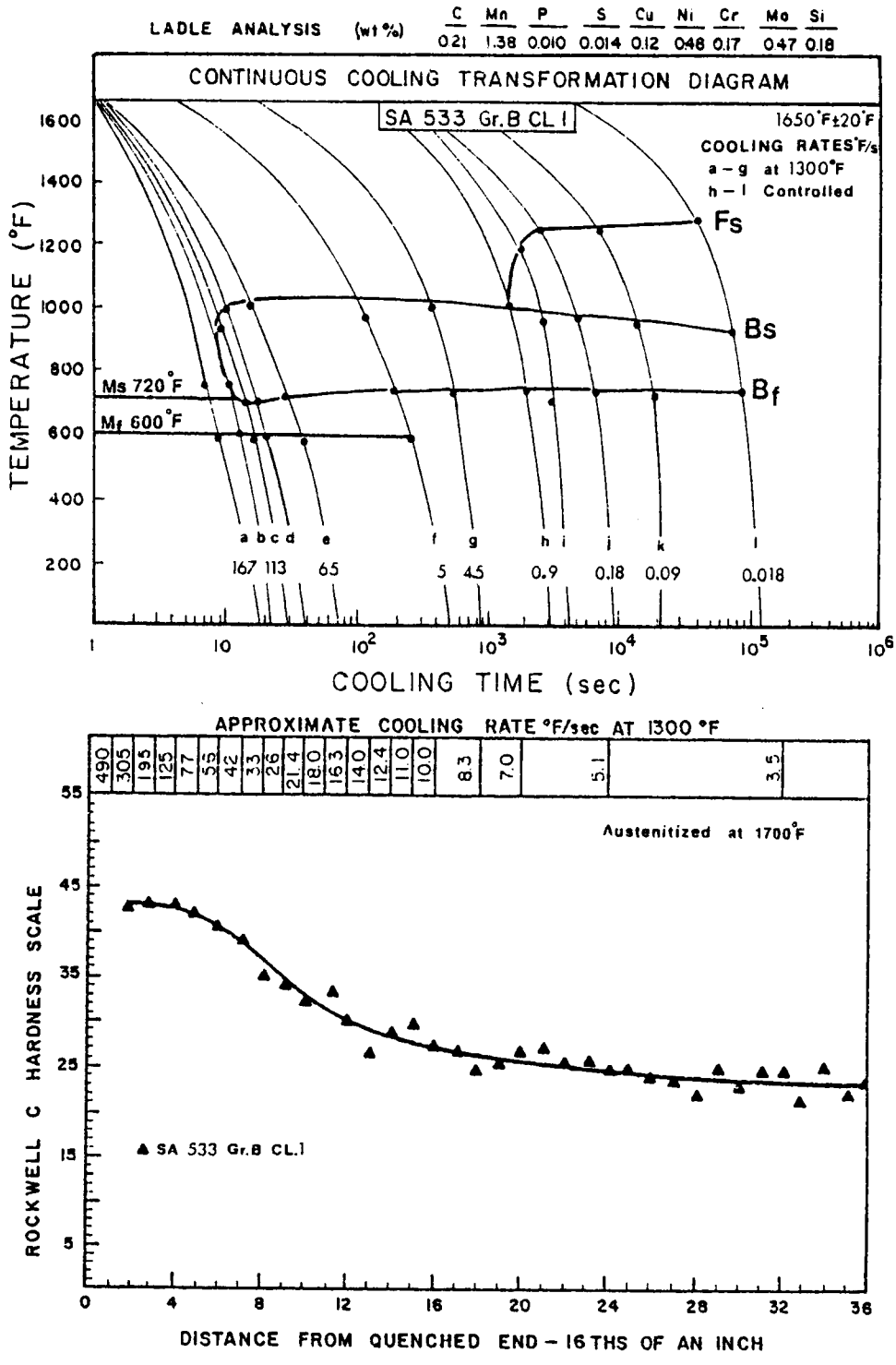

Figure 70. Correlation of CCT and hardenability curves of SA 533.

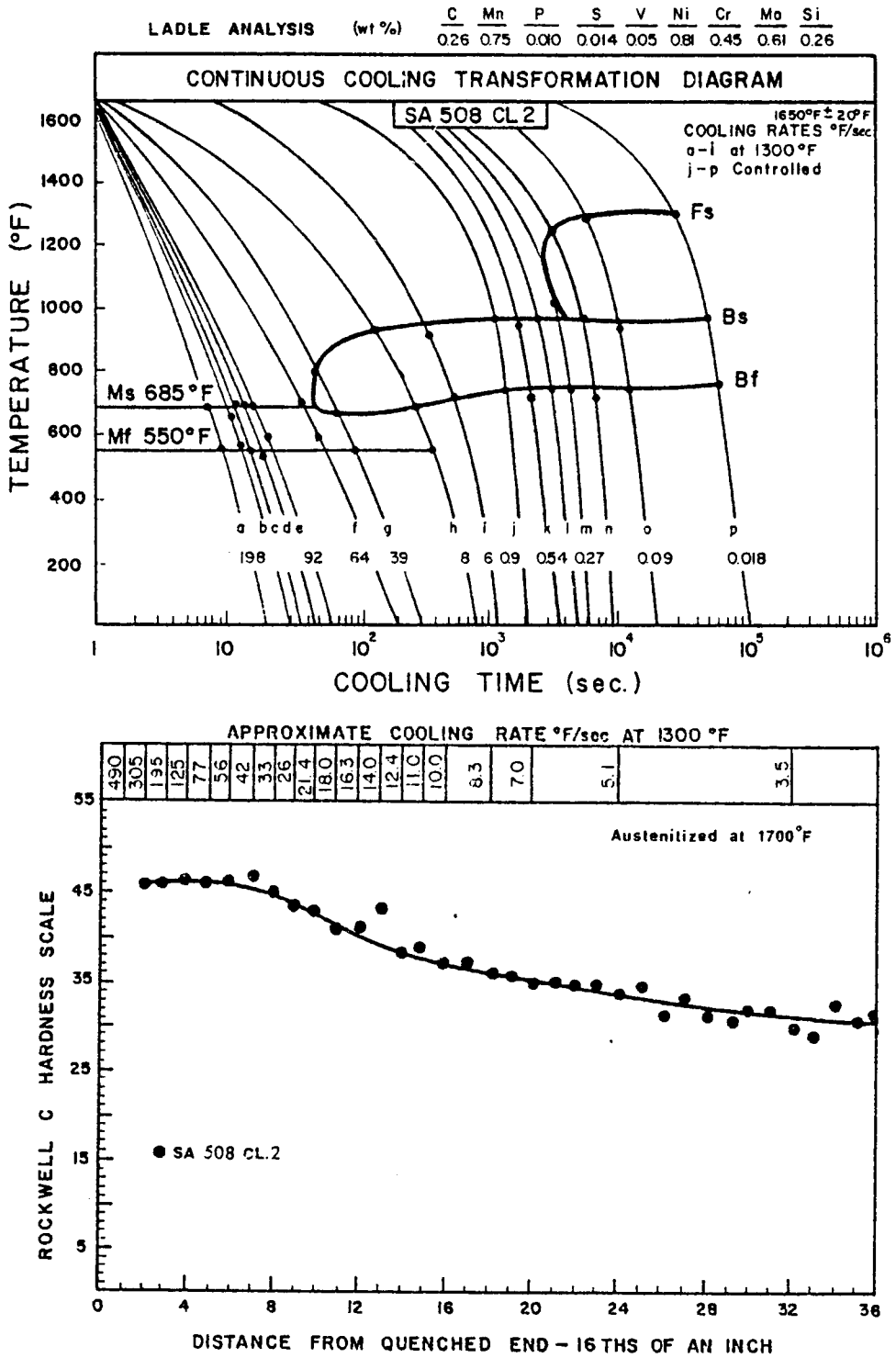

Figure 71. Correlation of CCT and hardenability curves of SA 508.

formation has occurred. Similarly, in SA 508 the critical cooling rate is approximately 50°F/sec at 1300°F, and the Jominy curve shows a drop in hardness at approximate cooling rate of 42°F/sec at 1300°F. This also proves that bainite formation has occurred.

Jominy bars were also austenitized at a higher temperature (2200°F) in addition to the standard 1700°F. The main purpose was to achieve a larger grain size. The larger grains affected the hardenability curves as shown in Figure 72. Due to the higher austenitizing temperature of 2200°F, the hardenability of both steels has increased further over that which was obtained for an austenitizing temperature of 1700°F. Note that the depth of hardness for both steels is almost identical, which indicates that at higher temperature, both steels have similar hardenability. This result agrees with the CCT diagrams for SA 533 and SA 508 as determined dilatometrically for peak temperature of 2400°F which was shown in Figure 58.

In order to better define the transformation characteristics of steel SA 533 and SA 508, the Jominy bars were also examined metallographically, by sectioning longitudinally. The microstructure was martensitic at the quenched-end and gradually changed to a martensitic-bainitic structure as the distance from the quenched end increased. The Jominy bar with the higher austenitizing temperature exhibited a larger grain size.

Cold Cracking

The most intensive research in the field of weldability has been that concerned with "cold cracking." This type of cracking originates primarily in the HAZ of base metals. The cracking is brought about through the embrittlement effects of hydrogen in a predominantly

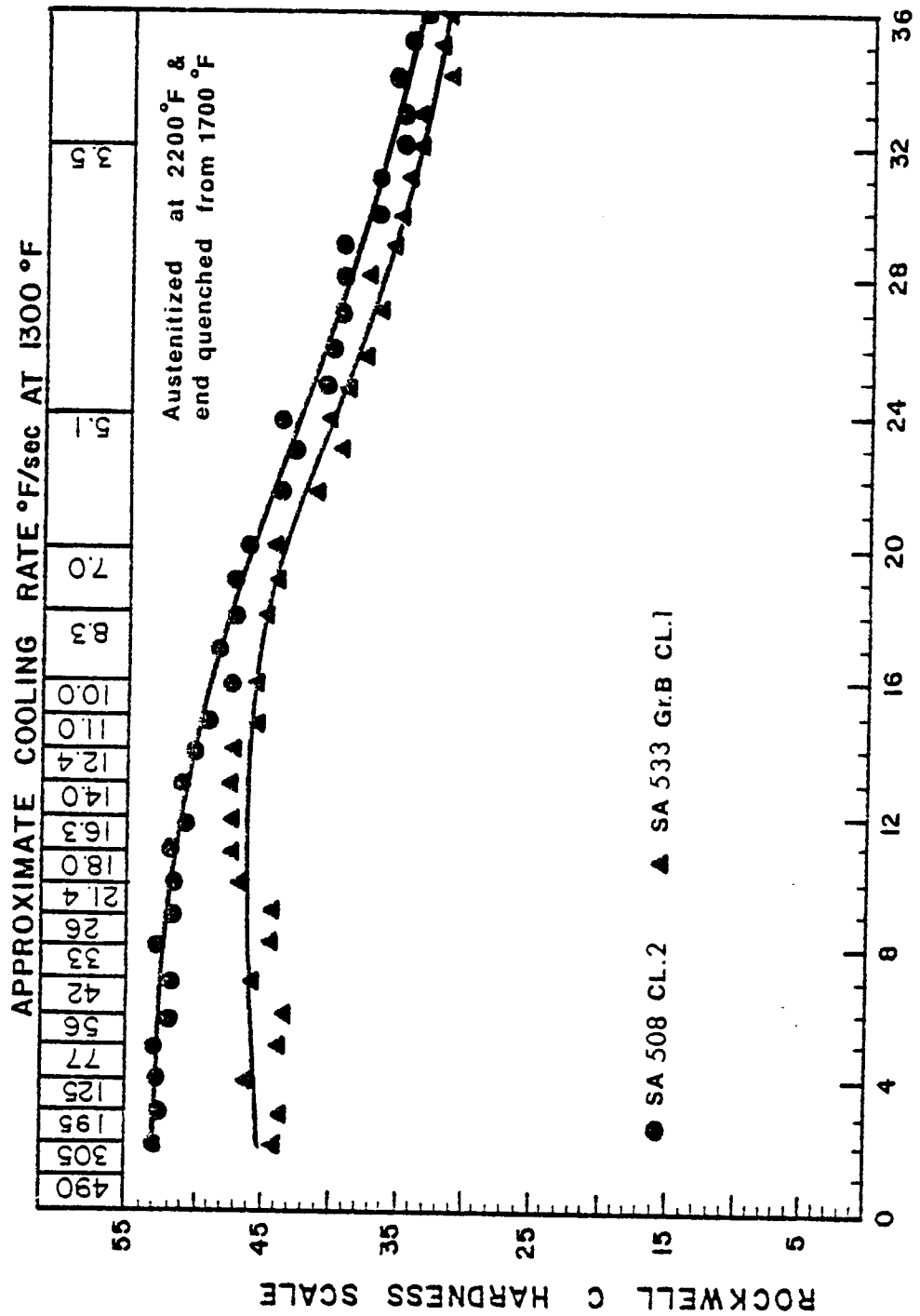

Figure 72. Hardenability curves for SA 508 and SA 533 steels, austenitized at 2200°F.

martensitic structure, the dynamic stresses of austenite-martensite transformation and/or residual stress state.

In the welding of certain low alloy steels, a better understanding of the mechanisms involved in hydrogen induced cold cracking is required. It is usually assumed that cold cracking is associated with hydrogen embrittlement of martensite or bainite and that it is initiated by high residual stresses developed in the weld joint during cooling.

Hydrogen induced cracking is brought about in the heat affected zone if four factors occur simultaneously:

1. Hydrogen is present. This is derived from the moisture in the fluxes used in welding and other sources. It is absorbed by the weld pool and transferred to the heat-affected zone by diffusion.
2. Tensile stresses act on the weld. These arise due to thermal contractions during cooling supplemented by stresses generated due to the rigidity of parts to be joined.
3. A susceptible HAZ microstructure is present. That region of the base metal which experiences a high temperature for the parent steel to transform rapidly from ferrite to austenite and back again produces microstructures which are more susceptible to hydrogen embrittlement than other regions of the HAZ.
4. A low enough temperature is reached. The greatest risk of cracking is close to ambient temperature and hence cracking may take place several hours after welding has been completed. Cracks in the HAZ may be in the weld toe, the weld root or in an underbead position.

Battelle Underbead Cracking Test

Underbead cracking is one of the forms of hydrogen-induced cracking. Introduction of hydrogen into weldments can result due to the dissociation of moisture in organic compounds present in the welding flux, moisture in shielding gas, moisture on steel surface, etc. The greatest problems arise in shielded metal-arc welding where the flux coating may often contain large amounts of hydrogen bearing materials.

The Battelle underbead tests for SA 533 and SA 508 were conducted at different preheat temperatures, ranging from 32°F to 300°F. The procedure applied was the one developed by Battelle Memorial Institute (discussed previously in the experimental section). After sectioning the specimen longitudinally (along the weld bead), the cross section of weld bead is polished, etched and examined microscopically. It was observed that SA 533 specimens welded at 32°F to 200°F showed underbead cracking, whereas specimens welded at 300°F showed no cracking. Similarly, for SA 508, underbead cracks appeared in specimens welded from 32°F to 300°F and at 400°F no cracking was observed. Table 6 summarizes results for both materials.

It is possible to avoid cracking in a susceptible microstructure by maintaining the material at a sufficiently high temperature until the microstructure has softened, by tempering, to render it less susceptible. This principle is employed as post weld hold treatments at the original preheat temperature.

An increase in temperature increases the diffusion rate of hydrogen and hence, accelerates its removal from the weld. Any measure which slows down the weld cooling rate is also helpful in reducing the

TABLE 6

RESULTS OF BATTELLE UNDERBEAD CRACKING TESTS

Materials	Pre-heat or Pre-cooled Temperature (°F)	Observations
SA 533 Gr.B Cl.1	32	crack
	85	crack
	200	crack
	300	no crack
SA 508 Cl.2	32	crack
	85	crack
	200	crack
	300	fine crack
	400	no crack

TABLE 7

RESULTS OF UNIVERSITY OF TENNESSEE HYDROGEN SUSCEPTIBILITY TESTS

Materials	Pre-heat or Pre-cooled Temperature (°F)	Observations
SA 533 Gr.B Cl.1	32	crack
	90	crack
	300	crack
	400	crack
	500	no crack
SA 508 Cl.2	32	crack
	90	crack
	300	crack
	500	crack
	600	no crack

hydrogen level and promoting softer microstructures. Thus, preheat, by slowing the cooling rate not only softens the microstructure but also helps hydrogen to escape. Two micrographs of underbead cracks are shown in Figure 73. The cracks are formed just below the weld bead and run parallel to the fusion line; the cracks tend to be transgranular but responsive to the orientation of the martensitic lath structure.

In the Battelle test the SA 508 was more susceptible to underbead cracking than was SA 533.

Results of Hydrogen Susceptibility Testing

The University of Tennessee Hydrogen Susceptibility Test was used to further document the sensitivity to hydrogen cracking using an augmented strain of 4%. The SA 533 welded from 32°F to 400°F cracked, whereas specimens welded at 500°F did not crack. Similarly, SA 508 cracks were observed in specimens welded from 32°F to 500°F, but no cracking was observed in specimen welded at 600°F. These results show that for the most critical situations, a preheat of 500°F for SA 533 and preheat of 600°F for SA 508 is sufficient to drive off hydrogen and prevent cracking. The results are summarized in Table 7. Macrographs of the cracking observed in the University of Tennessee Hydrogen Susceptibility Test are shown in Figure 74. The cracking is shown as a function of preheat temperatures.

It is concluded from both cracking tests, that SA 508 is more susceptible to hydrogen induced cracking than SA 533. The preheat required to prevent cracking in the University of Tennessee Hydrogen Susceptibility Test is higher than the preheat required to eliminate cracking in the Battelle Underbead Cracking Test. This result is in

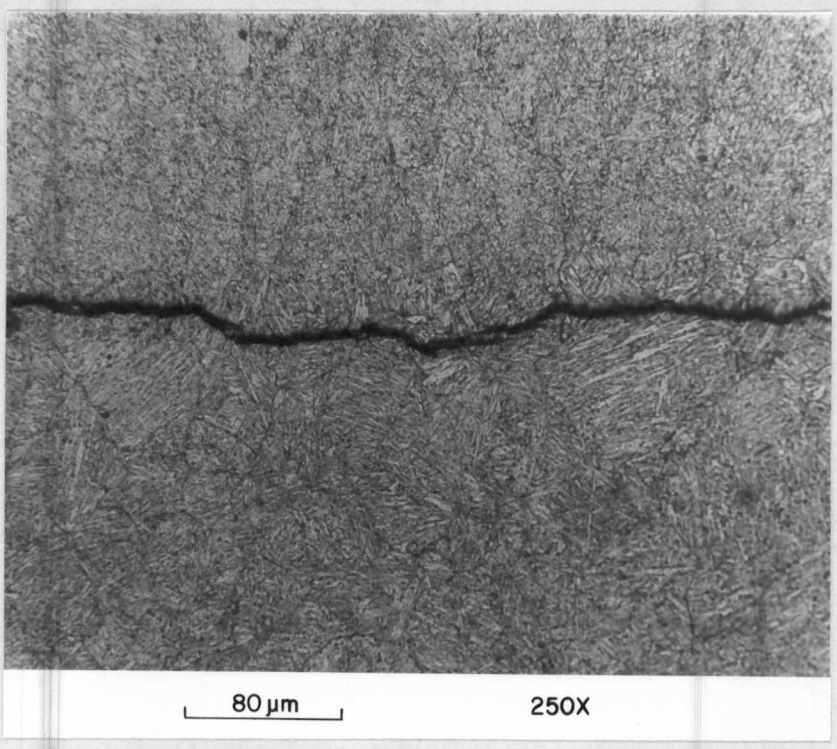

A) SA 533 Steel

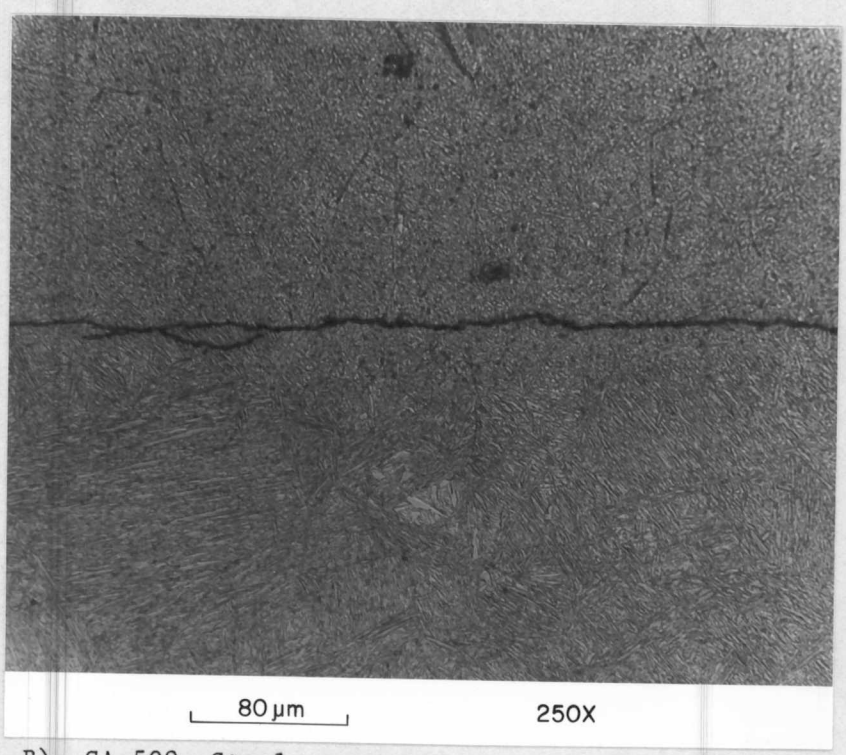

B) SA 508 Steel

Figure 73. Microstructures show underbead cracks for specimens welded @ 32°F. The top section of micrographs is weld metal. Super picral etch.



SA 533

32 90 300 400 500

PREHEAT TEMPERATURES °F

32 90 300 500 600

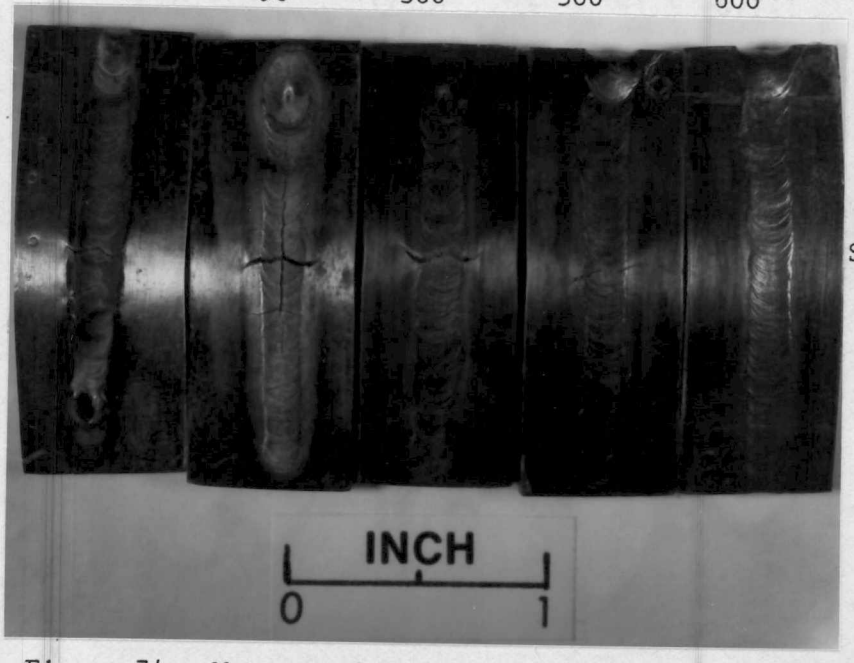

SA 508

Figure 74. Macrographs of cracks observed in University of Tennessee Hydrogen Susceptibility Test specimens.

line with other evaluations on carbon manganese steels. The preheat determined in the Battelle test has been shown to be adequate in fabrication situations.

For the University of Tennessee Hydrogen Susceptibility Test, the ease of ranking steels as to hydrogen susceptibility is good. However, the results (preheat temperatures) of the hydrogen susceptibility test are not sufficiently viable to be used for actual fabrication conditions. This is because the test is quite severe in its nature, and the results tend to be conservative. The advantage in this test lies in its ability to quickly rank the weldability of steels with respect to welding conditions, hydrogen levels and preheat temperatures.

Stress Relief Cracking (SRC)

Stress relief cracking (or reheat cracking) may be defined as intergranular cracking in the HAZ occurring during the exposure of welded assemblies to the elevated temperatures utilized for post weld heat treatments or in high temperature service. The cracks generally occur as a result of the redistribution of residual welding stresses coupled with HAZ metallurgical changes when sound weldments are heated to elevated temperatures after welding for PWHT.

The HAZ cracks are intergranular in nature and the material exhibits low ductility, showing little or no evidence of plastic deformation in the vicinity of the cracks. Since the cracks are usually confined to the coarse-grain region of the HAZ, cracking is directly related to prior high temperature exposure.

According to the experimental procedure described earlier, the

SRC tests were conducted for SA 533 and SA 508. The times to rupture and the reduction of areas for each specimen is a function of stress applied and the thermal treatment given to the specimen. The results are summarized in Table A-5 of Appendix A. The specimen with the bainitic microstructure produced by Cycle VI (136KJ/in, 500°F preheat) took longer to rupture than the one with the martensitic structure produced by Cycle II (50KJ/in, 80°F preheat).

In order to compare the steels on the basis of both stress-rupture strength and stress-rupture ductility, a plot of time-to-rupture versus percentage reduction in area and applied stress was drawn and is shown in Figure 75. It is to be noticed that SA 508 steel exhibited a higher stress to rupture, (for equivalent times) than did SA 533, indicating a stronger material at the PWHT temperature, whereas, SA 533 exhibited a higher creep rupture ductility than SA 508.

Pense et al.[24] performed considerable work on stress relief cracking in carbon and high strength steels. The results of tensile and stress relaxation tests on plain carbon and carbon-boron steels indicated that stress-relief cracking is not a problem in these steels, but A 517 F (Ni-Cr-Mo-B-V) was highly susceptible to stress relief cracking whereas, A 517 J (Mo-B) was not. Pense also observed that the plain carbon steel, consisting of upper bainitic structure, had reduction of area 76% and upon water quenching, the reduction of area reduced to 33% which was due to massive martensite produced. Similar ductility was also observed for carbon-boron steel, but for A 517 J the value dropped from 13% for the bainitic structure, to 5% for the martensitic structure.

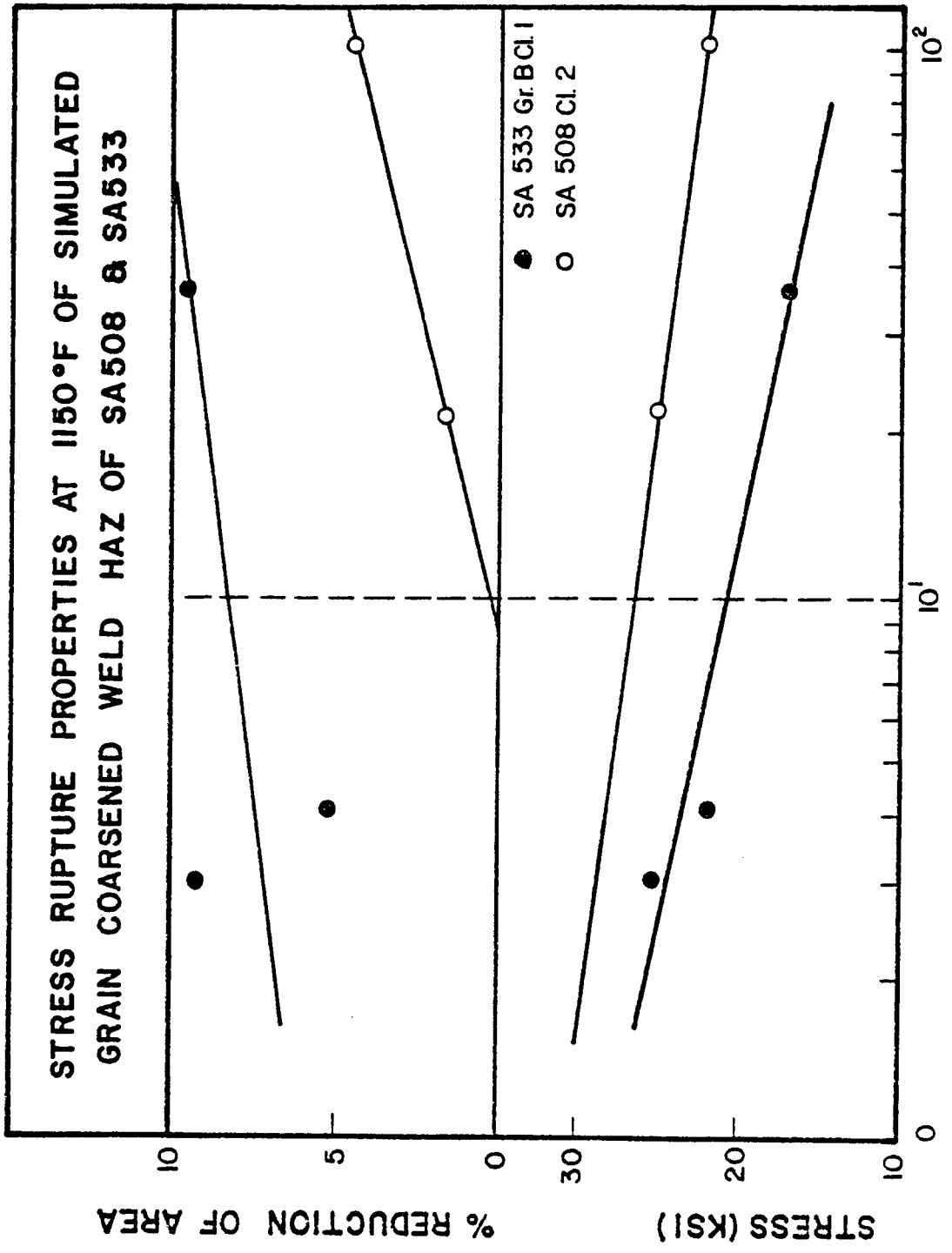

Figure 75. Stress rupture properties at 1150°F of simulated grain coarsened weld HAZ of SA 508 and SA 533.

Our results agree well with Pense, et al. in the sense that for steels not containing Ni, Cr and V the creep rupture ductility after a thermal cycle was quite high. In our study, the bainitic microstructure did not produce a higher creep rupture ductility than the martensitic structure as obtained by Pense.

The SRC susceptibility can be evaluated by a stress rupture parameter. The stress-rupture parameter is the product of the stress for a rupture life of 10 minutes and the corresponding reduction of area. For high strength steels (martensitic microstructure), if the value of this parameter is greater than approximately 15×10^4, then the stress-rupture strength and ductility are considered good and accordingly, a low susceptibility to cracking would be expected. Conversely, if the value is less than 15×10^4, then poor stress-rupture properties and increased crack susceptibility would occur. The stress-rupture parameter obtained for SA 533 is 16.8×10^4 and for SA 508 is 1.3×10^4 (as shown in Table 8). The results of stress-rupture testing, based upon the coarse-grained martensitic structure, lead to the conclusions that SA 508 is more susceptible to SRC than SA 533.

Using the data from the coarse-grained bainitic structure to evaluate stress-rupture parameter, it is predicted that a bainitic structure will have lower stress to rupture and creep rupture ductility for SA 533 and SA 508 steels, and consequently, a lower stress-rupture parameter is obtained, with SA 508 being the more susceptible to stress relief cracking with a bainitic microstructure.

The nature of the fracture surfaces of the stress-rupture specimens was examined with the Scanning Electron Microscope (SEM). The mode of fracture in the specimens was predominantly intergranular. Hamilton[37]

TABLE 8

THE VALUES OBTAINED IN SRC TEST
FOR RUPTURE LIFE OF 10 MINUTES

Steel	Stress for a Rupture Life of 10 Min (psi)	Reduction of Area %	Stress* Rupture Parameter
SA 533 Grade B Class 1	21,000	8	16.8×10^4
SA 508 Class 2	26,500	0.5	1.3×10^4

* The stress-rupture parameter is the product of the stress for a rupture life of 10 minutes and the corresponding reduction of area.

mentioned that precipitation hardening within the grain concentrates the strain on the grain boundaries which already have reduced ductility due to residual element segregation, and intergranular cracking results. The fractographs of the fractured surface for both steels are shown in Figures 76 through 79. Fractographs in Figure 76 are the result of Cycle II plus PWHT forming a martensitic structure. It is noticed that the grain size is large and the cracks are intergranular. Similar behavior is noted in Figure 77, except that the microstructure is bainitic, produced by Cycle VI plus PWHT. A similar trend for cracking and a related microstructure was observed in SA 508 steel and is shown in Figures 78 and 79. A careful review of SEM fractographs of the martensitic structure (Figures 76A and 78A) shows traces of microductility on the grain faces; this microductility is shown in Figure 78C at a higher magnification. Fractographs for the bainitic structures (Figures 77A and 79A) show no microductility, but there are oxides and inclusions on the grain faces. These defects are not considered to be related to the intergranular failure.

The results of the SRC test show that SA 508 steel is more susceptible to reheat cracking than SA 533. This conclusion is based on the stress-rupture strength and stress-rupture ductility of the specimens.

Careful handling of susceptible materials in terms of weld energy input, weld joint restraint and choice of PWHT conditions can prevent stress rupture cracking. However, in general, the prevention of reheat cracking is best accomplished by the correct selection of material and post-weld heat treatment.

SA 533

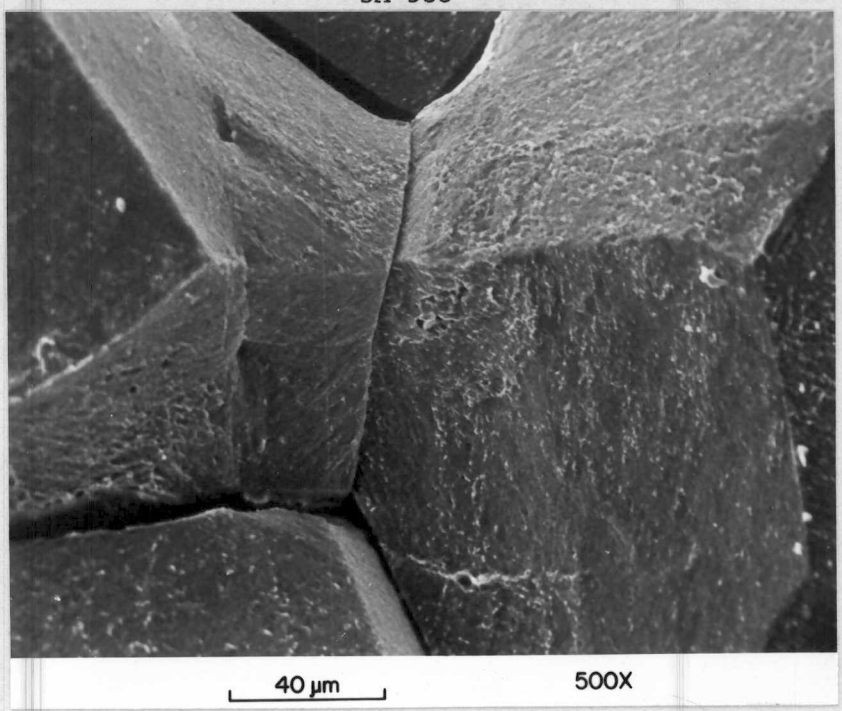

A) Intergranular rupture resulted by test No. 3 (Martensitic). SEM

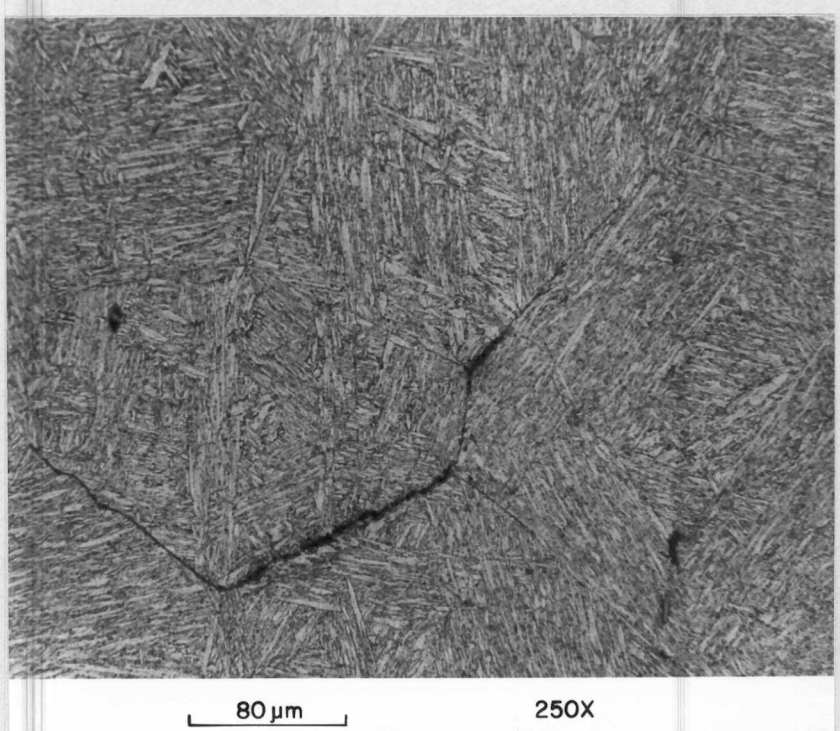

B) Metallographic section of A) above revealing grain boundary cracks. Super picral etch.

Figure 76. Fracture behavior observed in SRC test of SA 533 steel. (Martensitic structure.)

SA 533

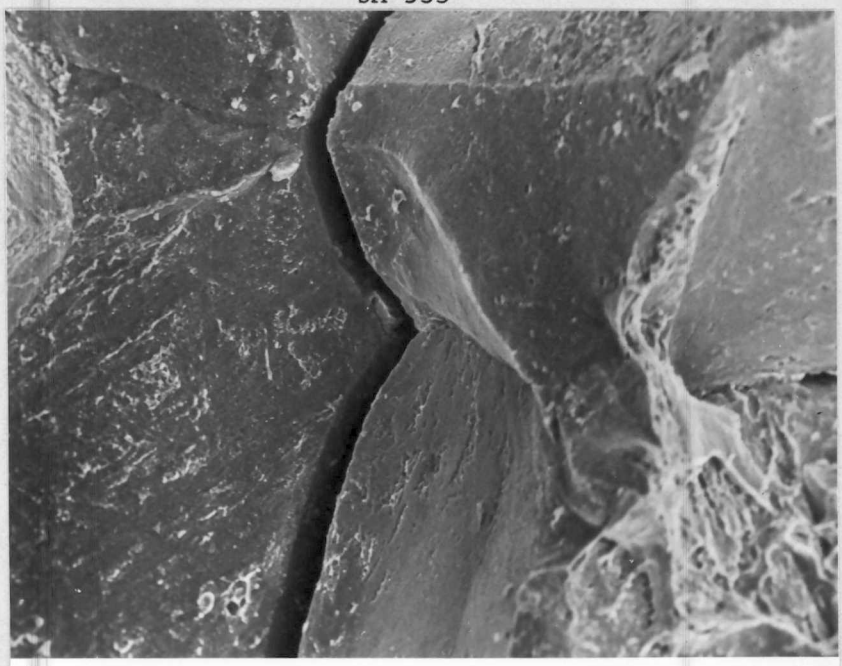

A) Intergranular rupture resulted by test No. 7 (Bainitic). SEM

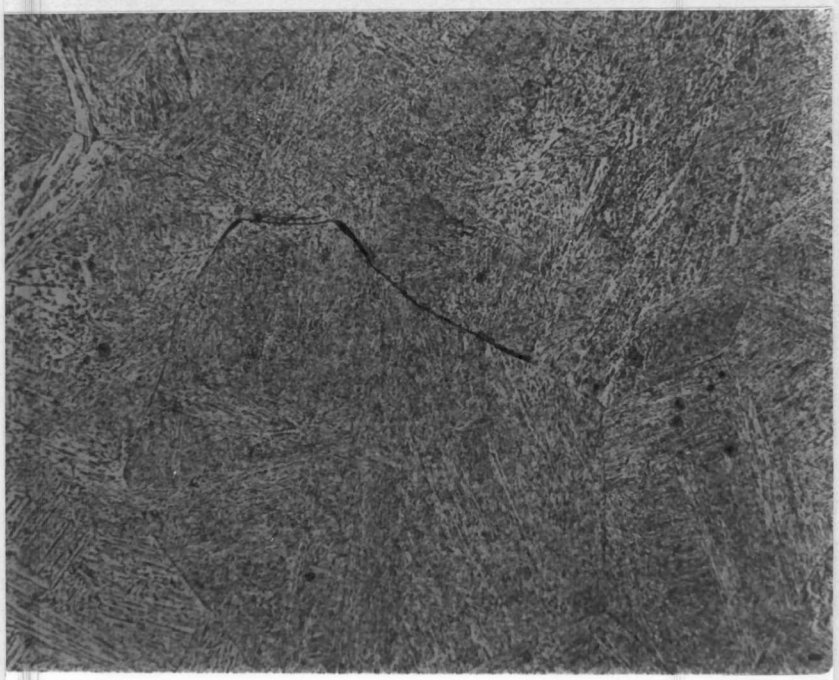

B) Metallographic section revealing grain boundary secondary cracks below the main rupture surface of A) above. Super picral etch.

Figure 77. Fracture behavior observed in SRC test of SA 533. (Bainitic structure.)

SA 508

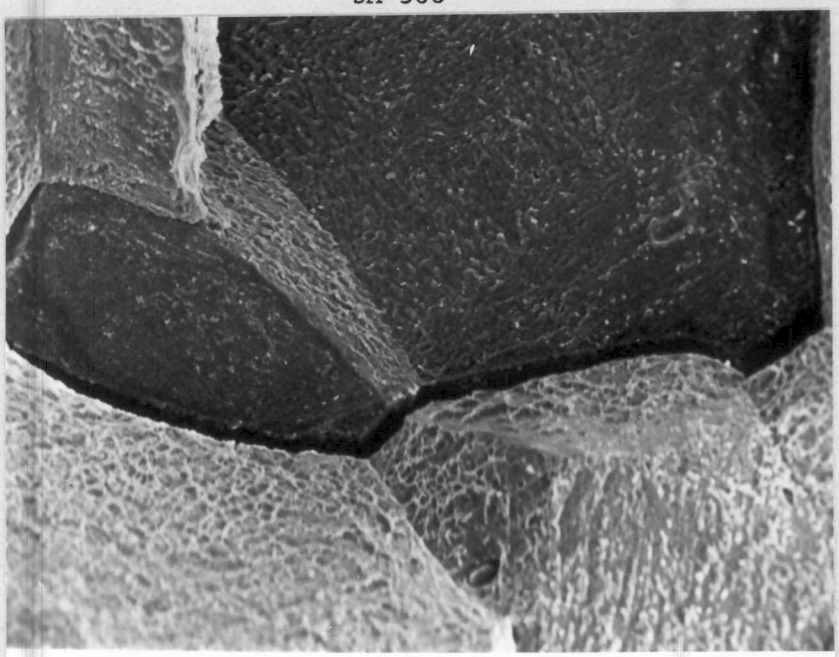

A) Intergranular rupture obtained by test No. 3 (Martensitic). SEM

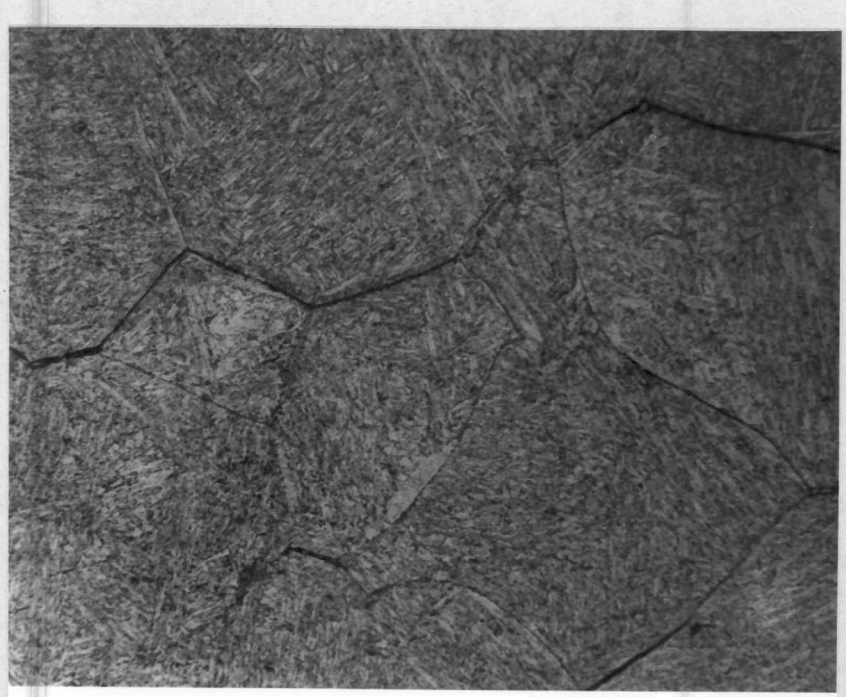

B) Metallographic section revealing grain boundary secondary cracks below the main rupture surface of A) above. Super picral etch.

Figure 78. Fracture behavior observed in SRC test of SA 508. (Martensitic structure.)

SA 508

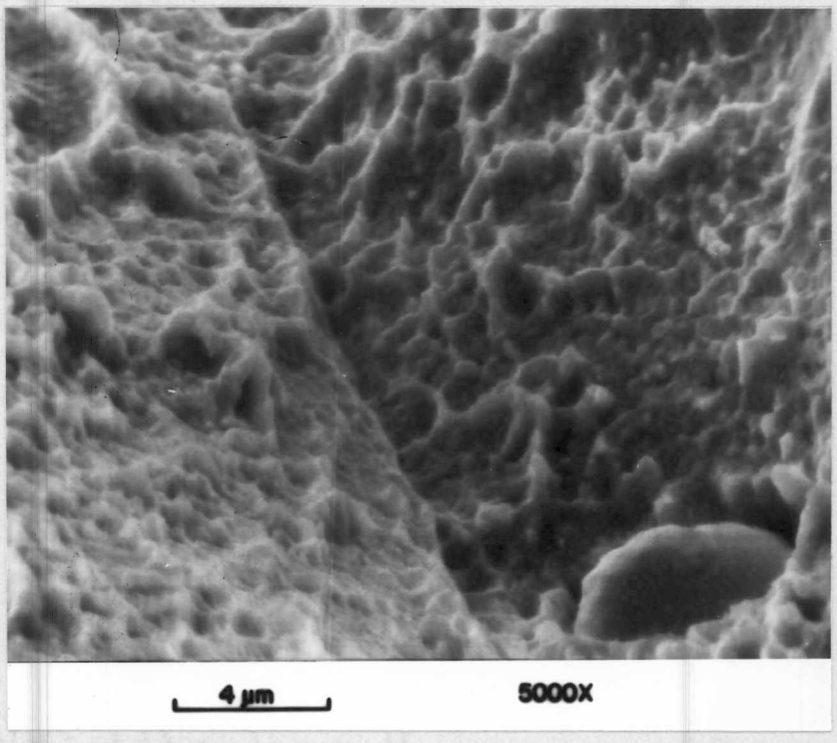

C) Microductility observed in A).

Figure 78. (continued)

SA 508

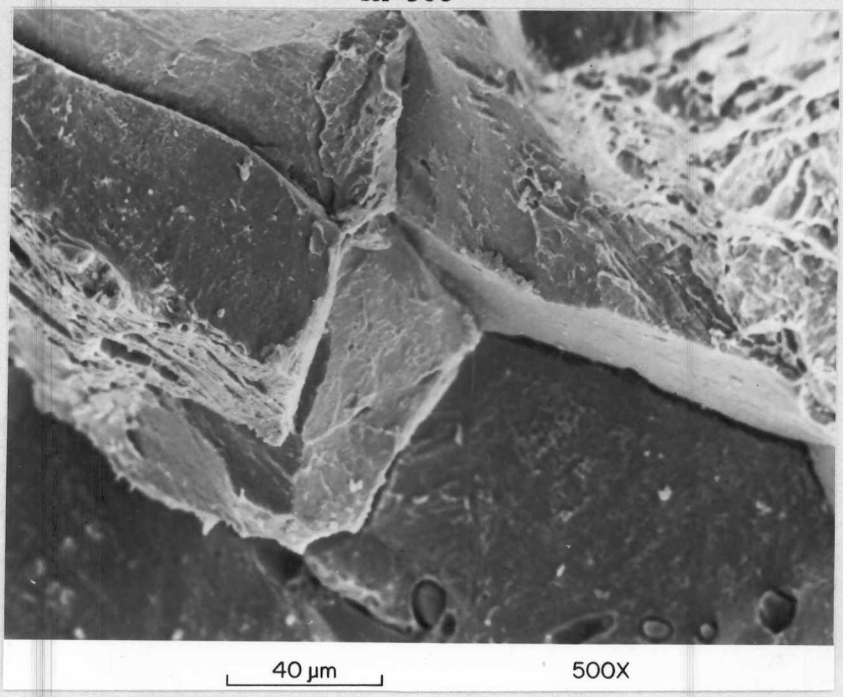

A) Intergranular rupture obtained by test No. 7 (Bainitic). SEM.

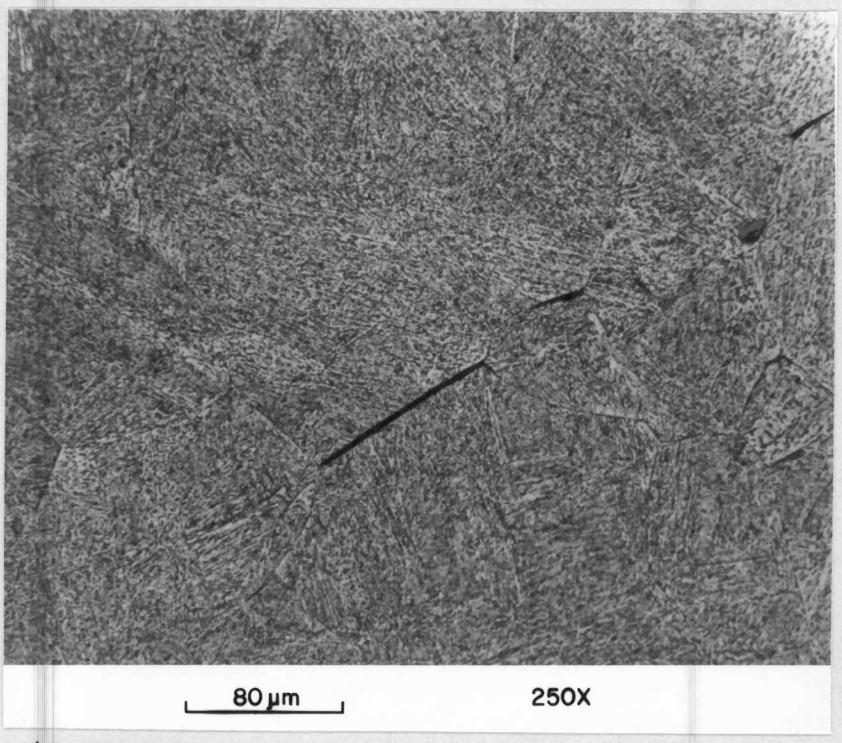

B) Metallographic section revealing grain boundary secondary cracks below the main rupture surface of A) above. Super picral etch.

Figure 79. Fracture behavior observed in SRC test of SA 508. (Bainitic structure.)

Charpy V-Notch Toughness of Simulated HAZ Microstructures

The toughness of any multipass HAZ microstructure is primarily determined by the final thermal cycle experienced at a particular location. Thus, the toughness of a steel subjected to a peak temperature of 2400°F would not be expected to be identical to the toughness of the same steel grain-coarsened at 2400°F and then recycled to 1650°F. After a material has been exposed to high peak temperature thermal cycle it will differ from the original base metal in prior austenite grain size, and in the amount of carbon and other alloy elements in solution. Thus, the influence of multiple HAZ cycles on properties is of interest.

Two energy input conditions were selected for weld thermal cycles with a 2400°F and 1650°F peak temperature. Cycle II (50KJ/in, 80°F preheat, 1" plate) was chosen to provide a fully martensitic transformation product and Cycle VI (136KJ/in, 500°F preheat, 1" plate) was chosen to provide a fully bainitic structure. A number of thermal treatments were employed for this test, among which was a dual-cycle treatment consisting of exposure to a higher peak temperature of 2400°F (sufficient to cause complete austenitization) followed by a lower peak temperature (1650°F), was employed to obtain grain-refined structure. This multicycle thermal excursion represents a multipass welding procedure. Another thermal treatment employed, consisted of exposure to a 2400°F peak temperature, followed by post weld hold at 600 or 300°F in order to temper the initial microstructure. A complete schedule of thermal heat treatments is shown in Table A-3 and charpy v-notch toughness is shown in Table A-6 and A-7 of Appendix A. These values are presented in bargraph form in Figures 80 and 88 for ready discussion. The lateral

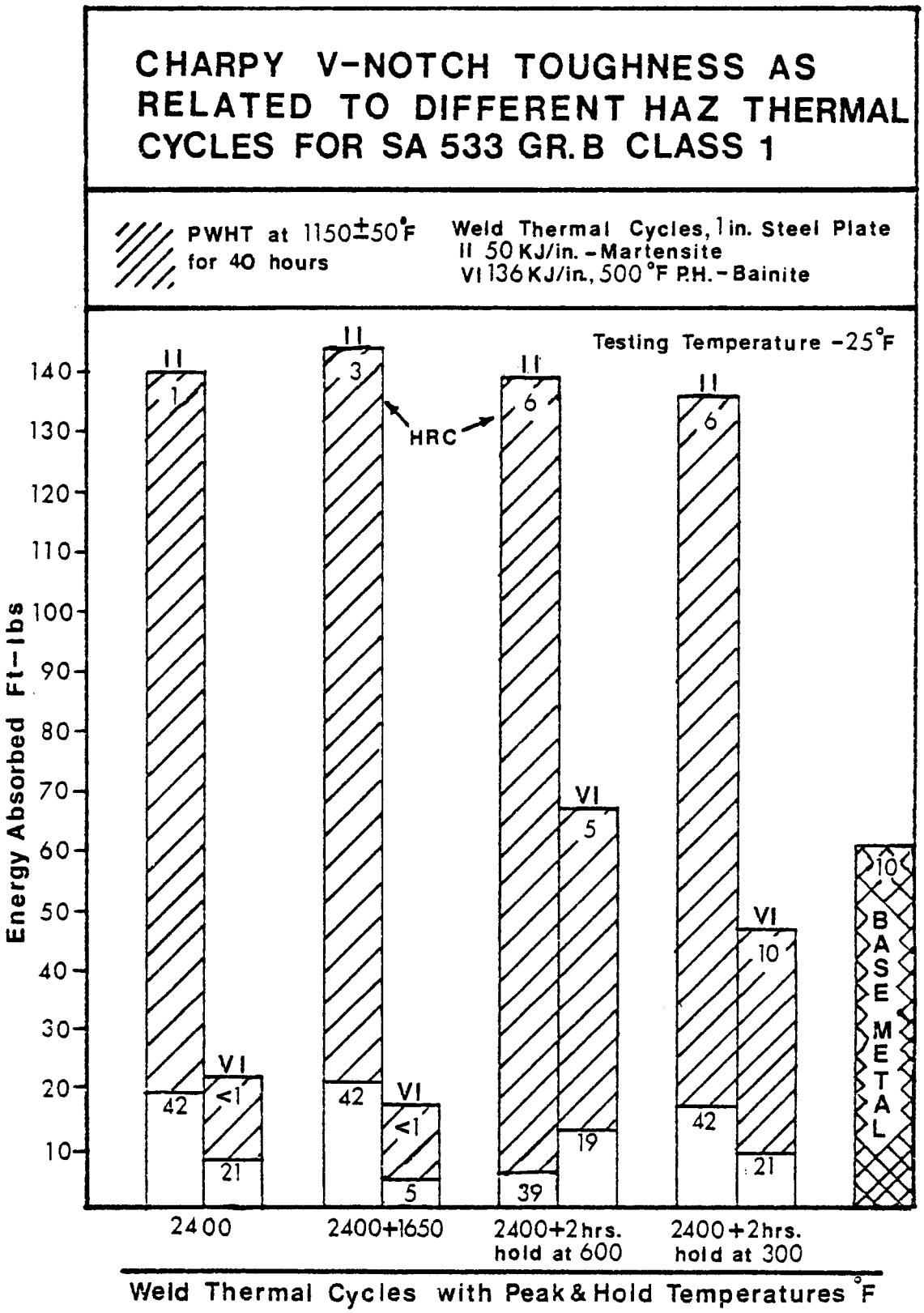

Figure 80. Charpy V-notch toughness as related to different HAZ thermal cycles for SA 533 Gr.B Cl. 1.

expansions comparable to these impact toughness values for SA 533 and SA 508 are shown in Figures A-1 and A-2 of Appendix B.

SA 533 Grade B Class 1

A bargraph of charpy v-notch toughness as related to different HAZ thermal cycles is shown in Figure 80. The impact test temperature selected was -25°F which corresponds to the transition temperature of the base metal. A toughness of 60 ft-lbs. was observed for the base metal. The coarse-grained martensitic structure (obtained by Cycle II) gave a toughness of about 20 ft-lbs. and upon PWHT the toughness increased significantly to 140 ft-lbs. The hardness decreased from HRC 42 to HRC 1 (HRB 83). For the coarse-grained bainitic structure (obtained by Cycle VI) an impact toughness of 10 ft-lbs. was recorded which upon PWHT increased to approximately 20 ft-lbs. The hardness dropped from HRC 21 to HRB 80. This result shows that the toughness of the bainitic structure is lower than the martensitic structure and that PWHT increases the toughness of martensite significantly but does not improve the toughness of bainite to a great extent. The respective microstructures are shown in Figures 81 and 82.

For SA 533 the optimum toughness of the martensitic structure was obtained by multiple cycles with different peak temperatures (2400°F followed by 1650°F peak) whereas the toughness for the bainitic structure was deteriorated by a double cycle. The thermal recycling duplicating multiple-pass welding resulted in properties largely determined by the peak temperature and cooling rate of the final cycle. This fact serves as a reminder that the HAZ's of multiple-pass welds comprise a complex conglomerate of microstructures produced by a wide

SA 533

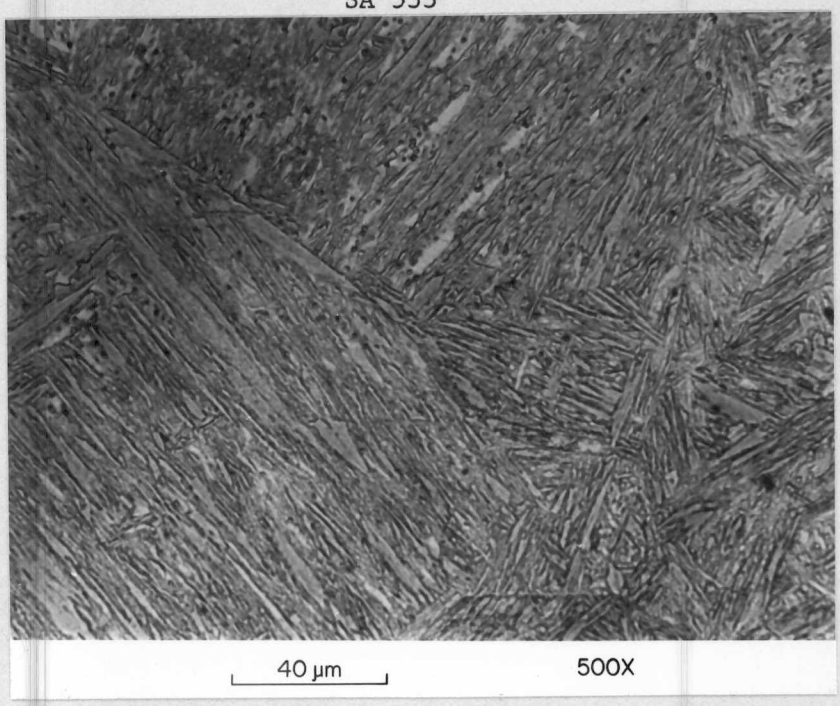

A) Cycle II (2400°F P.T.) Martensitic structure. HRC 42. Super Picral etch.

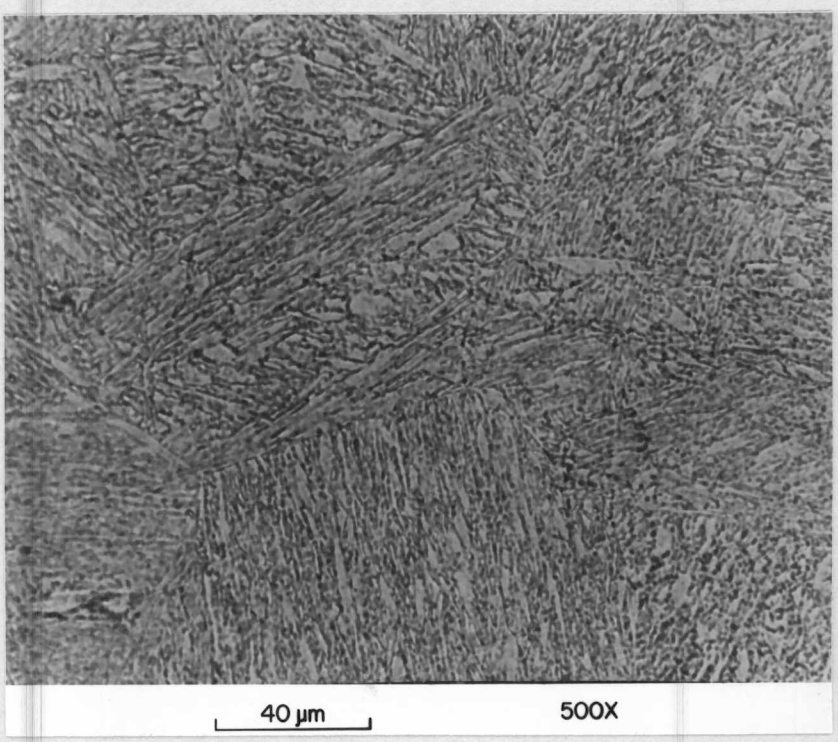

B) Cycle II (2400°F P.T.) + PWHT. Tempered Martensitic structure. HRC 1. Super picral etch.

Figure 81. Microstructural behavior observed in SA 533 steel for Cycle II.

SA 533

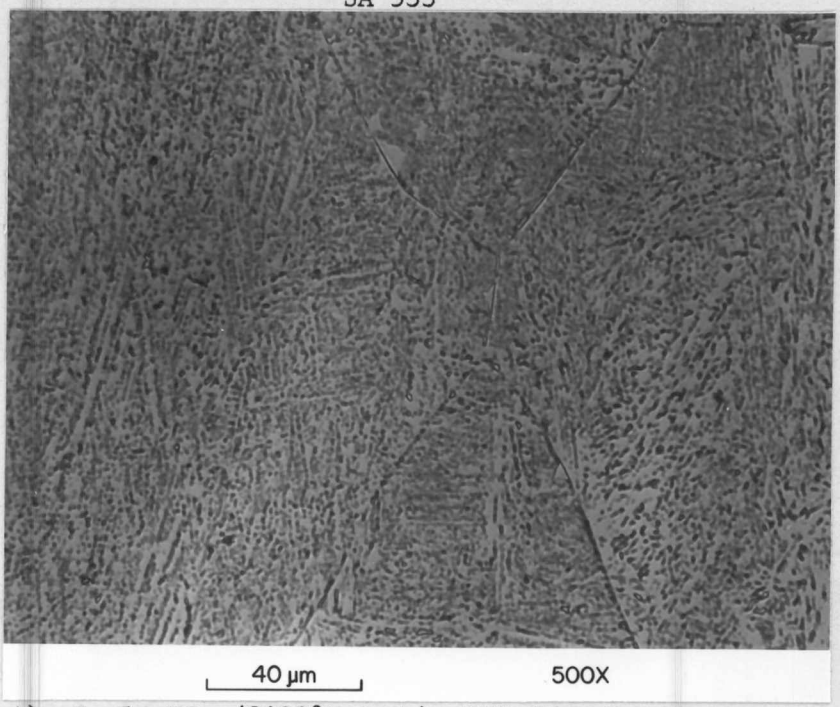

A) Cycle VI (2400°F P.T.) HRC 21. Bainitic structure. Super picral etch.

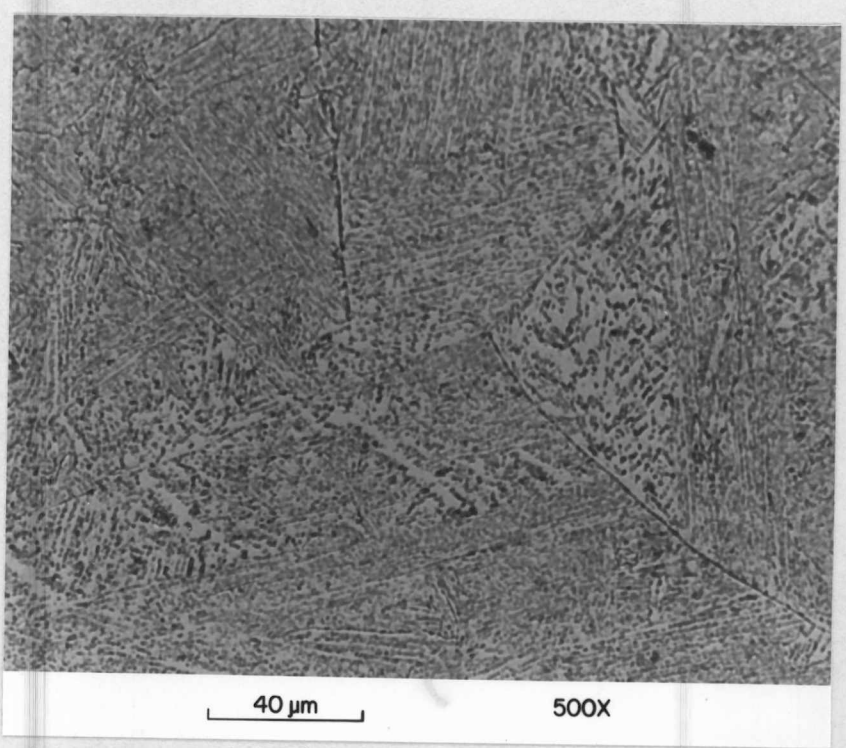

B) Cycle VI (2400°F P.T.) + PWHT HRB 82. Tempered Bainitic structure. Super picral etch.

Figure 82. Microstructural behavior observed in SA 533 steel for Cycle VI.

range of peak temperatures spatially distributed in a complicated pattern. It is not to be expected that hardness measurements will be usefully related to the notch toughness of such a conglomerate. The microstructures obtained after multiple cycles are shown in Figures 83 and 84.

Martensite, although very hard and basically strong, lacks toughness; however, tempered martensite can have a high strength and good toughness if it is heat treated appropriately. This is achieved because the brittle martensite is replaced by a fine dispersion of rigid carbide particles within a tough ferrite matrix. The untempered martensitic structure with post weld hold at 600°F showed the worst toughness of all treatments i.e., "as-welded," (note that this thermal treatment is similar to Martempering) but superior toughness was achieved after PWHT. The bainitic structure showed the best toughness when a post weld hold (at 600°F) and PWHT was employed. The micrographs for these thermal treatments are shown in Figures 85 and 86. The untempered martensitic and bainitic structure with a post-weld hold at 300°F showed toughness similar to that obtained without post-weld holds, but the bainitic microstructure upon PWHT showed the second best bainitic toughness. The respective microstructures are shown in Figure 87. It is clear from the above observations that martensitic structures showed better toughness than bainitic structures, and upon PWHT a tremendous increase in toughness was observed for martensitic structures. This indicates that weld HAZ regions containing tempered martensite will have better toughness than the base metal.

The hardness results showed that higher hardnesses were obtained for martensitic structures than for bainitic structures and that

SA 533

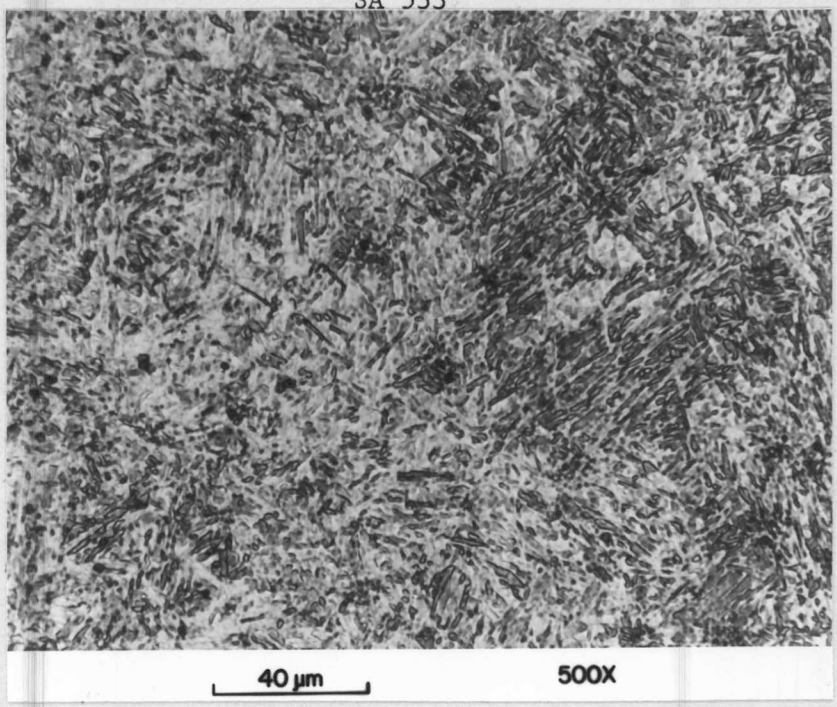

A) Cycle II (2400°F P.T.) + Cycle II (1650°F P.T.). Mixture of coarse and fine martensite. HRC 42. Super picral etch.

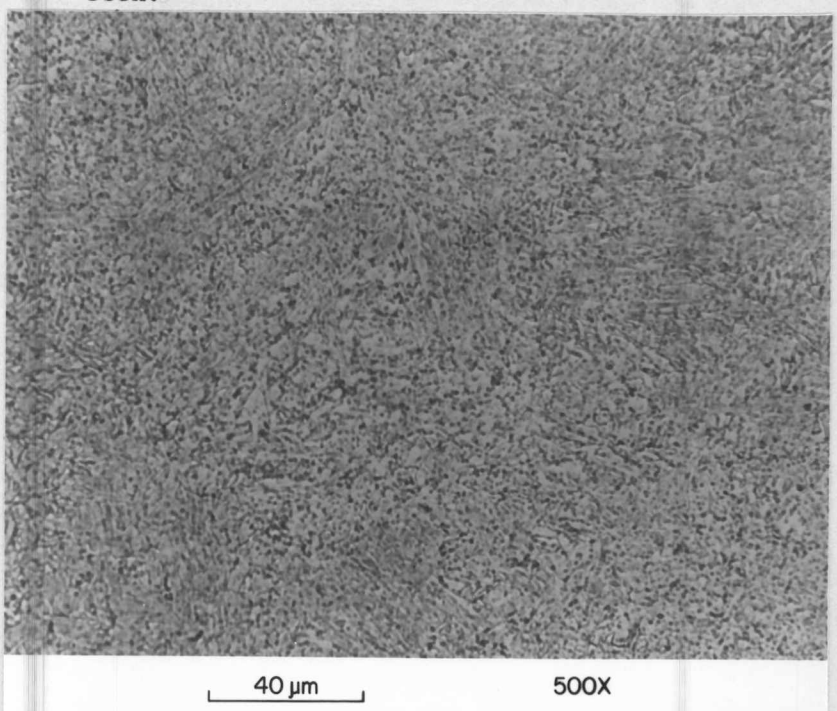

B) Cycle II (2400°F P.T.) + Cycle II (1650°F P.T.) + PWHT. Tempered Martensitic structure. HRC 3. Super picral etch.

Figure 83. Microstructural behavior observed in SA 533 steel for multiple cycles (Cycle II).

SA 533

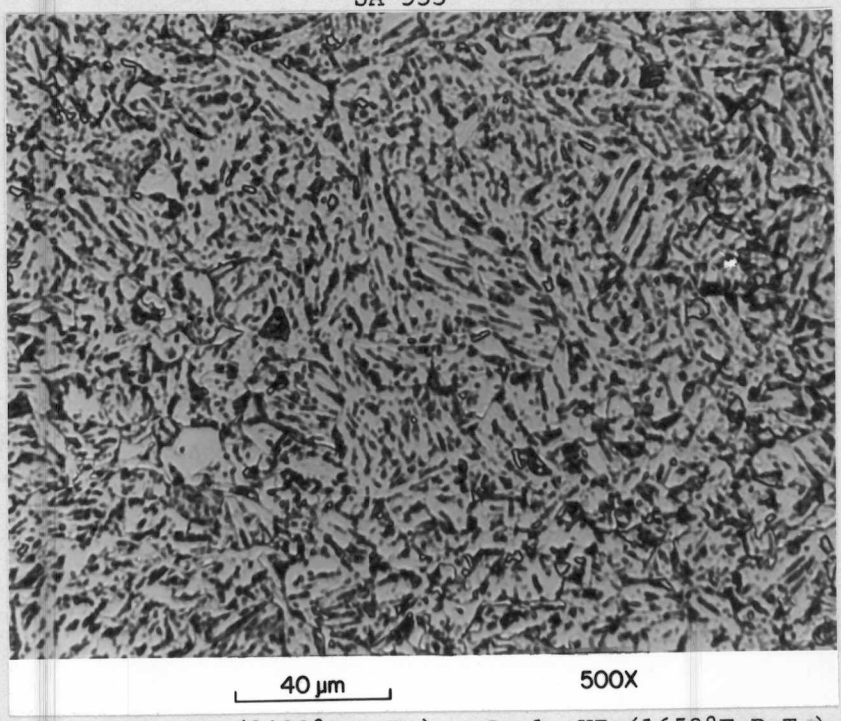

A) Cycle VI (2400°F P.T.) + Cycle VI (1650°F P.T.) Fine Bainitic structure. HRC 5. Super picral etch.

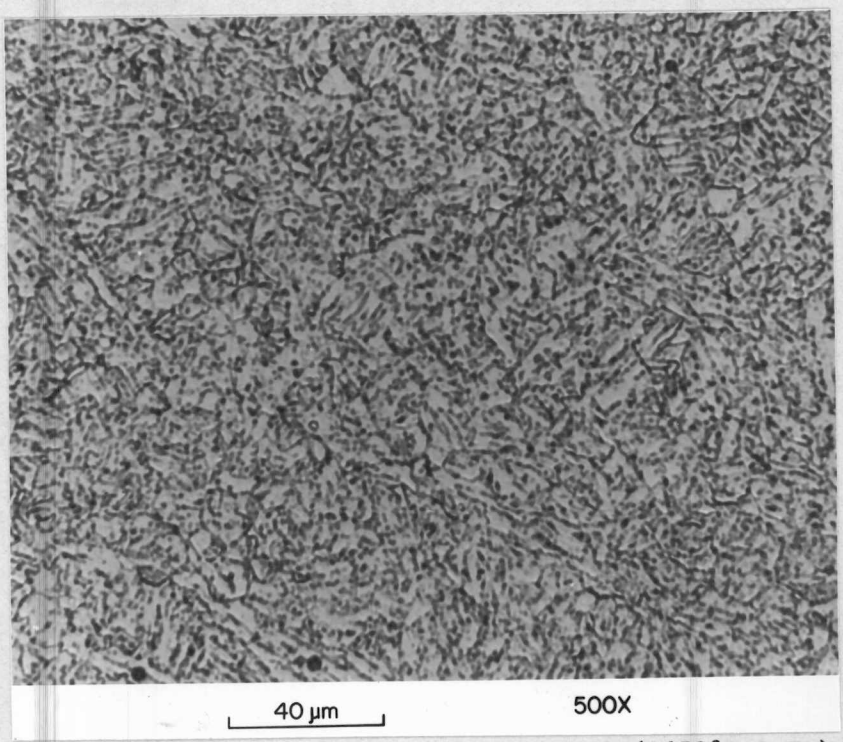

B) Cycle VI (2400°F P.T.) + Cycle VI (1650°F P.T.) + PWHT. Tempered Bainitic structure. HRB 82. Super picral etch.

Figure 84. Microstructural behavior observed in SA 533 steel for multiple cycles (Cycle VI).

SA 533

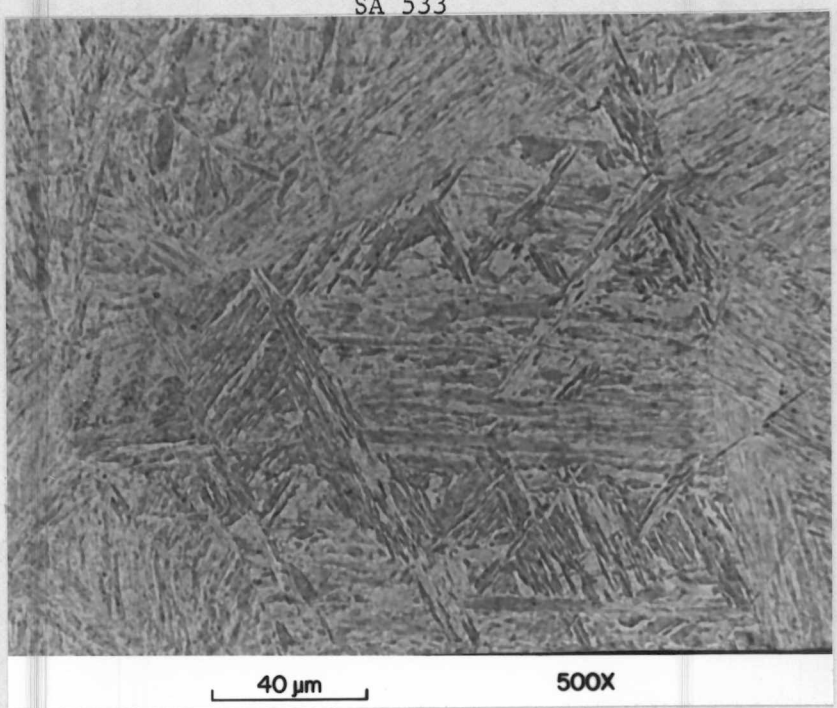

A) Cycle II (2400°F P.T.) + hold @ 600°F (2 hrs.) Martensitic structure. HRC 39. Super picral etch.

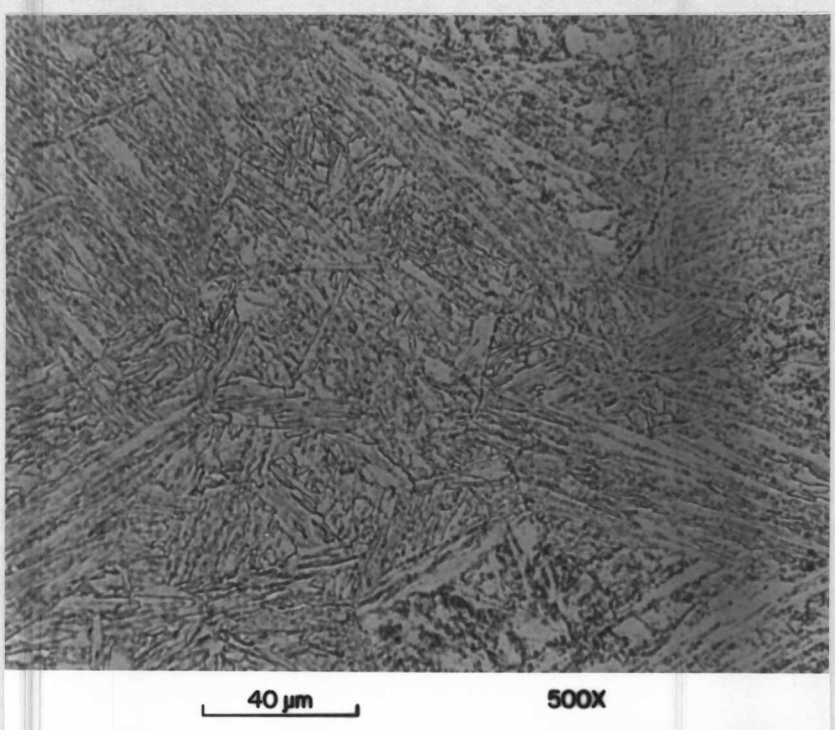

B) Cycle II (2400°F P.T.) + hold @ 600°F (2 hrs.) + PWHT. Tempered Martensitic structure. HRC 6. Super picral etch.

Figure 85. Microstructural behavior observed in SA 533 steel for Cycle II and held @ 600°F.

SA 533

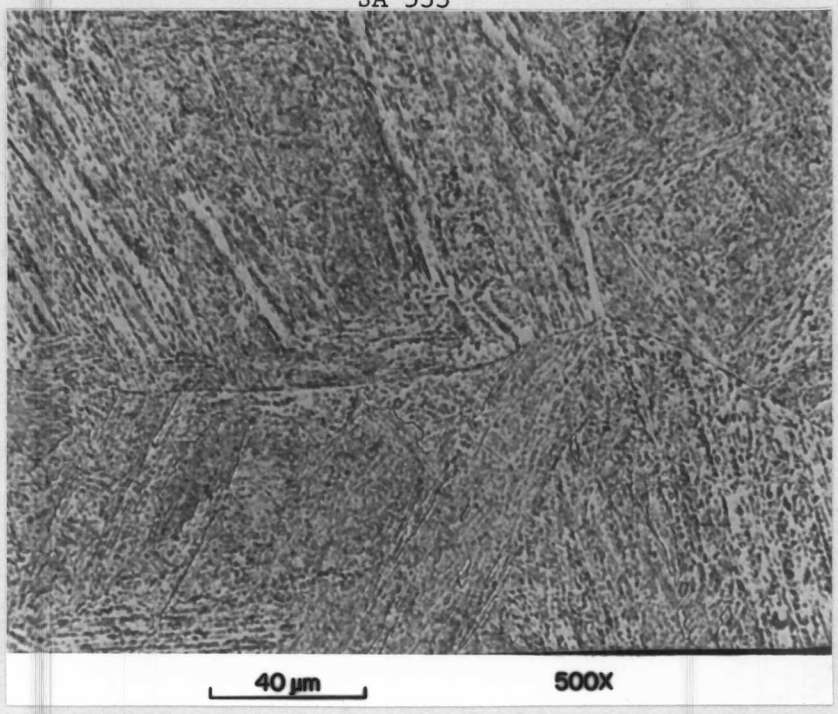

A) Cycle VI (2400°F P.T.) + hold @ 600°F (2 hrs.).
Tempered Bainitic structure. HRC 19. Super picral etch.



B) Cycle VI (2400°F P.T.) + hold @ 600°F (2 hrs.) + PWHT.
Tempered Bainitic structure. HRC 5. Super picral etch.

Figure 86. Microstructural behavior observed in SA 533 steel for Cycle VI and held @ 600°F.

SA 533

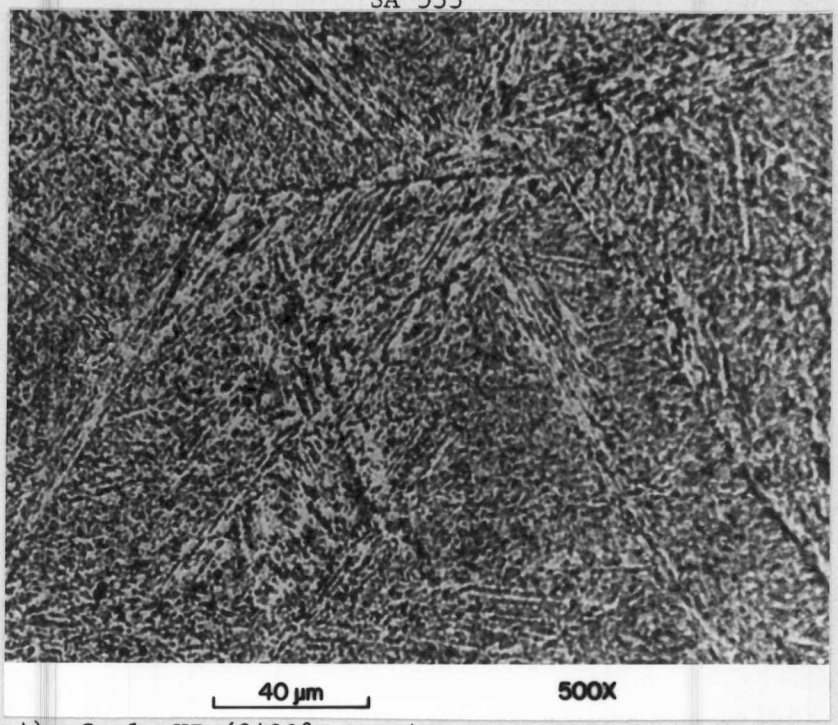

A) Cycle VI (2400°F P.T.) + hold @ 300°F (2 hrs.). Tempered Bainitic structure. HRC 21. Super picral etch.

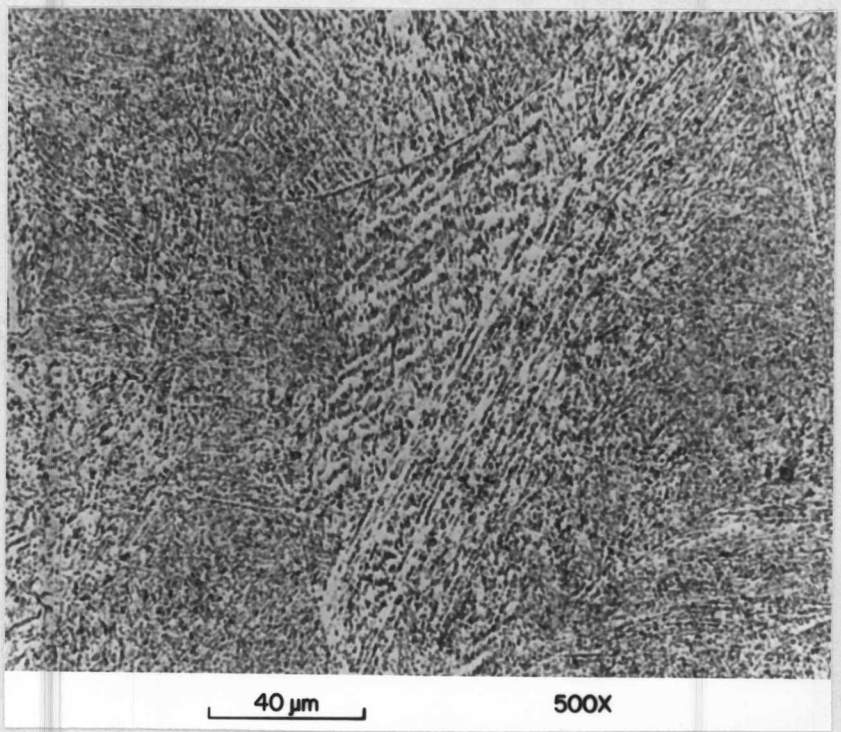

B) Cycle VI (2400°F P.T.) + hold @ 300°F (2 hrs.) + PWHT. Tempered Bainitic structure HRC 10. Super picral etch.

Figure 87. Microstructural behavior observed in SA 533 steel for Cycle VI and held @ 300°F.

hardness has no direct relation to the toughness. There is a general inverse relation in steel between hardness (strength) and ductility. As the cooling rate from austenitizing temperature is increased, the microstructure shifts from relatively soft aggregates of ferrite and carbide to harder bainitic or martensitic structures with accompanying loss in ductility. The degree of hardening observed in the HAZ of a welded steel will not be useful in judging the toughness of that region unless there is prior knowledge of the response of the steel to cooling rate and resulting microstructure.

SA 508 Class 2

The SA 508 Class 2 results are presented (Figure 88) in a manner similar to SA 533. The impact test temperature for this steel was selected to be room temperature (72°F), which corresponds to the transition temperature of the base metal. The base metal exhibited 70 ft-lbs. at 72°F. The coarse-grained martensitic structure gave a toughness of 37 ft-lbs. and upon PWHT the toughness increased to 45 ft-lbs. The hardness decreased from HRC 46 to HRC 28. For the coarse-grained bainitic structure, a toughness of 8 ft-lbs. was recorded, which upon PWHT, increased to 16 ft-lbs. The hardness dropped from HRC 28 to HRC 18 This result again shows that the toughness of the bainitic structures is lower than that of the martensitic structure. The respective microstructures are shown in Figures 89 and 90. The toughness of both microstructures was increased with multiple cycles with a grain refining peak temperature (2400°F followed by 1650°F peak), and upon PWHT the toughness was further increased. The microstructures are shown in Figures 91 and 92. These microstructures are similar to those observed for SA 533 (Figures 83 and 84).

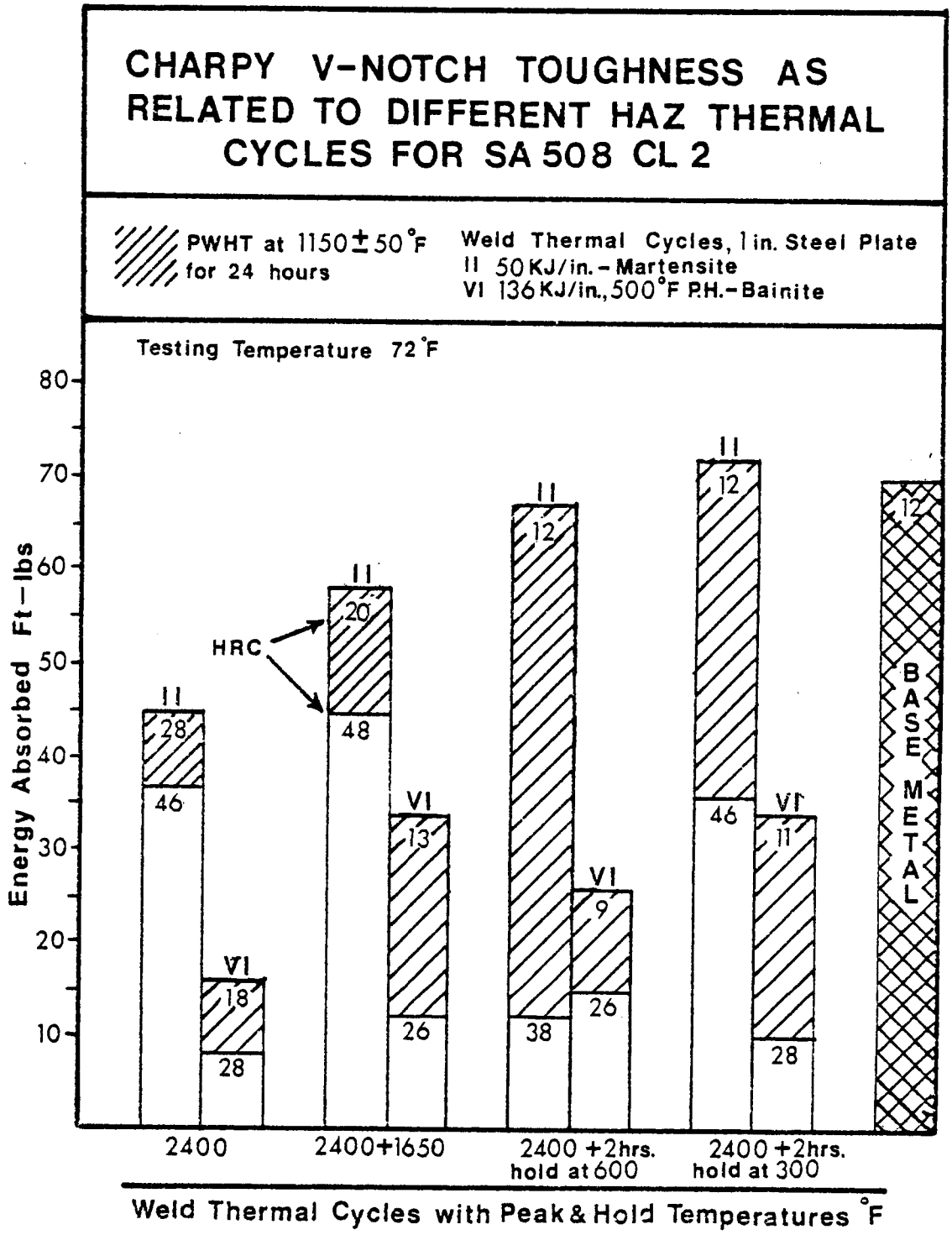

Figure 88. Charpy V-notch toughness as related to different HAZ thermal cycles for SA 508 Cl 2.

SA 508



A) Cycle II (2400°F P.T.) Martensitic structure. HRC 46. Super picral etch.

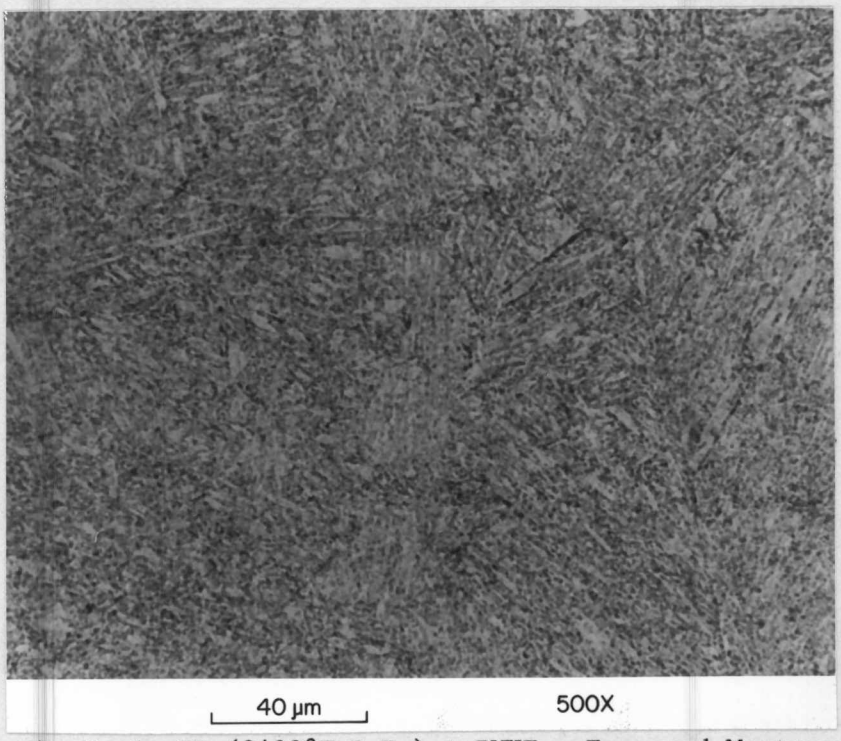

B) Cycle II (2400°F P.T.) + PWHT. Tempered Martensitic structure. HRC 28. Super picral etch.

Figure 89. Microstructural behavior observed in SA 508 steel for Cycle II.

SA 508

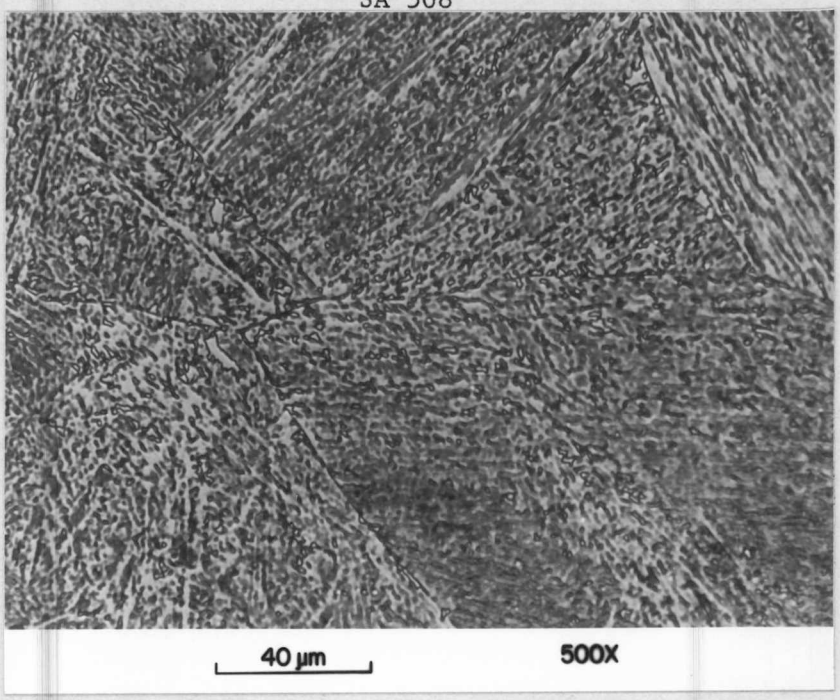

A) Cycle VI (2400°F P.T.) Bainitic structure. HRC 28. Super picral etch.

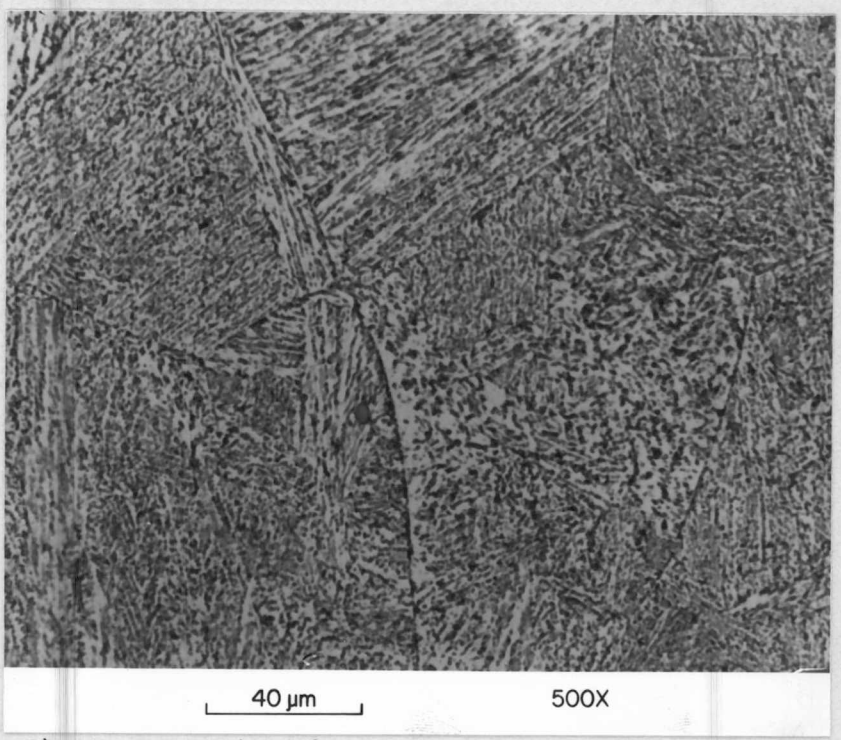

B) Cycle VI (2400°F P.T.) + PWHT. Tempered Bainitic structure. HRC 18. Super picral etch.

Figure 90. Microstructural behavior observed in SA 508 steel for Cycle VI.

SA 508

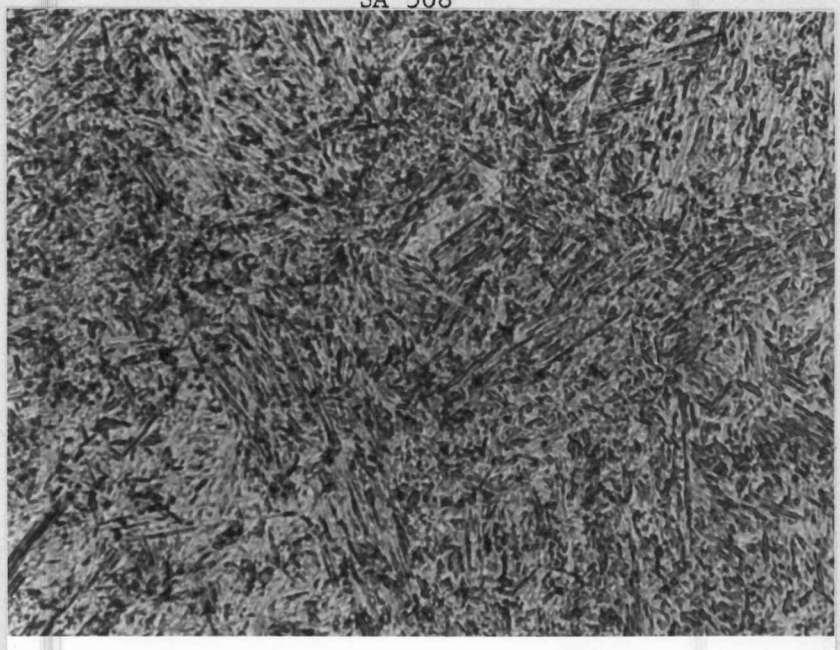

A) Cycle II (2400°F P.T.) + Cycle II (1650°F P.T.). Mixture of coarse and fine-grained martensite. HRC 48. Super picral etch.

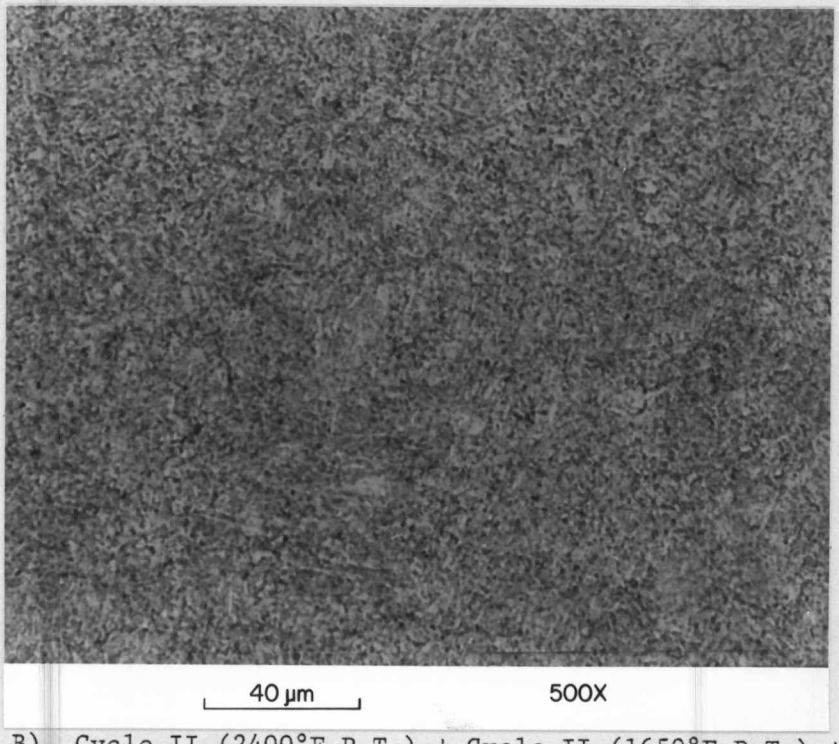

B) Cycle II (2400°F P.T.) + Cycle II (1650°F P.T.) + PWHT. Tempered Martensitic structure. HRC 20. Super picral etch.

Figure 91. Microstructure behavior observed in SA 508 steel for multiple cycles (Cycle II).

SA 508

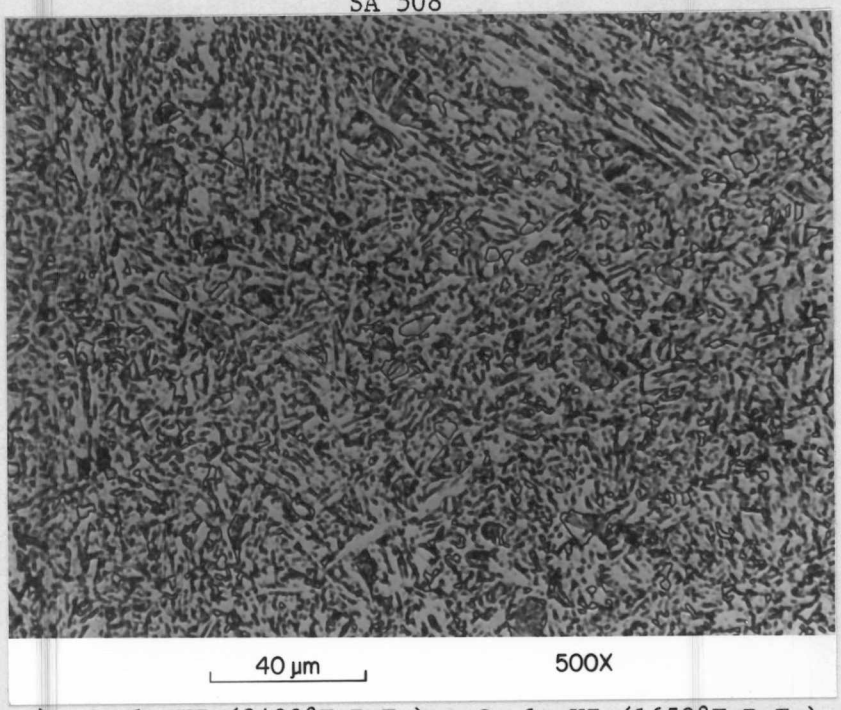

A) Cycle VI (2400°F P.T.) + Cycle VI (1650°F P.T.). Fine Bainitic structure. HRC 26. Super picral etch.

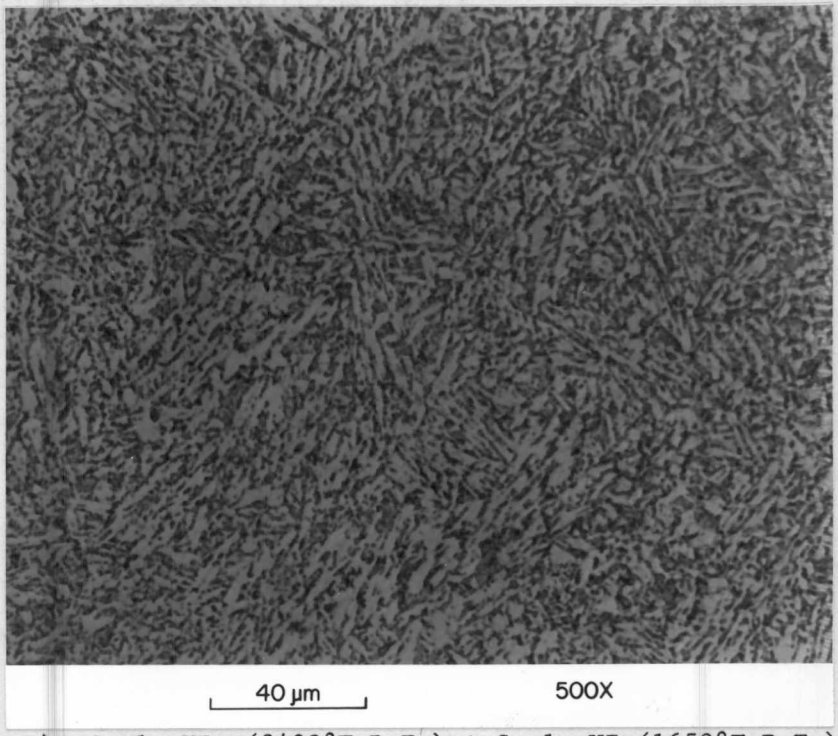

B) Cycle VI (2400°F P.T.) + Cycle VI (1650°F P.T.) + PWHT. Tempered Bainitic structure. HRC 13. Super picral etch.

Figure 92. Microstructural behavior observed in SA 508 steel for multiple cycles (Cycle VI).

The toughness of the untempered martensitic structure deteriorated when a post weld hold at 600°F was applied, but superior toughness was achieved by subsequent PWHT. This is in contrast to the results for untempered bainitic structure which showed the best toughness upon post weld holding at 600°F. These results are similar to the ones described for SA 533. The respective microstructures are shown in Figures 93 and 94. The untempered martensitic and bainitic structures with a post-weld hold at 300°F showed similar toughness to those obtained without post-weld hold, but upon PWHT both microstructures exhibited the best toughness of all thermal treatments (Figures 95 and 96.)

The hardness results showed that martensitic structure had higher hardness than bainitic structure and that the toughness is not related to hardness per se. It is noticed that the drop in hardness from untempered to tempered structure is greater for SA 533 than for SA 508. In general, the hardnesses obtained for SA 508 steel were higher than what were obtained for SA 533.

If the results of charpy toughness are compared with the results of Klumpes,[22] again, a total disagreement is evidenced. Klumpes mentioned that the increasing amount of martensite in the structure deteriorates the toughness and PWHT of fully martensitic structure does not benefit the toughness. Our results show just the opposite of his results, in that the best toughness is achieved by the PWHT of a martensitic structure, and this agrees with Canonico's[1] statement of untempered martensite being poor in toughness, whereas, properly tempered martensite has superior properties.

SA 508

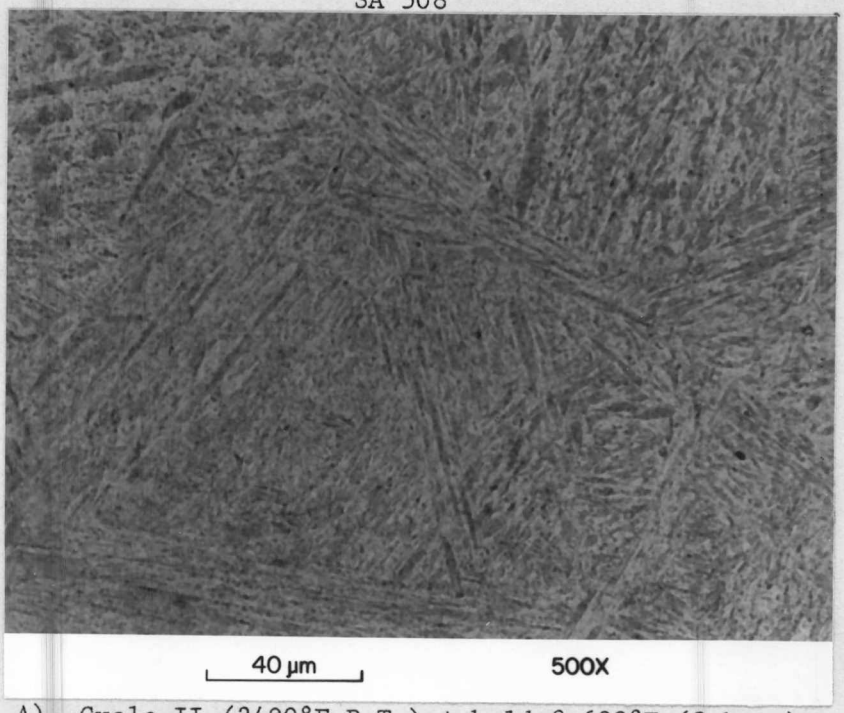

A) Cycle II (2400°F P.T.) + hold @ 600°F (2 hrs.). Tempered Martensitic structure. HRC 38. Super picral etch.

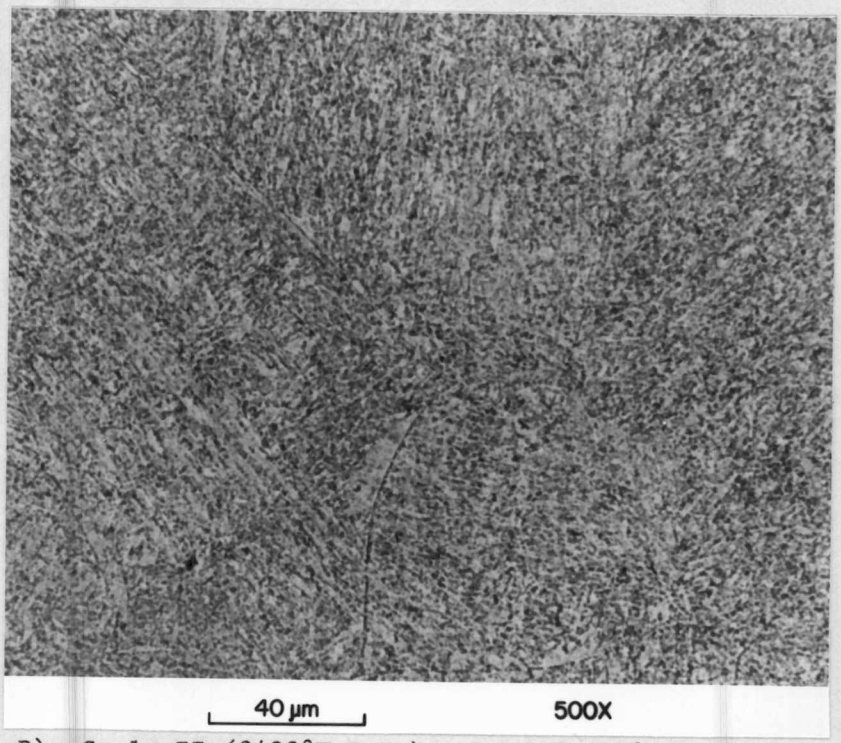

B) Cycle II (2400°F P.T.) + hold @ 600°F (2 hrs.) + PWHT. Tempered Martensitic structure. HRC 12. Super picral etch.

Figure 93. Microstructural behavior observed in SA 508 steel for Cycle II and held @ 600°F.

SA 508

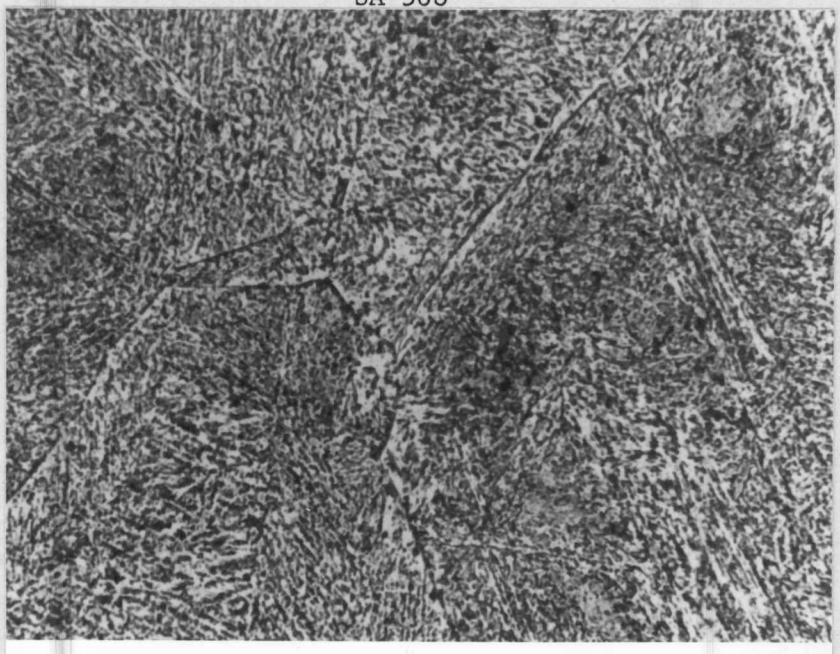

A) Cycle VI (2400°F P.T.) + hold @ 600°F (2 hrs.). Tempered Bainitic structure. HRC 26. Super picral etch.

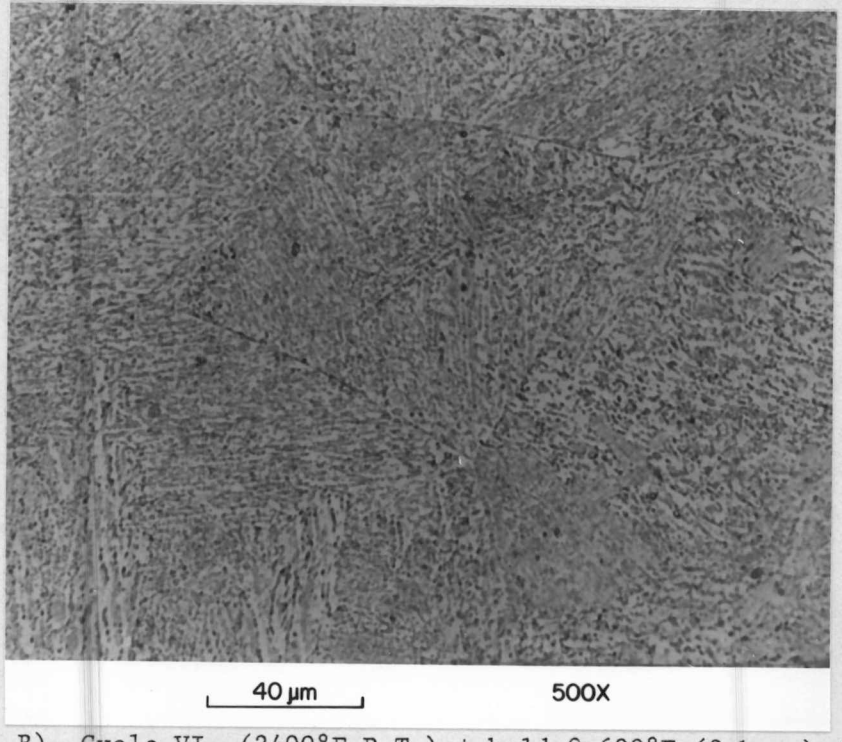

B) Cycle VI (2400°F P.T.) + hold @ 600°F (2 hrs.) + PWHT. Tempered Bainitic structure. HRC 9. Super picral etch.

Figure 94. Microstructural behavior observed in SA 508 steel for Cycle VI and held @ 600°F.

SA 508

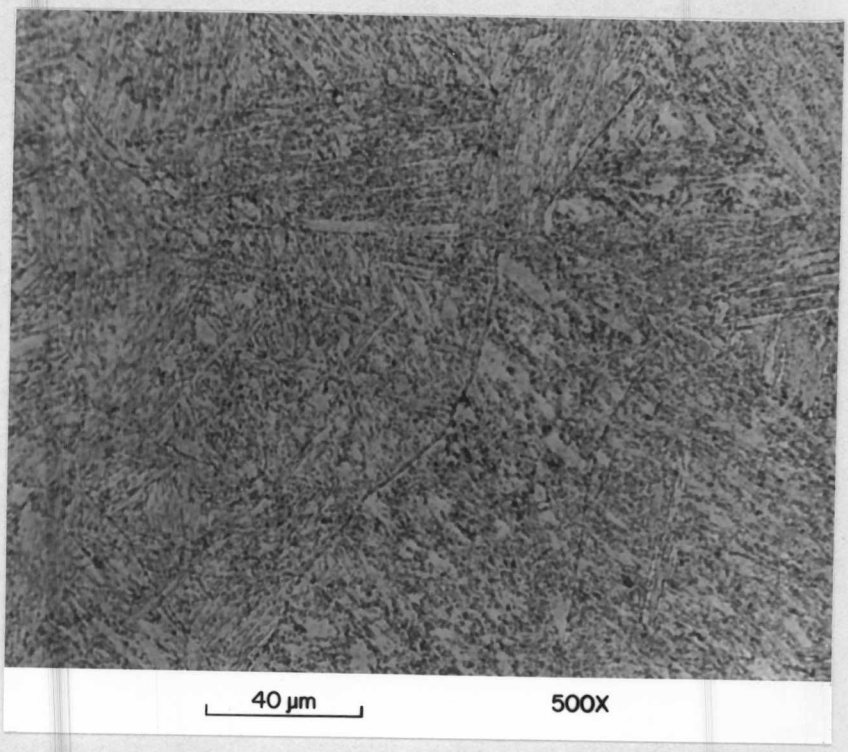

Cycle II (2400°F P.T.) + hold @ 300°F (2 hrs.) + PWHT. Tempered Martensitic structure. HRC 12. Super picral etch.

Figure 95. Microstructural behavior observed in SA 508 steel for Cycle II and held @ 300°F.

SA 508

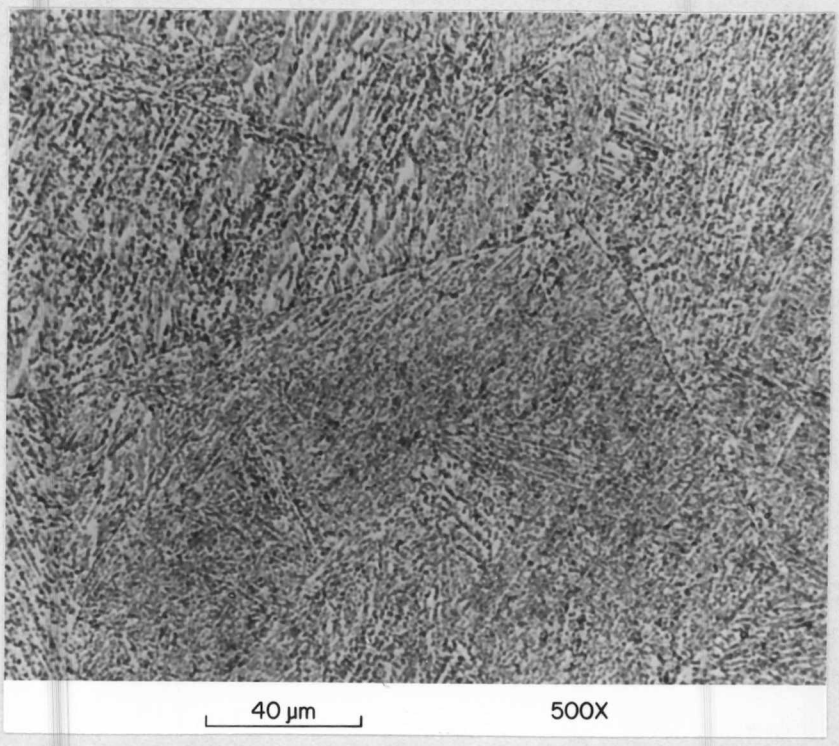

Cycle VI (2400°F P.T.) + hold @ 300°F (2 hrs.) + PWHT.
Tempered Bainitic structure. HRC 11. Super picral etch.

Figure 96. Microstructural behavior observed in SA 508 steel for Cycle VI and held @ 300°F.

The best toughness of the martensitic structure is attained when multiple cycles are employed (high peak temperatures followed by a grain-refining cycle) and this result agrees with Dolby,[6] who mentioned that the multipass HAZ's show higher toughness because of the increased proportion of grain-refined structure produced in the test specimen, whereas single pass unreheated HAZ regions show lower toughness. Canonico[1] noted that HAZ of welds generally possess superior tensile and toughness properties when compared to their chemically equivalent base metal. In our research it is found that HAZ of welds may or may not have a toughness superior to the base metal because the toughness depends upon the transformation products obtained in the HAZ.

It is concluded from these tests, that SA 533 and SA 508 behave similarly in the sense that both show a significant increase in toughness by tempering the martensitic structure. The tempered bainite structure showed poorer toughness in both steels. Therefore, it is recommended that bainitic structures be avoided in the HAZ.

It would have been very beneficial to obtain an impact transition curve for each thermal cycle schedule but due to the program scope, this could not be accomplished and this is suggested for future work.

CHAPTER V

CONCLUSIONS

Based on evaluation of the experiments for SA 533 and SA 508 steels in this program, the following conclusions have been reached.

1. The isothermal transformation behavior for SA 533 and SA 508 has been documented.
   a) The I-T behavior shows that the bainite nose for SA 508 steel lies at longer times than the bainite nose for SA 533 steel.
   b) Upon holding isothermally at 1250°F for 10,000 secs. some pearlite is formed in SA 508 steel, but for same time and temperature, no pearlite is observed in SA 533 steel.
   c) The ferrite nose location in both steels is identical.
   d) The bainite start temperature is lower for SA 508 steel than for SA 533 steel.
   e) The M_f temperature for SA 533 is higher than for SA 508 steel.
2. The continuous cooling transformation behavior for SA 533 and SA 508 determined by resistivity measurement and dilatometrical method, has been documented.
   a) The CCT behavior for both steels obtained by resistivity measurements is identical to the CCT behavior obtained by dilatometrical method using a peak temperature of 1650°F.
   b) The CCT diagrams show that the critical cooling rate for SA 508 is less than the critical cooling rate for SA 533.

c) In the welding situation the higher peak temperature of 2400°F, causes grain growth and shifts the bainite nose to longer times for both steels.

d) For heat affected zones the transformation behavior of SA 508 and SA 533 with peak temperaures of 2400°F is almost identical.

e) Thermal cycle with a hold of 5 secs. at 2400°F peak temperature, does not change the transformation behavior of SA 533 and SA 508 steels.

3. The CCT transformations occur at lower temperature and at longer times (below and to the right) as compared to the corresponding I-T behavior.

4. The CCT behavior of SA 533 steel obtained by Klumpes[22] does not correlate with the CCT behavior obtained in this study, because the critical cooling rate (90°F/sec) obtained by Klumpes is much lower than the critical cooling rate (140°F/sec) obtained in this study.

5. Hardenability results show that SA 508 has higher hardenability than SA 533.

6. In cold cracking tests, SA 508 was found to be more susceptible to hydrogen induced cracking than SA 533.

7. Stress relief cracking for SA 533 and SA 508 steels has been observed experimentally and metallographically.

a) The cracking behavior in both steels was intergranular.

b) For all the thermal treatments, it was observed that SA 533 has higher ductility than SA 508.

c) Stress rupture parameter in SRC test was much lower for SA 508 than for SA 533 indicating that SA 508 steel is more susceptible to reheat cracking than SA 533.

8. The charpy impact toughness of SA 533 and SA 508 for bainitic and martensitic structures, exposed to different thermal heat treatments, has been documented.
   a) Tempered martensite (in the coarse-grained region of HAZ) shows greater toughness than tempered bainite.
   b) An untempered, as-welded, coarse-grained, martensitic structure subjected to a post-weld hold at 600°F is injurious to the HAZ toughness.
   c) Multiple thermal cycles (2400°F peak, followed by 1650°F peak temperature) are beneficial to the martensitic structures of both SA 508 and SA 533 steels in terms of toughness.
   d) PWHT of the weld HAZ of SA 533 gives higher toughness than the PWHT weld HAZ of SA 508.
   e) The hardnesses observed for all identical thermal treatments were higher for SA 508 than SA 533 steel.
   f) The hardness drop from an untempered structure to tempered structure was greater for SA 533 than for SA 508.
9. Post weld-heat treatment has a significant effect on HAZ toughness.
10. Hardness cannot be used as a reliable indicator of notch toughness.

BIBLIOGRAPHY

BIBLIOGRAPHY

Cited References

1. D. A. Canonico, "Significance of Reheat Cracks to the Integrity of Pressure Vessels for Light-Water Reactors," Report ORNL/NUREG - 15. July 1977.

2. R. D. Stout and W. D. Doty, "Appendix," Weldability of Steels, 2nd Ed., eds. Samuel Epstein and R.E. Somers, WRC, New York, 1971.

3. M. W. F. Cane, R. E. Dolby, "Metallurgical Factors Controlling the HAZ Toughness of Submerged Arc Welded C-Mn Steels," Welding Research Institute, 1974.

4. R. E. Dolby, "The Effect of Nb on the HAZ Toughness of High Heat Input Welds in C-Mn Steels," Proceedings of Conference on Welding of HSLA (Microalloyed) Structural Steels, Rome, Nov. 1976, ASM.

5. N. E. Hannerz, "Effect of Stress Relieving Heat Treatment on the Toughness Properties of Simulated HAZ's in V-Alloyed Steels," Schweissen und Schneiden, 1976.

6. R. E. Dolby, "HAZ Toughness of Structural and Pressure Vessel Steels Improvement and Prediction," Welding Research Supplement, August 1979, pp 225s-238s.

7. T. U. Marston, W. Server, "Assessment of Weld Heat Affected Zones in a Reactor Vessel Materials," pp. 267-271, Transactions of the ASME Journal of Engineering Materials and Technology, Vol. 100 No. 3, July 1978.

8. R. E. Dolby, J. F. Knott, "Toughness of Martensitic and Martensitic Bainitic Microstructures with Particular Reference to Heat Affected Zone in Welded Low Alloy Steel," J. Iron Steel Inst., GB, Vol. 210 (1972) No. 11, pp. 857-865.

9. M. Suzuki, H. Takahashi, J. Kameda, "Microstructure and Fracture Toughness of Heat Affected Zone in a Welded Low Alloy Steel," J. Jap Welding Soc., Japan, Vol. 45 (1976), No. 6.

10. H. S. Chung, T. Takahashi, M. Suzuki, "Microstructural Gradient in HAZ and its Influence Upon Toe HAZ Fracture Toughness," pp. 248-261, Welding in the World, Vol. 16, No. 11/12, 1978.

11. C. E. Childress, "Fabrication Procedures and Acceptance Data for ASTM A 533 welds and a 10-inch thick ASTM A 543 Plate of the HSST Program," Documentary Report 3, ORNL-4313-3, Jan, 1971.

12. R. D. Stout and W. D. Doty, "The Properties of Steel Related to Weldability," Weldability of Steels, 2nd Ed., eds. Samuel Epstein and R. E. Somers, WRC, New York, 1971.

13. D. A. Canonico, "Heavy Section Steel Technology Program (HSST)," pp. 32-40, in Metal Progress, July, 1979.

14. D. A. Canonico, "Microstructure Studies of HSST Plate 01," pp. 20, 32 in HSST Program Semiannu. Prog. Rep, for period ending August 31, 1968, ORNL-4377 (April 1969).

15. J. R. Hester, "Correlation of Microstructure with Mechanical Properties for HSST Program Plate 01," M. S. Thesis, University of Tennessee (1970).

16. G. E. Grotke et al., "Reheat Cracking and Heat Affected Zone Toughness in SA 508 Class 2 Steel Weldments," Westinghouse Research Laboratory Report 76-ID4-Reheat-R1, (February 20, 1976).

17. A. G. Glover, J. T. McGrath, M. J. Tinkler and G. C. Weatherly, "The Influence of Cooling Rate and Composition on Weld Metal Microstructures in a C/Mn and a HSLA Steel," Welding Journal, September 1977, Res. Suppl. p. 267-s to 274-s.

18. E. S. Davenport, "Isothermal Transformation in Steels," Transactions, ASM, Vol 27, Dec. 1939, p. 837.

19. R. A. Grange and J. M. Kiefer, "Transformation of Austenite on Continuous Cooling and its relation to Transform at Constant Temperature," Transactions, March 1941.

20. K. E. Dorschu, "Control of Cooling Rates in Steel Weld Metal," Supplement to the Welding Journal, February 1968, p 49-s to 62-s.

21. H. Fuji Maki, T. Tsukamoto, S. Watanable, J. Imai, "Development and Manufacturing of Steel Forgings of ASTM-A508 Class 2 for Nuclear-Reactor Pressure Vessels," pp. 21-35, Nippon Steel Technical Report No. 7, November 1975.

22. H. Klumpes, "Peak Temperature Cooling Time Diagram of Pressure Vessel Steels ASME SA 508 Cl 2 and SA 533 Gr B Cl 1," tiDVS Berichte No. 32, Proceedings, 2nd International Colloquim on Welding in Nuclear Engineering, Dusseldorf, pp. 23024, October 1974.

23. J. D. Murray, "Stress-Relief Cracking in Carbon and Low Alloy Steels," Brit. Weld. J., 1967, 14, 8, pp. 447-56.

24. C. F. Meitzner and A. W. Pense, "Stress-Relief Cracking in Low Alloy Steel Weldments," Welding Journal, 48 (10), October 1969, Res. Supp., pp. 431-s to 440-s.

25. A. W. Pense, E. J. Galda and G. T. Powell, "Stress-Relief Cracking in Pressure Vessel Steels," Welding Journal, 50 (8), August 1971, Res. Suppl., pp. 374-s to 378-s.

26. R. W. Nichols, "Reheat Cracking in Welded Structures," Welding Research Abroad, pp. 36-44, March 1970.

27. K. Detert, W. Bertram, R. Banga, "Stress Relief Cracking in Strip-Weld Cladded Steel Plates," pp. 1269-1276 in Federation of Materials Societies, 1976. Publ. Metals Park, Ohio.

28. M. Lorenz and P. Luginbuhl, "Stress Relief Cracking in Overlay-Welded Components for Nuclear Reactor Pressure Vessels of a Heat-Resistant Structural Steel," pp. 51-60 in Sulzer Technical Review, Sulzer Research No. 1974, Sulzer Brothers Ltd., Ch-8401, Winterthur, Switzerland (1974).

29. C. J. McMahon, R. J. Dobbs, and D. H. Gentner, "Stress Relief Cracking in Mn, Mo, Ni and Mn, Mo, Ni, Cr Pressure Vessel Steels," Material Science and Engineering, 37 (1979), p179-186.

30. J. M. Brear, B. L. King, "Stress Relief Embrittlement in Mn - Mo - Ni Pressure Vessel Steels (ASME SA 533 B/SA 508)," Grain Boundaries, presented at Institution of Metallurgists conference, 1976.

31. L. G. Liljestrand, M. Ancouturier, G. Ostberg, P. Lindhagen, "Formation of Microcracks during Stress Relief Annealing of a Weldment in Pressure Vessel Steel of Type A 508 Cl 2," Aktiebolaget Atomenargi Studsvik, Sweden. IX-996-76.

32. S. Yukawa, "Evaluation of Periodic Proof Testing and Warm Prestressing Procedures for Nuclear Reactor Vessels," HSSTP-TR-1 ORNL, Tn 37830, July 1969.

33. C. E. Childress, "Fabrication and Mechanical Test Data for Acceptance of the First six 6-inch thick Intermediate Test Vessels of the HSST Program," ORNL Report No. TM-4351.

34. R. D. Stout, and W. D. Doty, Weldability of Steels, Welding Res. Council, 1978, pp. 252-254.

35. Emil G. Signes, "A Simplified Method for Calculating Cooling rates in Mild and Low Alloy Steel Weld Metals," Weldg. Journal, October 1972, Res. Suppl., pp. 473-S to 484-S.

36. Pravin Jhaveri, W. G. Moffatt, and C. M. Adams, Jr., "The Effect of Plate Thickness and Radiation on Heat Flow in Welding and Cutting," Welding Journal, January 1962, Res. Supple., pp. 12-S to 16-S.

37. I. G. Hamilton, "Ferritic Steel Plates for Pressure Vessels," Developments in Pressure Vessel Technology-3, edited by R. W. Nichols, 1980. pp. 1-33.

38. Tien Shou Lei, "The Effect of 0-8 Wt% Iron on Transformations of Alpha Phase Ni-Mo-Fe Alloys with Ni:Mo Ratio," A Dissertation Presented for the Ph.D degree. The University of Tennessee, Aug. 1979.

Other References

1. Bentley, K. P., "Precipitation During Stress Relief of Welds in Cr-Mo-V Steels," Brit. Welding Journal, October 1964. pp. 507-515.

2. Binckely, N. C., and R. W. Herrmann, "An Inservice Reactor Repair Simulation." DVS Berichte No. 32, Proceedings, 2nd International Colloquium, Welding in Nuc. Engr., Dusseldorf, October 1974, pp. 289-298.

3. Caplan, J. S., and E. Landerman, "Preventing Hydrogen-Induced Cracking After Welding of Pressure Vessel Steels by Use of Low Temperature Postweld Heat Treatments." WRC Bulletin 216, June 1976.

4. Debray, W., "Reheat Cracking in Low Alloy Steels," Metal Construction, February 1976. pp. 74-77.

5. Dhooge, A., et al., "A Review of Work Related to Reheat Cracking in Nuclear Reactor Pressure Vessel Steels," Int. J. Pres. Ves. and Piping (6) 1978. pp. 329-409.

6. Doane, D. V., and J. S. Kirkaldy, "Hardenability Concepts with Applications to Steel," Symposium, AIME, October 26, 1977.

7. Dolby, R. E., and G. G. Saunders, "A Review on the Problem of Reheat Cracking in Nuclear Vessels Steels," Report for the Nuclear Install. Inspectorate, Dept. of Energy, April 1975.

8. Dolby, R. E., and G. G. Saunders, "Underclad Cracking in Nuclear Vessel Steels," Part 1., Metal Construction, December, 1977. pp. 562-566.

9. Dolby, R. E., and G. G. Saunders, "Underclad Cracking in Nuclear Vessel Steels," Part II, Metal Construction, January 1978, pp. 20-24.

10. Doty, W. D., "Welding of Quenched and Tempered Alloy Steels," Metals Engr. Quarterly, ASM, February 1969, pp. 66-78.

11. Grotke, G. E., "Varestraint Weldability Testing of SA 508 Class 2 and SA 533 Grade B Class 1 Pressure Vessels Steels," Westinghouse Research Lab., 73-1D4-WELST-R1, February 1973.

12. Hodge, J. M., "Properties of Heavy Section Nuclear Reactor Steels," WRC Bulletin 217. pp. 14-22.

13. Jones, W. K. C., "Reheat Cracking Susceptibility of Some 2Cr-Mo Submerged Arc Weld Metals," Welding Res. Suppl., Welding Journal, February 1976, pp. 42-S to 46-s.

14. Kameda, J., H. Takahashi, and M. Suzuki, "Residual Stress Relief and Local Embrittlement in a SA 533 B Reactor Pressure Vessel Weldment," Int. J. Pres. Ves. and Piping (6), 1978. pp. 245-274.

15. Kottcamp, E. H., D. A. Canonico, and R. D. Stout, "Prediction of the Properties of Heavy Section Pressure Vessel Steels from End-Quench Tests," Welding Research Suppl., Welding Journal, August 1962. pp. 350-354s.

16. Lochead, J. C., and A. Speirs, "The Effect of Heat Treatment on Pressure Vessel Steels," Journal of the West of Scotland Iron and Steel Institute, Vol. 80, 1972-73, Paper No. 623.

17. Lundin, C. D., W. F. Savage, and J. L. Ledman, "Study of the Transformational Characteristics and the Weldability of HY-80 Steel," RPI, January 1963.

18. Meitzner, C. F., and R. D. Stout, "Microcracking and Delayed Cracking in Welded Quenched and Tempered Steels," Welding Res. Suppl., Welding Journal, September 1966. pp. 393-s to 400-s.

19. Mueller, R. A., D. G. Howden and F. B. Simmons, "HAZ Thermocycle and Structure Simulation," Welding Res. Suppl., Welding Journal, September 1973. pp. 411-s to 416-s.

20. Nippes, E. F., "The Weld Heat-Affected Zone," Welding Res. Suppl., Welding Journal. January 1959. pp. 1-s to 18-s.

21. Nippes, E. F., W. F. Savage, and J. M. Paez, "Transformational Behavior of Mn-Mo Armor Steels," Welding Res. Suppl., Welding Journal, December 1959. pp. 475-s to 481-s.

22. Nippes, E. F. and E. C. Nelson, "Prediction of Weld HAZ Microstructures from Continuous Cooling Transformation Data," Welding Res. Suppl., Welding Journal, June 1958. pp. 289-s 294-s.

23. Nippes, E. F., W. F. Savage and R. J. Allio, "Studies of the Weld Heat-Affected Zone of T-1 Steel," Welding Res. Suppl., Welding Journal, December 1957. pp. 531- s to 540- s.

24. Rogerson, J. H., "Welding Defects and Their Elimination," Development in Pressure Vessel Technology-3, edited by R. W. Nichols, 1980. pp. 327-355.

25. Savage, W. F., E. F. Nippes and E. S. Szekeres, "Hydrogen Induced Cold Cracking in a Low Alloy Steel," Welding Res. Suppl., Welding Journal, September 1976. pp. 276- s to 283- s.

26. Savage, W. F., E. F. Nippes and H. Homma, "Hydrogen Induced Cracking in HY-80 Steel Weldments," Welding Res. Suppl., Welding Journal, November 1976. pp. 368-s to 376-s.

27. Stout, R. D., "Hardness as an Index of the Weldability and Service Performance of Steel Weldments," WRC Bulletin 189, November 1973.

28. Suzuki, M., H. Takahashi and M. Saito, "Assessment of Allowable Maximum Crack Size in Toe HAZ of Welded Low Alloy Steel Components," Tohoku University, Sendai, Japan. IIW X-903-78.

29. Vanden Boom, J. E., and J. P. F. Mulder, "Mechanical Properties of Strip Clad Weld Heat Affected Zones Determined for Steels ASTM SA 508 Class 2, SA 533 Grade B Class 1, A 302, Grade B and A 387 Grade D, in View of Susceptibility to Stress Relief Cracking," Welding Res. Inter., Vol. 2, 1972 No. 2 pp. 20-36.

30. Vinckier, A. and A. Dhooge, "Reheat Cracking in Welded Structures During Stress Relief Heat Treatments," J. Heat Treating, Vol. 1 No. 1. June 1979, pp. 72-80.

31. Vinckier, A. G. and A. W. Pense, "A Review of Underclad Cracking in Pressure Vessel Components," WRC Bulletin 197 , August 1974.

APPENDICES

APPENDIX A

TABLE A-1

SCHEDULE OF SALT BATH HEAT TREATMENT OF
SA 533 (3T) AND SA 508 (8M) SPECIMENS

Time (secs)	Specimen @ 550°F	Specimen @ 800°F	Specimen @ 950°F	Specimen @ 1150°F	Specimen @ 1250°F
10^0	3TOA*	3TOB	3TOC	3TOD	3TOE
	8MOA*	8MOB	8MOC	8MOD	8MOE
10^1	3T1A	3T1B	3T1C	3T1D	3T1E
	8M1A	8M1B	8M1C	8M1D	8M1E
10^2	3T2A	3T2B	3T2C	3T2D	3T2E
	8M2A				
10^3	3T3A	3T3B	3T3C	3T3D	3T3E
	8M3A	8M3B	8M3C	8M3D	8M3E
10^4	3T4A	3T4B	3T4C	3T4D	3T4E
	8M4A	8M4B	8M4C	8M4D	8M4E

* 8 = Material SA 508 Class 2.

M = 1/2 T Section of Material.

3 = Material SA 533 Grade B Class 1.

T = Surface Section of Material.

0-4 = Different time periods i.e., 0 = 10^0, 1 = 10^1 sec. etc.

A-E = Different temperatures i.e., A = 550°F, B = 800°F etc.

TABLE A-2

THERMAL TREATMENTS AND STRESSES EMPLOYED
IN STRESS RELIEF CRACKING TEST

Test #	Thermal Treatment*	Stress Applied (Ksi)
1	Cycle II + PWHT	17
2	Cycle II + PWHT	22
3	Cycle II + PWHT	25
4	Base Metal PWHT	25
5	Cycle II + Cycle II (1650°F peak temp) + PWHT	22
6	Cycle II + hold @ (600°F for 2 hours) + PWHT	25
7	Cycle VI + PWHT	25
8	Cycle VI + hold @ (600°F for 2 hours) + PWHT	25

* All thermal cycles employed 2400°F peak temperatures unless otherwise mentioned. Cycle II and VI are simulated 50KJ/in. and 136KJ/in. (500°F preheat) heat input on 1 inch thick steel plate, producing martensitic and bainitic structures.
Temperature for PWHT for both materials is 1150°F.

TABLE A-3

THERMAL TREATMENTS EMPLOYED IN CHARPY V-NOTCH TEST

No. of Tests	Thermal Treatment*
1.	Run Cycle II
2.	" Cycle VI
3.	" Cycle II + PWHT
4.	" Cycle VI + PWHT
5.	" Cycle II + Cycle II @ Peak temperature of 1650°F.
6.	" Cycle VI + Cycle VI @ Peak temperature of 1650°F.
7.	" Cycle II + Cycle II @ Peak temperature of 1650°F. + PWHT
8.	" Cycle VI + Cycle VI @ Peak temperature of 1650°F. + PWHT
9.	" Cycle II and hold @ 600°F. for 2 hrs.
10.	" Cycle VI " " " " " " " "
11.	" Cycle II " " " " " " " " + PWHT
12.	" Cycle VI " " " " " " " " + PWHT
13.	" Cycle II and hold @ 300°F. for 2 hrs.
14.	" Cycle VI " " " " " " " "
15.	" Cycle II " " " " " " " " + PWHT
16.	" Cycle VI " " " " " " " " + PWHT

For each test, three charpy blanks were used. Material 508 was PWHT for 24 hrs. and 533 for 40 hrs., both at 1150 ± 50°F.

* All thermal cycles were run using 2400°F. peak temperature unless otherwise mentioned.

Cycle II and VI are simulated 50KJ/in. and 136KJ/in. (500°F. preheat) heat input on 1 inch thick steel plate, producing martensitic and bainitic structures.

TABLE A-4

ENERGY INPUTS AS A FUNCTION OF PLATE THICKNESS FOR SMAW PROCESS

Plate Thickness (inches)	Energy Inputs (KJ/in) - Preheat (°F)				
	Cooling Rates °F/sec. at 1300°F				
	84	35	23	14	8
1	50-72	100-72	136-72	136-300	136-500
2	54-72	130-72	175-72	190-300	200-500
3	54-72	130-72	175-72	190-300	220-500
4	54-72	130-72	175-72	190-300	220-500

TABLE A-5

DATA OBTAINED BY STRESS-RELIEF CRACKING TEST

Test No.	* Applied Stress (KSi)	SA 533 Gr.B Cl.1		SA 508 Cl.2	
		Time to Rupture (min)	% Reduction of Area	Time to Failure (min)	% Reduction of Area
1	17	36	9.8	No failure (120)	-
2	22	5	5.4	104	4.6
3	25	3	9.2	22	1.1
4	25	4	75.6	17	64
5	22	No failure (120)	-	-	-
6	25	8	6.8	61	1.6
7	25	37	4.5	69	4
8	25	No failure (120)	-	No failure (120)	-

* Test No. thermal treatment

1. Cycle II + PWHT
2. "
3. "
4. Base metal PWHT
5. Cycle II + Cycle II (1650°F. P.T.) + PWHT
6. Cycle II + hold @ 600°F. (2 hrs.) + PWHT
7. Cycle VI + PWHT
8. Cycle VI + hold @ 600°F. (2 hrs.) + PWHT

NOTE: All thermal cycles employed 2400°F P.T. unless indicated. Cycle II and VI produce martensitic and bainitic structures. PWHT was done at 1150°F.

TABLE A-6

DATA OF CHARPY TEST OBTAINED FOR
SA 533 STEEL, TESTED @ -25°F.

Test No	Energy (ft-lbs)	HRC	Lateral Expansion (mils)	%Shear
1	19	42	2	30
2	8	21	3	0
3	140	1	55	100
4	22	< 1	13	0
5	21	42	2	30
6	5	21	1	0
7	144	3.3	62	100
8	17	< 1	8	30
9	6	39	1	0
10	13	19	5	0
11	139	6	67	100
12	67	5	44	30
13	17	42	1	20
14	9	21	3	0
15	136	6	61	100
16	47	10	29	10
Base Metal	60	10	41	60

TABLE A-7

DATA OF CHARPY TEST OBTAINED FOR
SA 508 STEEL, TESTED @ 72°F.

Test No	Energy (ft-lbs)	HRC	Lateral Expansion (mils)	%Shear
1	37	46	5	40
2	8	28	4	0
3	47	28	24	50
4	16	18	8	0
5	45	48	4	40
6	12	26	6	5
7	58	20	31	100
8	34	13	23	30
9	12	38	2	5
10	15	26	8	5
11	67	12	39	100
12	26	9	17	15
13	36	46	6	30
14	10	28	6	0
15	72	12	44	100
16	34	11	20	15
Base Metal	70	12	47	60

APPENDIX B

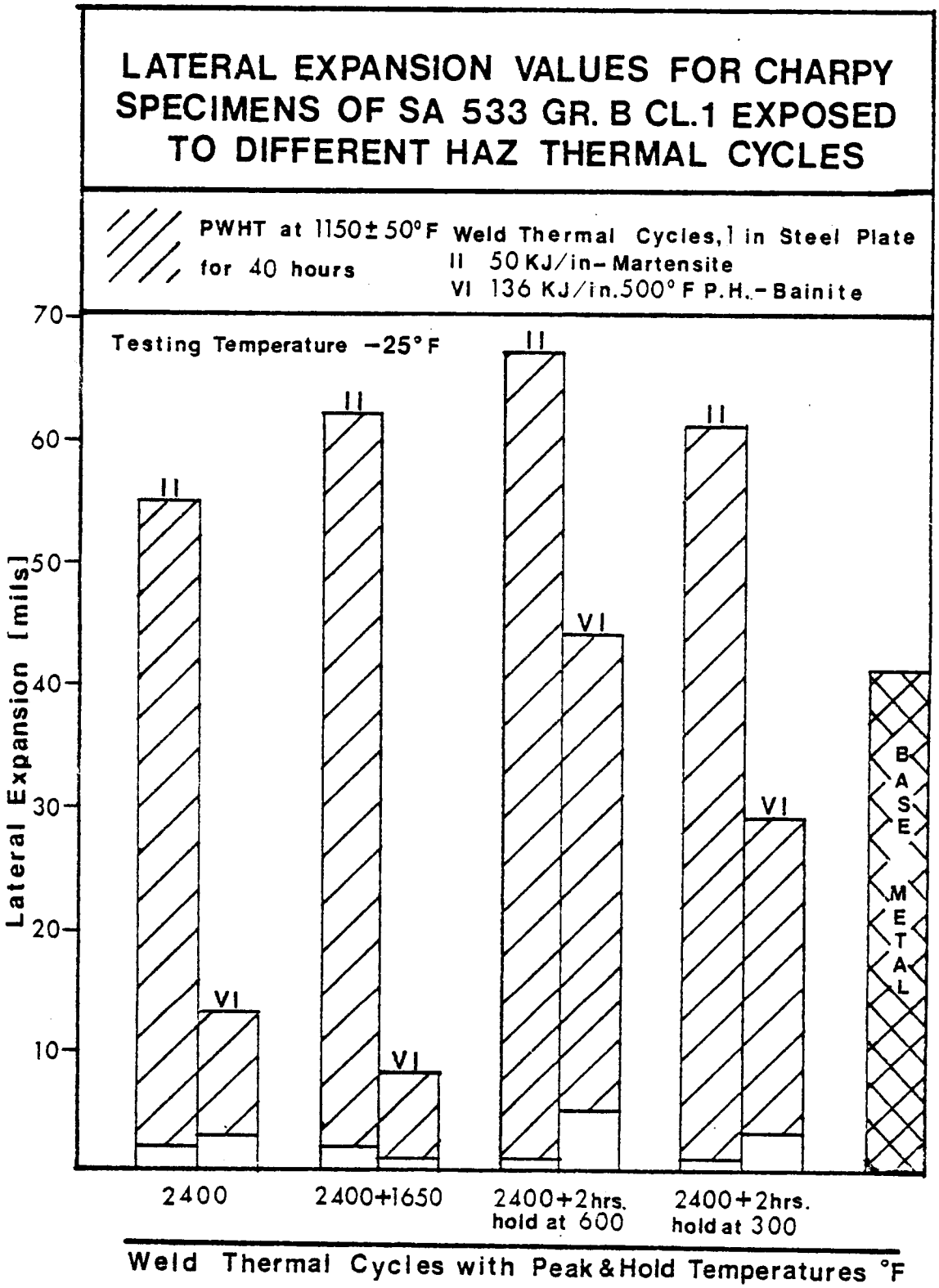

Figure A-1. Lateral expansion values for charpy specimens of SA 533 Gr. B Cl.1 exposed to different HAZ thermal cycles.

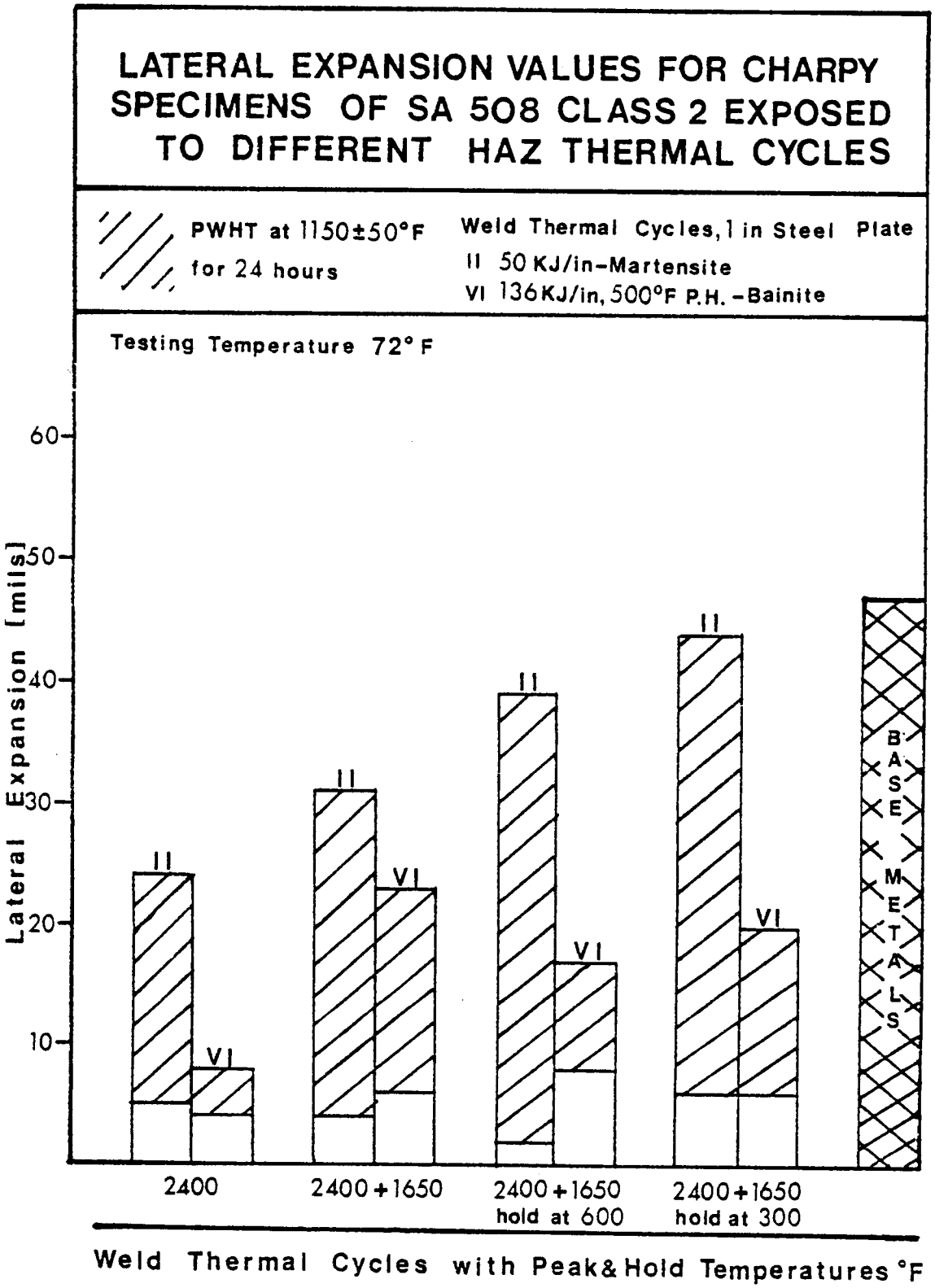

Figure A-2. Lateral expansion values for charpy specimens of SA 508 Cl.2 exposed to different HAZ thermal cycles.

VITA

The author was born September 5, 1954 in Sialkot, Pakistan. He came to the United States in 1974 to obtain higher education. He received his Bachelor of Science degree in the field of Metallurgy in June, 1978 at the University of Southern Colorado, Pueblo. He entered the Metallurgical Engineering Department of the University of Tennessee, Knoxville, in the spring of 1979, to continue studying toward his Master of Science degree in Metallurgical Engineering.

The author is a member of the American Welding Society and the American Society for Metals.